3-2007

Lamb Wave Propagation in Varying Thermal Environments

Jennifer P. Andrews

LAMB WAVE PROPAGATION IN VARYING THERMAL ENVIRONMENTS

THESIS

Jennifer Puri Andrews, First Lieutenant, USAF

AFIT/GA/ENY/07-M01

DEPARTMENT OF THE AIR FORCE
AIR UNIVERSITY

AIR FORCE INSTITUTE OF TECHNOLOGY

Wright-Patterson Air Force Base, Ohio

The views expressed in this thesis are those of the author and do not reflect the official policy or position of the United States Air Force, Department of Defense, or the United States Government.

AFIT/GA/ENY/07-M01

LAMB WAVE PROPAGATION IN VARYING THERMAL ENVIRONMENTS

THESIS

Presented to the Faculty

Department of Aeronautical and Astronautical Engineering

Graduate School of Engineering and Management

Air Force Institute of Technology

Air University

Air Education and Training Command

In Partial Fulfillment of the Requirements for the

Degree of Master of Science in Astronautical Engineering

Jennifer Puri Andrews, BS

First Lieutenant, USAF

March 2007

AFIT/GA/ENY/07-M01

LAMB WAVE PROPAGATION IN VARYING THERMAL ENVIRONMENTS

Jennifer Puri Andrews, BS

First Lieutenant, USAF

Approved:

Dr. Anthony N. Palazotto Chairman	Date
Major Eric D. Swenson Committee Member	Date
Dr. William P. Baker Committee Member	Date

Abstract

During flight, launch, and reentry, external surfaces on aerospace vehicles undergo extreme thermo-acoustic loads resulting in structural degradation. Structural health monitoring techniques are being devised to evaluate the health of these structures by locating and quantifying structural damage during and after flight. One such technique uses Lamb wave propagation to assess damage on the surface and through the thickness of thin materials.

The objective of this study was to assess the sensitivity of piezo-generated Lamb wave propagation to isothermal and thermal gradient environments using both theoretical and experimental methods. Experimental isothermal tests were conducted over a temperature range of 0-225°F. The changes in temperature-dependent material properties were correlated to measurable differences in the response signal's waveform and propagation speed. An analysis of the experimental signal response data demonstrated that elevated temperatures delay wave propagation, although the delays are minimal at the temperatures tested in this study. Both these results and experimental group velocity dispersion curves verified theoretical predictions. Subsequent experimental testing in thermal gradient environments, with peak temperatures ranging 114-280°F, also displayed an observable yet minimal delay in wave propagation. Finally, theoretical simulations at temperatures up to 600°F revealed significantly increased delays in wave propagation.

Acknowledgements

Over the course of the past year, I have had the privilege of working with Dr. Anthony Palazotto, my thesis advisor. His support and continual feedback were instrumental in my thesis work. I would also like to acknowledge and thank Mark Derriso, who had this research sponsored through the AFRL/VASA. The team supporting the efforts at the AFRL SHM Lab, which include Steve Olson, Martin DeSimio, Todd Bussey, and Kevin Brown provided me with continual support throughout my thesis work, for which I am very appreciative. Specifically, Martin DeSimio and Todd Bussey went above and beyond in their support and guidance. I would also like to acknowledge and thank my committee members, Dr. William Baker and Major Eric Swenson, who provided me with valuable feedback during my defense and at the concluding phase of this thesis. Finally, I would like to recognize my mother and my close friend Michael Hines. Their continual love and support over the past year and a half were beyond measure.

Table of Contents

List of Figures

Page

List of Tables

Page

List of Abbreviations

AFIT: Air Force Institute of Technology

AFRL: Air Force Research Laboratory

DAQ: Data Acquisition Unit

DOD: Department of Defense

NDT: Nondestructive Testing

NI: National Instruments

PSD: Power Spectral Density

PWAS: Piezoelectric Wafer Active Sensor

PZT: Lead Zirconate Titanate

SHM: Structural Health Monitoring

TOA: Time of Arrival

TOF: Time of Flight

VASA: Advanced Structural Concepts Branch

LAMB WAVE PROPAGATION IN

VARYING THERMAL ENVIRONMENTS

Chapter 1 Introduction

1.1 Motivation: Structural Health Monitoring

Structural health monitoring (SHM) has taken an active role in the evaluation of modern and aging structures around the world. "SHM is an emerging technology that can be defined as continuous, autonomous, real time, in-service monitoring of the physical condition of a structure by means of embedded or attached sensors with minimum manual intervention" (16). In particular, the Air Force has an urgent need for SHM systems due to aging air and spacecraft systems. Since these structures are continually exposed to harsh environments, the need to assess their health and re-certify them for flight within a matter of hours is mission critical (3).

In an evolving world where global threats are imminent on the United States and our Allies, there is a growing need to assure that our military assets are mission ready at all times. However, with a shortage of technical expertise in the developmental and operational fields and with the government pushing for a reduction in Department of Defense (DOD) expenditures, these tasks can be difficult to fulfill. Modern SHM systems are designed to meet these objectives.

SHM systems will assist maintenance crews in identifying structural degradation in a timely fashion in order to conduct preventative or corrective maintenance as needed. Additionally, these systems would provide an avenue for reducing the costs of the logistics required for replacement parts and would promote a long-term change in maintenance philosophy that would eventually evolve to a "fix when required approach" (5). Giurgiutiu stated, "the mounting costs of maintaining our aging infrastructure can be addressed through SHM systems that will reduce

unscheduled repairs while increasing safety and reliability" (8:1). Currently, Air Force maintenance costs exceed $13B a year (5).

1.1.1 Structural Mishaps Leading to SHM

In 1988, a catastrophic event occurred on an Aloha Airlines Boeing 737. "Multi-site cracks in the aircraft's skin joints were undetected, which led to an un-zipping of large segments of the fuselage" during flight (8:1). After the occurrence of this event, the Boeing Company took an active role in assuring that its new 7E7 aircraft were equipped with "full-time built-in SHM systems comprising sensors embedded in the structure to assess the state of structural health" (8:1). This event also led to the government's focus on early crack detection in structural joints (5).

The Tacoma Narrows Bridge collapse, which occurred on 7 November 1940, was due to a torsional or twisting mode that was never seen before in a structure of its kind. Prior to its destruction "the bridge would sway and buckle in a dangerous manner" suggesting that the implementation of a SHM system may have prevented the foreshadowed collapse (23). Unfortunately, this event occurred at a time when SHM was nonexistent.

Several SHM technologies have emerged in the last fifteen years due to a push for civil and aerospace engineering companies to meet specifications and standards that were not implemented over 60 years ago. It is "approximated that out of 576,600 bridges in the national inventory, 32% are either 'structurally deficient' or 'functionally obsolete' and in need of replacement" (8:1). Many of these bridges were built in the mid-1900s, when SHM was nonexistent. Similarly, aerospace engineers designed airframes in the mid-1900s lacking SHM technology. A prime example is the National Aeronautics and Space Administration's Space Shuttle fleet. Since the Space Shuttle Columbia tragedy in 2003, in which the orbiter's structure disintegrated upon reentry, there has been a strong push for the implementation of an Integrated Structural Health

Management (ISHM) system for the remaining Shuttle fleet and for future space vehicles. Similarly, military airframes designed over half a century ago were not equipped with SHM technology. A prime example is the B-52H Stratofortress. At present, B-52s are projected to sustain operational duties over the next few decades. Over the years, these airframes will undergo depot maintenance after every six to eight years. During the period in which these aircraft are operational, the airframes can be subjected to temperature swings (-40°F to 150°F) and the corrosive effects of salts, de-icing agents, and several types of fuels, fluids, and lubricants (5). The integration of a SHM system on an older airframe such at the B-52 would provide maintenance crews with critical feedback regarding the health of the airframe, thus assisting crew members with the upkeep of the fleet.

1.1.2 Levels of SHM

SHM systems have been broken down into four distinct levels (3):

- Level I: Damage Detection
- Level II: Damage Localization
- Level III: Damage Assessment
- Level IV: Life Prediction

Level I SHM assesses whether damage is existent within a structure. If damage is present, Level II pinpoints the location of the damage. Level III provides a quantitative analysis of the damage and Level IV provides an estimate of the structure's life expectancy. These levels of damage assessment are dependent on the capabilities of the SHM system implemented. A structure may be excited using actuator's, which is referred to as active SHM, or it may be subjected to operational loading called passive SHM. The structure's response to loading is monitored, collected, and processed in an effort to provide a prognosis of its condition (1). The research presented in this thesis employs active SHM technology.

1.1.3 Nondestructive Evaluation SHM Techniques

A variety of nondestructive SHM techniques have been studied in both industry and the DOD in recent years. Typical Nondestructive Evaluation (NDE) techniques include ultrasonic technology, acoustic emission, magnetic field analysis, penetrant testing, eddy current techniques, X-ray analysis, impact-echo testing, global structural response analysis, and visual inspections. Since some of these techniques have disadvantages, other methods such as vibration-based and impedance-based techniques, have been developed. Vibration-based methods are associated with changes in the modal properties of a system, such as frequencies, damping, and mode shapes. These methods are generally used to detect damage using low frequencies. On the other hand, impedance-based methods use high-frequency signals to excite a structure and monitor changes in a material's electro-mechanical impedance (10:222).

Electro-mechanical Impedance Techniques

Mechanical impedance is the ratio of an applied force to the resulting velocity of a system. Electrical impedance is the ratio of an applied voltage to the resulting current of a system. With the use of an equation that correlates both a structure's mechanical impedance and a sensor's electrical impedance, changes in the electrical impedance of a sensor can be directly correlated to changes in the mechanical impedance of a specimen. The high-frequency signals used in impedance-based SHM are generated by small piezoceramic Lead Zirconate Titanate (PZT) patches that are attached to the host structure. When a structure is damaged, a change occurs in the mechanical impedance of the material and a PZT patch senses this change in the mechanical impedance as a change to its electrical impedance. As an example, if the same voltage is applied to a specimen over several trials, but the resulting currents differ, this can be attributed to a change in the mechanical impedance of the material (10:222-223). Characterizing the electro-mechanical impedance spectrum of a specimen before it is damaged provides a baseline to which subsequent tests can be compared in order to identify and quantify damage.

Impedance-based techniques have been determined to be useful in the detection of near field damage. Near field damage is damage that is within close proximity of a sensor. Therefore, they have been combined with other NDE techniques to identify the location of damage in larger structures. The pitch-catch method is one technique that uses wave propagation to identify damage using PZT patches. One PZT patch is used to generate a signal and another is used to detect the wave transmitted within the material. If a wave's time of flight (TOF) changes due to damage, this technique can help to pinpoint the damage location. On a large structure, this technique is extremely useful since one patch can be used as an actuator and several other patches can be used as sensors. This approach enables analyzing a larger area for the purpose of SHM. Additionally, "the coupling of impedance-based and wave propagation techniques makes the damage identification process more robust such that the loss of a particular patch does not render the health monitoring system nonfunctional" (24:390). Two groups who integrated the local impedance method with the wave propagation approach are Wait, Park, and Farrar, from Los Alamos National Laboratory, and Grisso, Leo and Inman from the Virginia Polytechnic Institute (VPI) and State University (10;24).

Piezoelectric Wafer Active Sensor Ultrasonics

One new method implemented in the NDE of structures is the use of the Piezoelectric Wafer Active Sensor (PWAS). As opposed to conventional ultrasonic transducers, Giurgiutiu, Bao, and Zhao characterized a PWAS as small, inexpensive, unobtrusive, and non-invasive. In some of the older technologies, for example a piezoelectric resonator (i.e. piezoelectric stack, proof mass, and damper), the casing and the electric cord were both expensive and bulky. The large size of these sensors made them impractical to use on various structures. Consequently, there has been a push to reduce the cost, size, and complexity of modern sensors (7:428-429).

The PWAS acts as both an emitter and detector. Initially, the PWAS is electrically excited, which induces a strain in the wafer that transmits to the structure as an interaction force

and moment at the piezo-structure interface. The force and moment, together, act as a 'pinching' mechanism that generates structural waves. On the receiving end, the elastic wave propagating through the material induces a strain that is detected by the sensor as a voltage quantity (7:429).

Giurgiutiu and his partners used both theoretical and experimental techniques to study PWAS embedded ultrasonic waves in beams and plates. They conducted research furthering the detection of damage on aging aircraft by using active SHM on thin metallic plates (7:428). The ultrasonic waves were excited over a range of frequencies (10 kHz to low MHz) and Giurgiutiu's team discovered an optimal excitation frequency at 300 kHz for pulse-echo studies. An optimal excitation frequency generates a maximum response signal based on the size of a PWAS and the thickness of a specimen. Additionally, the aircraft-grade aluminum plate study was used to verify wavespeed dispersion characteristics (7:428). Techniques similar to these are implemented in the current study.

1.1.4 SHM Studies

The following is a compilation of pertinent studies that implemented NDE techniques using Lamb wave technology. The actual features of Lamb waves are discussed in Chapter 2. A number of researchers stressed the importance of studying environmental effects on this technology.

Temperature Influences on Wave Propagation

A study by Grisso et al. simulated the affects of a varying temperature environment on damage detection (9; 10). The impedance-based SHM approach was applied in their studies. Additionally, theoretical results incorporating temperature changes indicated a potential influence on the calculation of damage location using the wave propagation approach.

Wavespeed, which is used to determine damage location, is based on material properties including the modulus of elasticity and density. Their previous studies have confirmed that

increasing temperature results in a diminished modulus of elasticity for metals, which would result in an alteration of wavespeed calculations. Therefore, it was concluded that a temperature differential would affect the localization of structural damage (9; 10). On the other hand, their study demonstrated that a change in material density would not play a significant role when determining damage location in a large specimen. A typical relationship between the modulus of elasticity for aluminum and temperature is seen in Figure 1. Grisso generated a best fit curve to modulus of elasticity data obtained from a reference by Callister (2).

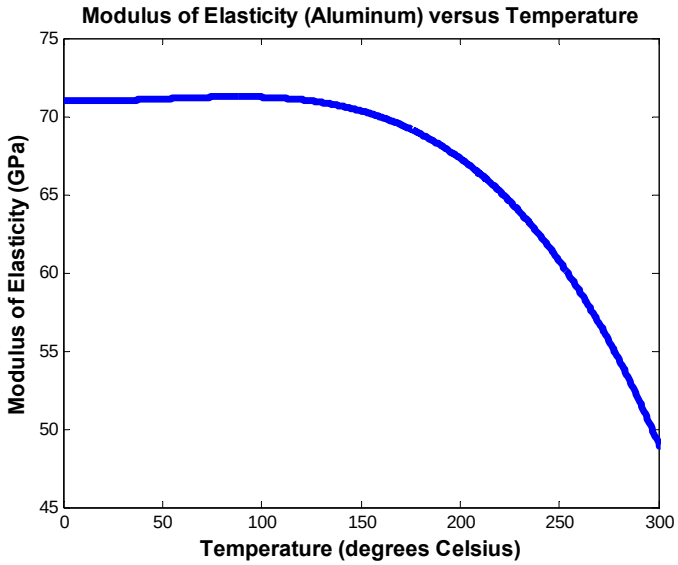

Figure 1: Modulus versus Temperature (2; 9; 10)

From the results of their study, they concluded that temperatures between -100-200°C had little effect on locating damage; however, extreme temperatures, above 200°C and below 100°C, had a significant affect on determining damage location. The theoretical predictions were based on a wavespeed calculated at room temperature. Therefore, continually recalculating the wavespeed in a varying temperature environment is necessary to confirm the location of the damage (10:232). Prior knowledge of wavespeed as a function of temperature would also be useful in this analysis.

New Results in the Use of PWAS for SHM

Giurgiutiu's study addressed the durability and survivability of PWAS transducers exposed to varying environmental conditions and the importance of adequate adhesive and protective coating design (5:1-14). The environmental exposures included temperature cycling, environmental outdoors exposure, submersion exposure, large strains, and fatigue cycle loading. PWASs were placed in an oven, both free and bonded, at temperatures ranging 100-175°F. After eleven months of testing, the results showed that a free PWAS survived 1700 oven cycles without any significant changes in the electro-mechanical impedance spectrum. The bonded PWAS survived 1400 cycles without significant changes. However, there were marked changes in the bonded PWAS after 1700 cycles due to the disbond between the PWAS and the substrate, which indicated that repeated differential expansion can lead to PWAS failure (5:7). In this thesis, several isothermal tests were conducted over a similar range of temperatures.

An additional topic of interest addressed by Giurgiutiu was the testing of a round PWAS on a 2024-T3 aluminum alloy thin-plate (1.07-mm) specimen. The sweet-spot for the fundamental symmetric mode (S_0) response was at 300 kHz and the sweet-spot for the fundamental anti-symmetric mode (A_0) response was at 50 kHz. A sweet-spot occurs at frequencies where one modal amplitude (A_0 or S_0) is very small relative to the other. A slightly thicker specimen (3.15-mm) yielded results that were much more complex in nature, since additional modes were excited. Therefore, the use of a thin plate is sufficient when exciting the fundamental modes (5:3). These modes will be discussed in detail in Chapter 2 under Lamb wave theory.

Durability of METIS Design Lamb Wave Sensors

Wardle and Chambers designed a PZT-based Lamb wave sensor for the SHM of aerospace structures (25). As of October 2006, they have experimentally tested the sensors for electromagnetic interference and radiation resistance. They expressed the necessity for future

performance testing under varying temperature and moisture conditions in addition to long-term exposure at these conditions. "A range of testing including high and low temperature, saturated moisture, electrical and vibrational noise, large strain, and long-term exposure will be undertaken" (25). These tests, and more, are necessary to establish a reliable operating envelope for the sensor. As publicized in the study by Wardle and Chambers, environmental concerns are relevant to any new sensor on the market (25).

Durability Requirements for Aircraft

In a study by Kessler, Amaratunga, and Wardle, the durability requirements for SHM sensors were addressed (12). One of the test standards discussed was environmental susceptibility. Specifically, two temperatures were specified: operational and shock. In the case of operational testing, the following test regimen was recommended. Sensors would be saturated for three hours at extreme temperatures (-55°C and 85°C). Subsequently, the sensors would be functionally tested for two hours at these conditions. Shock tests would involve starting a sensor at a cold extreme and ramping up the heat rate by 10°C per minute until the hot extreme was obtained. After two minutes the sensor would be ramped down to the cold extreme and functional testing would be implemented for a one hour period before additional cycling was continued. Ultimately, combining thermal testing with other environmental testing such as pressure, moisture, and vibration testing is necessary to simulate the actual conditions aircraft are subjected to in operational environments.

Integrated Assessment Using Piezoelectric Active Sensors

Wait's team from Los Alamos National Laboratory used the impedance-based qualities of their piezoelectric active sensors to locate and detect connection damage in a scaled building structure. Additionally, they used the transducer's ability to generate and sense propagating waves toward the detection of simulated cracks in a plate. They discovered a sweet-spot Lamb

wave input at 300 kHz in the wave propagation study. In addition, they focused on the S_o response since it traveled much faster than the A_o response (24).

Fundamental Lamb Wave Propagation

In studies by Derriso et al., piezoelectric transducers were used to both generate and detect Lamb waves (3). Since the propagation distance, the distance between the sender and receiver transducers, and the TOF values were known, the group velocities could be calculated for the received signals. From these calculated values, experimental group velocity dispersion curves were generated and compared to theoretical group velocity dispersion curves. Techniques similar to these were applied in this thesis and are discussed in greater detail in Chapter 2.

1.2 Research Objective

Lamb waves are sensitive to internal and surface cracks in a thin material. However, little research has been conducted on the sensitivity of Lamb wave propagation to external environments. Consequently, the objective of this study was to measure the sensitivity of Lamb wave propagation to both isothermal environments, ranging 0-225°F, and thermal gradient environments.

In the isothermal testing, experimental and theoretical investigations were conducted. The experiments measured each signal's TOF, which was effected by the change in modulus due to temperature. An experimental modulus of elasticity versus temperature curve was used to correlate changes in material properties due to varying temperatures. These changes were incorporated in theoretical wave response computations that were subsequently compared to the experimental wave response results. Any changes to the waveforms of the received signals and their TOF calculations were documented for analysis. Power spectral densities (PSD) were also used to identify differences in the frequency content of the received signals. Additionally, theoretical group velocity dispersion curves were generated from solutions to the Lamb wave equations. Group velocity dispersion curves generated from the isothermal experimental test data

were compared to the theoretical curves in the final analysis. Additional studies were conducted on the varying specimen supports and on wave propagation in thermal gradient environments. Analysis methods similar to the methods used in the isothermal testing were implemented in these subsequent studies. Finally, theoretical simulations were conducted to demonstrate the sensitivity of Lamb wave propagation to isothermal and thermal gradient conditions at elevated temperatures in the region of 600°F.

Chapter 2 Theory

2.1 Wave Theory

There are several methods of defect detection implemented in the field of SHM. A primary method is the use of guided elastic waves, or more specifically ultrasonic Lamb waves. To fully understand the significance of Lamb waves and how they are both generated and implemented in SHM to assess damage, the fundamentals of waves and wave propagation must first be addressed.

2.1.1 The 1-D Wave Equation

Maxwell derived the one-dimensional wave equation, which displays the property of displacement for scalar functions, f (26):

$$\frac{\partial^2 f}{\partial x^2} - \frac{1}{v^2}\frac{\partial^2 f}{\partial t^2} = 0 \qquad 2.1.1$$

where the independent variables x and t are distance and time, and v is the wavespeed. The general solution for the wave equation is $f(x,t) = f_1(x+vt) + f_2(x-vt)$. Specifically, the function $f(x,t)$ can be displaced to the left and right based on its argument $(x \pm vt)$. The function $f_1(x-vt)$ will shift right and is considered a forward propagating wave. Conversely, the function $f_2(x+vt)$ will shift left and is considered a backward propagating wave. In the present study, the focus is on forward propagating waves.

2.1.2 Solution to the 1-D Wave Equation

One solution to the governing wave equation, equation 2.1.2, is essential to understanding wave propagation and its associated phenomenon such as attenuation and phase changes (21:18). The displacement of a particle (u) is a function of the spatial parameter x and the temporal parameter t.

$$u(x,t) = A\cos\left[\left(kx - \omega t\right) - \theta\right] \qquad 2.1.2$$

The variables used in equations 2.1.1 and 2.1.2 along with parameters associated with wave propagation are displayed in Table 1.

Table 1: Sinusoidal Wave Parameters

Wave Parameters			
Variable	**Name**	**Equations**	**Unit**
A	Peak Amplitude		length
λ	Wavelength		length
T	Period		sec
θ	Absolute/Initial Phase Shift		rad
f	Frequency (cycles/sec)	$1/T$	Hz
ω	Circular/Angular Frequency (temporal)	$2\pi f$	rad/sec
k	Circular Wave Number (spatial)	$2\pi/\lambda$	rad/length
v, c_p	Phase Velocity / Wavespeed	$\lambda/T = \omega/k = \Delta x/\Delta t$	length/sec

The total phase of a propagating wave, temporal and spatial, is $\varphi = (kx-\omega t)$ (15:16). If there is an initial phase shift, this is accounted for using θ in equation 2.1.2.

Waves can be used to characterize particle motion within a medium that is strained. When a medium is strained, the resulting elastic forces cause particles in the medium to oscillate. The oscillation of these particles can be characterized as wave movement from both spatial and temporal perspectives. Wave propagation can be characterized spatially by illustrating the displacement of an infinite number of particles within a medium at an instant in time (t_0), where the displacement is simply a function of the distance (x). In this characterization, a wave can be displayed moving in the direction of the x-axis with a constant speed (c_P). After an interval of time (Δt), the argument of the function f becomes $(x–v(t+\Delta t))$. The function f will not change if there is a simultaneous increase in x (Δx) corresponding to $c_P\Delta t$. Wave propagation can also be characterized temporally. The oscillating motion of one point within a medium can be characterized as wave movement over time. The particle's position is taken to be x_0 and its displacement $u(x_0)$ can be shown with respect to time. Figure 2 is an example of wave propagation using both methods described above. The frequency, angular frequency, circular wavenumber, and phase velocity can be determined from the period (T) and wavelength (λ)

parameters identified in the figure below. Temporal propagation was relevant to this study since the locations of two piezoelectric transducers were fixed in the spatial dimension and Lamb waves propagating through those points were characterized as particle displacements over time.

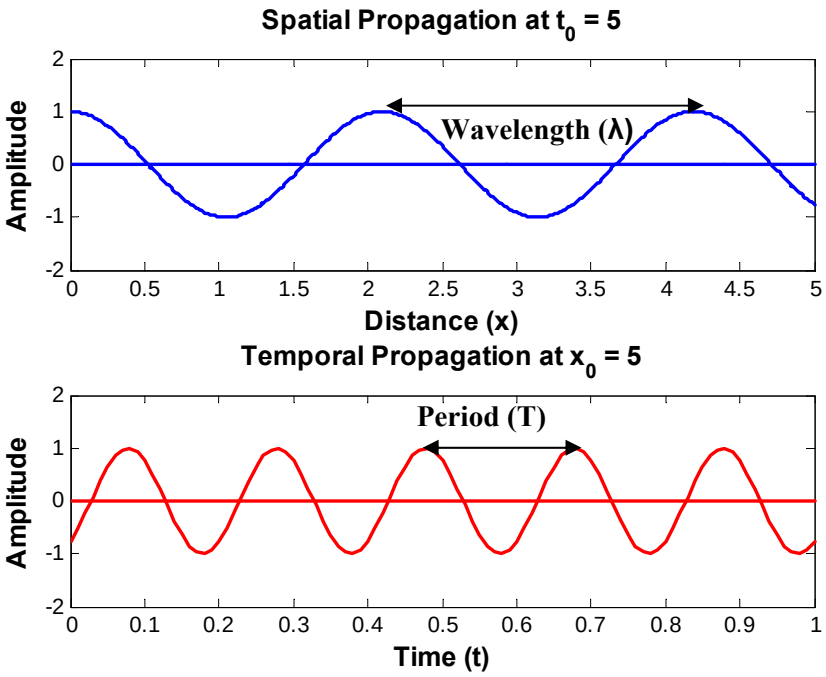

Figure 2: Sinusoidal Wave Parameters

For a given wave, angular frequency is equal to the wave number multiplied by the phase velocity, or $\omega=kc_p$. Therefore, the wave equation can also be modeled as in equation 2.1.3 if we replace ω with its equivalent (kc_p):

$$u(x,t) = A\cos\left(k\left(x - c_p t\right)\right) \qquad 2.1.3$$

Equation 2.1.3 can be used to theoretically model wave propagation in a structure, given a wave's phase velocity (c_p), which is displayed in equation 2.1.4:

$$c_p = \frac{\omega}{k} = \lambda f \qquad 2.1.4$$

The phase velocity is also a function of the properties of a medium.

2.1.3 Phase and Group Velocities

Phase velocity is the velocity at which a wave of a single frequency propagates. Group velocity, on the other hand, is the term given to the propagation velocity of a wave packet. A wave packet is a group of waves that travel together at similar frequencies but varying wavespeeds (21:17). As an example, consider an excitation signal that has energy over a range of frequencies. When this excitation pulse is transmitted in a specimen, the propagating wave is actually comprised of several component waves of varying frequencies and phase speeds. If these waves of varying phase speeds are superimposed, the speed of the resulting wave is the group velocity. The group velocity is also referred to as the signal velocity, or velocity at which the energy of a wave packet is conveyed through a structure:

$$c_g = \frac{\partial \omega}{\partial k} \tag{2.1.5}$$

When the phase velocity or wavespeed is independent of frequency, the phase velocity is equivalent to the group velocity. However, in dispersive mediums the phase velocity is dependent on frequency. When the wavespeed decreases with frequency, the group velocity is less than the phase velocity. Conversely, when the wavespeed increases with frequency the group velocity is greater than the phase velocity (15:48).

In a dispersive medium, which will be discussed further in the section on Lamb wave theory, a wave packet will generally propagate at a group velocity slower than the phase speed of the original excitation signal. Stokes gave a simple theoretical explanation of phase and group velocities in 1876. He considered two propagating harmonic waves of equal amplitude but of varying frequencies, ω_1 and ω_2 (21:17). The waves are added together, as seen in equation 2.1.6, and manipulated in a method that displays the effects of phase and group velocity on the propagation of the signal:

$$u(x,t) = A\cos\left(k_1 x - \omega_1 t\right) + A\cos\left(k_2 x - \omega_2 t\right) \tag{2.1.6}$$

Equation 2.1.6 can be rewritten as

$$u(x,t) = A\cos\left(k_1\left(x - c_1 t\right)\right) + A\cos\left(k_2\left(x - c_2 t\right)\right) \quad 2.1.7$$

Additionally, using the trigonometric identity:

$$A\left[\cos(\alpha) + \cos(\beta)\right] = 2A\left[\cos\left(\frac{\alpha - \beta}{2}\right) * \cos\left(\frac{\alpha + \beta}{2}\right)\right] \quad 2.1.8$$

Equation 2.1.7 can be displayed as

$$u(x,t) = 2A\cos\left(0.5(k_2 - k_1)x - 0.5(\omega_2 - \omega_1)t\right) * \cos\left(0.5(k_2 + k_1)x - 0.5(\omega_2 + \omega_1)t\right) \quad 2.1.9$$

Since cosine is an even function, the following substitutions can be made: $\Delta\omega=\omega_2-\omega_1$, $\Delta k=k_2-k_1$; $\frac{1}{2}(\omega_2+\omega_1)=\omega_{AV}$, $\frac{1}{2}(k_2+k_1)=k_{AV;}$ $c_{AV}= \omega_{AV}/k_{AV}$. The resulting equation has a low-frequency term, containing $\Delta\omega$ and Δk, which has a propagation velocity of $c_g=\Delta\omega/\Delta k$. It also possesses a high-frequency term, which has a propagation velocity ($c_p=\omega/k$).

$$u(x,t) = 2A\cos\left(0.5\Delta k x - 0.5\Delta\omega t\right) * \cos\left(k_{AV}x - \omega_{AV}t\right) \quad 2.1.10$$

As an example, Figures 3 and 4 depict wave motion based on the superposition of two sinusoidal signals. Figure 3 depicts the waves from a temporal perspective. The oscillating motion of a point at a given distance ($x_0=10$) is characterized as wave movement over time. Figure 4 depicts the waves from a spatial perspective. A stress wave moving through a medium, captured at an instant in time ($t_0=10$), is characterized with respect to distance. The wave parameters are as follows: $k_1 = 3$, $k_2 = 5$, $\omega_1 = 4\pi$, and $\omega_2 = 5\pi$. The first subplot in each figure depicts two sinusoidal signals before they are superimposed and the following subplot depicts the high and low frequency terms of the superimposed signal. The low frequency term represents the propagation of the wave envelope or the group velocity of the resulting wave packet and the high frequency term reflects the carrier speed or average phase velocity of the resulting wave packet. Finally, the product of these terms along with the amplitude factor ($2A$) yields wave packets as

seen in the final subplot of Figure 3. The superposition of several waves, as opposed to just two, is pertinent to this thesis and is discussed further in the section on superposition.

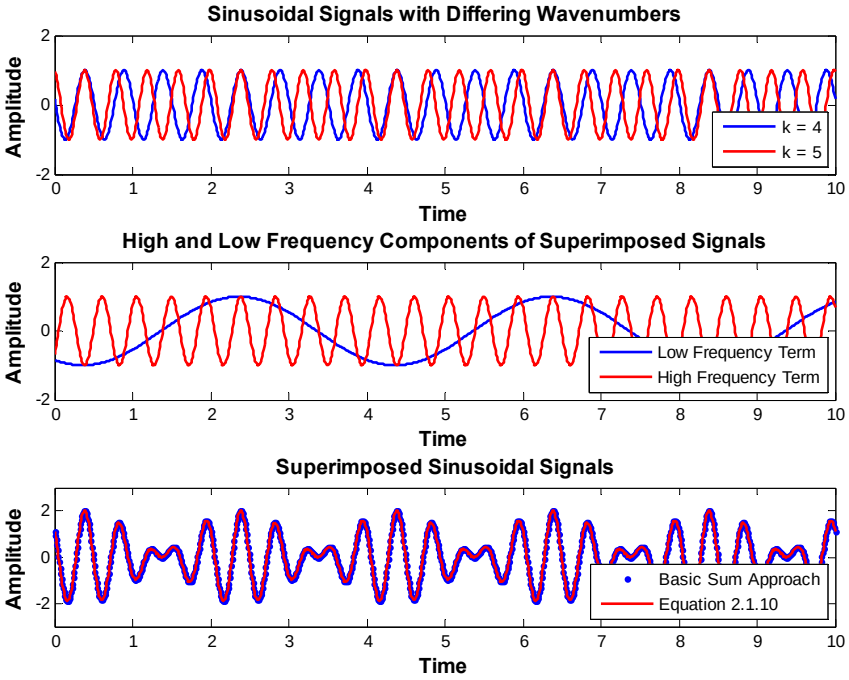

Figure 3: Wave Superposition Relative to Time

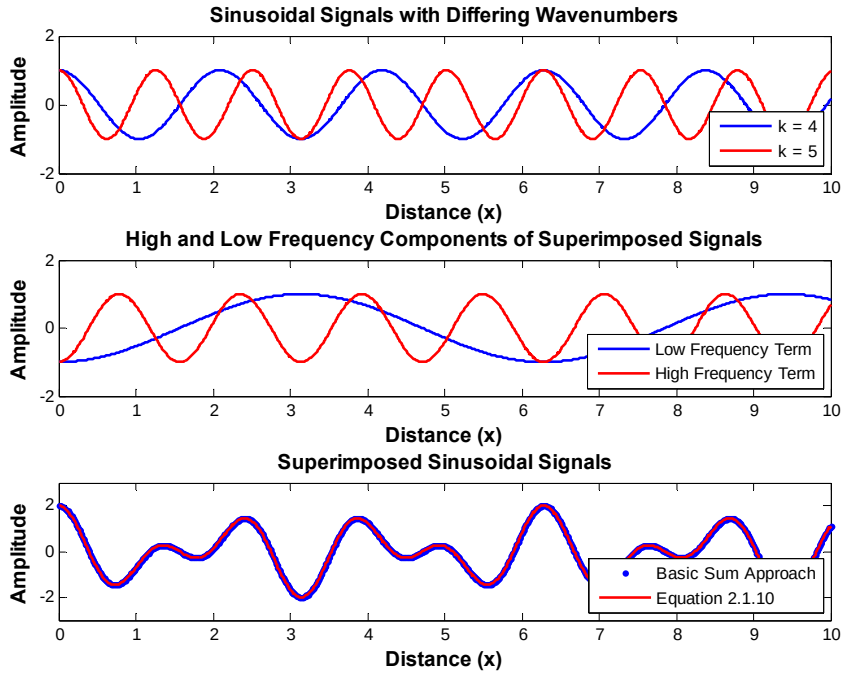

Figure 4: Wave Superposition Relative to Distance

2.1.4 Wave Modes

A wave mode refers to the manner of particle oscillation during wave propagation. In a solid material, particles can oscillate in four primary modes: as longitudinal waves, shear waves, surface waves, and in thin materials as plate waves. The two modes of propagation that are most widely used in ultrasonic testing and which occur in a uniform, unbounded, isotropic medium are transverse or shear waves and longitudinal or pressure waves. These waves occur as a result of a material that is elastically displaced. Particles are displaced from their equilibrium positions and as a result internal (electrostatic) restoring forces between particles combined with their inertias generate oscillatory motions. The oscillatory motions can also be referred to as elastic waves. When transverse waves occur a structure's particles can move in two directions, both of which are perpendicular to the line of propagation. One wave can occur within the plane of the plate, horizontal shear waves, and vertical shear waves can propagate normal to the plate (through the thickness). In contrast, longitudinal waves generate oscillations in the direction of wave propagation (11). As an example, consider the motion of a slinky. Transverse waves travel perpendicular to the orientation of the slinky and longitudinal waves propagate in the direction of the stretched slinky. Figure 5 is a pictorial view of transverse and longitudinal waves. The black lines depict the direction of particle motion and the red arrows depict the direction of wave propagation (11).

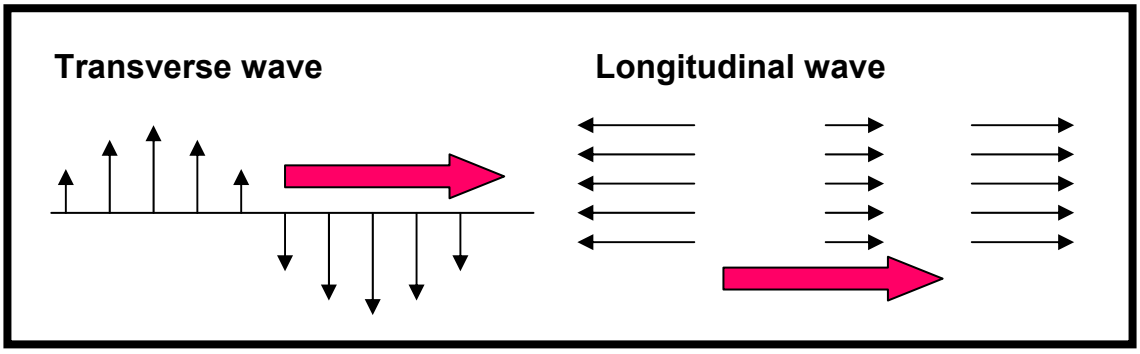

Figure 5: Transverse and Longitudinal Waves (11)

Wave propagation is dependent on the density (ρ) and elastic properties of a medium (11). The wavespeed corresponding to longitudinal waves is characterized by Young's Modulus (E) as follows:

$$c_L = \sqrt{\frac{E}{\rho}} \qquad 2.1.11$$

Similarly, the wavespeed of shear or transverse waves is characterized by the shear modulus (G):

$$c_T = \sqrt{\frac{G}{\rho}} \qquad 2.1.12$$

In the present study, plate waves were used in the experiments. Plate waves are "complex vibrational waves that travel through the entire thickness of a material" and are commonly referred to as guided Lamb waves (11). These waves result from conversion between transverse and longitudinal modes.

2.1.5 Dispersion Behavior

Waves propagated through a dispersive medium result in multiple waveforms with varying wavespeeds, which are a function of frequency. This results in an increase in the spatial extent of the original pulsed signal, which corresponds to spreading in the wave packet. As an example, exciting a structure with a finite duration sinusoidal burst will result in several component waves traveling at differing wavespeeds. The superposition or synthesis of these component waves results in a wave packet or group wave. The speed of the wave packet is the group velocity, which was discussed in Section 2.1.3. Quantifying wave dispersion is critical to SHM since damage identification is directly dependent on a signal's TOF, which can be determined from the group velocity (c_g) of a wave and the known propagation distance of the signal (d) as TOF = d/c_g.

The following figures and numbers are a prime example of wave dispersion. A 5 ½-cycle Hanning-window excitation signal, seen in Figure 6, was propagated over 300 mm at a frequency of 300 kHz. As a result of windowing, the sinusoid's frequency content is spread over a finite bandwidth. Figure 7 captures the resultant packet, which is comprised of component waves over a close range of frequencies. If the fast Fourier transform is taken of this time signal, it can be seen that the peak of the signal's energy content is concentrated at its center frequency, or 300 kHz, as seen in Figure 8.

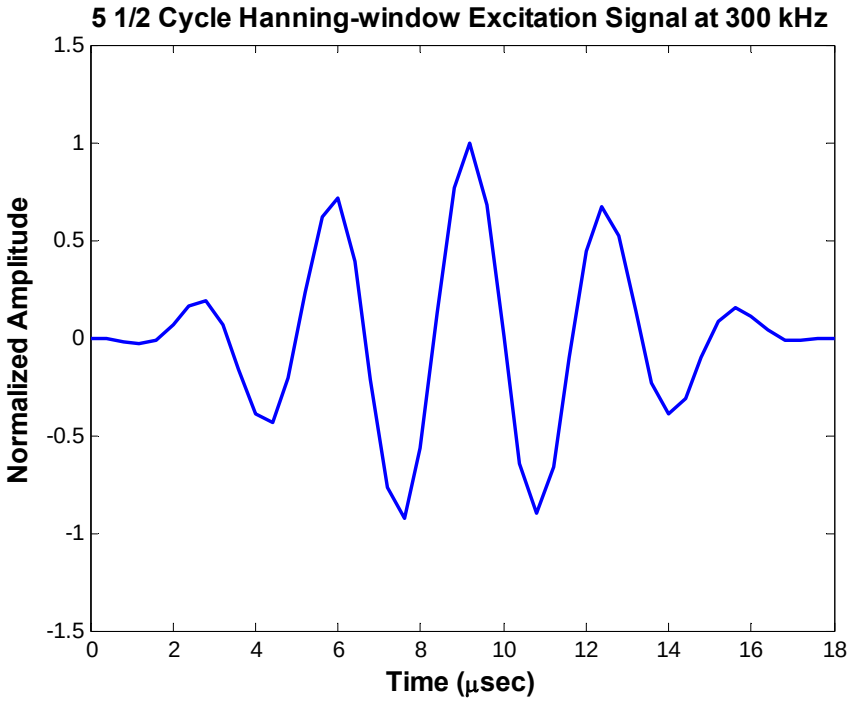

Figure 6: 5 1/2 Cycle Hanning-window Excitation Signal at 300 kHz

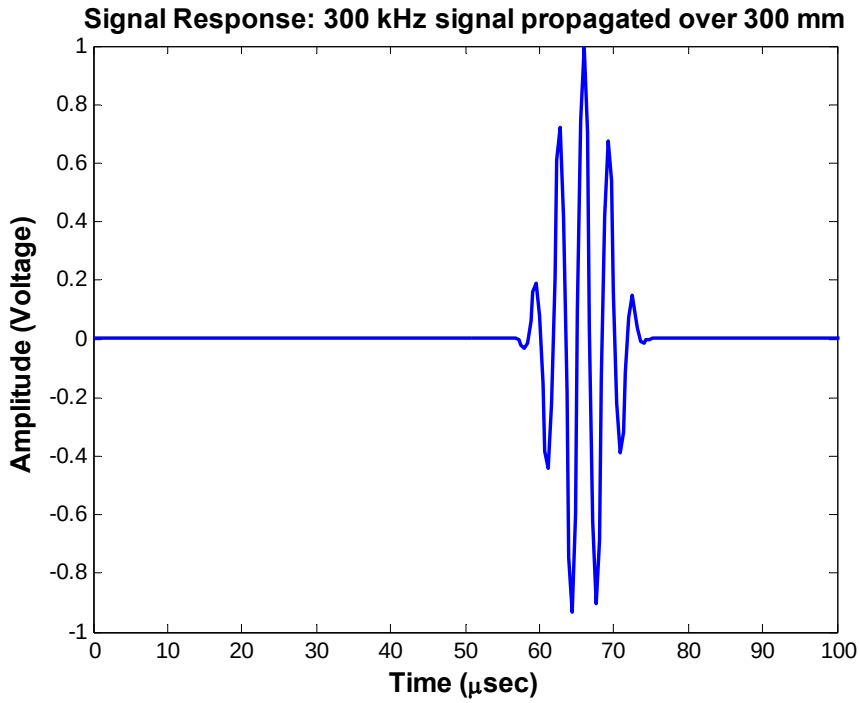

Figure 7: Theoretical S_0 Response at 300 kHz

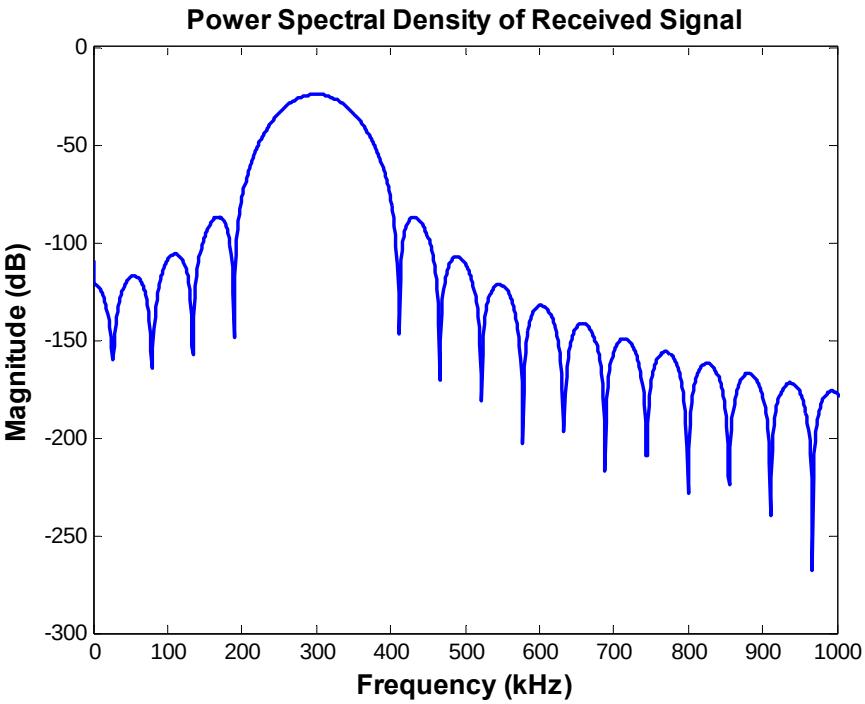

Figure 8: PSD of Theoretical S_0 Response

Superposition

The superposition principle applies when several waves are collocated so that the sum of the displacements of the individual waves is equivalent to the total wave displacement (26). Equation 2.1.13 can be used to display this concept by adding together the displacements of several component waves (21:18).

$$u = \sum_{i=1}^{n} A_i \cos(k_i x - \omega_i t) \qquad 2.1.13$$

The next few figures display the concept of superposition. In Figure 9, 100 component waves were added to a center frequency wave of 300 kHz. Figure 10 and Figure 11 incorporate additional component waves until the full response signal is obtained in Figure 12. Clearly, the response signal becomes more distinct as the signal content increases around the center frequency. As seen, capturing the full extent of the frequency content in a signal is critical in theoretical simulations.

The theoretical response signals generated in this study were obtained by implementing equation 2.1.14 in Matlab®

$$u(k) = 2 * real\left(\sum_{k=1}^{N-1} S(k) * \exp\left(j\omega \left(\frac{d}{c_P(k)} - t \right) \right) \right) \qquad 2.1.14$$

$S(k)$ is the fast Fourier transform of the input signal and is a function of the frequency index k. This element of the equation carries the magnitude and phase of the signal. The exponential term of the equation represents the time-harmonic factor, where d is the propagation distance of the signal and the phase velocity is a function of the frequency index, $c_P(k)$. Finally, only the real values for real or pure imaginary numbers are taken into consideration since this represents the undamped propagating modes of a structure.

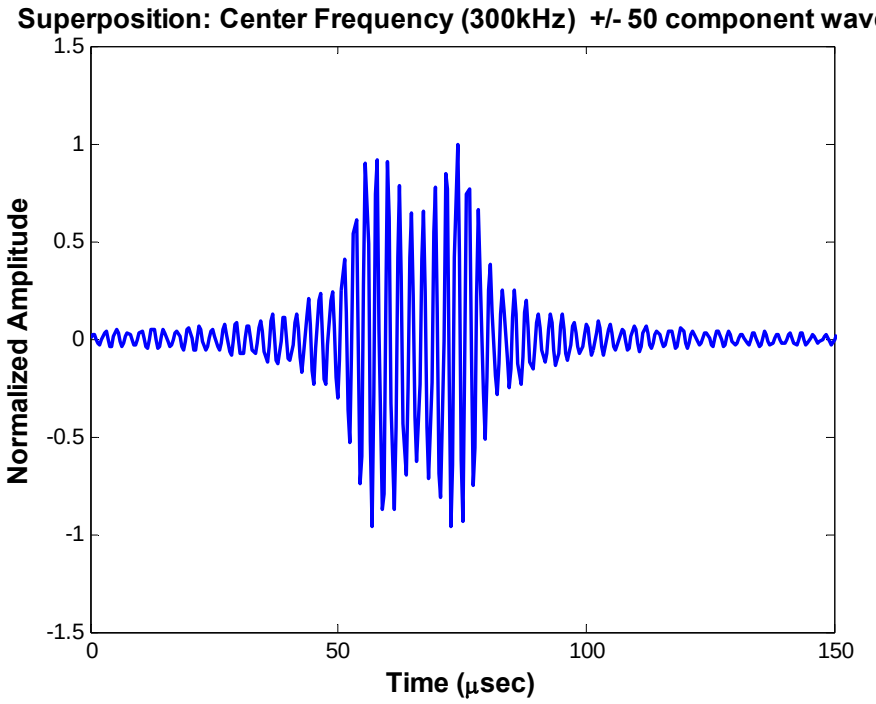

Figure 9: Superposition of 100 Component Waves

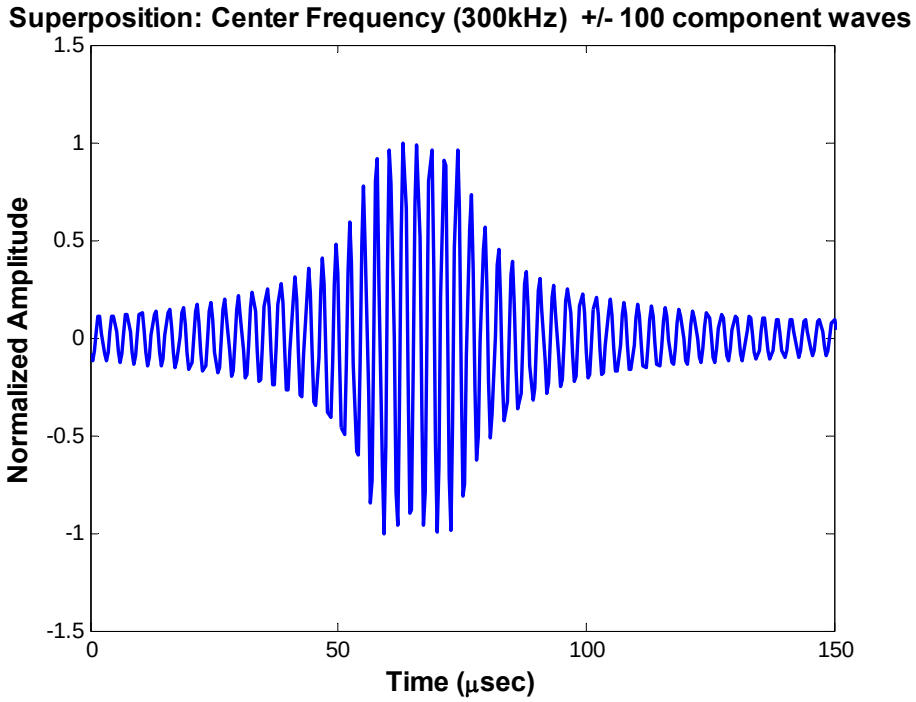

Figure 10: Superposition of 200 Component Waves

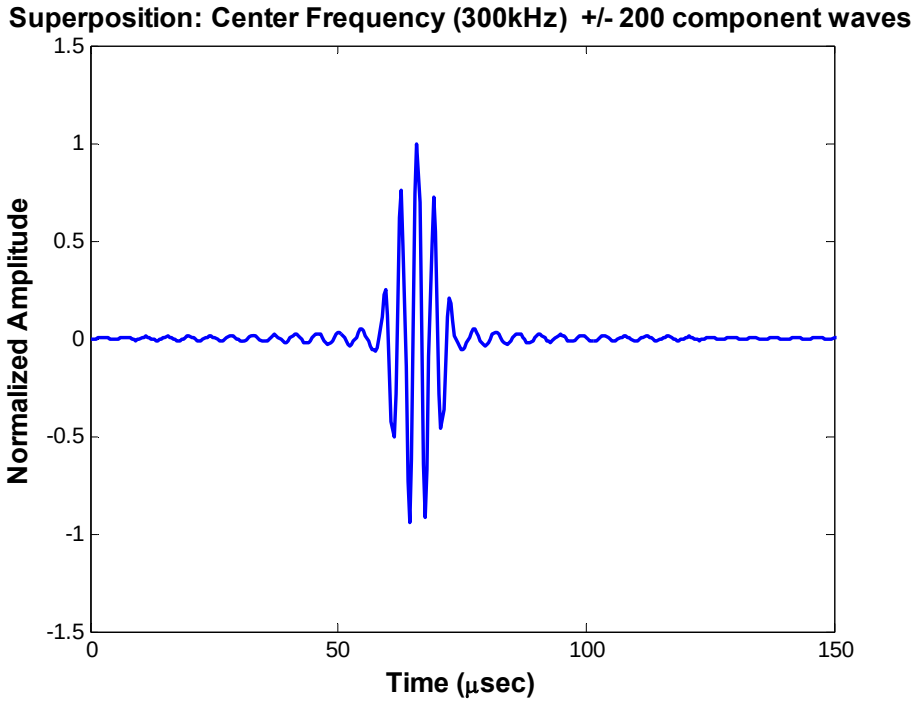

Figure 11: Superposition of 400 Component Waves

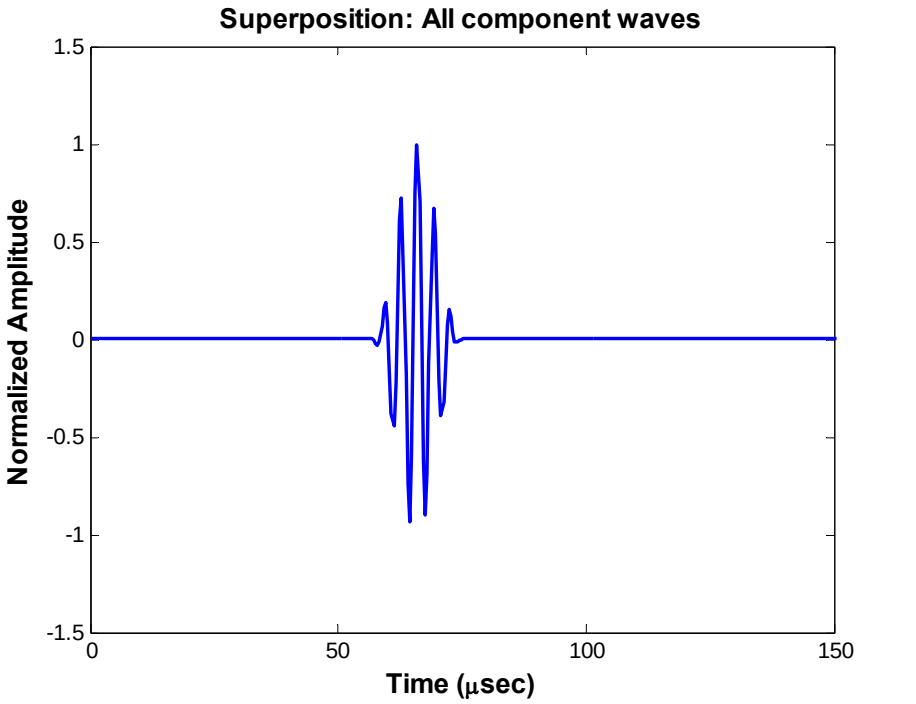

Figure 12: Superposition of all Component Waves

2.1.6 Elastic Waves

When elastic waves are sent out in a medium, they transmit changes in stress and velocity inside the material (15:9). Additionally, they exhibit quantitative wave characteristics to include the frequency, period, phase, wavelength, wavespeed, wave number, and amplitude of particle displacement due to changes in stress and velocity. These characteristics were discussed in the section on wave theory. Elastic waves are categorized as either bulk or guided waves. Bulk waves travel within the interior of a material and exhibit a finite number of wave modes. On the other hand, guided waves exhibit an infinite number of wave modes since they travel on the surface of a material and through the thickness of thin materials. Both waves obey the same governing equations; however, only guided waves are affected by boundary conditions (21:101).

Guided waves can be categorized as either Rayleigh or Lamb waves. Both result from the coupling between longitudinal and vertical shear waves that are reflected and refracted at the free surfaces of a material. Specifically, "Rayleigh waves are free waves on a surface of a semi-infinite solid. Traction forces must vanish on the boundary, and the waves must decay with depth. Lamb waves are waves of plane strain that occur in a free plate and the traction forces must vanish on the upper and lower surface of the plate" (21:101-102). Due to their respective characteristics, Rayleigh waves are useful in detecting surface cracks in relatively thick structures and Lamb waves are useful in detecting damage in plate and shell structures (3).

2.2 Ultrasonic Lamb Wave Theory

The study of ultrasonic waves "is the science and exploitation of elastic waves in solids, liquids, and gases, which have frequencies above 20 kHz" (15:1). When ultrasonic waves propagate through a material, an internal crack will "produce an early echo or reflection with less attenuation than that from the back face of an object" (15:3). This fact supports the notion that the interaction of these elastic waves with structural damage will alter the behavior of the waves. Specifically, ultrasonic waves have been used to identify highly localized structural damage using

both pitch-catch and pulse-echo techniques. The pitch-catch technique is implemented by actuating a signal with one transducer and sensing the response signal with a second transducer. The pulse-echo technique simply uses one transducer to both transmit and detect the signal. The present study focused on Lamb wave propagation using the pitch-catch approach.

Horace Lamb gave the first introduction to Lamb wave theory in 1917 (14); however, the first use of Lamb waves in SHM can be attributed to Worlton in 1957 (28). Lamb waves are unique because they are "mechanical waves corresponding to vibration modes of plates with a thickness on the same order of magnitude as their wavelength" (24:390). Therefore, these waves propagate through the entire thickness of a material. Over the past few decades, the use of Lamb waves in the NDE of structural damage has provided both advantages and disadvantages. Since Lamb waves are capable of propagating over long distances, these waves have generally been used to monitor large surface areas. Additionally, Lamb waves provide through-the-thickness interrogation, which is advantageous when detecting internal defects in thin materials. Wave attenuation, wave reflection, and changes in transmission velocity are parameters that make this possible (24:391). A difficulty using Lamb waves is that they are dispersive in nature (3). Therefore, understanding the dispersive behavior of these waves and more importantly how their behavior is altered by varying environmental conditions is necessary if Lamb waves are to be used in SHM applications. The present study is a step towards meeting that objective.

Free Plate Problem

Since Lamb waves are waves of plane strain that occur in a free plate, the following is an explanation of the free plate problem based on a discussion in the Rose text (21:101-107). The geometry of the free plate problem is seen in Figure 13.

The equations of motion for particle displacement in this medium are characterized as:

$$\mu u_{i,jj} + (\lambda + \mu) u_{j,ji} + \rho f_i = \rho \ddot{u}_i \qquad 2.2.1$$

The Lame constants are μ and λ, u is displacement, and f is an applied force. Additionally, the subscripts i and j equal 1, 2, or 3. Refer to Saada's text for additional information on elasticity theory (22). Since the domain of the free plate problem is finite, surface tractions are the applicable boundary conditions to these equations of motion.

$$t_i = \sigma_{ji} n_j \qquad 2.2.2$$

In the case of a free plate, the surfaces at $y = d/2 = h$ and $y = -d/2 = -h$ are considered traction free. Once excitation occurs at a point in the plate, the resulting energy encounters the upper and lower bounding surfaces of the plate, enabling mode conversion between longitudinal and transverse modes. Additionally, as the energy propagates through the plate, superposition causes the formation of wave packets, or guided wave modes in the plate (Figure 22:101-107).

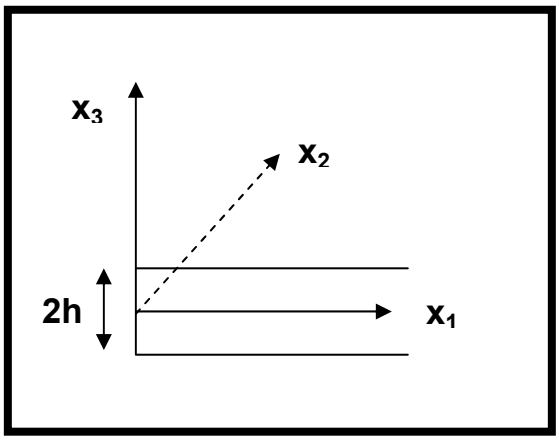

Figure 13: Free Plate Geometry (21:103)

Since Lamb waves are waves of plane strain, only displacements through the thickness (x_3 direction) and in the direction of wave propagation (x_1 direction) are taken into consideration. Displacements in the x_1 direction correspond to longitudinal waves and displacements in the x_3 direction correspond to vertical shear waves. If the x_2 direction was considered in Lamb wave propagation, the resulting waves in this direction would be referred to as horizontal shear waves. Similar to vertical shear waves, horizontal shear waves propagate perpendicular to longitudinal waves.

The solution to the equations of motion for particle displacement is obtained using the method of displacement potentials. Isotropic plates require this simple solution method. For plate waves in an anisotropic plate, the appropriate method to apply is the partial wave technique. Two uncoupled wave equations for the case of plane strain are obtained if the displacement vector (field) is decomposed according to Helmholtz decomposition and the result is plugged into equation 2.2.1. Equation 2.2.3 corresponds to the governing longitudinal waves:

$$\frac{\partial^2 \phi}{\partial x_1^2} + \frac{\partial^2 \phi}{\partial x_3^2} = \frac{1}{c_L^2} \frac{\partial^2 \phi}{\partial t^2} \tag{2.2.3}$$

Equation 2.2.4 corresponds to the governing shear waves:

$$\frac{\partial^2 \psi}{\partial x_1^2} + \frac{\partial^2 \psi}{\partial x_3^2} = \frac{1}{c_L^2} \frac{\partial^2 \psi}{\partial t^2} \tag{2.2.4}$$

Since a plane strain scenario is assumed, the displacements (u) and stresses (σ) can be written in terms of the potentials as

$$u_1 = u = \frac{\partial \phi}{\partial x_1} + \frac{\partial \psi}{\partial x_3} \tag{2.2.5}$$

$$u_2 = v = 0 \tag{2.2.6}$$

$$u_3 = w = \frac{\partial \phi}{\partial x_3} - \frac{\partial \psi}{\partial x_1} \tag{2.2.7}$$

$$\sigma_{31} = \mu \left(\frac{\partial u_3}{\partial x_1} + \frac{\partial u_1}{\partial x_3} \right) = \mu \left(\frac{\partial^2 \phi}{\partial x_1 \partial x_3} - \frac{\partial^2 \psi}{\partial x_1^2} + \frac{\partial^2 \psi}{\partial x_3^2} \right) \tag{2.2.8}$$

$$\sigma_{33} = \lambda \left(\frac{\partial u_1}{\partial x_1} + \frac{\partial u_3}{\partial x_3} \right) + 2\mu \frac{\partial u_3}{\partial x_3} = \lambda \left(\frac{\partial^2 \phi}{\partial x_1^2} + \frac{\partial^2 \phi}{\partial x_3^2} \right) + 2\mu \left(\frac{\partial^2 \phi}{\partial x_3^2} - \frac{\partial^2 \psi}{\partial x_1 \partial x_3} \right) \tag{2.2.9}$$

The analysis begins by assuming solutions to equations 2.2.3 and 2.2.4:

$$\phi = \Phi(x_3) \exp[i(kx_1 - \omega t)] \tag{2.2.10}$$

$$\psi = \Psi(x_3) \exp[i(kx_1 - \omega t)] \tag{2.2.11}$$

These solutions represent standing or transverse waves in the x_3 direction and traveling or longitudinal waves in the x_1 direction. Substituting these assumed solutions into equations 2.2.3 and 2.2.4 yields equations governing the unknown functions Φ and Ψ:

$$\Phi(x_3) = A_1 \sin(px_3) + A_2 \cos(px_3) \tag{2.2.12}$$

$$\Psi(x_3) = B_1 \sin(qx_3) + B_2 \cos(qx_3) \tag{2.2.13}$$

The parameters p and q can be expressed in terms of the angular frequency (ω), the circular wavenumber (k), and the longitudinal and transverse wavespeeds (c_L and c_T):

$$p^2 = \frac{\omega^2}{c_L^2} - k^2 \tag{2.2.14}$$

$$q^2 = \frac{\omega^2}{c_T^2} - k^2 \tag{2.2.15}$$

Before proceeding, it should be noted here that the longitudinal and transverse wavespeeds seen in equations 2.1.11 and 2.1.12 are modified for this problem. Since the modulus values for an isotropic material are constant in all directions, the values can be replaced with the Lamé constants (λ and μ). Additionally, the modulus originally used for longitudinal wavespeeds has been modified. When the lateral parameters of a medium are much greater than the wavelength, which is the case in this problem, the modulus is sometimes referred to as the plane wave modulus (M). The plane wave modulus is equivalent to $\lambda + 2\mu$ and the shear modulus is equivalent to μ (22:199-201). The new equations for the longitudinal and transverse wavespeeds, along with the plane wave modulus, are as follows:

$$c_L = \sqrt{\frac{M}{\rho}} = \sqrt{\frac{\lambda + 2\mu}{\rho}} \tag{2.2.16}$$

$$M = \frac{E(1-\upsilon)}{(1-\upsilon-2\upsilon^2)} \tag{2.2.17}$$

$$c_T = \sqrt{\frac{G}{\rho}} = \sqrt{\frac{\mu}{\rho}} \tag{2.2.18}$$

The dependence of the Lamé constants on E and Poisson's ratio, υ, is displayed in the following equations:

$$\mu = G = \frac{E}{2(1+\upsilon)} \tag{2.2.19}$$

$$\lambda = \frac{E\upsilon}{(1+\upsilon)(1-2\upsilon)} \tag{2.2.20}$$

At this point, the longitudinal and transverse waves are non-dispersive since their wavespeeds are only a function of material properties, not frequency.

Returning to equations 2.2.12 and 2.2.13, these equations can now be substituted into the original displacement and stress equations (2.2.5-2.2.9) resulting in the following stress and strain equations in terms of Φ and Ψ:

$$u_1 = \left[ik\Phi + \frac{\partial \Psi}{\partial x_3} \right] \tag{2.2.21}$$

$$u_3 = \left[\frac{\partial \Phi}{\partial x_3} - ik\Psi \right] \tag{2.2.22}$$

$$\sigma_{31} = \mu \left(2ik\frac{\partial \Phi}{\partial x_3} + k^2\Psi + \frac{\partial^2 \Psi}{\partial x_3^2} \right) \tag{2.2.23}$$

$$\sigma_{33} = \lambda \left(-k^2\Phi + \frac{\partial^2 \Phi}{\partial x_3^2} \right) + 2\mu \left(\frac{\partial^2 \Phi}{\partial x_3^2} - ik\frac{\partial^2 \Psi}{\partial x_3} \right) \tag{2.2.24}$$

The solution can be split into two modes, the symmetric and anti-symmetric modes, since the waves propagate along a symmetry axis or the midplane of the plate. A comprehensive development of these modes can be referenced in the Rose text (21:105-106). Since the constants A_1, A_2, B_1, and B_2 are still unknown the traction free boundary conditions are applied at $x_3 = \pm h$:

$$\sigma_{31} = \sigma_{31} = 0 \tag{2.2.25}$$

After some manipulation and simplification, the equations obtained for the symmetric and anti-symmetric modes are as follows:

$$\frac{\tan(qh)}{\tan(ph)} = -\frac{4k^2 pq}{(q^2 - k^2)^2} \tag{2.2.26}$$

$$\frac{\tan(qh)}{\tan(ph)} = -\frac{(q^2 - k^2)^2}{4k^2 pq} \tag{2.2.27}$$

These equations are commonly referred to as the Rayleigh-Lamb frequency equations. The parameters parameters p and q were defined in equations 2.2.14 and 2.2.15, k is the wavenumber, and h is half the specimen thickness. Equations 2.2.26 and 2.2.27 can be considered as relating either the circular frequency to the wavenumber (ω to k), which results in the frequency spectrum, or the phase velocity to the circular frequency (c_P to ω), which results in dispersion curves. To conclude, these equations can be solved using numerical methods to determine the velocities at which a wave of a particular frequency-thickness product will propagate within a plate (21:101-111).

2.2.1 Numerical Solution of the Rayleigh-Lamb Frequency Equations

Lamb wave dispersion can be predicted based on solutions to the Rayleigh-Lamb frequency equations. There are an infinite number of wavenumbers (k) that will satisfy these equations; however, only real values for real or pure imaginary wavenumbers are necessary since they supply information about the undamped propagating modes of a structure (21:110-111). Additionally, when plotting dispersion curves only the real solutions of the Rayleigh-Lamb frequency equations are taken into consideration. Equations 2.2.26 and 2.2.27 are modified before implementing the numerical solution routine:

$$\frac{\tan(qh)}{q} + \frac{4k^2 p \tan(ph)}{(q^2 - k^2)^2} = 0 \qquad 2.2.28$$

$$q\tan(qh) + \frac{(q^2 - k^2)^2 \tan(ph)}{4k^2 p} = 0 \qquad 2.2.29$$

The objective of the numerical method outlined by Rose is to find roots corresponding to particular phase velocities at a given frequency-thickness product. Initially, equations 2.2.28 and 2.2.29 are evaluated for a frequency-thickness product $(\omega h)_0$ and an initial phase velocity estimate $(c_p)_0$. Phase velocity estimates are incrementally increased until a sign change occurs between a consecutive pair of estimates. A sign changes indicates that the expression has gone through a zero and a root exists between two points. An iterative root-finding algorithm is implemented to provide a better estimate of the phase velocity until it is close to zero. The process just outlined is continued for additional frequency-thickness products, as required (21:110-111). Once a phase velocity estimate is obtained for a given frequency-thickness value, a corresponding group velocity estimate can be determined from equation 2.2.30 (21:113):

$$c_g = c_p^2 \left[c_p - (fd)\frac{dc_p}{d(fd)} \right]^{-1} = \frac{\partial \omega}{\partial k} \qquad 2.2.30$$

The estimate is equivalent to the original dispersion relation given in equation 2.1.5.

Dispersion curves are generated by plotting either phase or group velocity values against their corresponding frequency-thickness products. From a mathematical standpoint, the frequency-thickness product drives dispersion and is used as an independent variable when representing wavespeed functions and generating phase and group velocity dispersion curves (21:111-112).

Figure 14 and Figure 15 are examples of theoretical phase and group velocity dispersion curves for a 1 mm thick aluminum specimen at 0, 75, 150, 190, 225, and 600°F. If a component wave is propagating at a specified frequency in the range of 100-600 kHz, its corresponding

phase velocity can be obtained from Figure 14. Similarly, if a wave packet is propagating at a center frequency in the range of 100-600 kHz, its corresponding group velocity can be obtained from Figure 15. The temperature based curves demonstrate that phase and group velocities decrease with an increase in temperature, which is expected due to the decrease in the modulus of elasticity over increasing temperatures, as seen in Figure 16. Figure 16 was based on an interpolation of values taken from MIL-HDBK-5. Therefore, a preliminary conclusion is that elevated temperatures decrease the material strength of an aluminum specimen and as a result reduce the phase and group velocities of traveling waves.

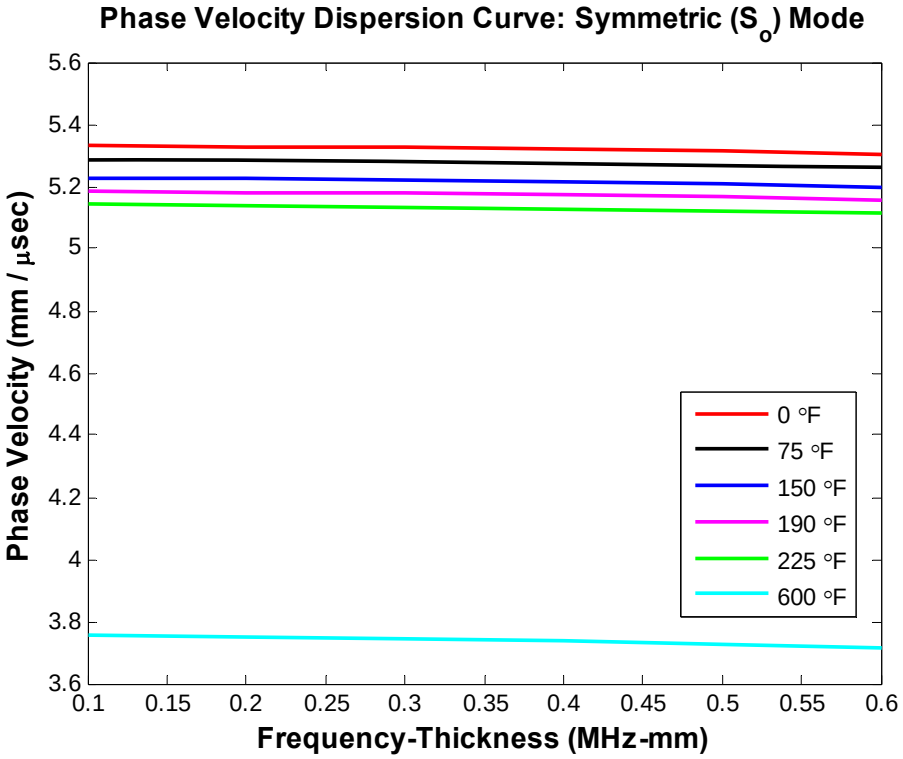

Figure 14: Theoretical Phase Velocity Dispersion Curve for Varying Temperatures

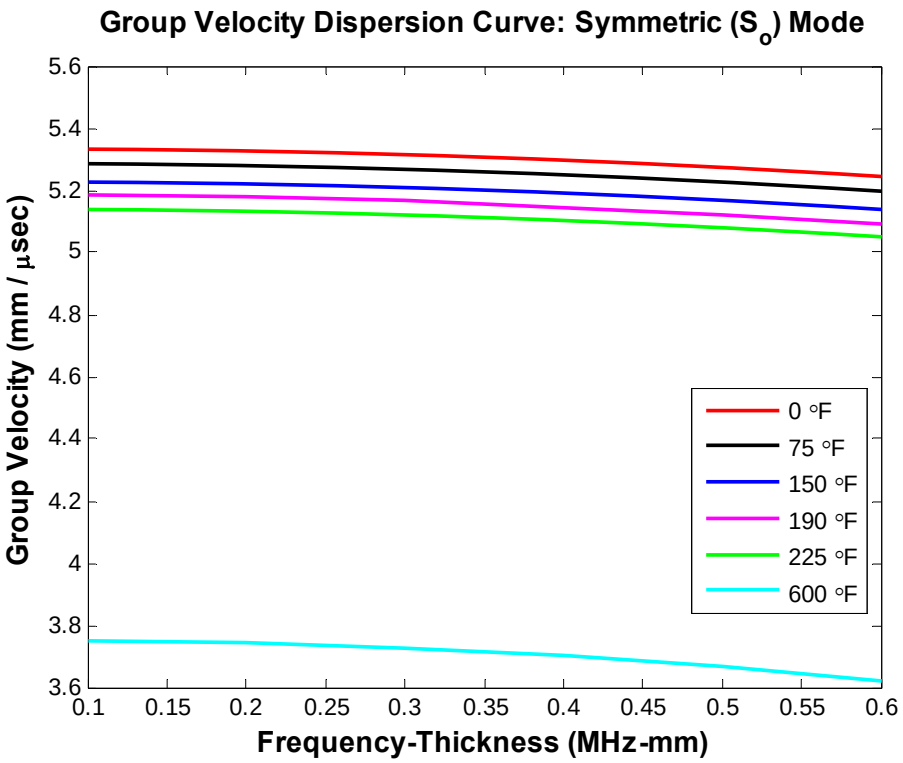

Figure 15: Theoretical Group Velocity Dispersion Curve for Varying Temperatures

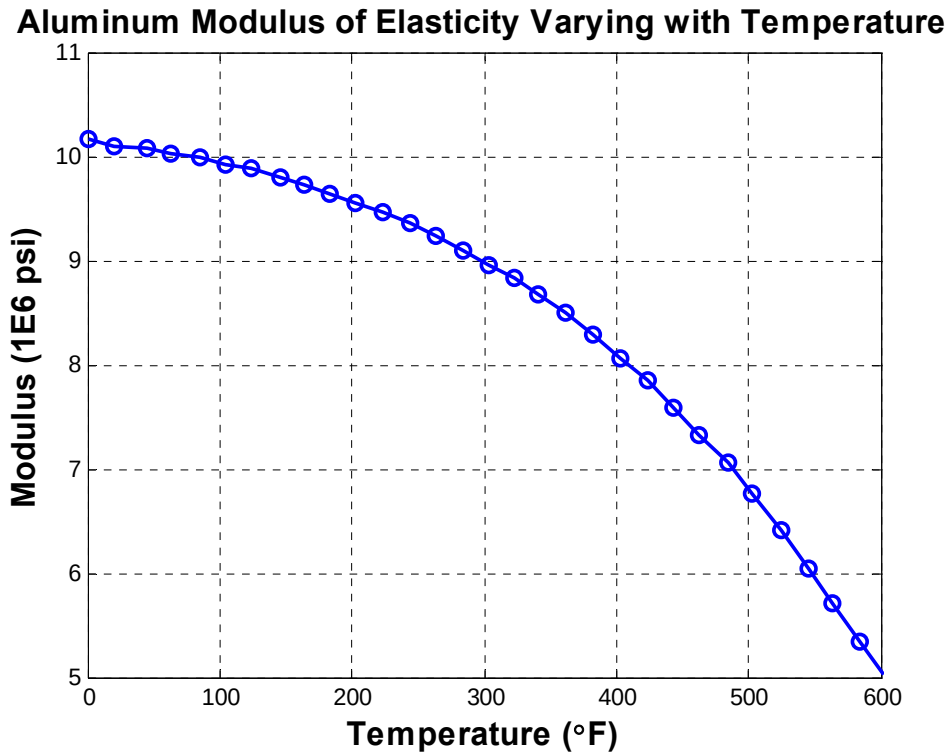

Figure 16: Aluminum Modulus of Elasticity Varying with Temperature

2.2.2 Lamb Wave Modes

Multiple symmetric and asymmetric (anti-symmetric) Lamb wave modes can exist at a given signal frequency. Figure 17 depicts these waveforms as displacements through a thickness cross-section, depicted by the dotted lines in the figures. Symmetric modes are most efficiently generated when an exciting force is parallel to the plate. Their motion is symmetric to the midplane of the plate and they are sometimes referred to as the 'extensional mode' since the waves stretch and compress a plate in the direction of wave propagation, similar to longitudinal waves. Asymmetric waveforms generate motion primarily in a normal direction to the plate with little motion within the plane of the plate. Often termed the 'flexural mode', asymmetric modes cause the body of the plate to bend when two surfaces move in unison, similar to transverse waves (11).

The number of coexisting wave modes goes up as the frequency-thickness product increases, as seen in Figure 18. To control this behavior, and in an effort to isolate the A_o and S_o responses used for Lamb wave damage detection, the frequency-thickness product is kept below 1.8 MHz-mm (1). The fundamental modes are isolated since additional modes would add complexity to the received signal due to an increase in the number of edge reflections.

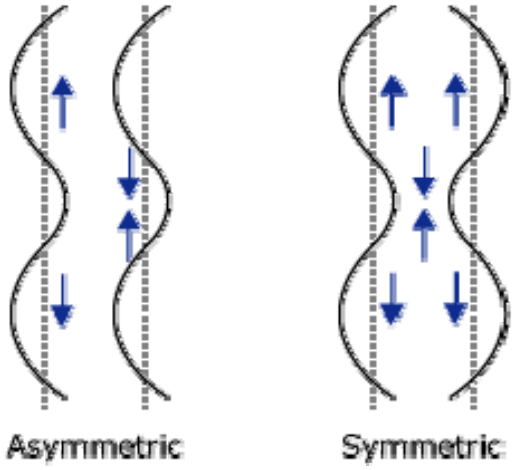

Figure 17: Symmetric and Asymmetric Waveforms (11)

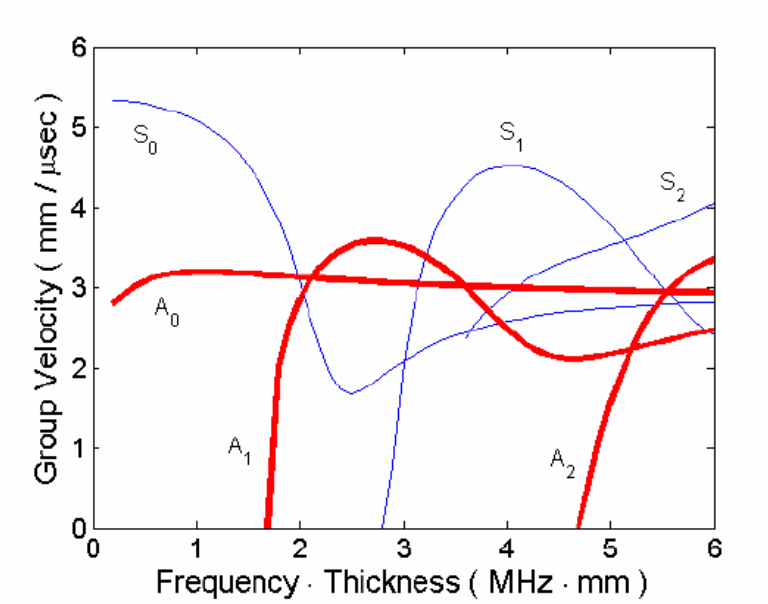

Figure 18: Theoretical Group Velocity Dispersion Curve for an Aluminum Plate

Symmetric modes generally propagate through aluminum at a faster group velocity than the anti-symmetric modes (Figure 18). As an example, below 1.8 MHz-mm the S_0 response is easily traceable in the received signal since it arrives at the receiver before the A_0 response and any wave reflections off the edges of the plate. Hence, identifying changes in the S_0 response is easier to accomplish than identifying traceable changes in the latter portion of a received signal since reflections off the ends of the plate need to be taken into consideration. For the purpose of this thesis, the S_o response was selected for analysis since it was not considered necessary to analyze the entire received signal in order to determine the effects of varying temperature environments on Lamb wave propagation. The frequencies of the excitation signals were limited to 150-500 kHz and the specimens used ranged in thickness (0.6-1.1 mm). These parameters were selected since the frequency-thickness product was required to stay below a threshold of 1.8 MHz-mm.

2.3 Theory on Piezoelectric Transducers

Piezoelectric transducers can be used for both actuating and sensing Lamb wave signals. The piezoelectric transducers used in this study are thin disks of the ceramic material PZT (Figure 19) and they were purchased from APC International Ltd. (Material 850). When transducers are attached to a test specimen for SHM, a transducer that sends out a wave is commonly referred to as an actuator, while a transducer that receives a wave is referred to as a receiver. Piezoelectric transducers are polarized such that a voltage differential applied across the thickness of the disk causes the radius of the disk to contract or expand. The radial displacement actuates a mechanical wave within the host material that propagates through a medium and eventually strains a receiver. A gain property relates strain to voltage, thus the resulting compressions and expansions of the sensing transducer generate voltage differentials which are captured as voltage amplitudes over time.

Figure 19: Piezoelectric Transducer

The following description is a detailed explanation of piezoelectric transducers (Figure 20).

The conversion of electrical pulses to mechanical vibrations and the conversion of returned mechanical vibrations back into electrical energy is the basis for ultrasonic testing. The active element is the heart of the transducer as it converts the electrical energy to acoustic energy, and vice versa. The active element is basically a piece of polarized material (i.e. some parts of the molecule are positively charged, while other parts of the molecule are negatively charged) with electrodes attached to two of its opposite faces. When an electric field is applied across the material, the polarized molecules will align themselves with the electric field, resulting in induced dipoles within the molecular or crystal structure of the material. This alignment of molecules will cause the material to change dimensions. This phenomenon is known as electrostriction. In addition, a permanently-polarized material such as quartz (SiO_2) or barium titanate ($BaTiO_3$) will produce an electric field when the material changes dimensions as a result of an imposed mechanical force. This phenomenon is known as the piezoelectric effect. (11)

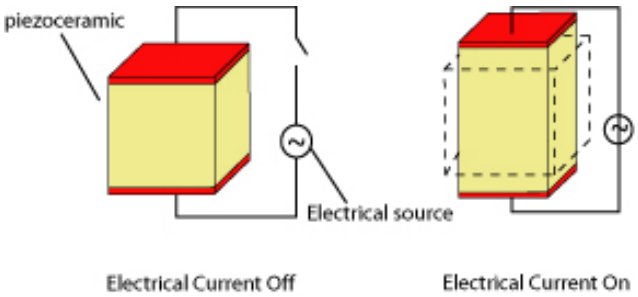

Figure 20: Piezoelectric Transducer (11)

Generating the 5 ½ Cycle Hanning-window Excitation Signal

A 5 ½ cycle Hanning-window excitation signal has been used in several Lamb wave studies by Derriso et al. and was consequently used in this study (1). In general, Hanning-window sine bursts are used to excite Lamb waves because they reduce energy at frequencies other than the excitation or 'center' frequency (18). The addition of the half cycle, to an integer number of cycles, provides a distinct peak in the excitation signal and provides its symmetry (1; 18). Since the frequency content is narrow relative to the center frequency, this is considered a narrow-band signal. Additionally, since the signal is based on a limited cycle sinusoidal tone burst undesired reflections between packets are reduced, thereby allowing for TOF calculations. Once generated and amplified, the signal is sent to an actuator. The excitation signal is transmitted into the medium surrounding the outer edge or circumference of the radial actuator and the signal leaves the actuator at the end of its 5 ½ cycle duration.

Determining the length and duration of the excitation signals is fairly simple. As an example,, the length of one cycle for a 300 kHz signal is approximately 18 mm. This value can be determined from the theoretical phase velocity and signal frequency given the equation ($c=f\lambda$). The length of the entire 5 ½ cycle signal is approximately 97 mm. In addition, the duration of an excitation signal can be determined by dividing the number of cycles in the signal by the excitation frequency (cycles/sec). In the case of the excitation signal just discussed, the duration

is approximately 18.3 microseconds. Reference Appendix C for a complete analysis of the excitation signals used in this study.

Chapter 3 Experimental Set-up

The experimental lab work was carried out at both the Air Force Research Laboratory (AFRL) Air Vehicle Directorate and the Vibrations Laboratory at the Air Force Institute of Technology (AFIT), Wright Patterson Air Force Base. The AFRL SHM Lab in Building 65 housed the primary equipment used to set up the test specimens and run the experiments. Additionally, the Vibrations Lab at AFIT provided a location to capture infrared images using a thermal imaging camera.

The primary equipment used in the experiments included an Agilent 33250 Function/Arbitrary Waveform Generator, a LeCroy WaveSurfer 454 Oscilloscope, National Instruments data acquisition equipment (DAQ) including the PXI-6133 analog to digital converter and the BNC-2110 terminal block, and a Newport RP Reliance Sealed-Hole Tabletop for equipment and specimen set-up (Figure 21). Additionally, Wave Editor Software® (Agilent, Version 1.3.55) was used to generate the excitation pulses and LabVIEW® Software was used to capture the real-time excitation and response signals.

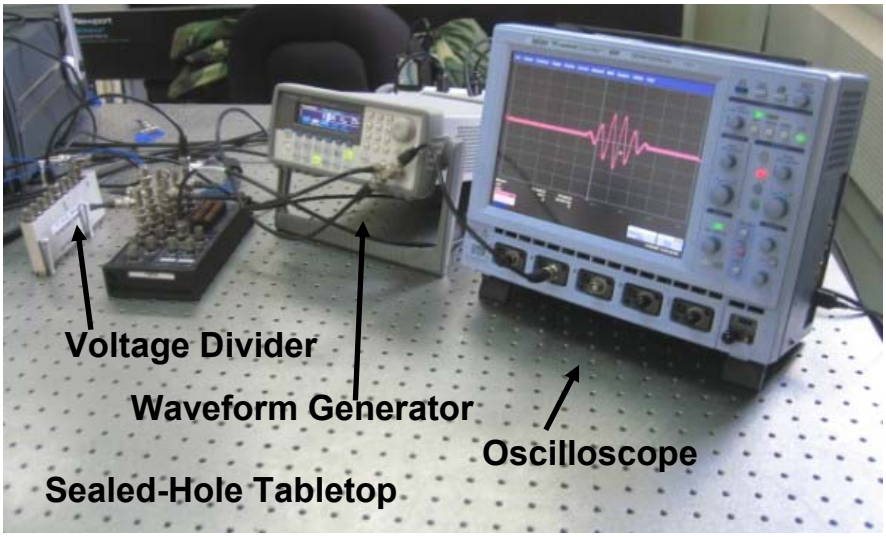

Figure 21: Equipment Set-up

Figure 22 is an illustration of the lab set-up with arrows designating communication between the equipment.

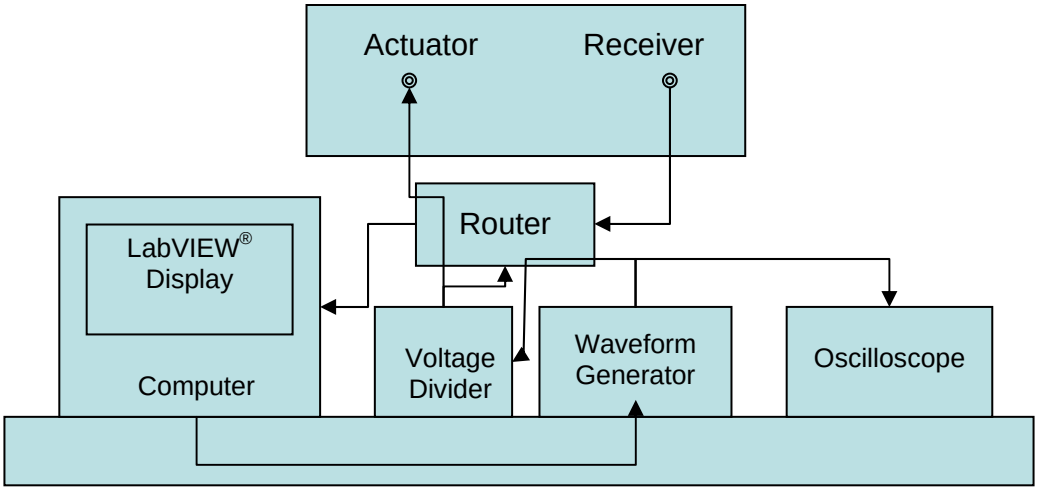

Figure 22: Lab Equipment Diagram

A range of frequencies for the excitation signals were input to LabVIEW® (Figure 23). When the testing began, these frequency signals were digitized at a sampling rate of 2.5 MHz with 14 bits of amplitude quantization. LabVIEW® sent the excitation signals sequentially to the waveform generator where they were amplified to 18 volt peak-to-peak signals. Subsequently, the waveform generator sent the excitation signals to the DAQ and an actuating piezoelectric transducer via a voltage divider. The voltage divider provided a reduced amplitude version of the excitation signals to be recorded without overdriving the 6133 analog to digital converter.

Each excitation signal was sent to the actuating transducer ten times, which allowed ten wave transits to be averaged. Electrical noise was minimized by this data averaging technique. Additionally, the short duration of a pulse assured that the echo of the signal had died down before the next signal arrived (15:76). The waveform generator also sent the excitation signal to the oscilloscope, where it was continuously viewed during testing. Response signals were sent to the DAQ and subsequently viewed in LabVIEW®, as seen in Figure 23. The excitation and response signals were saved to disk for further analysis.

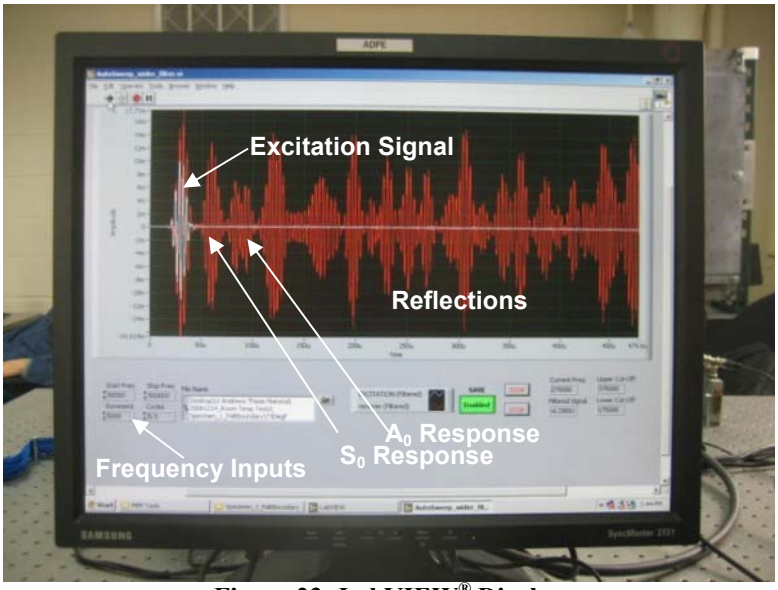

Figure 23: LabVIEW® Display

Supplementary equipment used in the isothermal tests included a Micro-Climate Oven (Model: MCBH-1.2-.33-.33-H/AC) and a BK Precision 725 Humidity/Temperature Meter. The oven, shown in Figure 24, was manually set to the pre-determined temperatures during isothermal testing. Once the specimen was placed in the oven, a temperature meter (thermocouple) attached directly to the specimen provided continuous temperature readings. The specimen was soaked at a given temperature for over 30 minutes before each new test.

Figure 24: Micro-Climate Oven

For the thermal gradient tests, a 14 inch PROTHERM 40 Series Infrared Heater, Model PH 120 14, an OMEGA Single Benchtop Indicator (MDS41), OMEGA Type-K Thermocouples, and two National Instruments (NI) multi-input thermocouple platforms were incorporated in the test set-up. Figure 25 displays the set-up of the infrared heater over the specimen. The heater was placed half an inch to 1 inch above the table using two end supports constructed in the lab. Placing the heater close to the specimen minimized the heat radiated across the plate and placing the heater at the center of the plate generated a symmetric thermal gradient.

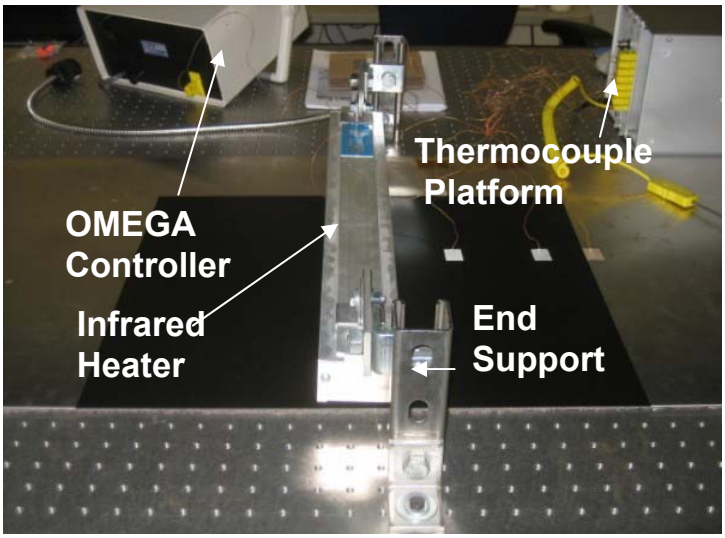

Figure 25: Heater (20) and End Supports

During the thermal gradient experimentation, the heater was manually run using the OMEGA controller (Figure 26). The controller used a Type-K thermocouple as a temperature gauge; hence, the thermocouple was placed under the heater to control the peak value of the thermal gradient. Once the thermocouple reached a pre-set temperature, the controller stabilized the temperature of the heater at this value.

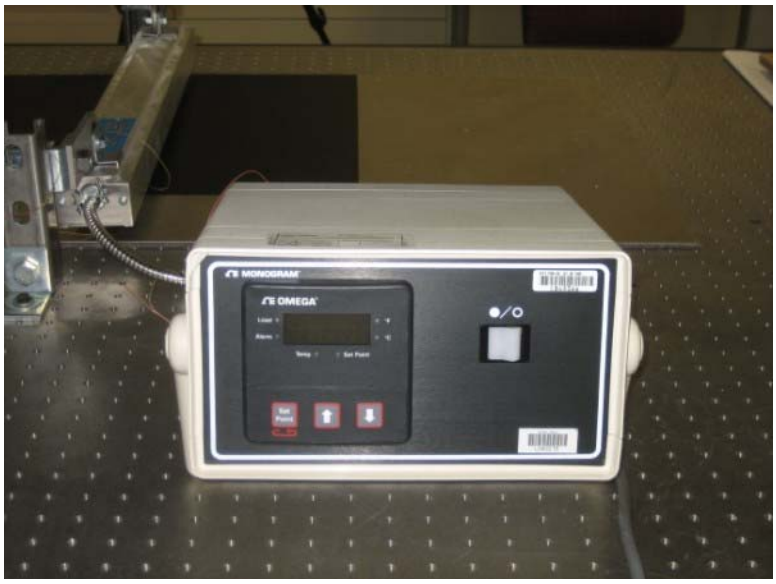

Figure 26: Omega Benchtop Indicator (19)

Figure 27 displays the thermocouple platforms. The first platform included eight thermocouple ports and was designed using the following NI devices: a NI SCXI Chassis: NI SCXI 1000, a 16-bit USB data acquisition and control module: NI SCXI-1600, and an 8-channel thermocouple input module: NI-SCXI-1112 (17). The NI SCXI-1600 plugged into the chassis and provided data acquisition and control for the thermocouple input module, while communicating with the computer using a USB 2.0 connection. This platform was available for use during preliminary thermal gradient testing at AFIT. The second thermocouple platform was designed using five one-channel NI SCC-TC02 Thermocouple Input Modules attached to a NI E Series Board. Both interfaces were available during testing at the SHM Lab, which enabled the use of 13 thermocouples to characterize the thermal gradient profiles.

Figure 27: National Instruments (17) Multi-input Type-K Thermocouple Interfaces

Additionally, a FLIR ThermaCAM P Series Infrared Camera PM695 was used by a lab technician to capture infrared images during the thermal gradient testing. The camera, as seen in Figure 28, was placed on a tripod and angled to capture a side view of the specimen. Once the testing began, images were taken at various times to display the progression of the thermal gradient. The thermal images were saved and downloaded to PDF files for further use.

Figure 28: ThermaCAM (4)

3.1 Specimen Design and Preparation

In both the isothermal and thermal gradient experiments, 2024-T3 aluminum sheet specimens were selected and cut to size at the AFIT Model Shop. The dimensions of the specimens are displayed in Table 1. Length and width dimensions were determined using a meter stick and thickness values were printed on the sheet metal in English units (i.e. 0.025 and 0.040 inches). These values were converted to metric units as seen in Table 2.

Table 2: Specimen Dimensions

Specimen	Length (mm)	Width (mm)	Thickness (mm)
I	475.9	247.7	1.015
II	1218	648.0	0.6345
III	1217	645.0	0.6345

Specimen I was used in the isothermal testing. The length and width dimensions of the plate were maximized by pre-determining the specimen's set-up inside of the oven. The specimen was placed in the oven diagonally, with two rubber blocks supporting either end of the plate. The block positions are pointed out in Figure 29; however, they are not easily seen due their small size. This set-up minimized contact between the plate and the metal surfaces inside the oven.

Figure 29: Specimen I Placed Diagonally in Oven

Two additional aluminum plate specimens were selected for the thermal gradient testing. Their length and width dimensions increased over that of Specimen I, which allowed for a greater propagation distance between actuator and receiver. Additionally, larger specimens were needed due to the size of the infrared heater. The use of larger specimens assured that the transducers were close to room temperature while the center of the specimen was heated to temperatures exceeding 200°F. The thickness of Specimens II and III was less than the thickness of Specimen I. The change in specimen thickness was based on the availability of aluminum sheet material at the AFIT Model Shop. Additionally, a water jet was used to cut Specimen II to size.

Once the plates were selected, the placements of an actuator and a receiver transducer were determined for each specimen. Transducers were centered along the width of the plates and placed along the length such that the boundary reflections would not affect the S_0 response and the length of the propagation distance would allow time for changes in the signal to occur. Refer to Table 3 for the signal propagation distance between actuator and receiver for each specimen.

Table 3: Signal Propagation Distances

Specimen	Signal Propagation Distance (mm)
1	158
2	509
3	512

Before attaching the transducers to a specimen, each plate was cleansed using Isopropanol and a gauze sponge. This process removed any residue on the surface to ensure strong adhesion between the transducers and the metal. The transducers were handled using a disposable cotton-tipped wood applicator and wax and an M-BOND adhesive was used to attach them to the specimen. Once attached, the adhesive residue around the transducers was cleaned using acetone and a gauze sponge. Removing the residue on and around the transducers assured that the signals were not affected by additional deposits on the surface of the plate. Wiring was soldered on to the transducers and subsequently attached to the lab equipment during experimental testing.

3.2 Isothermal Testing Data Acquisition

Once the piezoelectric transducers and thermocouple were attached to Specimen I, the specimen was placed in the Micro-Climate Oven and the sensor wiring was directly connected to the primary equipment through a port in the side of the oven. Refer to Figure 30 and Figure 31. All of the isothermal testing was conducted in the same fashion. Forty-six excitation signals, ranging from 50-500 kHz in increments of 10 kHz, were sent to the actuator. Additionally, ten trials were run at each temperature.

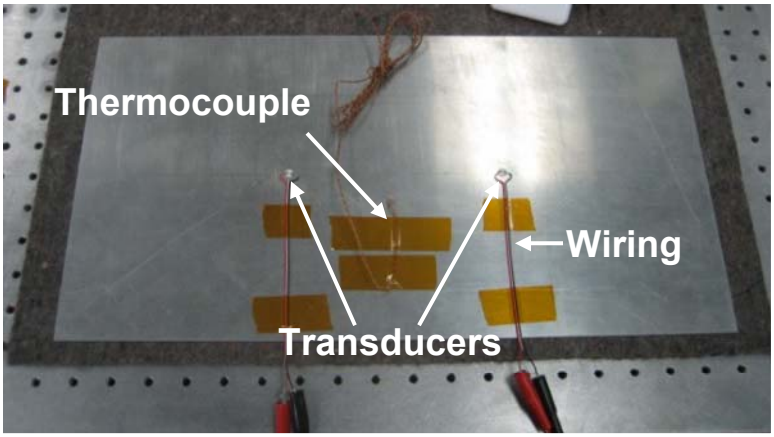

Figure 30: Specimen I with Piezoelectric Transducers and Thermocouple

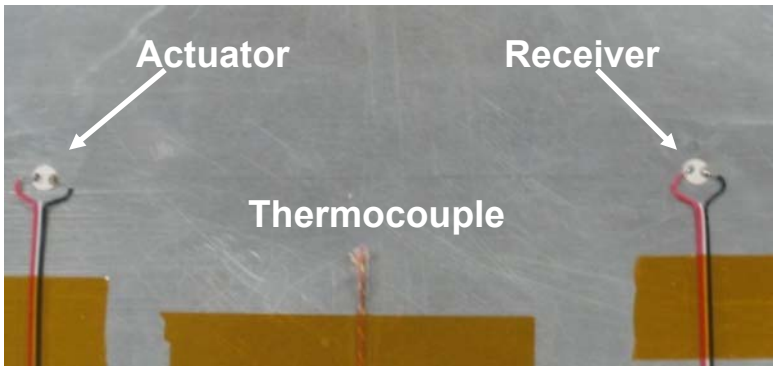

Figure 31: Magnified View of Actuator, Receiver, and Thermocouple

Baseline Lamb wave propagation tests were conducted at room temperature and the remaining isothermal tests were conducted at temperatures in the range of 0-225°F. The maximum test temperature for testing was based on the functional limitations of the piezoelectric

transducers and the adhesive used to attach the transducers to the specimen. In previous studies conducted at the SHM Lab, temperatures at 250°F and above appeared to have an adverse effect on the transducers since the response signals were reduced in amplitude. Therefore, the tests in this study were kept below 250°F.

3.3 Support Testing Data Acquisition

In the transition from isothermal to thermal gradient testing, two experiments were conducted on Specimen I using different plate supports. The purpose of these tests was to identify changes in Lamb wave propagation due to the direct contact between a plate and its support. In the first set-up, the plate was placed on two small rubber blocks. Each block was approximately two inches square and half an inch thick. The plate was essentially free from contact with any external surfaces, as seen in Figure 32. In the second set-up, the specimen was placed on a felt mat; hence, the plate made direct contact with a material surface (Figure 30). Since these tests were conducted at room temperature outside of the oven, the S_0 responses for the two support conditions were also compared to S_0 responses obtained from the isothermal oven testing at room temperature.

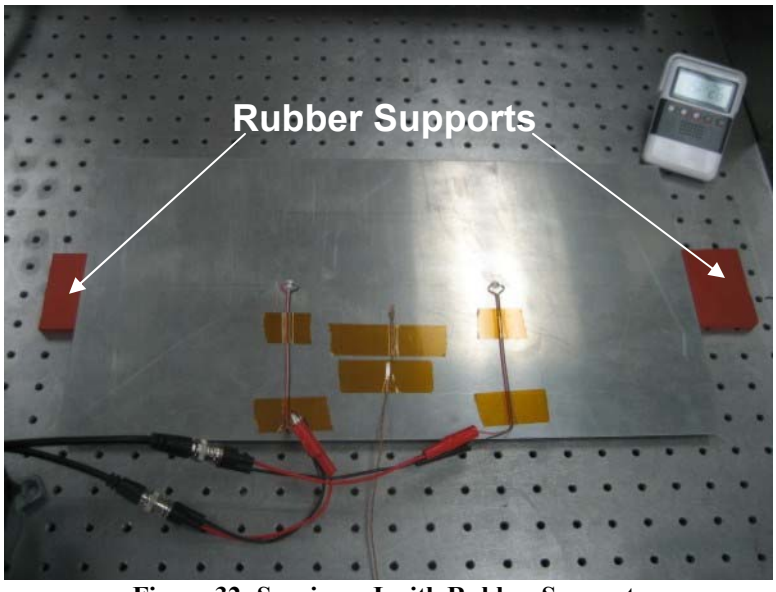

Figure 32: Specimen I with Rubber Supports

3.4 Thermal Gradient Testing Data Acquisition

In real-world environments, it is also likely that thermal gradients are present in the body of a structure due to heat spots. Consequently, the next step was to take a look at the affects of thermal gradient environments on Lamb wave propagation. Initially quantifying the affects of isothermal environments on Lamb wave propagation provided a foundation to this new area of research. The primary objective of the thermal gradient testing was to generate a sharp gradient in the specimen. The peak temperature, under the heater, was set as high as possible while maintaining the thermocouples near room temperature. This set-up was more likely to confirm a measurable change in Lamb wave propagation since higher temperatures reduce the modulus of elasticity for aluminum.

Preliminary thermal gradient tests using Specimen II were conducted in the Vibrations Lab at AFIT. The focus of this testing was to capture infrared images of the thermal gradients using a thermal imaging camera. These images could potentially supplement temperature readings taken by Type-K thermocouples attached to the plate. The thermocouple readings were displayed real-time using LabVIEW® and were the primary means of capturing the thermal gradients data in the SHM Lab. In order to efficiently use the infrared camera, the imaging area on the plate was spray-painted black to prevent heat reflection off the surface of the plate. The painted region fell between the piezoelectric transducers along the length of the specimen and between a row of thermocouples and the opposite edge of the plate along the width (Figure 33). When this testing was discontinued, as will be discussed in Chapter 4, the specimen set-up was taken back to the SHM Lab and subsequent testing was conducted using Specimen III.

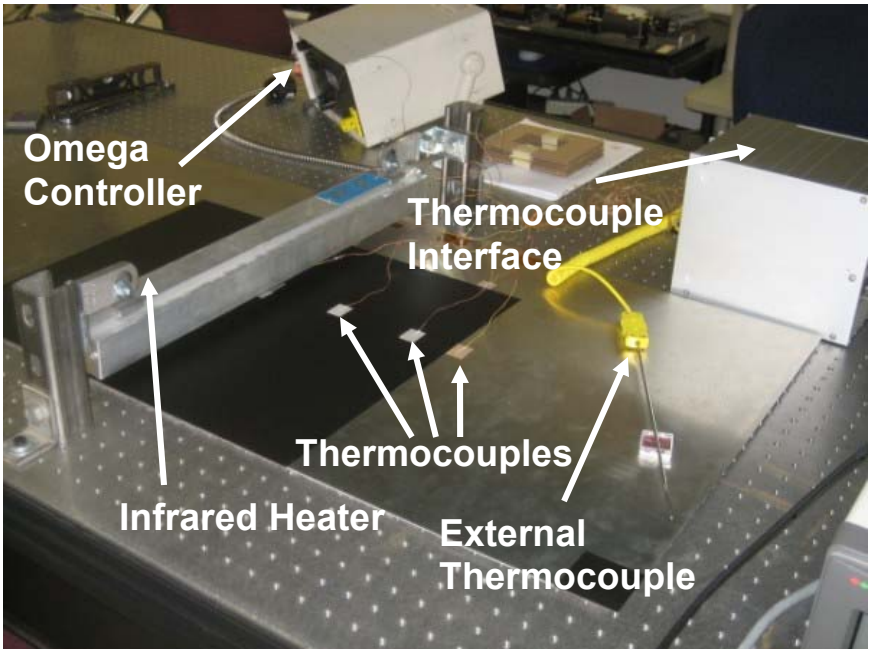

Figure 33: Specimen II Set-up

Figure 34 captured the set-up for Specimen III. Due to the set-up in the SHM Lab, the gradient testing on Specimen III required the use of two LabVIEW® displays to capture signal and thermal gradient data. One display was used to transmit and receive the Lamb wave signals, as implemented earlier for the isothermal testing, and a second display was used to store the temperature readings as seen in Figure 35. All measurements were captured over time. As a result of this arrangement, the temperature and signal readings were not synchronized. The temperature readings were started immediately after the excitation signals were sent to the specimen.

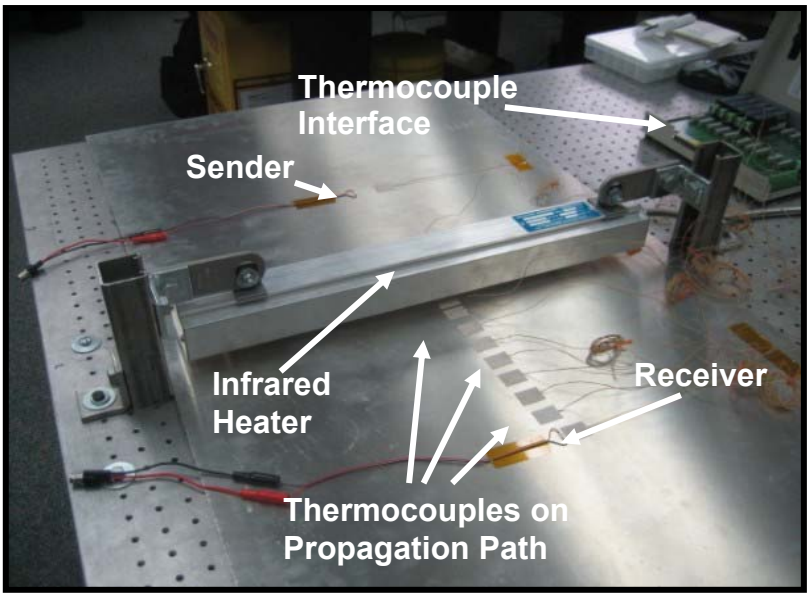

Figure 34: Specimen III Set-up

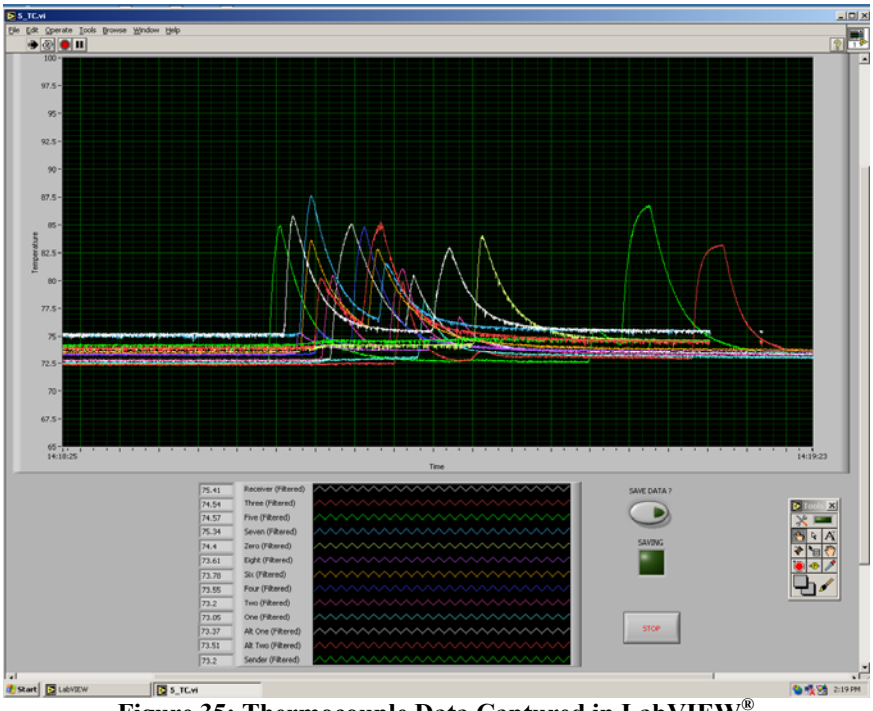

Figure 35: Thermocouple Data Captured in LabVIEW®

Both thermocouple interfaces were used for data capture, which enabled the use of 13 thermocouples to characterize the thermal gradients. Since the gradients were approximately symmetric, ten thermocouples were used to characterize half the gradient. The first

thermocouple, located at the zero position, was placed directly under the lamp. Nine additional thermocouples were placed after the center point (zero position) of the propagation path and up to the receiver transducer. Figure 36 displays the placement of thermocouples four through nine. The remaining three thermocouples were placed on the opposite side of the heater and were used to verify the symmetry of the thermal gradient across the plate. Thermocouple positions can be referenced in Table 4. The negative positions denote the thermocouples placed on the opposite side of the heater.

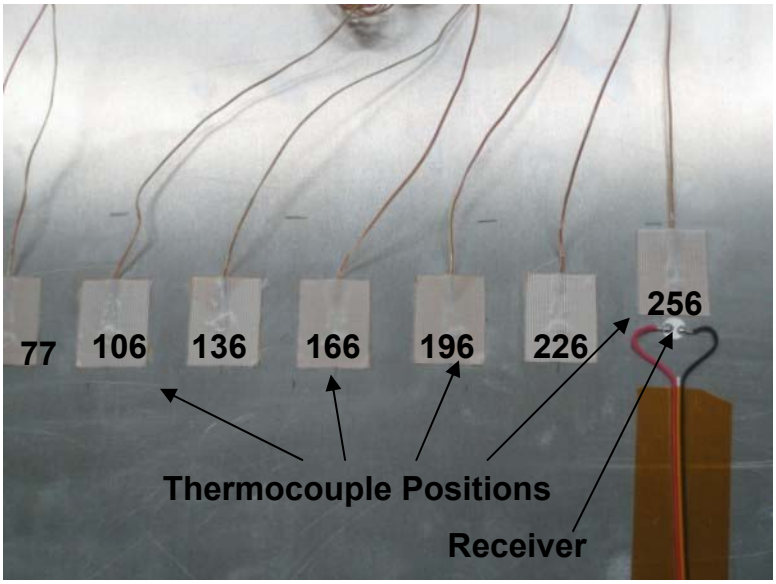

Figure 36: Specimen III Thermocouple Placements (mm)

Table 4: Specimen III Thermocouple Positions

Thermocouple	1	2	3	4	5	6	7	8	9	10	11	12	13
Placement (mm)	0	24	47	77	106	136	166	196	226	256	-47	-106	-256

3.5 Matlab® Analysis

Matlab® Software was used to analyze the experimental signal data and to implement theoretical Lamb wave propagation simulations. The foundation of the theoretical code was provided by unpublished Matlab® algorithms developed at the AFRL/VASA under a subcontract supporting Anteon [Air Force Contract #FA8650-04-D-3446-012]. The common objective for

both the isothermal and thermal gradient data was to generate plots for specific frequency signals over varying thermal conditions. Isolated S_0 responses were analyzed to identify changes in the signal waveforms and times of arrival (TOA). The TOA for a response signals is determined by identifying the time index corresponding to the peak in the signal waveform. Additionally, group velocity dispersion curves were generated from the isothermal data over the range of tested temperatures. All of the isothermal experimental results were used to verify theoretical predictions, where the theoretical simulations were generated given the solutions to the Rayleigh-Lamb frequency equations. The thermal gradient data was more difficult to predict theoretically, so only the experimental data was analyzed in this study.

3.5.1 Generating Excitation and Response Signal Time Plots

Throughout the experiments, excitation and response signals were captured for further analysis. Specifically, the raw signal data was captured as voltage values versus time, as shown in Figure 37. In cases where several test trials were run at a particular temperature or support condition, the signal data was averaged. Once the signals were plotted using Matlab®, each S_0 response was isolated based on a visual analysis of the waveform. The S_0 response was analyzed to determine time delays in signal propagation and to observe changes in the waveform due to temperature variations.

Notice, in the plot of the response signals, there is a waveform present at the same point in time the excitation signals were transmitted to the specimen. This anomaly was due to induction between the wires transmitting the signals. Induction occurs when the magnetic field generated from a current in one wire generates an electric current in an adjacent wire. Since the wires were in close proximity to each other during testing, the magnetic field around the current carrying the excitation signal transmitted the same signal over to the receiving current.

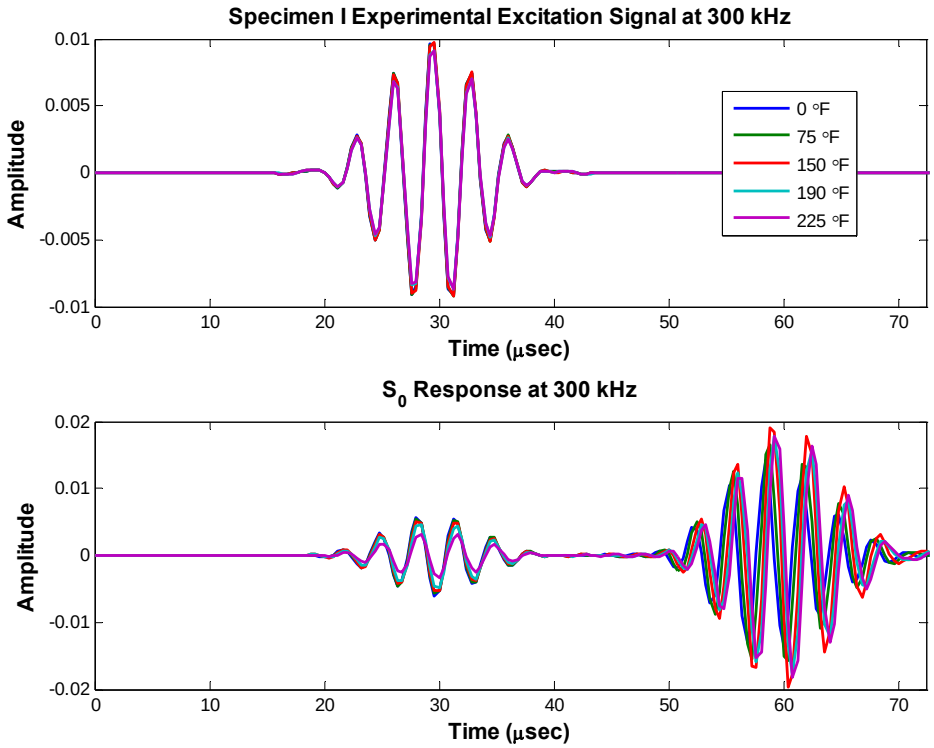

Figure 37: Specimen I Raw Signals at 300 kHz

Theoretical S_0 response simulations served as a comparison to the experimental S_0 response signals and were generated using the concept of superposition discussed in Chapter 2 (refer to equation 2.1.14). The phase velocity values required to compute the superimposed waves were extracted from theoretical phase velocity dispersion curves. These curves were generated from the solutions to the Lamb wave equations based on the method addressed in Section 3.5.2.

Before conducting an analysis on the raw experimental data, the time delay between the theoretical and experimental excitation signals was determined and accounted for in the theoretical predictions. As an example, Figure 38 displays the theoretical and experimental excitation signals for a 300 kHz signal. Since the experimental excitation signal did not begin at time zero, a time delay existed between the two signals. This time delay was approximately

20-30 microseconds for all of the tests. Once the time delay was calculated and added to the theoretical excitation signal, the signals aligned with each other as seen in Figure 39.

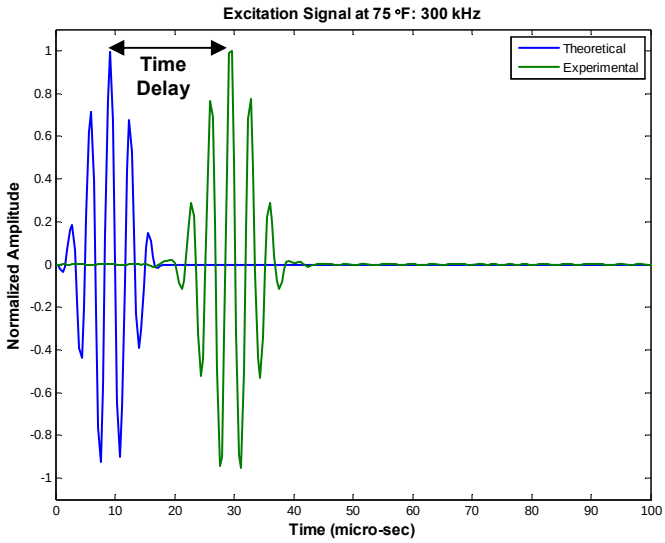

Figure 38: Time Delay in Experimental Excitation Signal

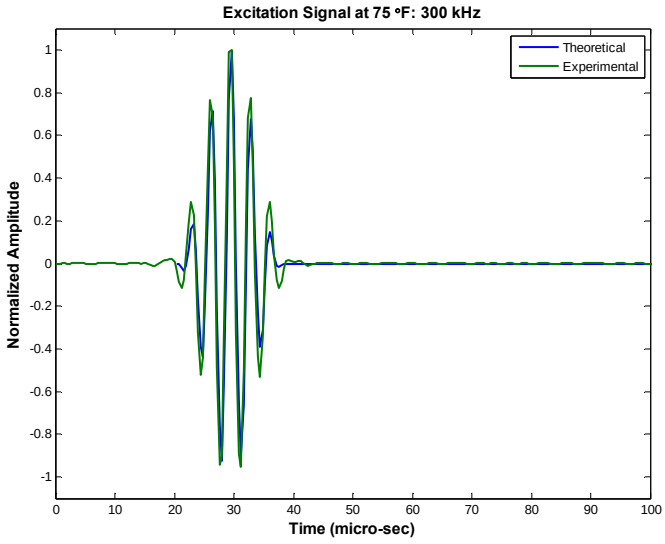

Figure 39: Time Delay Added to Theoretical Excitation Signal

The time delay was also factored in to the theoretical response signal calculations. Lastly, the excitation and S_0 response signals were normalized with respect to the peak amplitude in each waveform. An important note here is that the maximum point on each signal does not always

fall positive with respect to a signal's amplitude; therefore, the maximum point must be taken with respect to the absolute value of a signal. As an example, Figure 40 displays normalized excitation signals at a frequency of 300 kHz. Once these modifications were made to the raw data, direct comparisons could be made between the experimental and theoretical results.

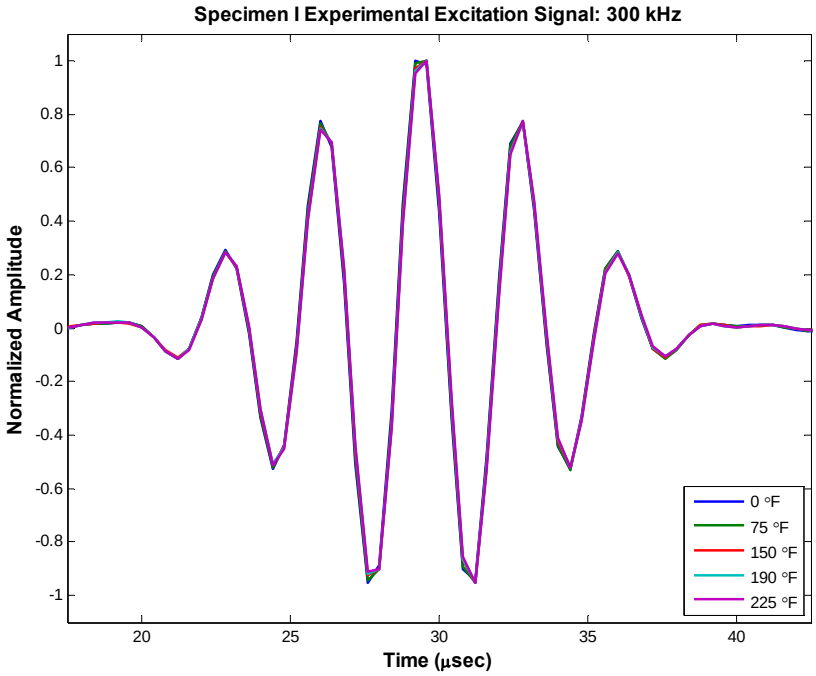

Figure 40: Specimen I Experimental Excitation Signals at 300 kHz

3.5.2 Generating Group Velocity Dispersion Curves

Theoretical group velocity dispersion curves were generated using the equations and numerical method outlined by Rose and covered in Chapter 2. Generating the solutions required the following experimental parameters: the thickness of the specimen, the propagation distance, signal frequencies, the sampling rate of the signal, and the temperature of the medium. Recall, the Lamé constants used in the theoretical calculations require values for Young's modulus (E), the shear modulus (G), and the density of the material (ρ). Values for E varying with temperature were obtained from Figure 16. Subsequently, G was determined from E and the density used for

aluminum sheet specimens was 2768 kg/m^3. Given the parameters specified above, the polyfit command in Matlab® was used to find the coefficients of a polynomial p(x) of degree n that fit the data, p(x(i)) to y(i), in a least squares sense. The coefficients corresponding to each solution were saved in a Matlab® file and subsequently used to generate theoretical group and phase velocity dispersion curves. Polynomials of degree five were obtained for solutions at temperatures below 200°F and polynomials of degree 11 were obtained for solutions at temperatures exceeding 200°F. The Matlab® code used to generate these solutions can be referenced in Appendix C..

Experimental group velocity dispersion curves were generated given the thickness of the specimens, the signal frequencies, the propagation distance, and by determining the TOF of the S_0 responses. The TOF was determined by taking the difference in the time indices corresponding to the peaks in the excitation and response signals. The peak of the S_0 response was determined after using a window to gate this portion of the received signal. The window was based on a theoretical algorithm implemented in Matlab® and this algorithm can be referenced in Appendix C. Once the TOF values were determined, the corresponding group velocity values were calculated by dividing the known propagation distance of the signals by their TOF values. The frequency of each signal was multiplied by the thickness of the specimen to obtain the abscissa values for the plots.

Group velocity dispersion curves are presented in Chapter 4 to display the correlation between the theoretical and experimental results. Figure 41 captures a general theoretical group velocity prediction for 75°F plotted with upper, lower, and mid-window group velocity estimates. Therefore, if the peak of an experimental signal falls within close proximity of a window limit or at the center of the window, the corresponding experimental group velocity value will fall near the maximum, minimum, or mean velocity lines depicted in the graphs.

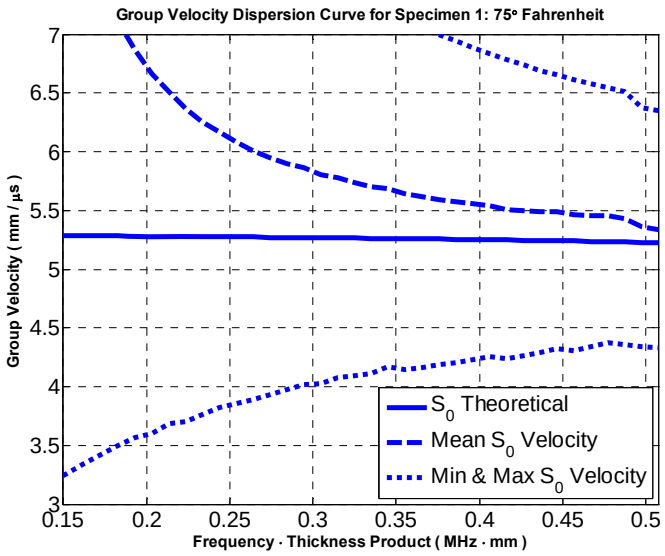

Figure 41: Theoretical S_0 Group Velocity Dispersion Curve with Window Limits

3.5.3 Generating Thermal Gradient Curves

A thermal gradient curve was generated per test trial using the thermocouple data and the measured placements of the thermocouples along the propagation path. Temperature values were plotted along the y-axis and the corresponding positions of the thermocouples were plotted along the x-axis. For each trial, seven signals were sequentially tested in the range of 200-500 kHz. The total time of the wave transits was fairly short so there were only minor fluctuations in the temperature readings over each test trial. Due to this fact, the temperature at each thermocouple was taken as the average over a test trial.

Chapter 4 Results and Discussion

Chapter 4 presents the results obtained from both the isothermal and thermal gradient experiments. The data obtained for the isothermal testing was based on the use of Specimen I and the data obtained for the thermal gradient testing was based on the use of Specimens II and III. Specifically, Section 4.1 covers the isothermal testing to include theoretical and experimental wave propagation results, power spectral densities, and group velocity dispersion curves. Section 4.2 explores the effects of varying specimen supports on Lamb wave propagation. Thermal gradient testing in covered in Section 4.3, followed by theoretical simulations at temperatures up to 600°F in Section 4.4.

4.1 Isothermal Testing

The isothermal data presented was taken from theoretical and experimental tests at 0, 75, 150, 190 and 225°F. Data was obtained from signals at 46 frequencies signals in the range of 50-500 kHz at increments of 10 kHz. Of these, ten signals were analyzed. The results of the 300 kHz S_0 responses will be presented in the following sections, while the additional frequency signals can be referenced in Appendix C.

4.1.1 Wave Propagation Analyses

Figure 42 displays the theoretical and experimental S_0 responses at a frequency of 300 kHz. The transient decay or ringing in the experimental signals around the 65 microsecond timeframe was an observable difference between the theoretical and experimental waveforms and it can be traced back to the experimental excitation signals. A data filter used in the data collection hardware stored the signals over time and there were approximately 128 delays (0.4 microseconds per delay) during this process. As a result, the signals were stretched out in the temporal domain.

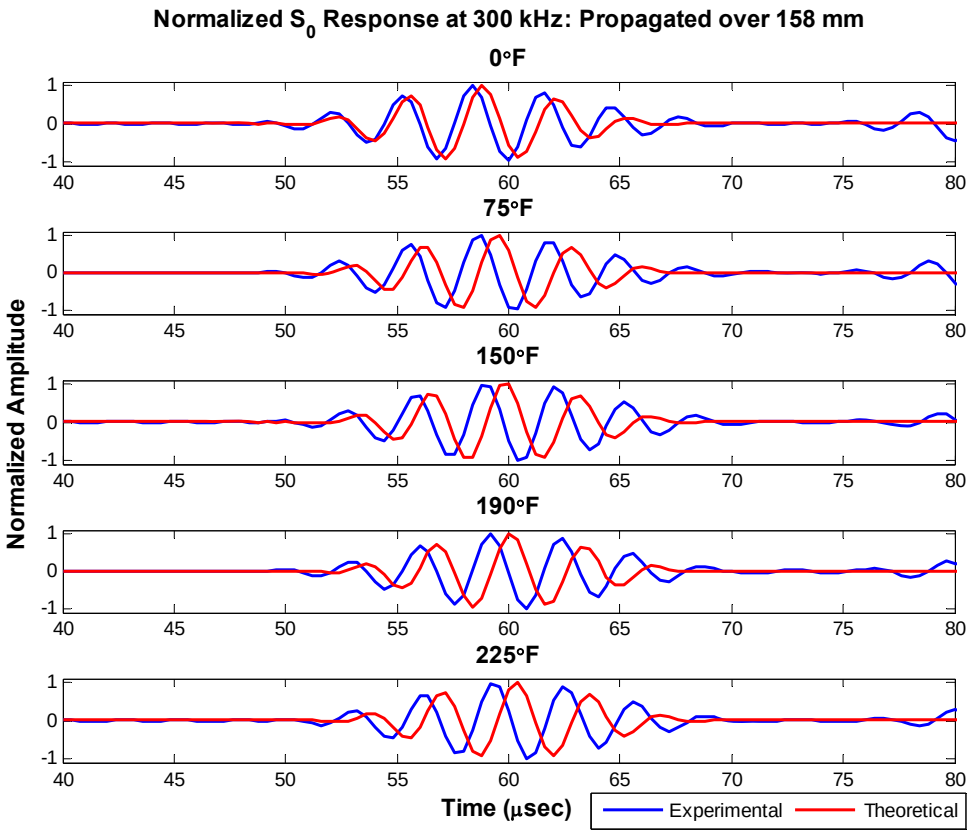

Figure 42: Specimen I Experimental versus Theoretical S_0 Response at 300 kHz

In addition to the observed waveform differences, there were measurable time differences in the TOA of the signals. Table 5 presents these differences, which were determined by calculating the differences between time indices corresponding to the peaks of the theoretical and experimental S_0 responses. In each case, the theoretical time index was subtracted from the corresponding experimental time index. It should be noted here that sampling error may have affected time difference calculations between any two signals compared in subsequent analyses, to include this analysis. Sampling error occurs when the determination of a signal's peak is off by plus or minus one sample. Due to the error associated with determining the peak of a response signal, this error is doubled when the TOA difference is determined between two response signals. Positive time differences indicate that the theoretical waveforms propagated at a slightly faster group velocity than the experimental waveforms. Overall, the differences

between the S_0 responses in the range of 150-500 kHz were generally on the order of 0.4–1.2 microseconds, or 1-3 samples; however, in some isolated cases the differences were off by several samples. The TOA differences calculated for the lower frequencies (<150 kHz) were noticeably high. Recall, at low frequencies in the range of approximately 50-150 kHz the amplitude of the A_0 waveform is dominant. As a result, the peak of the S_0 response is not distinct. Since the time differences are based on the peaks of the waveforms, this variability is reflected in the notably high time differences between these signals. Based on the signals with frequencies above 150 kHz, the theoretical calculations were highly accurate in predicting the TOA for the experimental results in this study.

Table 5: TOA Differences between Theoretical and Experimental S_0 Responses

Theoretical versus Experimental S_0 Responses										
TOA Differences (μsec)										
°F versus KHz	**50**	**100**	**150**	**200**	**250**	**300**	**350**	**400**	**450**	**500**
0	-29.2	-28.8	0	-0.4	-2.4	-0.4	-0.4	0.8	0.4	0.8
75	-19.6	-28.8	2.8	-0.4	-0.4	-0.8	2.4	0.4	-0.4	0.8
150	-19.2	9.6	0	-3.2	-0.4	0.4	1.2	0.4	0.4	2
190	-20.0	-29.6	0	-3.2	-0.8	-0.8	-0.4	0.4	-0.8	0.8
225	-38.8	4.4	-0.4	-3.2	-0.4	0.4	0.8	0.4	0.4	1.6

4.1.2 Power Spectral Densities

PSD plots were used to display the frequency content of the S_0 responses. Generally, the bulk of a signal's magnitude is centered about its center frequency or frequency at which the excitation signal is transmitted. This is evident in Figure 43 and Figure 44, which display the magnitude of the frequency content for both the theoretical and the experimental 300 kHz S_0 response signals discussed in Section 4.1.1. In this case, the main lobe of the signal falls between 200-400 kHz, with the peak falling at the center frequency of 300 kHz. However, the main lobe of the experimental PSD plots has shifted slightly to the right. In addition, there is an observable decrease in the magnitude of the frequency content as the temperature increases from 0°F to 225°F. These observations were similar to those made by Konstantinidis (13:972), who observed

changes in the frequency response of a transducer at higher temperatures. Changes in the piezoelectric properties and bond stiffness of the transducers led to these observable differences. As a final note, if these plots are expanded to display additional frequency content, the magnitude levels of the lower and higher frequencies falls within the noise level of the measurements. Therefore, characterizing the frequency content of signals in this study is limited to magnitudes greater than approximately -120 dB.

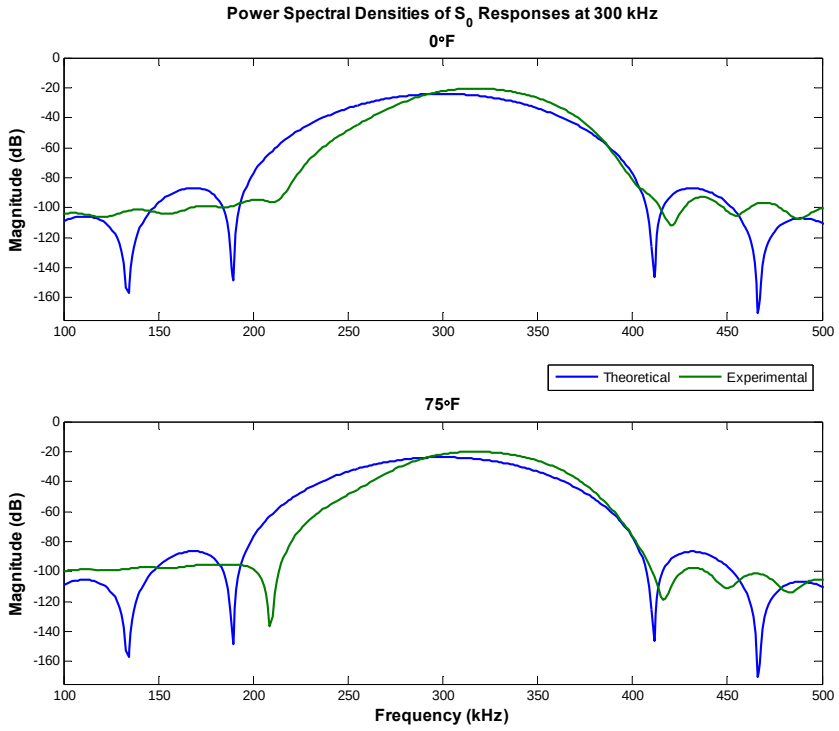

Figure 43: Power Spectral Densities of S_0 Responses at 300 kHz (0°F and 75°F)

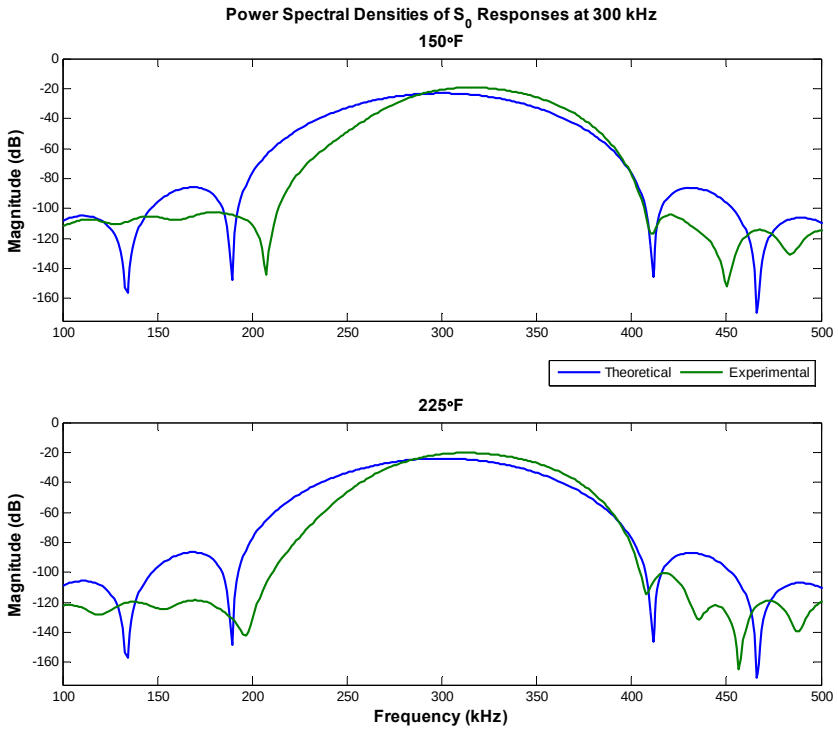

Figure 44: Power Spectral Densities of S_0 Responses at 300 kHz (150°F and 225°F)

4.1.3 Signal Delays Attributed to Elevated Temperatures

Figure 45 displays theoretical S_0 responses propagated over 158 mm at a frequency of 300 kHz to demonstrate the affects of elevated temperatures on wave propagation. These predictions are a function of the modulus of elasticity, which was a function of temperature as discussed in Chapters 2 and 3. There are no apparent changes to the waveforms; however, there are measurable time delays between the signals. Table 6 displays the TOA differences between the individual waveforms. Again, these differences are based on the peak-to-peak difference between the wave packets, where the time index of the lower temperature peak is subtracted from the time index of the higher temperature peak. The TOA differences demonstrate that the higher temperature waveforms are propagating at a slower group velocity than the lower temperature waveforms on the order of 0.4 to 1.2 microseconds. Table 6 also contains time

delay calculations for signals that can be referenced in Appendix C. When the temperature difference between two signals is 75 degrees or less, the time differences between waveforms are generally on the order of one sample, or 0.4 microseconds. These minor differences can be attributed to the effects of elevated temperatures; however, they can also be attributed to the sampling error associated with TOA calculations. The TOA differences between the higher temperature signals relative to signals propagated at 0°F consistently fall between 0.8-1.2 microseconds and in a few cases 2 microseconds. Although minor sampling errors may have occurred between these peak-to-peak calculations, there is consistent evidence of time delays in the signals over these higher temperatures.

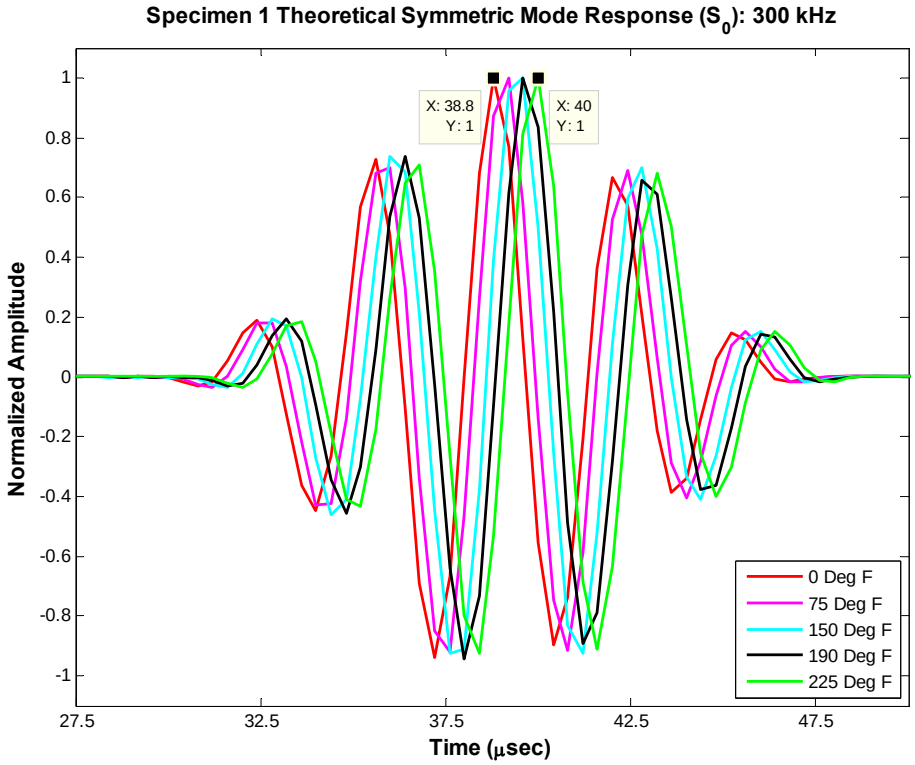

Figure 45: Specimen I Theoretical S_0 Response at 300 kHz

Table 6: Theoretical S_0 Response Temperature Based Time Delays

Theoretical S_0 Responses						
Temperature Based Time Delays (µsec)						
Frequency (kHz)	**0-75°F**	**75-150°F**	**150-190°F**	**190-225°F**	**0-190°F**	**0-225°F**
50	0	0.4	0.4	0	0.8	0.8
100	0	0.4	0.4	0.4	0.8	1.2
150	0.4	0	0.4	0.4	0.8	1.2
200	0.4	0.4	0.4	0	1.2	1.2
250	0	0.4	0.4	0	0.8	0.8
300	0.4	0.4	0	0.4	0.8	1.2
350	-1.2	1.6	0.4	0.4	0.8	1.2
400	0.4	0.4	0.4	0	1.2	1.2
450	1.2	0.4	0.4	0	2	2
500	0.4	-0.8	1.2	0.4	0.8	1.2

The same concept was illustrated experimentally using the experimental S_0 responses over the same frequency and temperature ranges. Figure 46 is an example of the experimental S_0 responses propagated at 300 kHz. Similar to the theoretical waveforms presented in Figure 45, there is little variability between the experimental waveforms. Additionally, there are measurable TOA differences between the S_0 responses as displayed in Table 7. The TOA differences are comparable to the theoretical differences; however, there is more amplitude variability in the lower frequency experimental signals. The notably high TOA difference between the 100 kHz signals is due to this variability. Beyond the low frequency analysis and into the higher temperature ranges there are consistent TOA differences on the order of 0.8 to 2.4 microseconds between signals at 0°F and 190-225°F. Refer to frequencies above 150 kHz in the last two columns of Table 7. These numbers were slightly higher than the theoretical differences under the same conditions; however, the trend of TOA differences greater than 0.8 microseconds is consistent for signals propagated at temperatures over an approximate 200 degree temperature range.

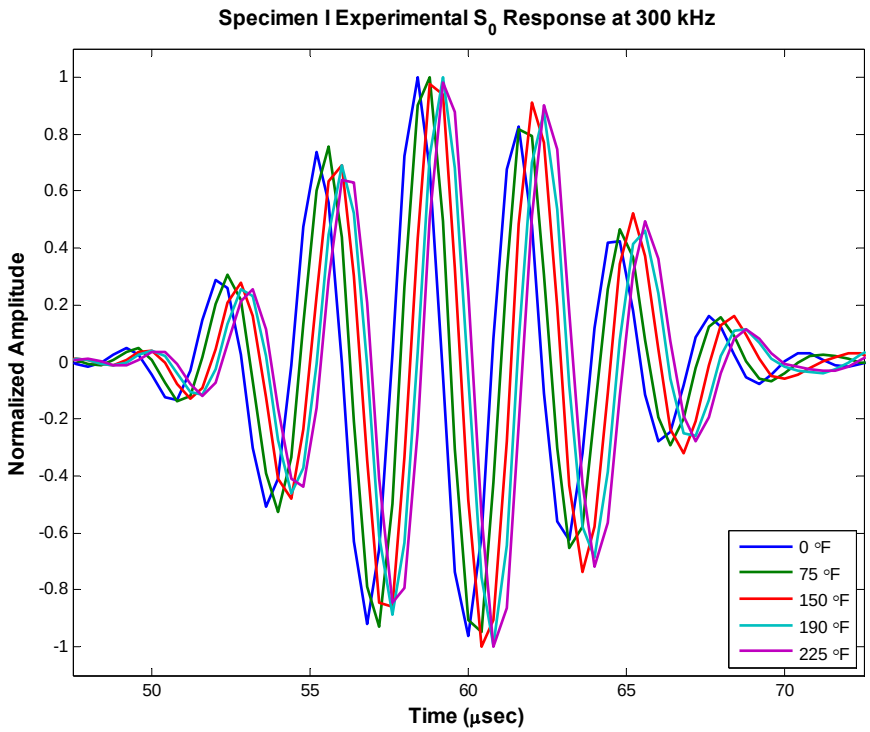

Figure 46: Specimen I Experimental S_0 Response at 300 kHz

Table 7: Experimental S_0 Response Temperature Based Time Delays

Experimental S_0 Waveforms						
Temperature Based Time Delays (µsec)						
Frequency (kHz)	**0-75°F**	**75-150°F**	**150-190°F**	**190-225°F**	**0-190°F**	**0-225°F**
50	9.6	0.8	-0.4	0.8	10	10.8
100	0	61.6	0	-2.8	61.6	58.8
150	3.2	-2.8	0.4	0	0.8	0.8
200	0.4	-2.4	0.4	0	-1.6	-1.6
250	2	0.4	0	0.4	2.4	2.8
300	0.4	1.6	-1.2	1.6	0.8	2.4
350	1.6	0.4	-1.2	1.6	0.8	2.4
400	0	0.4	0.4	0	0.8	0.8
450	0.4	1.2	-0.8	1.2	0.8	2
500	0.4	0.4	0	1.2	0.8	2

4.1.4 Group Velocity Dispersion Curves

Figure 47 and Figure 48 display theoretical predictions and experimental results for Specimen I at 75°F and 225°F. Additional plots can be referenced in Appendix C. Since ten test trials were run at each temperature, the experimental mean group velocity values are displayed

with error bars. The error is based on a confidence level of approximately 67%, or one standard deviation from the mean. As seen in Figure 47, data points for frequency-thickness values below 0.15 MHz-mm reveal significant experimental deviations from the theoretical predictions. Again, given the thickness of Specimen I, the S_0 response was not easily traceable at these low frequencies since the A_0 response was dominant. Other group velocity deviations can be attributed to the sampling error associated with the TOF calculations. Standard deviations were commensurate with sampling error since the group velocities were determined by a constant propagation distance divided by the TOF values. Overall, experimental data above 150 kHz came within close approximation of the theoretical predictions throughout the isothermal tests.

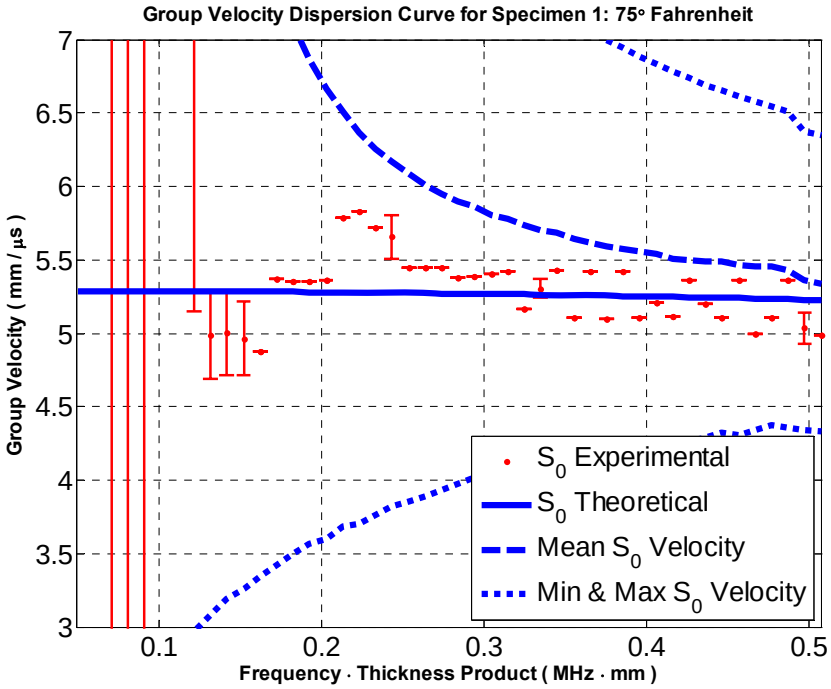

Figure 47: S_0 Group Velocity Dispersion Curve at 75°F

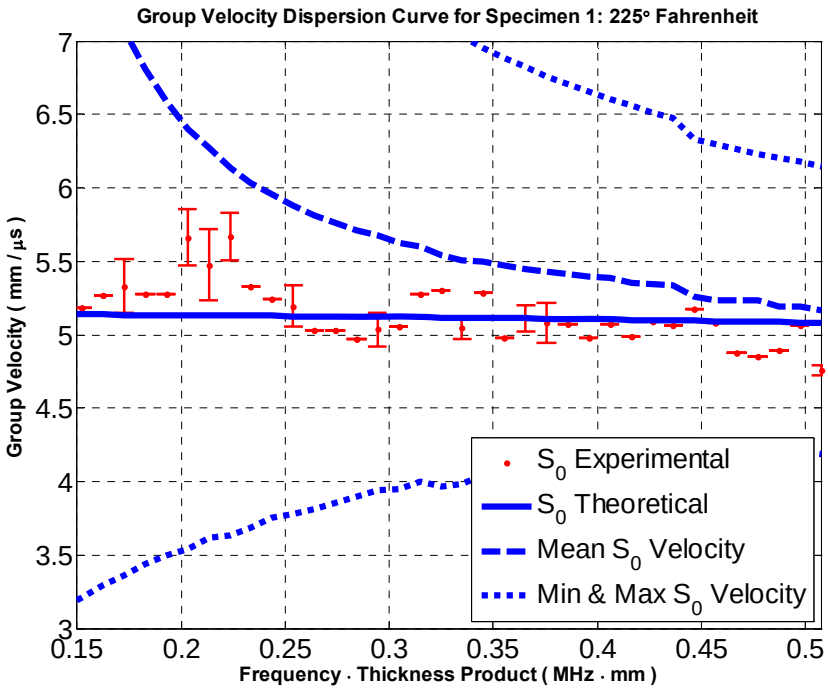

Figure 48: S_0 Group Velocity Dispersion Curve at 225°F

4.2 Specimen Support Testing

Before proceeding with the thermal gradient testing, the use of varying support conditions was examined. Supports were used to prevent specimen contact with other surfaces. Rubber supports were used during the oven testing on Specimen I. Since the supports were placed at the ends of the plate, they had no affect on the propagation path of the transmitted signals. In the case of Specimens II and III, a felt mat was placed under the plates to prevent direct contact with the table surface. The specimens were too large to suspend with end supports since the plates concaved in this situation. Since the felt placed under the specimens made direct contact with the entire surface of the plate there was potential for this type of support to adversely affect wave propagation.

In order to determine if there were any measurable changes in the S_0 responses due to these varying supports, Specimen I was used as a test case. It was placed on both felt and rubber supports outside of the oven, as shown in Figure 30 and Figure 32. Three wave propagation tests

were conducted using each support set-up. The mean results from these trials were compared to the mean results obtained from the oven-based tests at room temperature. These results are captured in Figure 49. In the analysis, the wave propagation plots showed no TOA differences and minimal waveform differences for signals propagated at 300 kHz and additional frequencies (refer to plots in Appendix C). However, there were visible differences between the group velocity dispersion curves in Figure 50, which meant that frequency signals that were not plotted would have revealed evidence of these TOF differences. Specifically, there were noticeably higher standard deviations in the range of 300-400 kHz for the felt support case. These results imply that the signals may have had interaction with the surface of the felt support, thus resulting in fluctuating signal or group velocities. Since these deviations were only based on three tests the analysis was limited in this area; hence, the use of varying supports needs to be explored further to confirm that the signals were not altered by some other cause such as user or equipment error. Since the specimen set-up was limited to the use of a felt support, the thermal gradient testing was continued despite these variations seen in the results.

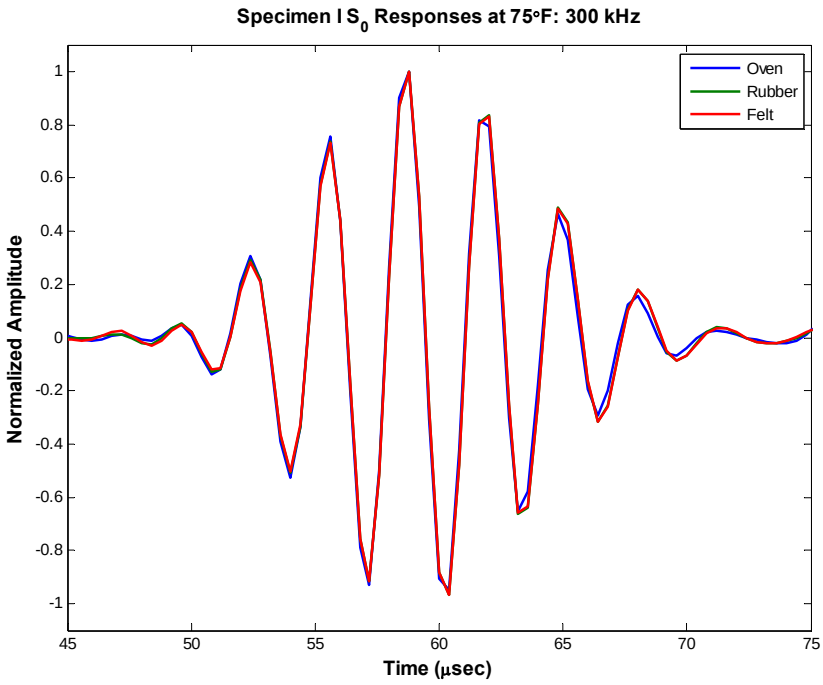

Figure 49: Specimen I S_0 Responses at 300 kHz for Varying Supports

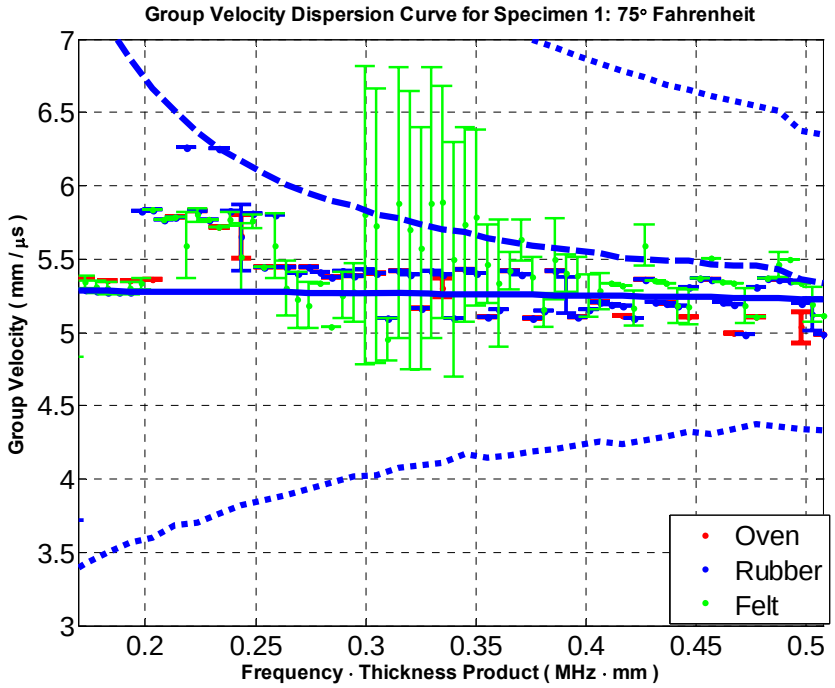

Figure 50: S_0 Group Velocity Dispersion Curve for Specimen I with Varying Supports

4.3 Thermal Gradient Testing

The objectives of the initial testing on Specimen II were to generate thermal gradients in the plate using the infrared heater and to capture their profiles using a thermal imaging camera and thermocouples. Since the thermal imaging camera was only available for use at AFIT, the specimen set-up was taken to AFIT's Vibrations Lab. Once the testing began, the infrared images captured by ThermaCAM were used to verify the data obtained by the thermocouples as seen in LabVIEW®. Since the initial data comparisons proved reliable, subsequent testing in the SHM Lab was conducted using thermocouples to quantify the gradient.

Figure 51 and Figure 52 were two images taken by ThermaCAM. The thermal imaging camera has the benefit of depicting the temperature profile across the whole plate, while thermocouples only provide point estimates. Since the heat lamp was placed approximately an inch above the center of the plate, in an effort to minimize radiation flow due to air, it was captured in the images and is the reason why the center of the images appears lower in temperature. In actuality, the midpoint of the plate was the hottest region of the gradient. The horizontal lines depicted in the figures were used to identify the center line along the specimen, since this line coincided with the propagation path during Lamb wave testing. The thermal gradient along this line appears symmetric with respect to the heater. Due to this fact, capturing thermal data for at least half of the gradient during testing was sufficient to characterize the entire gradient. Therefore, during subsequent testing on Specimen III thermocouples were only placed from the midpoint of the gradient, directly under the lamp, to the receiving transducer. The temperature range of the gradients depicted in the infrared images is depicted by the color scheme displayed in the legend to the right of the figures. Figure 51 captured the gradient developing, with a visibly high temperature near the lamp at approximately 150°F. In the second figure the gradient had increased approximately 20 degrees near the lamp and the overall gradient had spread further into the plate.

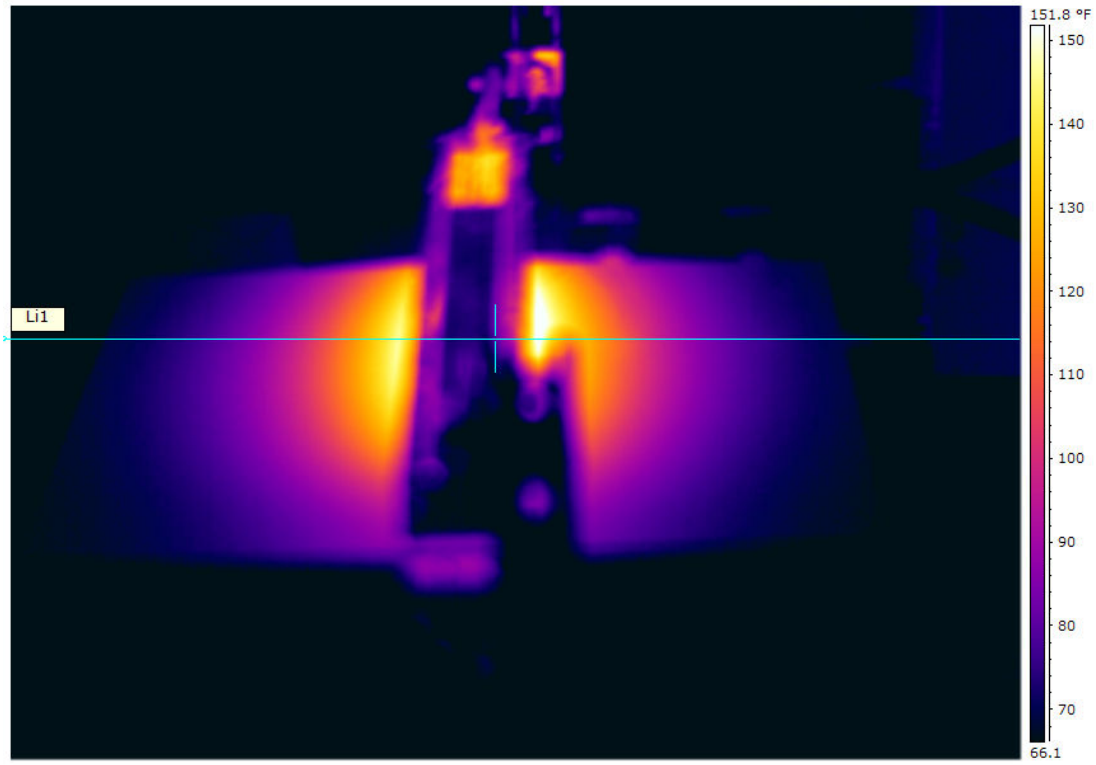

Figure 51: Specimen II Infrared Image I

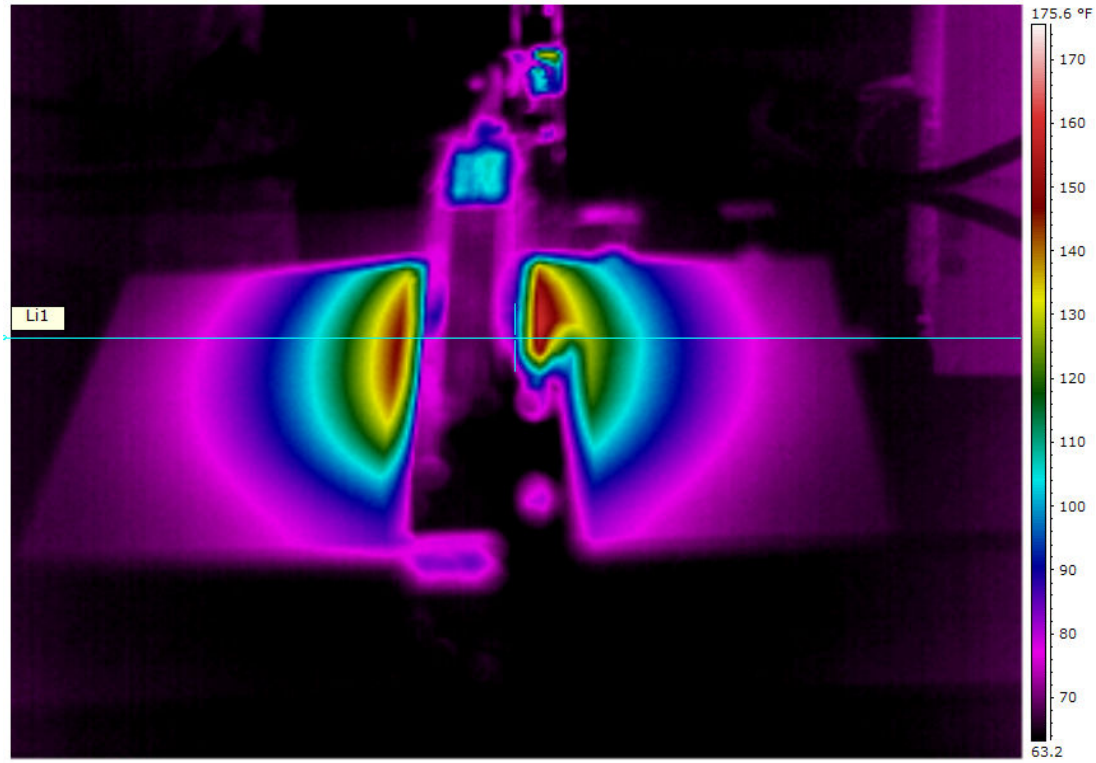

Figure 52: Specimen II Infrared Image II

During the first few thermal gradient tests trials, the plate bowed up due to elevated residual stresses in the aluminum plate. The black spray-paint was a contributing factor to the high amount of heat absorbed by the plate since there was little to no heat reflection off the specimen under these conditions. Due to this event, the thermal gradient tests were discontinued on Specimen II and the plate was taken back to the SHM Lab. No baseline wave propagation measurements were taken prior to the thermal gradient testing on Specimen II, so the post-bowing analysis was limited to comparisons between theoretical and post-bowing experimental wave propagation results conducted at room temperature.

As seen in Figure 53, the experimental S_0 responses arrived a few microseconds before the theoretical S_0 response; however, this was also seen in the theoretical versus experimental isothermal wave propagation results where no bowing occurred. Thus, there were no significant changes in the signal's TOF. The experimental waveform consisted of approximately eight cycles, as opposed to the five and half cycles seen in the theoretical waveform. The increased number of cycles in the experimental signal is likely due to the use of the data filter, as previously mentioned in the isothermal analyses. Additionally, when the experimental S_0 responses from Specimen II were compared to the experimental S_0 responses from the Specimen I tests under varying support conditions, it can be seen that the same frequency signals are almost identical in waveform; refer to Figure 54 and Figure 46. Since Specimen I did not undergo any gradient testing, and since the results were comparable to those of Specimen II, it can be suggested that any permanent deformation (plasticity) to the plate did not have observable effects on the Lamb wave propagation at room temperature. Although there were no observable effects on the Specimen I results due to the use of felt, the use of felt may have altered the Specimen II results due to the variation in thickness between the two specimens. Specimen II was 0.635 mm thick as opposed to Specimen I, which was 1.02 mm thick.

As a final comparison, a group velocity dispersion curve was generated using the experimental data and theoretical predictions as seen in Figure 55. The experimental group velocity values appeared slightly higher than expected, since the isothermal results generally fell around the theoretical group velocity predictions. The group velocity values from these tests primarily fell above the mean S_0 velocity threshold, whereas the results from the Specimen I tests fell closer to the theoretical S_0 line. Based on the scope of testing in this study, there was no way to determine if the use of felt as a support and long-term deformation would affect subsequent test results. Hence, testing on Specimen II was discontinued and Specimen III was used for additional thermal gradient experimentation. The differences between the two specimens were only their length and width dimensions.

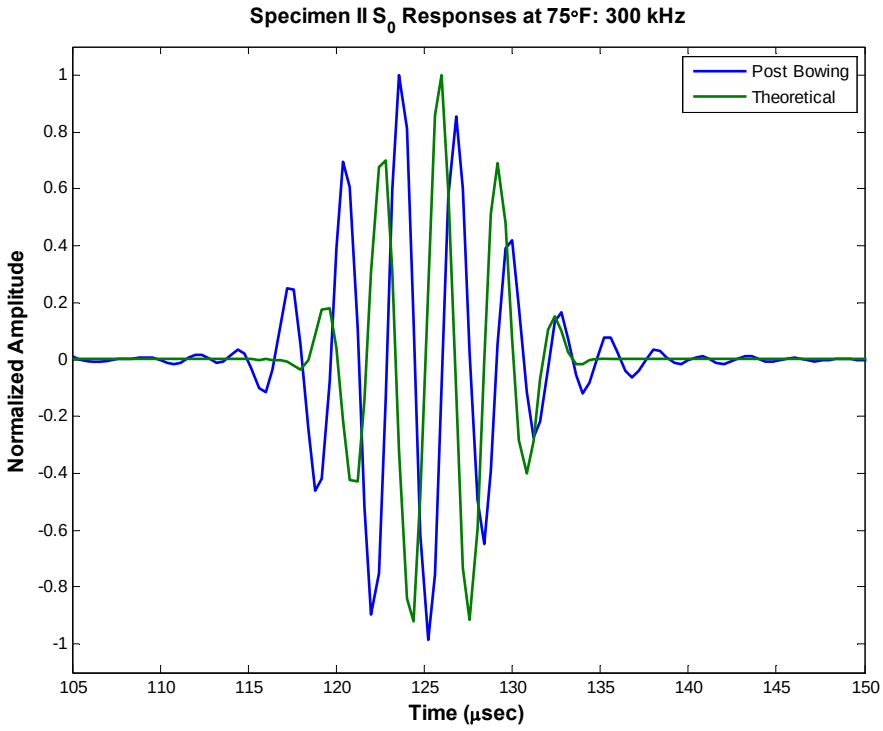

Figure 53: Specimen II Theoretical versus Experimental S_0 Response Comparison

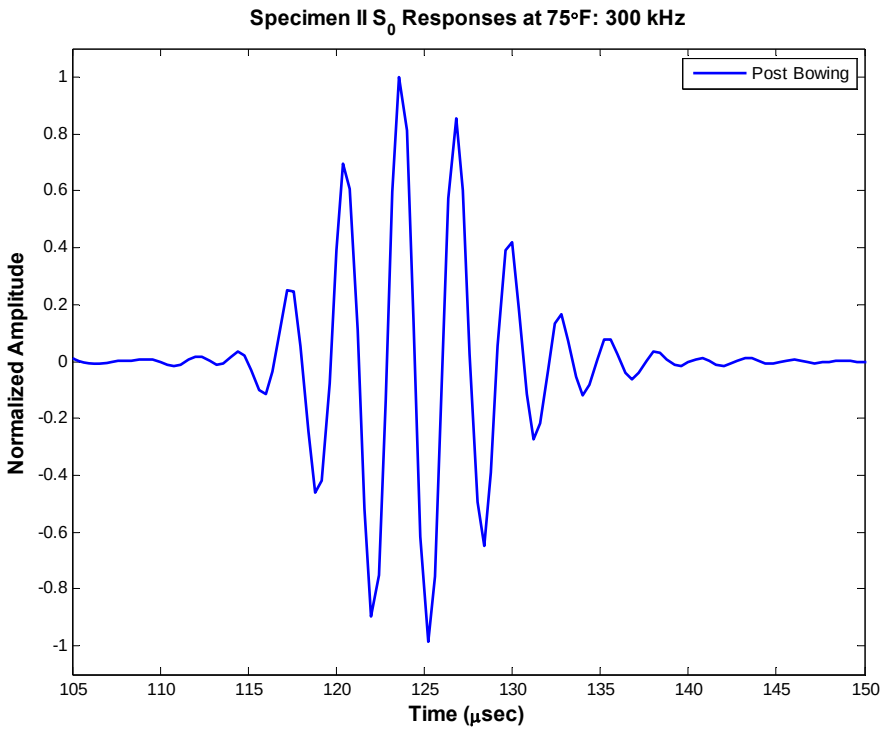

Figure 54: Specimen II S_0 Experimental Response

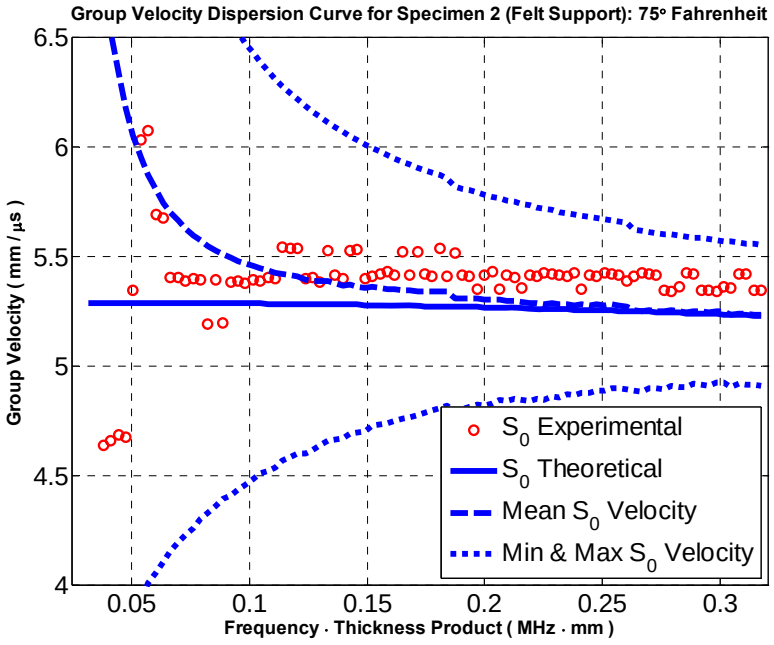

Figure 55: Specimen II Group Velocity Dispersion Curve (Post-bowing)

Before thermal gradient testing was initiated on Specimen III, baseline tests were conducted at room temperature. Figure 56, the pre-bowing group velocity dispersion curve for Specimen III, is similar to the post-bowing group velocity dispersion curve for Specimen II.

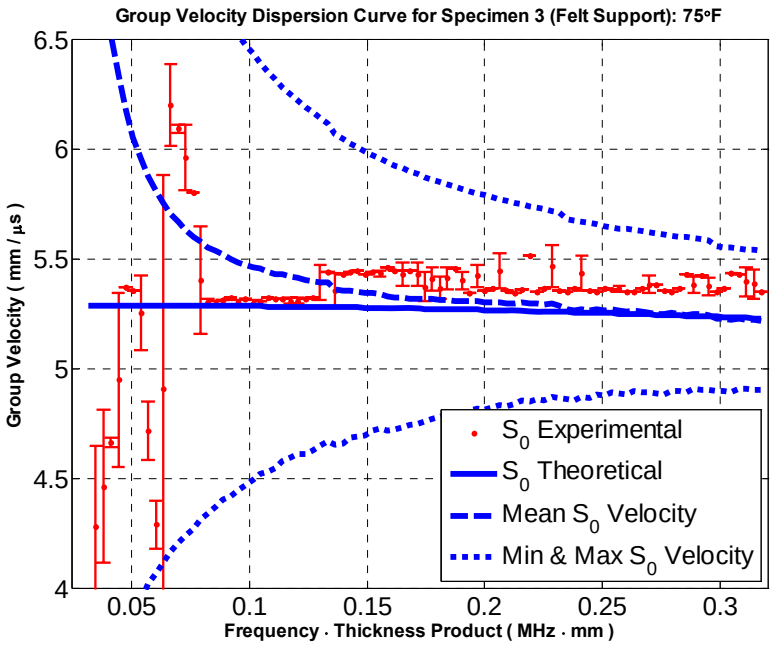

Figure 56: Specimen III Group Velocity Dispersion Curve (Pre-bowing)

Therefore, it can be further surmised that the long-term structural damage from bowing did not have observable effects on the Specimen II TOF calculations at room temperature. After support and bowing issues had been taken into consideration, one final concern was given to the placement of the thermocouples along the propagation path of the signals. Since Lamb waves are sensitive to small material defects, they could potentially show signs of sensitivity to any object attached to the surface of a plate. For that reason, wave propagation tests were conducted at room temperature with and without the thermocouples placed along the propagation path. Only five thermocouples were placed along the path during these tests. Later in the study, several more thermocouples were placed along the propagation path to characterize the thermal gradients.

Looking at Figure 57, there is a distinct change in the number of cycles at the end of the waveforms when compared to the theoretical waveform. The additional cycles are noticeably amplified and the transient nature of the waveforms lasted 10-15 microseconds longer than previous signal analyses. Since these differences are evident in both baseline tests, with and without the thermocouples placed along the propagation path, these changes are likely attributed to the use of a felt support. This analysis contradicts the analysis from the Specimen I tests, which showed no noticeable signal effects due to the use of a felt support. However, the thickness of Specimen III was approximately half the thickness of Specimen I; hence, the use of a much thinner specimen may have been the reason why these results were distinctly different. The S_0 response obtained from the thermocouple testing did exhibit slightly higher amplitudes for a few of the cycles in the transient response; thus, the effects of placing thermocouples along the signal's propagation path should not be overlooked. However, since the felt support had direct contact with the entire propagation path along the plate, as opposed to the thermocouples, it is more likely that any effects the thermocouples had on signal propagation were overshadowed by the effects of the felt.

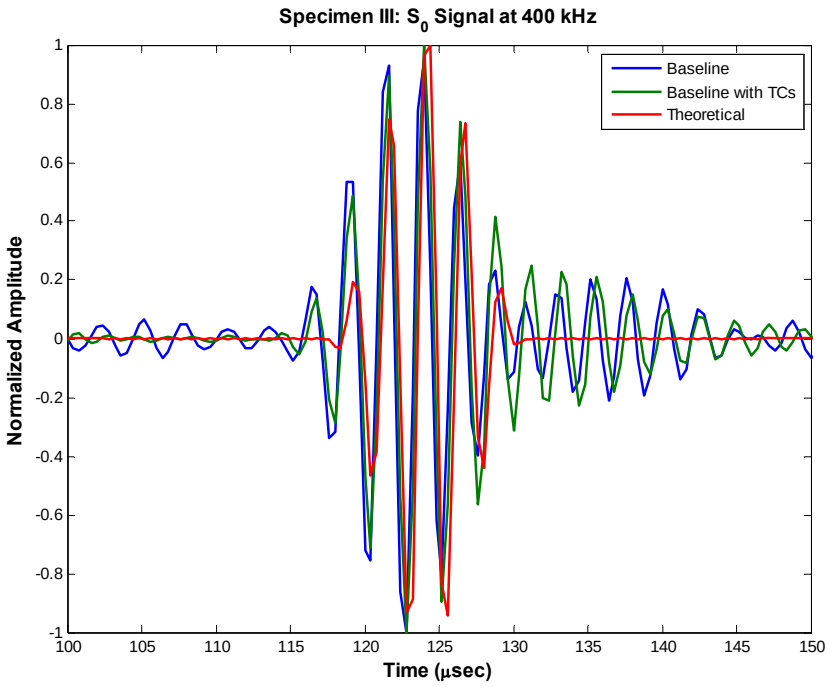

Figure 57: Specimen III S_0 Responses at 400 kHz - Thermocouple Placement Analysis

Knowing the potential effects on Lamb wave propagation due to the use of a felt support, long-term deformation in the specimen, and the placement of thermocouples along the propagation path, the gradient testing was continued. Additional changes in the S_0 responses could be attributed to the thermal gradient conditions and/or the occurrence of real-time bowing during the tests. The first few tests were run using five thermocouples placed along the propagation path (Figure 58). Once again, the heater was placed one inch above the specimen to create a sharp gradient in the plate. However, when the testing began the residual stresses in the plate were still significant enough to cause bowing for a second time in this study. The legend in the following figure captures two thermal gradients. One gradient, seen in green, was captured before the specimen began to bow. The second gradient, seen in red, was captured while the specimen was actively bowing.

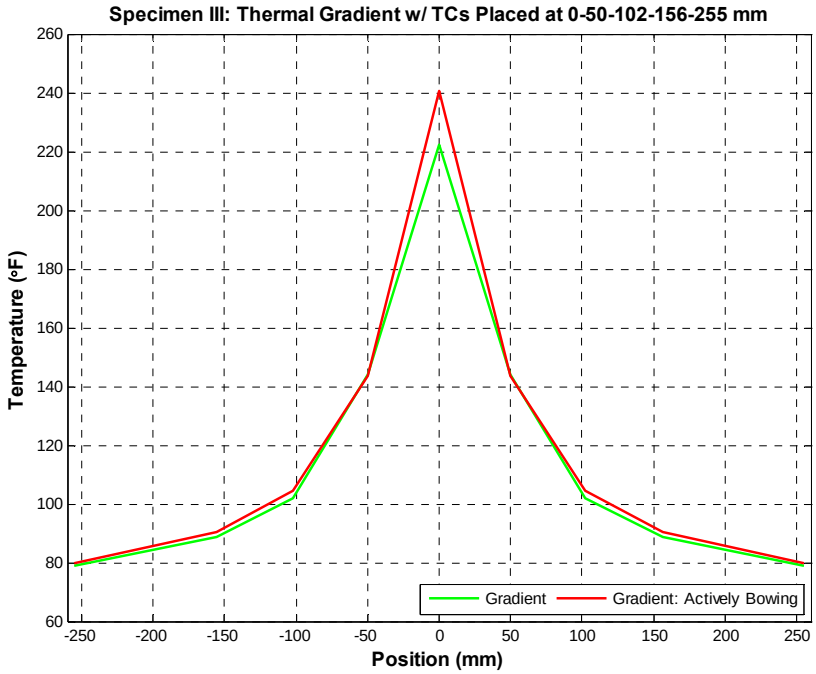

Figure 58: Specimen III Thermal Gradient Profiles Using Five Thermocouples

Before the final segment of gradient testing, additional wave propagation tests were run at room temperature to identify any observable changes to the transmitted signals due to deformation in the plate. These results were then compared to the baseline tests. The waveform changes observed in the baseline tests were apparent once again in the post-bowing analysis. Results from the post-bowing analysis confirmed amplification in some of the cycles trailing the primary waveform (i.e. the segment of the signal closely matching the theoretical waveform), both with and without the thermocouples attached to the specimen. Hence, deformation may have had a small effect on the signal responses, but once again the thermocouples did not appear to have any significant effect on the S_0 responses.

The thermal gradient profiles for the final segment of gradient testing are displayed in Figure 60. The abscissa values depict positions along the propagation path, with the center of the path at position zero. The point at -252 mm depicts the location of the actuating transducer and the point at 252 mm depicts the location of the receiving transducer. The lowest thermal gradient

captured had a peak temperature of approximately 114°F and the highest thermal gradient had a peak temperature of approximately 281°F. Refer to Table 8 for all of the peak temperatures.

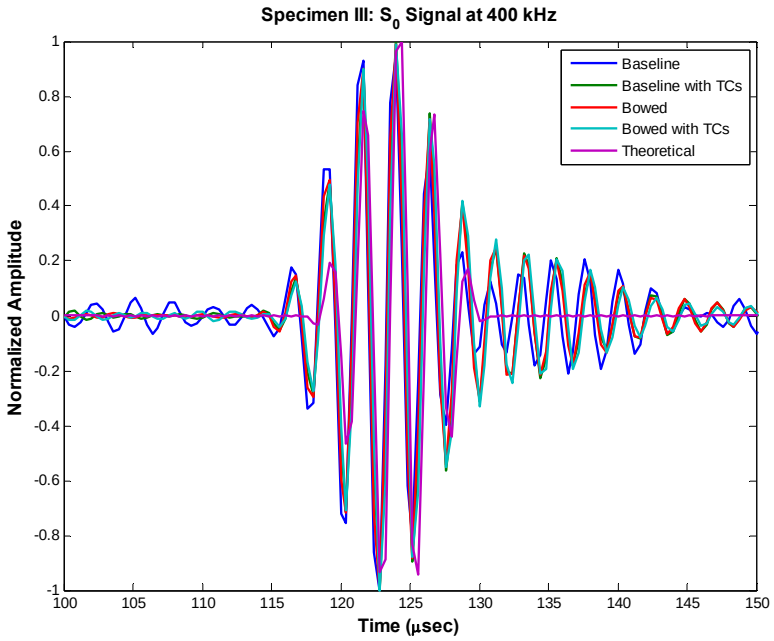

Figure 59: Specimen III Post-bowing S_0 Responses at 400 kHz

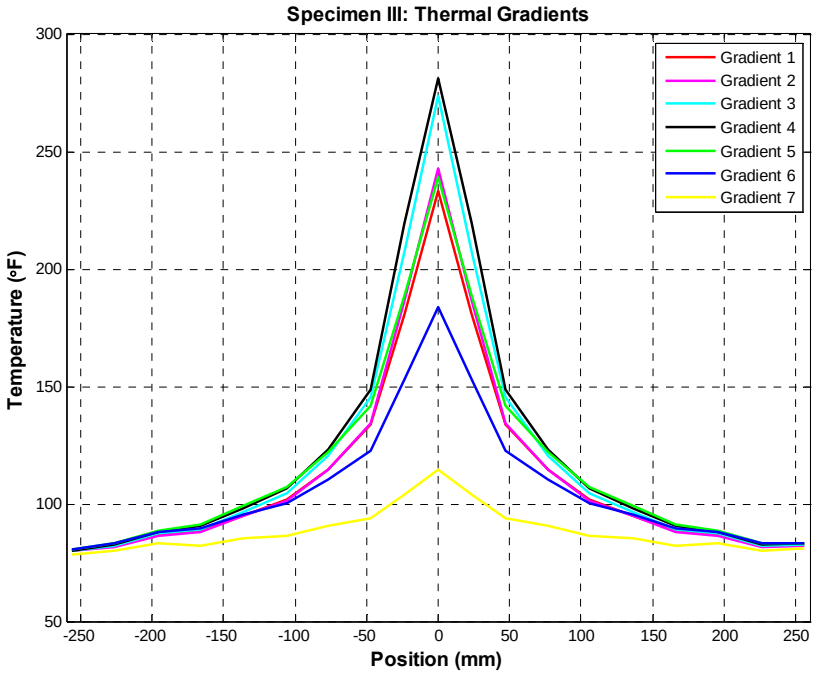

Figure 60: Specimen III Thermal Gradient Profiles Using 13 Thermocouples

Table 8: Thermal Gradient Peak Temperatures

Gradient	1	2	3	4	5	6	7
Peak Temperature (°F)	281	274	243	239	233	184	114

The following S_0 response plots captured the changes between signals at 450 kHz and 300 kHz, as seen in Figure 61 and Figure 62. Additional frequencies can be referenced in Appendix C. There is a noticeable delay in the S_0 responses obtained from all of the thermal gradient tests with respect to the baseline and post-bowing room temperature tests. However, the range of thermal gradients tested appeared to have the same effect on the TOA differences in the S_0 responses. Since the signals only traveled through an extremely heated region of the plate for roughly 20 microseconds, the minimal changes in group velocity were to be expected. It is more likely that wave propagation through an isothermally heated plate at these high temperatures would show greater changes in wave propagation speeds. An additional factor to consider was the occurrence of real-time bowing during all of the tests, which could have been a short-term contributing factor to the consistent delay observed in the signals.

Shifting from TOF to waveform observations, the added waveform cycles seen in the earlier tests were amplified once again in the high frequency signals. The waveform differences suggest that the sensitivity of the higher frequency signals to real-time bowing and/or thermal effects enhanced the amplification already seen in the post-bowing analysis. There were minimal changes in the frequency signals at roughly 350 kHz and below. Additionally, a perturbation appeared in the beginning of the baseline signal. The observed disturbance was attributed to noise in the signal. Generally, noise in the system is reduced by data averaging.

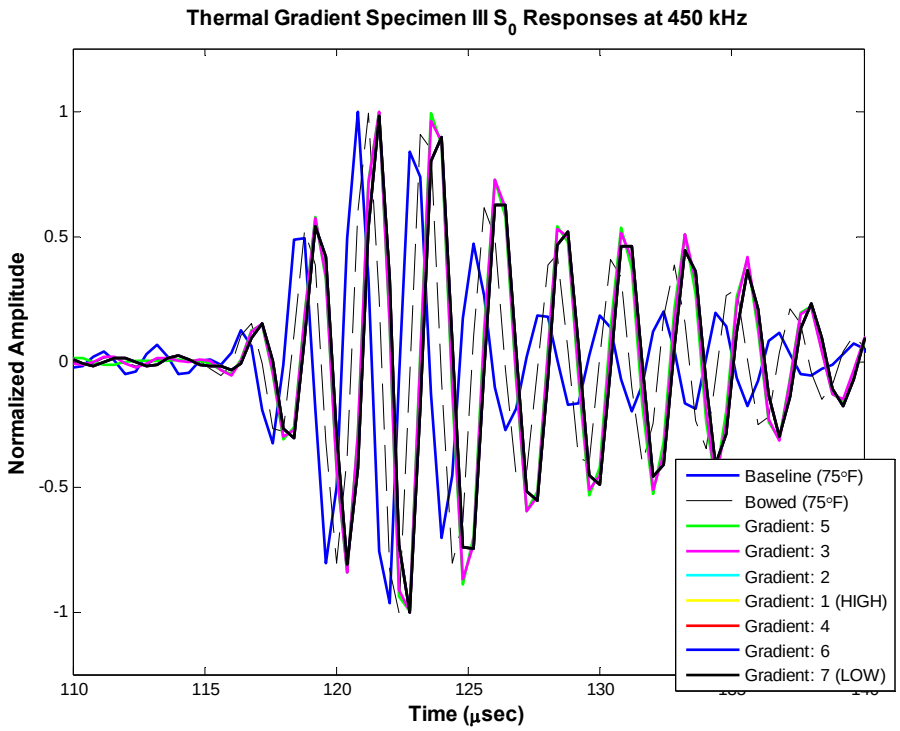

Figure 61: Specimen III Baseline versus Thermal Gradient S_0 Responses at 450 kHz

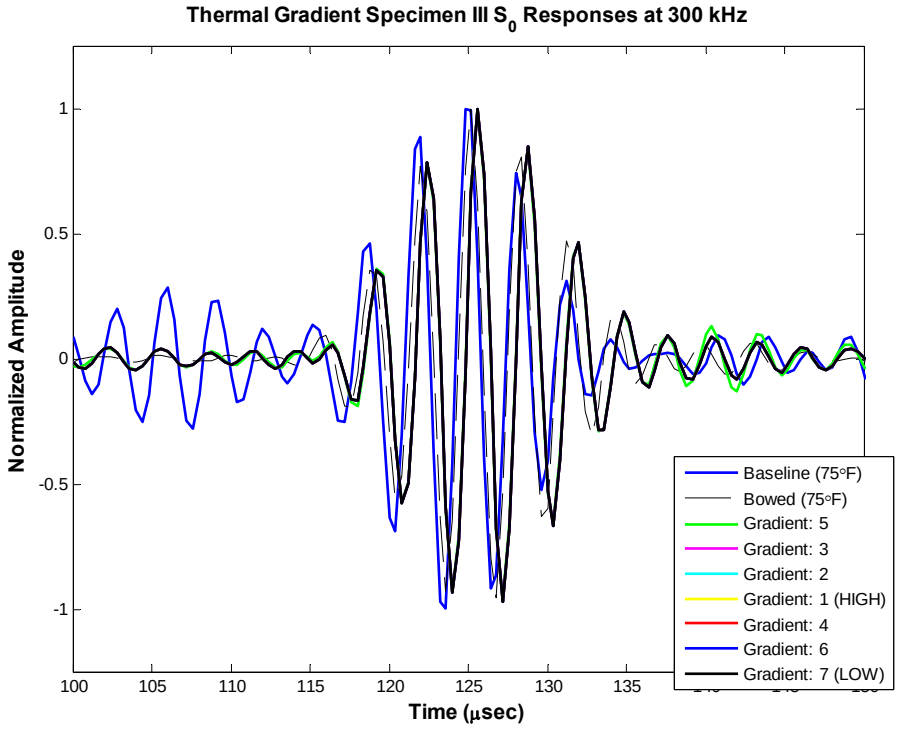

Figure 62: Specimen III Baseline versus Thermal Gradient S_0 Responses at 300 kHz

4.4 Theoretical Simulations at Elevated Temperatures

On a final note, a few theoretical predictions were run using Matlab® to demonstrate the potential affect of significantly higher temperatures on wave propagation in isothermal and thermal gradient environments. The isothermal results are captured in Figure 63. Although the theoretical S_0 responses are not sufficient in characterizing waveform changes in the signals, they do indicate significant TOA changes over increasing temperatures, as displayed in Table 9. Thus, further experimental research is necessary to verify these predictions. As an example, a Lamb wave propagated over a distance of 1000 mm in the temperature range of 600°F showed a 77.6 microsecond TOA difference when compared to a wave propagated at 75°F over this same distance. There was only a 5.6 microsecond TOA difference between waves propagated at 75°F and 225°F. The noticeable differences in time propagation are due to the reduction in the modulus of elasticity from 10E6 psi at 75°F to approximately 5E6 psi at 600°F.

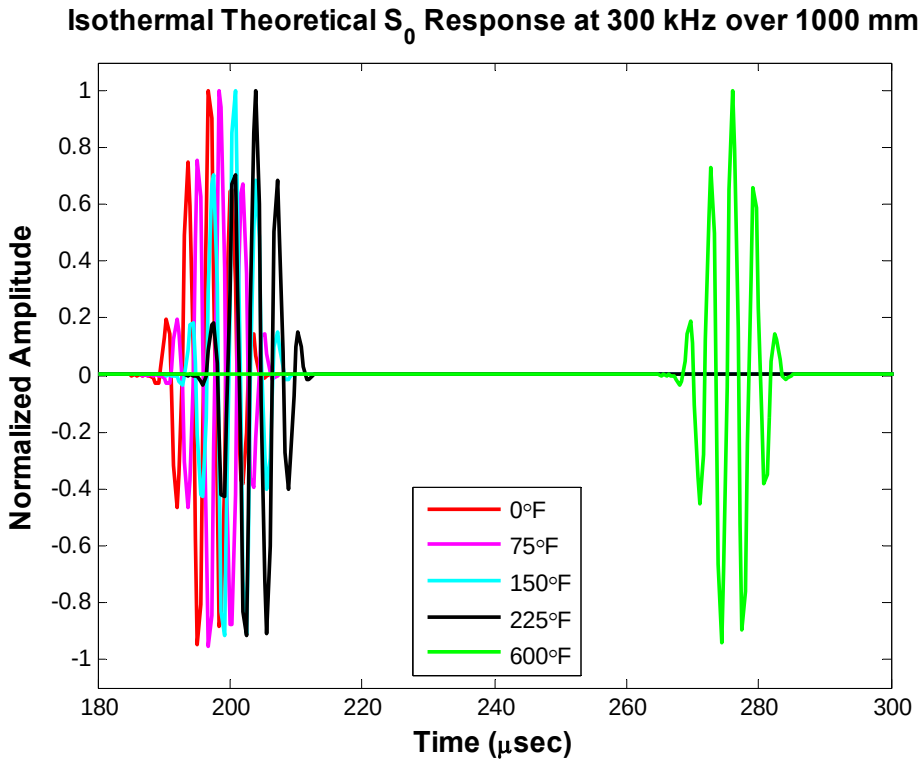

Figure 63: Isothermal Theoretical S_0 Responses at Elevated Temperatures over 1000 mm

Table 9: Theoretical S_0 Responses over Elevated Temperatures

Theoretical S_0 Response Signals		
Time Differences in Wave Propagation		
Distance(mm)	75-225°F	75-600°F
500	2.4 µsec	38.8 µsec
750	4 µsec	58 µsec
1000	5.6 µsec	77.6 µsec

The thermal gradient prediction was generated by segmenting the propagation path and sequentially propagating a new signal over each element, so the received signal at the end of one segment was established as the excitation signal over the following segment. Each element was subjected to new temperature conditions that were considered to be isothermal. The simulated gradient had a peak of 600°F and the actuator and receiver transducers were at room temperature (75°F). The temperature corresponding to the regions between the sensors and the heat source was 225°F. A simple plot of the gradient is displayed in Figure 64.

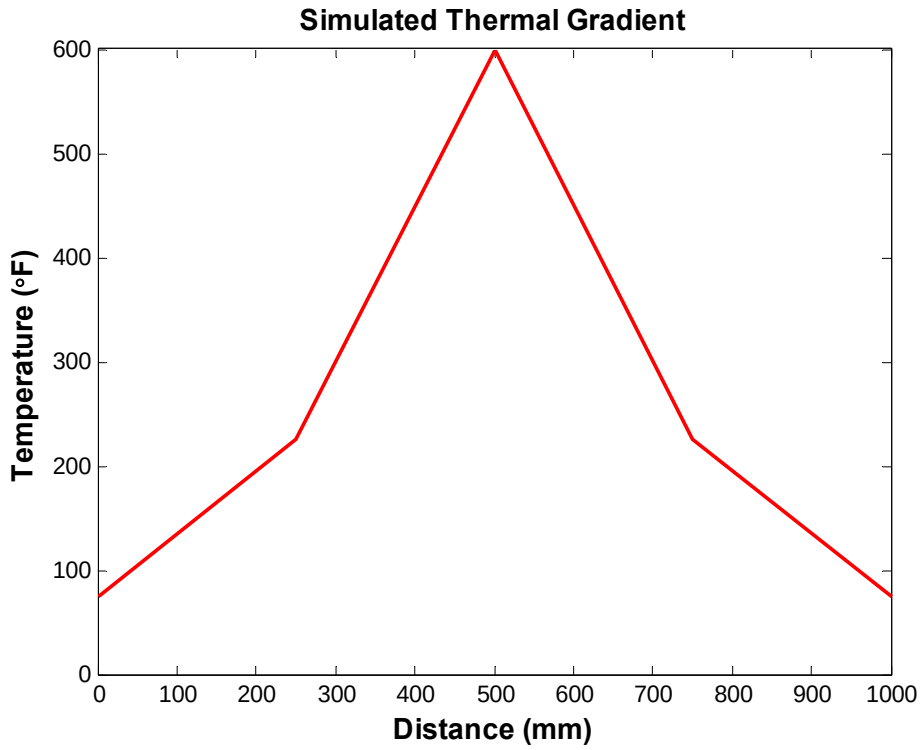

Figure 64: Simulated Thermal Gradient

As can be seen in Figure 65, the time difference was approximately 17.6 microseconds between a signal propagated at room temperature (75°F) and a signal propagated over this thermal gradient. Although the TOA difference for the thermal gradient simulation is not as high as the differences seen in the isothermal gradients, there is evidence that thermal gradients will affects Lamb wave propagation and must be taken into consideration in real-world SHM testing.

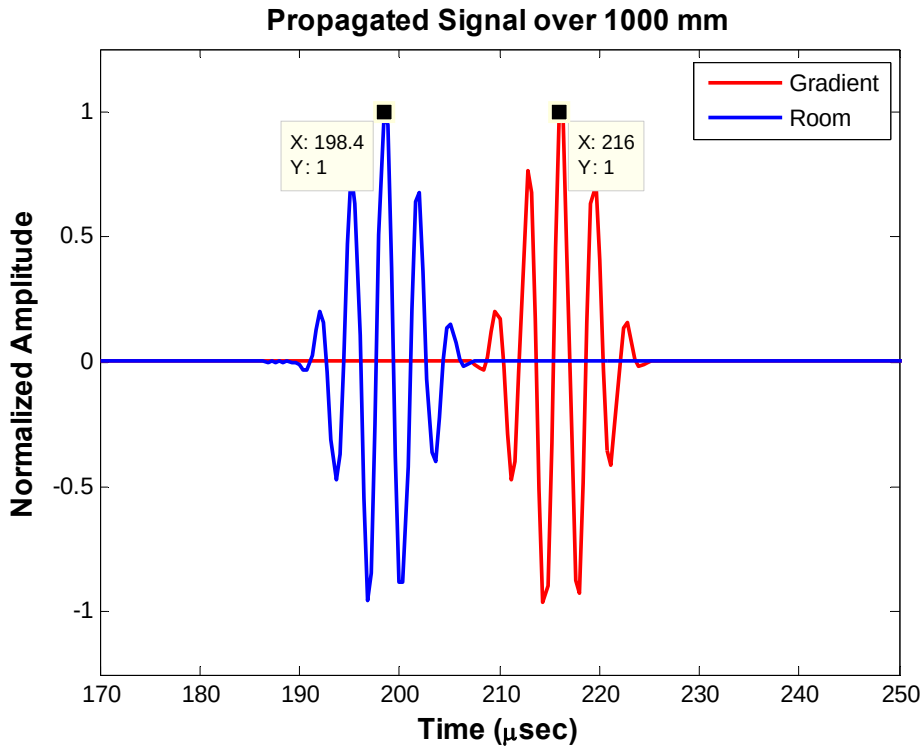

Figure 65: Theoretical Thermal Gradient S_0 Responses over 1000 mm

Additionally, a group velocity dispersion curve was generated from the thermal gradient simulation. Since the temperature and frequency-thickness product were known for each segment of the path, the theoretical group velocity could be determined for each segment. Additionally, since the propagation distance was known over each segment, a signal's TOF over a segment could be determined by dividing the propagation distance by the theoretical group velocity. At the end of the simulation, the individual TOF calculations were added together to obtain the total TOF for the response signal. The total TOF was divided by the full propagation distance of the

response signal to obtain an estimate of the signal's group velocity through the entire thermal gradient. Figure 66 captures group velocity dispersion curves for signals propagated over a thermal gradient and at 75°F, 225°F, and 600°F. As expected, the group velocities of the signals propagated over the thermal gradient have decreased due to the decrease in the modulus of elasticity. The thermal gradient curve is lower than the curves for 75°F and 225°F, yet much higher than the curve for 600°F. Since the signals were propagated over a temperature range primarily below 300°F, it was expected that the signals would not be significantly delayed over signals propagated at 225°F.

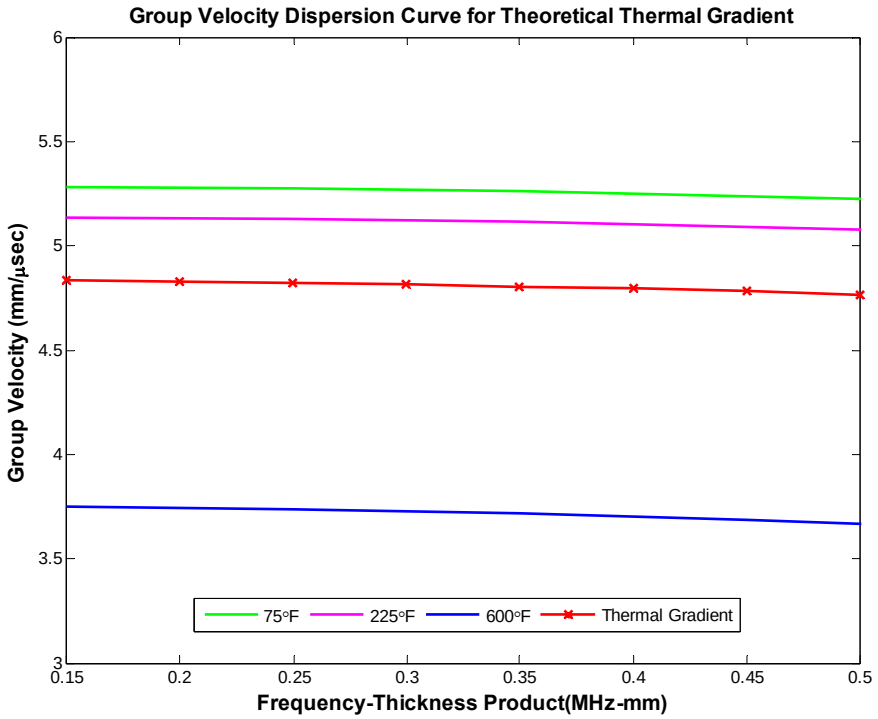

Figure 66: Theoretical Thermal Gradient Group Velocity Dispersion Curve (Peak: 600°F)

Chapter 5 Conclusions

The initial objective of this study was to quantify the sensitivity of Lamb wave propagation in an aluminum plate subjected to varying thermal environments. Specifically, the TOA, TOF, and the waveform of the signals were taken into consideration in this analysis. Experimental results validated theoretical predictions in the isothermal studies. Thermal gradient experiments were implemented independently of theoretical predictions; however, the experimental results showed similar delays in signal propagation over elevated temperatures. Essentially, if Lamb wave propagation is implemented in the SHM of aircraft subjected to thermal conditions ranging 0-225°F, ideally the wave propagation results will show minimal changes due to temperature. Finally, isothermal and thermal gradient simulations over longer distances and at much higher temperatures indicate that the change in a signal's TOA can be significantly altered under these conditions.

From the experimental results presented in Chapter 4, it is evident that elevated temperatures delay Lamb wave propagation. The parallel between the theoretical and experimental results from the isothermal tests demonstrated that theoretical predictions are excellent indicators for the TOA of a response signal, under these conditions, since the experimental results validated the theoretical predictions. However, there were some noticeable differences between the waveforms of the response signals due to the use of a data collection filter. At this point in time, the waveform differences were not accounted for theoretically since their effects on the experimental signals were not known until the concluding phase of this research.

Over the range of temperatures tested in this study, the theoretical versus experimental TOA differences were minimal (0.4-1.2 microseconds) and in some cases fell within the sampling error of the signals. The theoretical responses appeared to arrive slightly faster or at the same

time as the experimental response signals for higher frequencies. Similarly, these signals appeared to slow down when compared to the experimental responses for lower frequency signals. Overall, these minor fluctuations were on the order of a few samples and had minimal affects on the theoretical TOA predictions. Additionally, the resulting changes in group velocity were minimal, which was expected due to theoretical predictions from previous studies.

Time differences between the TOA for same frequency signals propagated at varying temperatures were fairly consistent between theoretical and experimental results. Although the temperature based differences were minimal, time delays were observed between theoretical signals and were on the same scale as the time differences observed between the experimental signals. Generally, the largest differences occurred between signals propagated at 0°F and 225°F.

One consistent observation throughout the thermal gradient testing was the sensitivity of the high frequency signals to changes along the wave propagation path. In the baseline thermal gradient tests, the S_0 responses at higher frequencies were altered from the waveforms observed in the isothermal tests. There was a significant increase in the number of cycles in the waveforms. Since these waveforms were also altered in the post-bowing analysis at room temperature, it was evident that either actual damage present in the material or the use of felt as a support distinctly affected the response waveforms. If the waveform changes were due to the support, this could be attributed to potential resistance (traction) between the surfaces. From the response signals acquired during the actual thermal gradient tests, delays in the TOA for all of the signals indicated that the signals were affected by the thermal gradient conditions. These results were similar to the isothermal test results. Additionally, the waveforms of the high frequency S_0 responses revealed the same increase in the number of cycles and over increasing temperatures these additional cycles were amplified when compared to the baseline and post-bowing room temperature results. A number of factors could have contributed to the amplification of these

cycles. The out-of-plane shape of the plate due to real-time bowing and elevated thermal conditions are two factors to take into consideration.

Lastly, the theoretical isothermal and thermal gradient predictions at temperatures up to 600°F indicated that much higher temperatures have a significant affect on the TOF for a signal. A significant reduction in Young's modulus is the factor contributing to these large time differences. Hence, conducting experimental investigations to validate theoretical predictions at these high temperatures is the next course of action in this line of research.

5.1 Impacts of Experimental Set-up

The experimental set-up had direct impacts on the research in this study. These impacts include the sampling rate, inductance between wiring, the specimen support set-up, and the use of thin specimens in thermal gradient testing. The first two concerns dealt with lab equipment. Since several of the TOA differences were under 0.8 microseconds, these values fell within the error of the sampling rate (± 0.8 microseconds). A higher sampling rate would reduce the sampling error, and the accuracy of the TOA measurements would increase. Secondly, using a higher sampling rate would better characterize signals at higher frequencies. The higher frequency signals (400-500 kHz) were not adequately characterized at a sampling rate of 2.5 MHz. The second issue dealing with the lab set-up was the occurrence of inductance between the wires transmitting the excitation and response signals. A test set-up using wires with better shielding would reduce the coupling between the excitation and response signals. In future studies, initial tests should be conducted to assure that these issues are minimized if not eliminated.

The last two impacts dealt with the specimen and its set-up. The use of felt as a specimen support posed a critical factor in the thermal gradient testing. In fact, the anomalies observed in the received waveforms were attributed to the placement of felt under the specimen. Hence, there is a need to establish a better support set-up for large specimens that must be placed horizontally.

A new set-up should only come into contact with the edges of a specimen and should not interfere with the intended signal propagation path. In this study, it was necessary to place the plate horizontally such that the heater could be placed over it; however, there was no existing set-up for horizontally placed specimens. One current set-up in the SHM Lab has a thin plate specimen vertically situated with a frame mounted around its edges and secured to the table. If a method is established to heat the plate vertically, this set-up can be used in future studies. Lastly, the use of a thin specimen in the gradient testing may have led to the early occurrence of bowing at the temperatures tested. The use of a thicker specimen to potentially offset bowing is advised for future testing. However, the thickness of the specimen should not exceed the wavelengths of the signals tested. Generally, the use of a thin specimen also requires Lamb wave testing at higher signal frequencies in order to generate the peak modal response or sweet-spot from a specimen. If the use of high frequencies is limited by the sampling rate, as it was in this study, then the specimen thickness must be increased to assure the frequency-thickness product generates this peak response.

5.2 Proposed Topics for Future Consideration

There are several areas in this study that have opened up avenues for future research. Beyond correcting the issues outlined in the previous section, some of the future work areas include conducting analyses on the A_0 response, testing Lamb wave propagation at higher temperatures, using larger ovens for isothermal testing, automating experimental thermal gradients, and predicting Lamb wave propagation in thermal gradient environments using theoretical methods. To begin with, only the S_0 response was considered for analysis in this study. In future studies, the effects of varying thermal environments on the A_0 response should be taken into consideration. Since symmetric and anti-symmetric wave modes provide varying feedback in damage identification, understanding their differences under varying temperature conditions should also be taken into consideration.

If the primary objective is to continue testing Lamb wave propagation at elevated temperatures exceeding 225°F, piezoelectric transducers and adhesives that can withstand temperatures in the range of 600°F are currently available for purchase (http://www.piezo-kinetics.com). The SHM Lab is currently purchasing these transducers for future studies that will deal with elevated thermal environments. Once the effects of varying thermal environments on Lamb wave propagation are characterized experimentally, the next step would be to test Lamb wave damage detection in real-world environments. If the location and severity of a defect can be determined in a thermally variant environment, then substantial progress has been made in characterizing the behavior of Lamb waves.

If future studies necessitate isothermal and thermal gradient testing, the use of a larger oven is recommended for isothermal testing. This would enable the use of a larger specimen that could potentially be used in subsequent thermal gradient testing, thus allowing the use of only one specimen per study. An additional benefit of using larger specimens is that the signal propagation distance will increase while minimizing boundary reflections in the received signals. Since the purpose of using Lamb waves is to detect structural defects over large areas and long distances, the use of a large plate specimen ensures that in-house testing is relevant to real-world applications.

In future thermal gradient testing, establishing an automated method to generate experimental thermal gradients will ensure repeatability in the Lamb wave propagation results. Additionally, theoretically characterizing Lamb wave propagation in thermal gradient environments will provide useful if the results can be experimentally verified. One theoretical approach was initiated in this study. Another approach would involve taking the average temperature of an experimental thermal gradient, simulating wave propagation at this constant temperature, and comparing these wave propagation results to results obtained from actual thermal gradient tests. If the results are similar, it can be demonstrated that simply approximating

the average temperature of a thermal gradient is sufficient in characterizing Lamb wave propagation through a thermal gradient region.

The affects of varying thermal environments on Lamb wave propagation have been touched upon in this study using both theoretical and experimental methods. However, only a few studies prior to this research conducted both theoretical and experimental tests over varying thermal conditions. In the future, using experimental investigations to validate theoretical simulations is highly recommended. Additionally, these tests should be more closely aligned with the extreme conditions of real-time environments. Ultimately, the complexities of this research will require several more in-house studies and increased collaboration between experts in the SHM field.

APPENDIX A: TECHNICAL TERMS

Amplitude: The peak magnitude reached in a wave cycle.

Attenuation: The combined effect of scattering and absorption is called attenuation. Scattering is the reflection of the sound in directions other than its original direction of propagation. Absorption is the conversion of the sound energy to other forms of energy. Ultrasonic attenuation is the decay rate of the wave as it propagates through material (11).

Asymmetric Mode: The asymmetrical Lamb wave mode is often called the "flexural mode" because a large portion of the motion moves in a normal direction to the plate, and a little motion occurs in the direction parallel to the plate. In this mode, the body of the plate bends as the two surfaces move in the same direction (11).

Bulk Waves: Waves that travel within the interior or bulk of a material (i.e. away from the boundaries) (21:101).

Component Wave: A wave traveling at a single frequency.

Dispersion: The frequency dependence of wavespeed, manifests itself in a waveform which stretches or shrinks in time. It can be analyzed in the time domain through zero-crossing or in the frequency domain through the phase spectrum (15:93).

Dispersion Curve: The relation between wavespeed and frequency (15:47).

Elastic Wave: A wave that carries changes in stress and velocity of the medium through which it propagates (15:9).

Excitation Pulse: A high voltage signal, or main bang, sent out electrically to excite a transducer. It originates from a pulse generator and is amplified by a power amplifier (15:75).

Free Plate: The geometry of a free plate problem simply contains the x_1 (longitudinal) and x_3 (transverse) directions where the surfaces of a plate $\pm h$ are traction free (21:103). Hence,

the plate has no supports or boundary conditions. Note: the thickness of the plate is $2h$ in the x_3 direction.

Frequency: The number of oscillations per unit of time (f) (15:15).

Path Length: The distance of a wave's propagation path.

Gait: A time interval, or window, is selected to ensure that only the event of interest in a pulse is examined (15:90).

Group Velocity: Group Velocity is associated with the propagation velocity of a group of waves of similar frequency (21:17).

Group Wave: Waves traveling in the same direction at differing speeds and frequencies interact constructively to form a group wave (15:45-46).

Guided Wave: Similar to bulk waves; however, when the guided wave problem is solved it must include some physical boundary conditions (21:101).

Hanning-window: A general purpose window for use with random signal analysis. Windows are used to reduce leakage when a signal is not periodic. Essentially, windowing a time signal forces the signal to zero at the beginning and end of a period thus eliminating discontinuities across samples (1).

Impedance: Acoustic impedance (z) relates the amplitudes of stress (σ) and velocity (v)in a wave (i.e. $\sigma = zv$). It is a product of the density (ρ) and wavespeed (c). If wavespeed is dependent on frequency, then the relationship can only be applied to individual frequency components (15:16).

Isotropic Material: A material that has not directional dependence. It has two independent elastic constants, commonly Young's Modulus and Poisson's ratio (15:20).

Lamb Wave: Waves of plane strain that occur in a free plate. The traction forces must vanish on the upper and lower surface of the plate (21:101-102).

Lamb Wave Propagation: Wave motion associated with a traction-free homogeneous and isotropic plate (21:101).

Phase Velocity: The wavespeed, or speed at which a wave moves. It is determined by the material properties, the body shape, and sometimes the frequency. If it is independent of frequency, it is equivalent to the group velocity. For non-isotropic materials, the phase velocity depends on the direction of propagation (15:16,170).

Piezoelectric Transducer: The piezoelectric (pz) effect creates a mechanical stress in a pz material, usually a crystal (i.e. lead zirconate (PZT)) when an electric field is applied as a voltage across it, or conversely. An oscillating voltage produces an oscillating stress which excites propagating oscillatory waves. High-frequency transducers are sometimes made of small deposits of pz material (15:66-67).

Pitch-Catch: One transducer actuates a signal and a second transducer receives the transmitted signal.

Plane Strain: There are no displacements in the x_3 direction (i.e. $u_3(x_3) = 0$). Therefore, there is a state of plane strain in the OX_1/OX_2 plane (22).

Pulse-Echo (PE): A wave is emitted from a transducer on a surface of an object to be examined, and its echo (i.e. reflection from another surface) is detected by the same transducer at a later time, after the wave has passed through the body and returned. This method is viable for use on thick specimens (15:70).

Rayleigh Waves: Free waves on the surface of a semi-infinite solid. Traction forces must vanish on the boundary, and the waves must decay with depth (21:101).

Semi-infinite Solid: A solid with a boundary and one dimension that is considered to be infinitely long. This is similar to having an axis with one direction of positive numbers and another axis with directions of positive and negative numbers.

Spectrum: Collection of amplitudes of several component waves. If the component waves are superimposed, they create a waveform (15:16).

Superposition: Superposition occurs when component waves that have the same phase superimpose and interfere constructively to form a wave of increased amplitude (15:169).

Symmetric Mode: Symmetrical Lamb waves move in a symmetrical fashion about the median plane of the plate. This is sometimes called the extensional mode because the wave is "stretching and compressing" the plate in the wave motion direction. Wave motion in the symmetrical mode is most efficiently produced when the exciting force is parallel to the plate (11).

Time of Flight (TOF): (1) The time taken for a wave to travel a designated path, or travel time. It is the difference between the onset time of the inserted wave and that of the received wave (15:90). (2) The time difference between the initial bang and the wave-package arrival represents the time-of-flight. The TOF is consistent with the distance traveled by the wave (5).

Time Period: The time taken for one oscillation ($T = 1/f$) (15:15).

Transducer: A device which converts one form of energy into another (i.e. electrical energy into mechanical energy, and vice versa) (15:65).

Transverse Motion: Motion in the z-direction, transverse to the x-y plane (15:167).

Ultrasonics: The science and exploitation of elastic waves in solids, liquids, and gases, which have frequencies above 20 kHz (15:1).

Waveform: The sequence in time of the motions of a wave, which can change by dispersion and attenuation (15:9,89).

Wavelength: The distance occupied by one spatial cycle of the wave at an instant of time (λ) (15:15).

Wavenumber: The number of radians in one cycle ($k = 2\pi/\lambda$) (15:15).

Wave Packet: A group of spatially localized waves that propagate together.

Wave Propagation: The movement of a wave through a medium.

Wavespeed: See phase velocity.

Windowing: Selecting a portion of a signal for analysis. The signal is truncated before and after preset times (15:100).

APPENDIX B: SOLUTION TO 1-D WAVE EQUATION

Forward Propagating Solution to the 1-D Equation

The solution *f(x-vt)* satisfies the 1-D wave equation as demonstrated below.

The first step involves taking the second derivative of the solution with respect to x.

$$\frac{\partial^2 f}{\partial x^2} = f''(x - vt)$$

The second derivative is then taken with respect to t.

$$\frac{\partial^2 f}{\partial t^2} = f''(x - vt)v^2$$

The original 1-D wave equation is manipulated to get all terms on the left hand side.

$$\frac{\partial^2 f}{\partial x^2} - \frac{1}{v^2}\frac{\partial^2 f}{\partial x^2} = 0$$

Once the terms are substituted in, it is evident that the solution satisfies the 1-D equation.

$$\therefore f''(x - vt) - \frac{1}{v^2} f''(x - vt)v^2 = 0$$

APPENDIX C: TABLES AND FIGURES

Table 10: Length of One Cycle for Specimen I Excitation Signals

Length of One Cycle for Excitation Signals: Specimens I (mm)											
Frequency (kHz)	**0°F**	**25°F**	**50°F**	**75°F**	**100°F**	**125°F**	**150°F**	**175°F**	**190°F**	**225°F**	**600°F**
150	35.54	35.39	35.34	35.23	35.12	35.01	34.84	34.67	34.55	34.27	25.01
200	26.65	26.54	26.50	26.42	26.33	26.25	26.12	25.99	25.90	25.69	18.75
250	21.31	21.22	21.19	21.13	21.06	21.00	20.89	20.79	20.72	20.55	14.99
300	17.75	17.68	17.65	17.60	17.54	17.49	17.40	17.32	17.26	17.12	12.49
350	15.21	15.15	15.12	15.08	15.03	14.98	14.91	14.84	14.79	14.66	10.69
400	13.30	13.25	13.23	13.19	13.14	13.10	13.04	12.98	12.93	12.82	9.34
450	11.82	11.77	11.75	11.71	11.68	11.64	11.58	11.53	11.49	11.39	8.29
500	10.63	10.58	10.57	10.53	10.50	10.47	10.42	10.37	10.33	10.24	7.45

Table 11: Length of Specimen I 5.5 Cycle Hanning-window Excitation Signals

Length of 5.5 Cycle Hanning-window Excitation Signals: Specimen I (mm)											
Frequency (kHz)	**0°F**	**25°F**	**50°F**	**75°F**	**100°F**	**125°F**	**150°F**	**175°F**	**190°F**	**225°F**	**600°F**
150	195.45	194.67	194.35	193.77	193.16	192.57	191.61	190.68	190.02	188.48	137.56
200	146.55	145.96	145.72	145.29	144.83	144.39	143.67	142.97	142.47	141.32	103.12
250	117.20	116.74	116.54	116.20	115.83	115.48	114.90	114.34	113.94	113.02	82.47
300	97.63	97.24	97.08	96.79	96.49	96.20	95.71	95.25	94.92	94.14	68.69
350	83.65	83.32	83.18	82.93	82.67	82.42	82.00	81.60	81.32	80.65	58.82
400	73.15	72.86	72.74	72.53	72.30	72.08	71.71	71.36	71.12	70.52	51.40
450	64.99	64.73	64.62	64.43	64.22	64.03	63.70	63.39	63.17	62.64	45.61
500	58.45	58.21	58.12	57.94	57.76	57.58	57.29	57.01	56.81	56.33	40.97

Table 12: Duration of 5.5 Cycle Hanning-window Excitation Signals

Excitation Signal	
Frequency (kHz)	**Duration (μsec)**
150	36.67
200	27.50
250	22.00
300	18.33
350	15.71
400	13.75
450	12.22
500	11.00

Table 13: Length of One Cycle for Specimens II and III Excitation Signals

Length of One Cycle for Excitation Signals: Specimens II & III (mm)											
Frequency (kHz)	**0°F**	**25°F**	**50°F**	**75°F**	**100°F**	**125°F**	**150°F**	**175°F**	**190°F**	**225°F**	**600°F**
150	35.55	35.40	35.35	35.24	35.13	35.02	34.85	34.68	34.56	34.28	25.03
200	26.66	26.55	26.51	26.43	26.34	26.26	26.13	26.00	25.91	25.70	18.77
250	21.32	21.24	21.20	21.14	21.07	21.01	20.90	20.80	20.73	20.56	15.01
300	17.76	17.69	17.66	17.61	17.56	17.50	17.42	17.33	17.27	17.13	12.50
350	15.22	15.16	15.14	15.09	15.05	15.00	14.92	14.85	14.80	14.68	10.71
400	13.32	13.27	13.24	13.20	13.16	13.12	13.06	12.99	12.95	12.84	9.37
450	11.84	11.79	11.77	11.73	11.70	11.66	11.60	11.55	11.51	11.41	8.33
500	10.65	10.61	10.59	10.56	10.53	10.49	10.44	10.39	10.35	10.27	7.49

Table 14: Length of Specimens II and III 5.5 Cycle Hanning-window Excitation Signals

Length of 5.5 Cycle Hanning-window Excitation Signals: Specimens II & III (mm)											
Frequency (kHz)	**0°F**	**25°F**	**50°F**	**75°F**	**100°F**	**125°F**	**150°F**	**175°F**	**190°F**	**225°F**	**600°F**
150	195.50	194.72	194.40	193.83	193.22	192.63	191.66	190.73	190.07	188.52	137.69
200	146.60	146.02	145.78	145.35	144.89	144.45	143.72	143.03	142.53	141.37	103.21
250	117.27	116.80	116.61	116.26	115.89	115.54	114.96	114.40	114.01	113.08	82.53
300	97.71	97.32	97.16	96.87	96.56	96.27	95.78	95.32	94.99	94.22	68.76
350	83.73	83.40	83.26	83.01	82.75	82.50	82.09	81.69	81.40	80.74	58.92
400	73.25	72.96	72.84	72.62	72.39	72.17	71.81	71.46	71.21	70.63	51.54
450	65.10	64.84	64.73	64.54	64.34	64.14	63.82	63.51	63.29	62.77	45.80
500	58.57	58.34	58.24	58.07	57.89	57.71	57.42	57.14	56.94	56.48	41.20

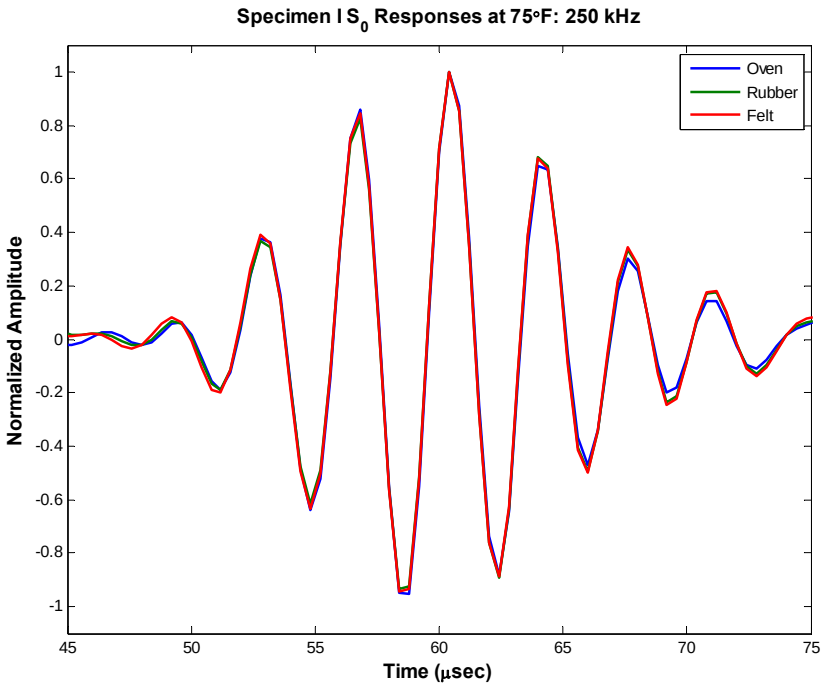

Figure 67: Specimen I S_0 Responses at 250 kHz for Varying Supports

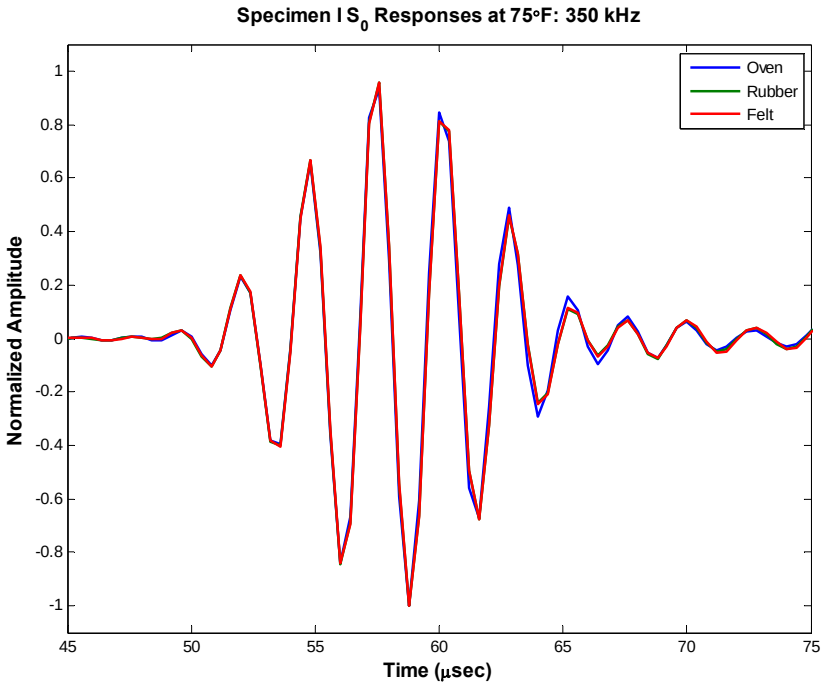

Figure 68: Specimen I S_0 Responses at 350 kHz for Varying Supports

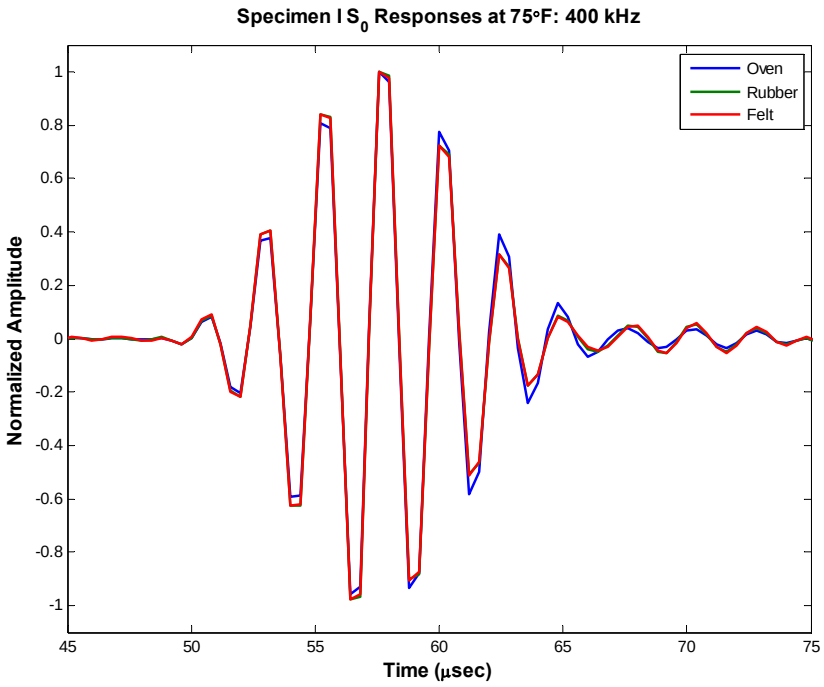

Figure 69: Specimen I S_0 Responses at 400 kHz for Varying Supports

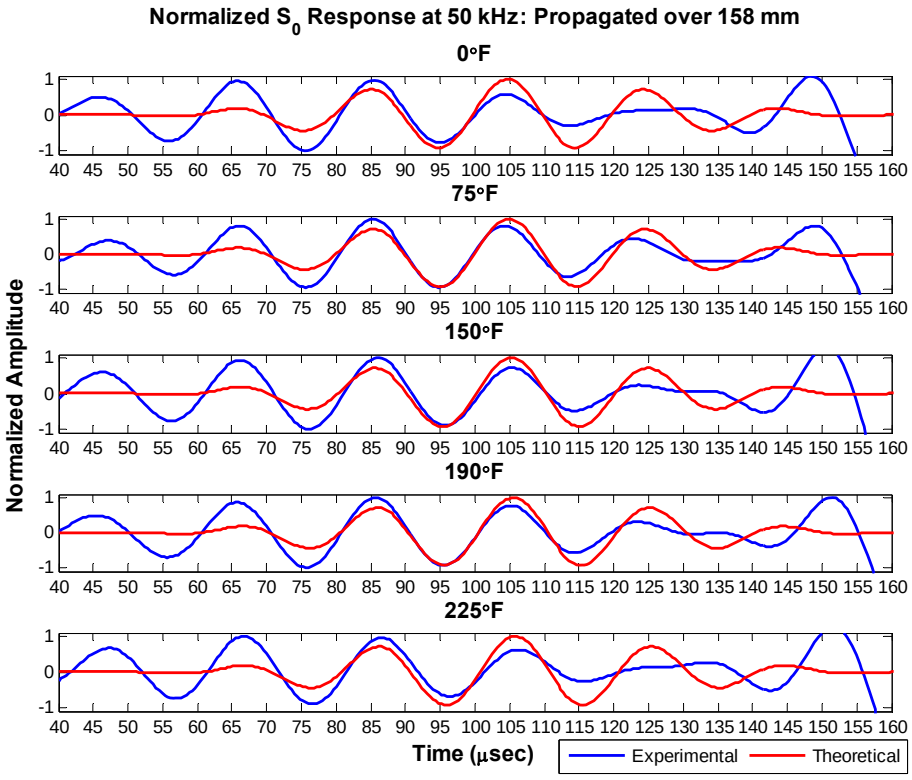

Figure 70: Experimental versus Theoretical S_0 Response at 50 kHz

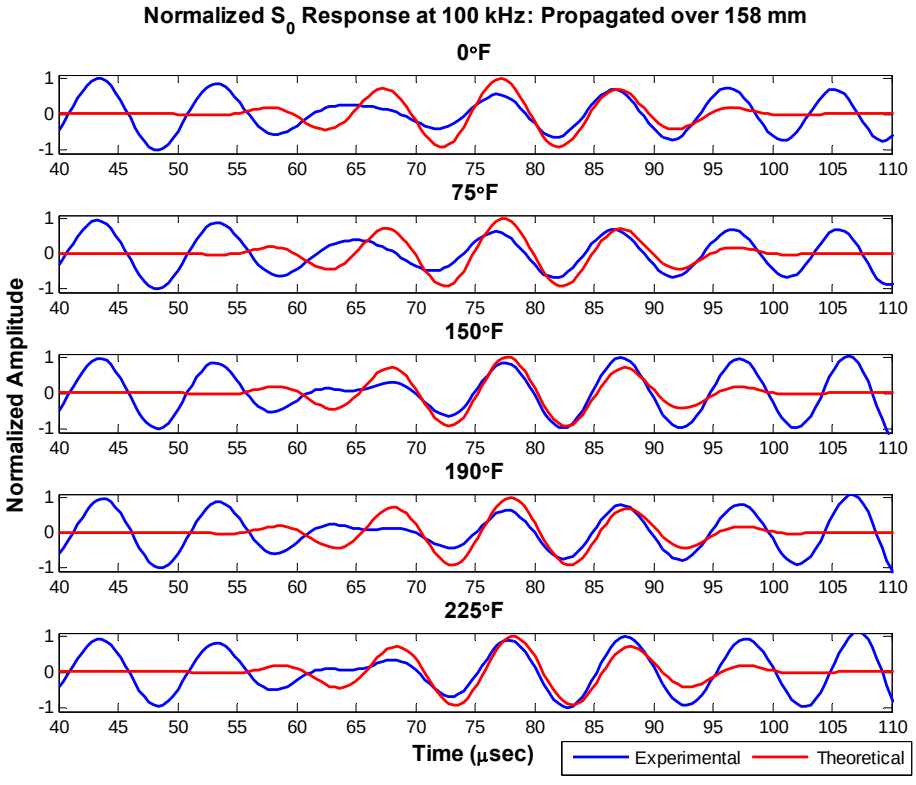

Figure 71: Experimental versus Theoretical S_0 Response at 100 kHz

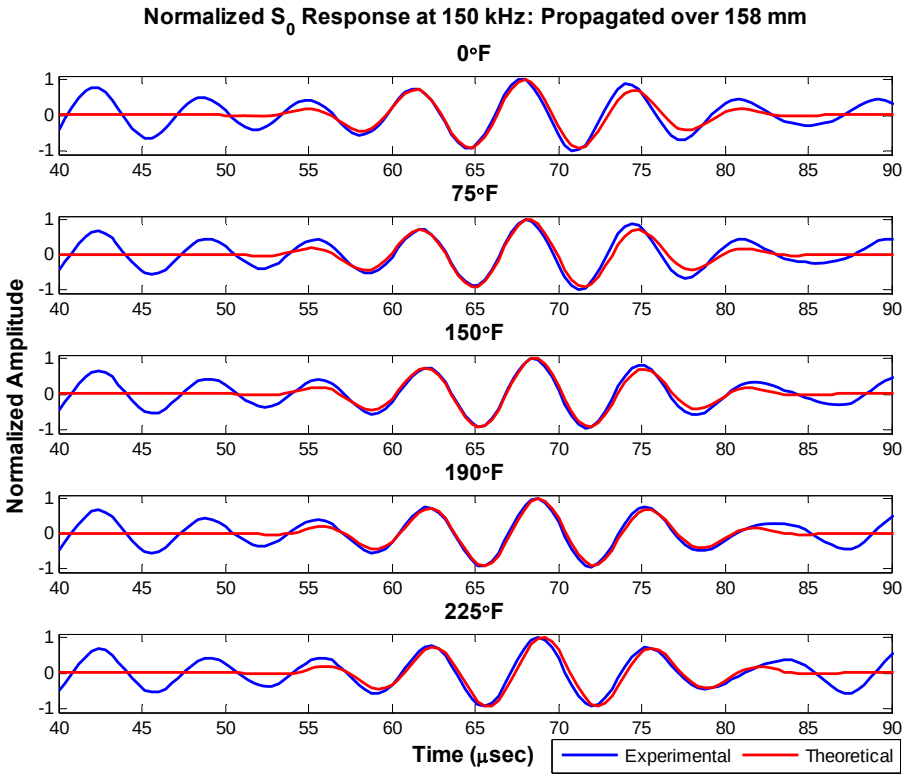

Figure 72: Experimental versus Theoretical S_0 Response at 150 kHz

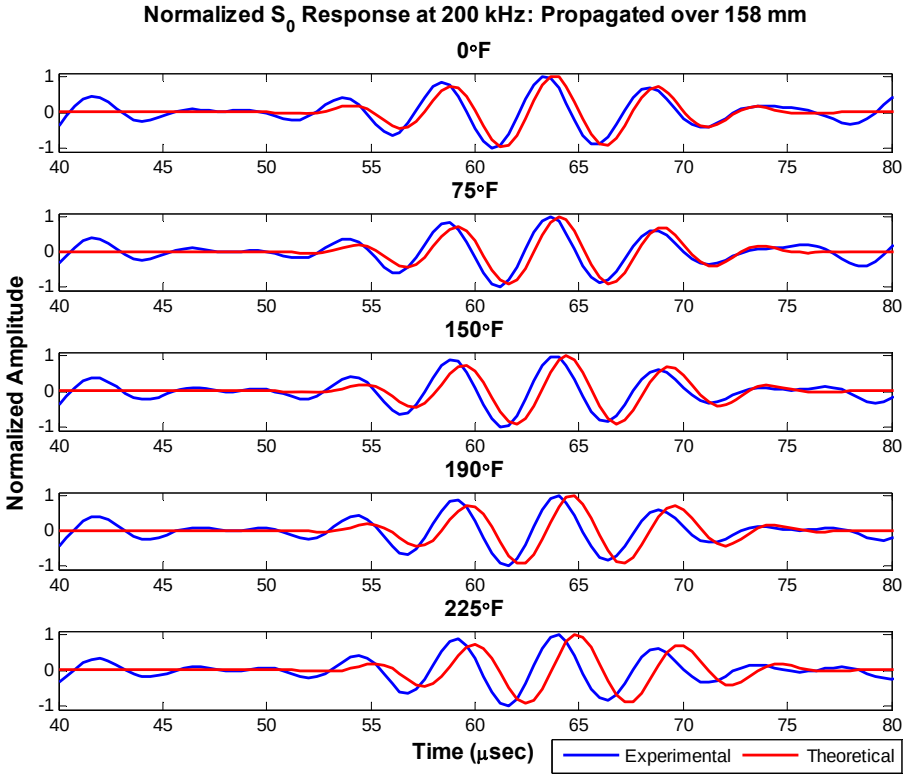

Figure 73: Experimental versus Theoretical S_0 Response at 200 kHz

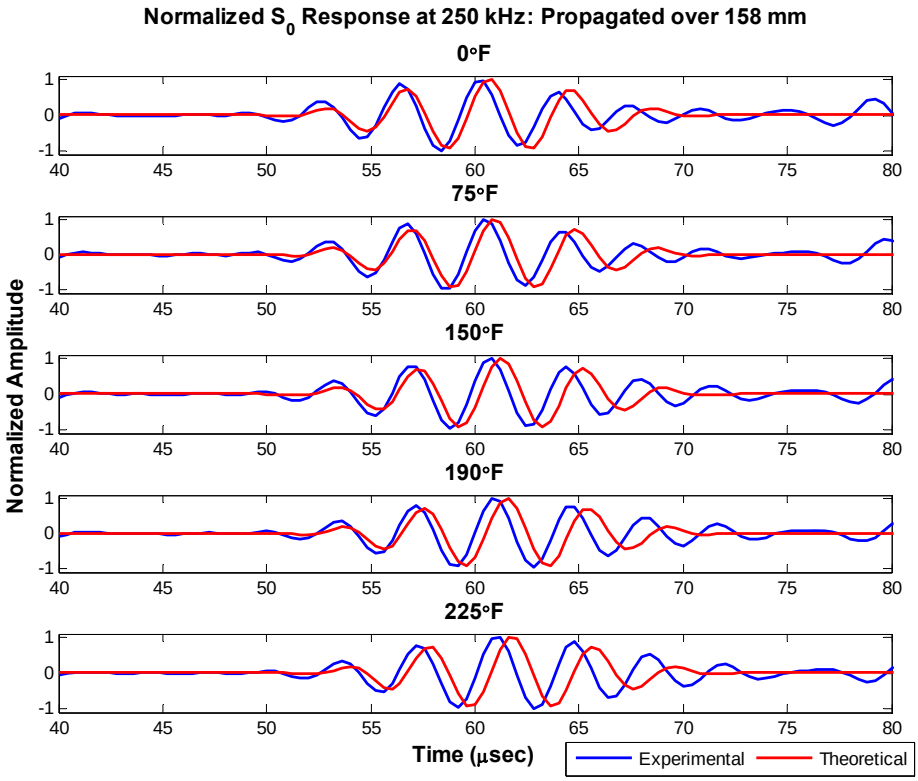

Figure 74: Experimental versus Theoretical S_0 Response at 250 kHz

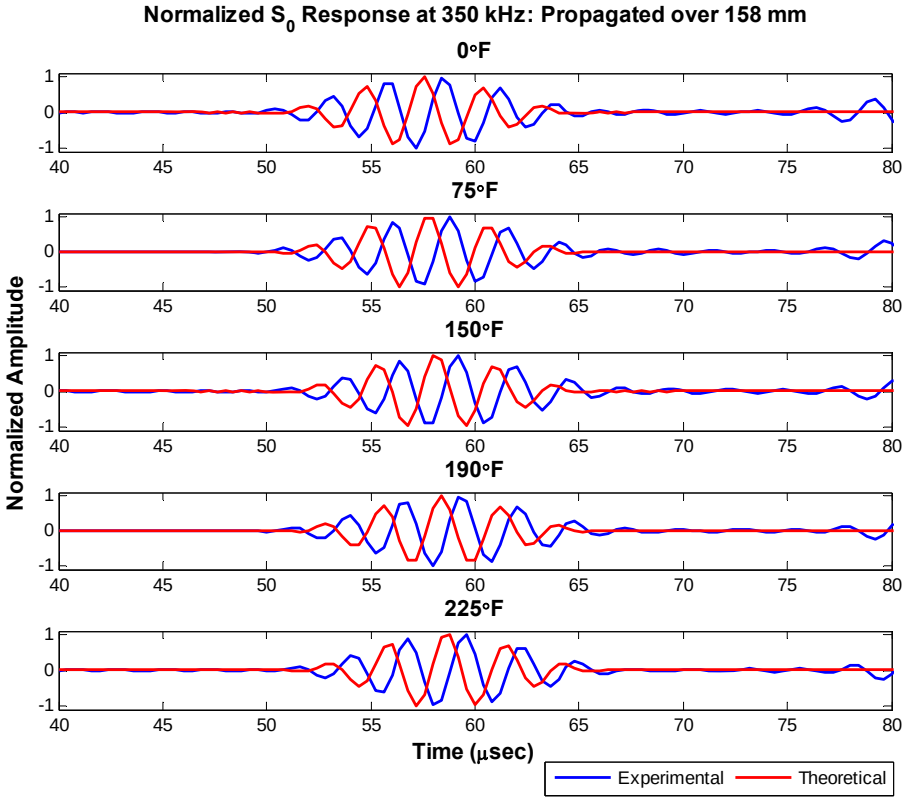

Figure 75: Experimental versus Theoretical S_0 Response at 350 kHz

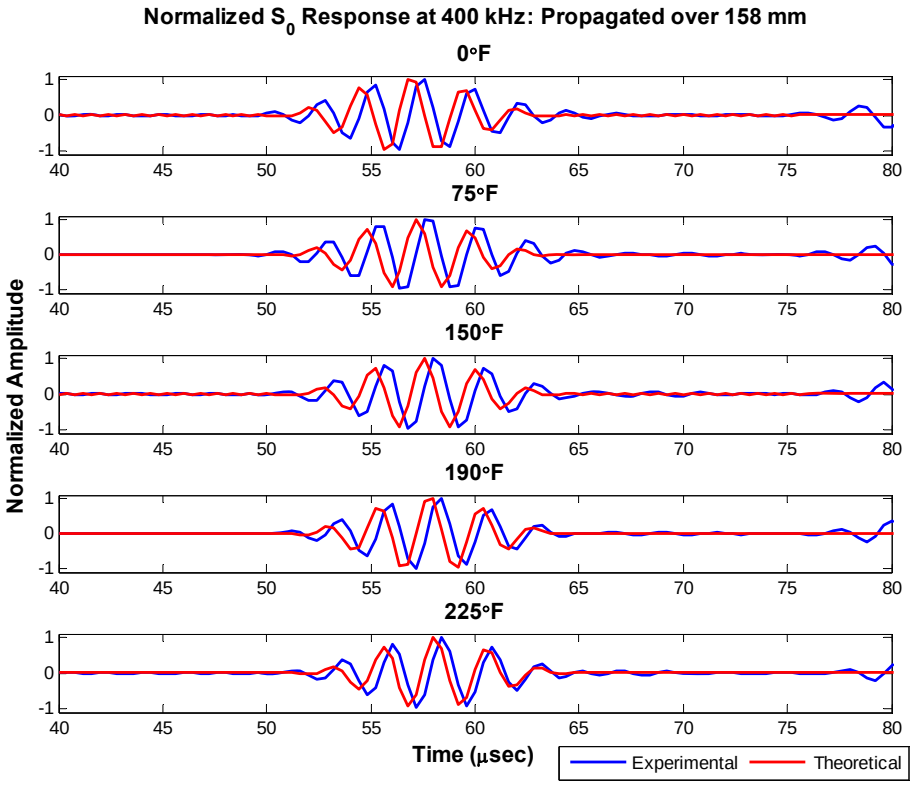

Figure 76: Experimental versus Theoretical S_0 Response at 400 kHz

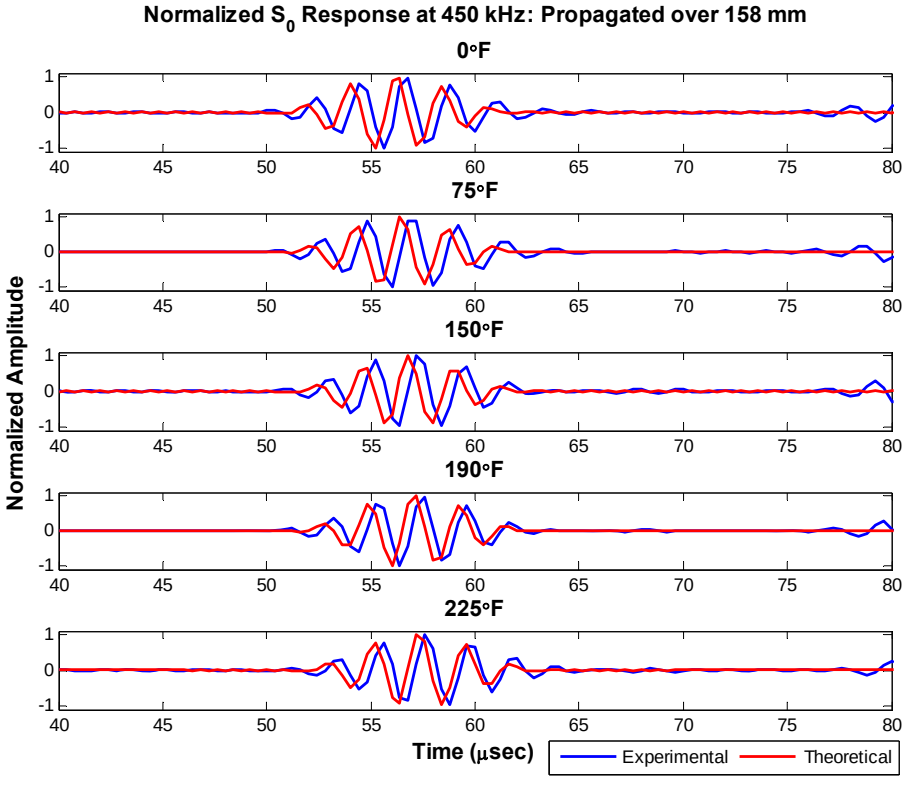

Figure 77: Experimental versus Theoretical S_0 Response at 450 kHz

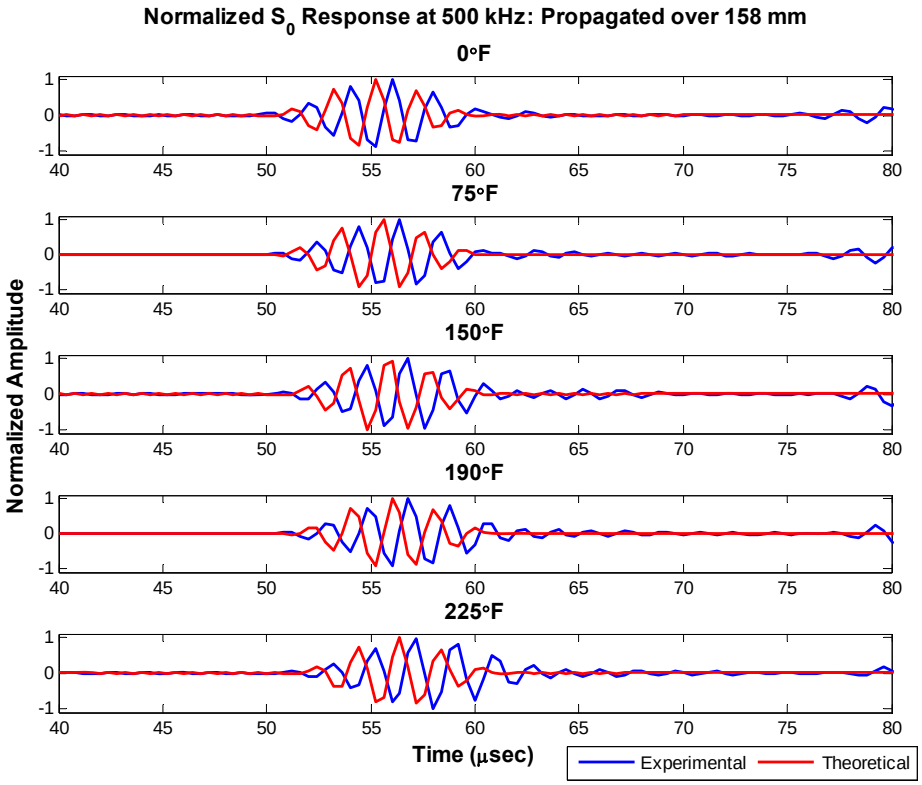

Figure 78: Experimental versus Theoretical S_0 Response at 500 kHz

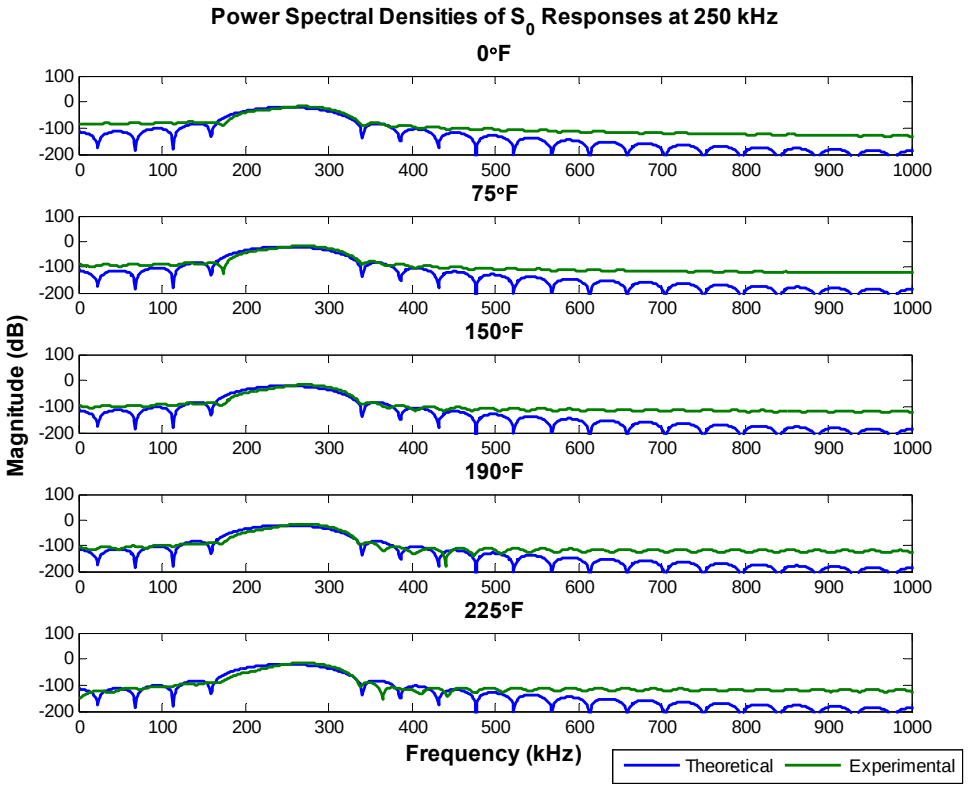

Figure 79: Power Spectral Densities of S_0 Responses at 250 kHz

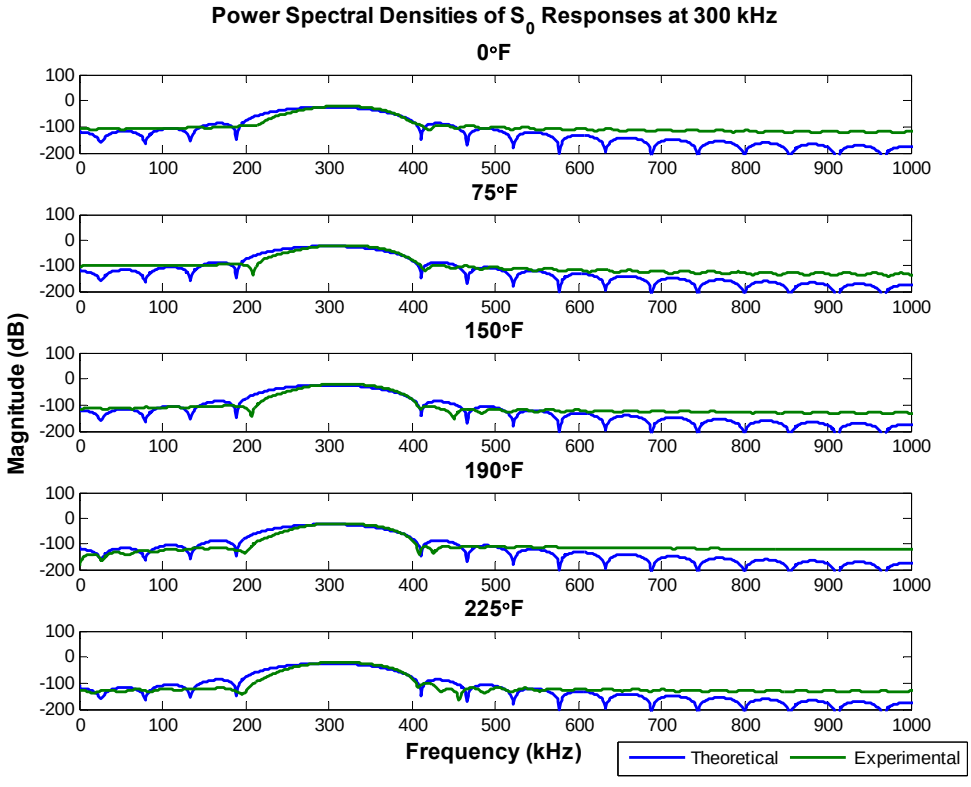

Figure 80: Power Spectral Densities of S_0 Responses at 300 kHz

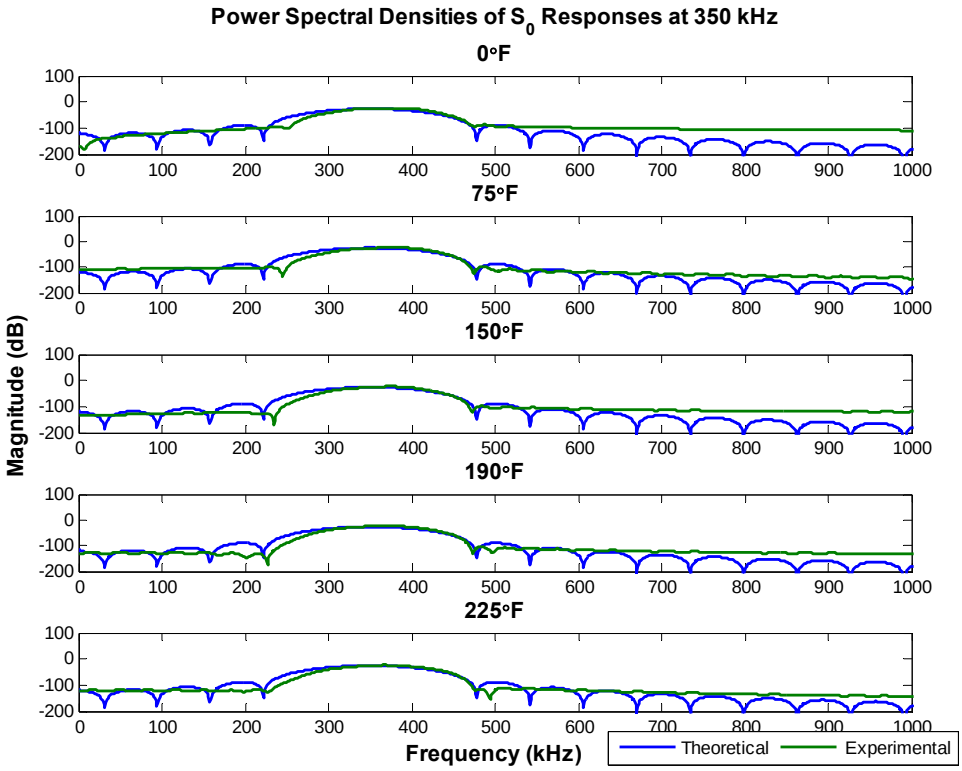

Figure 81: Power Spectral Densities of S_0 Responses at 350 kHz

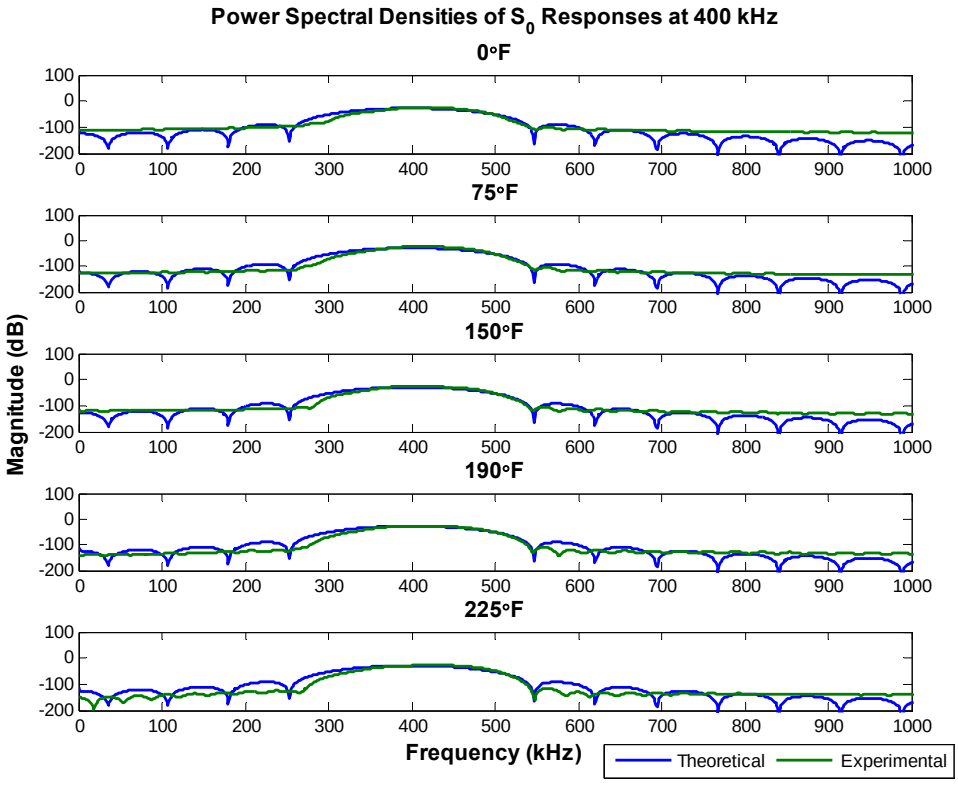

Figure 82: Power Spectral Densities of S_0 Responses at 400 kHz

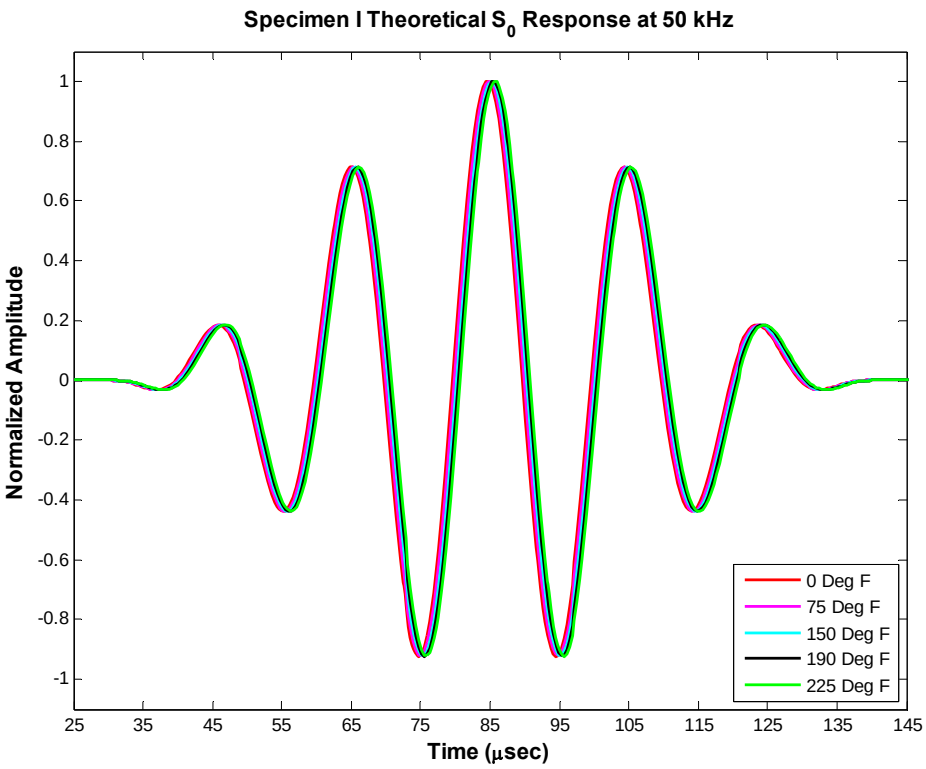

Figure 83: Specimen I Theoretical S_0 Response at 50 kHz

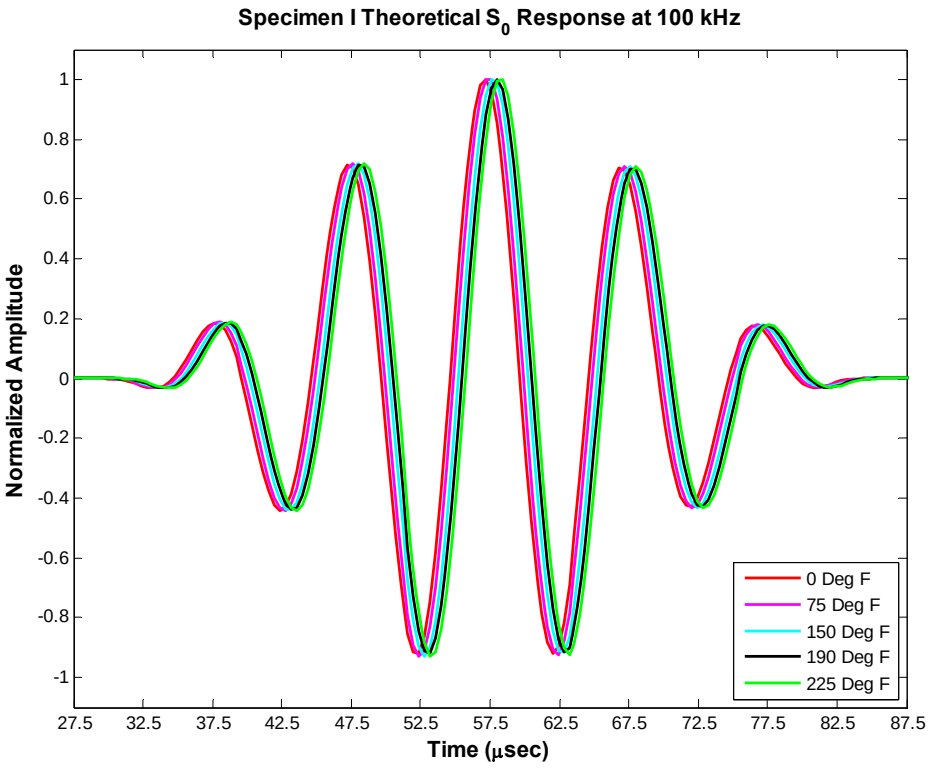

Figure 84: Specimen I Theoretical S_0 Response at 100 kHz

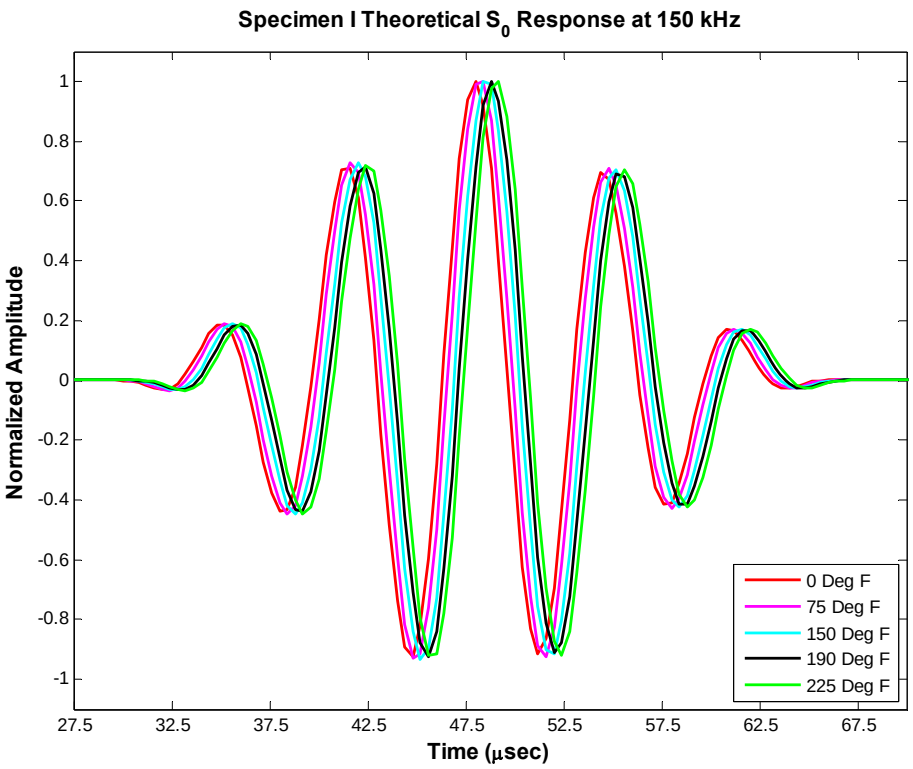

Figure 85: Specimen I Theoretical S_0 Response at 150 kHz

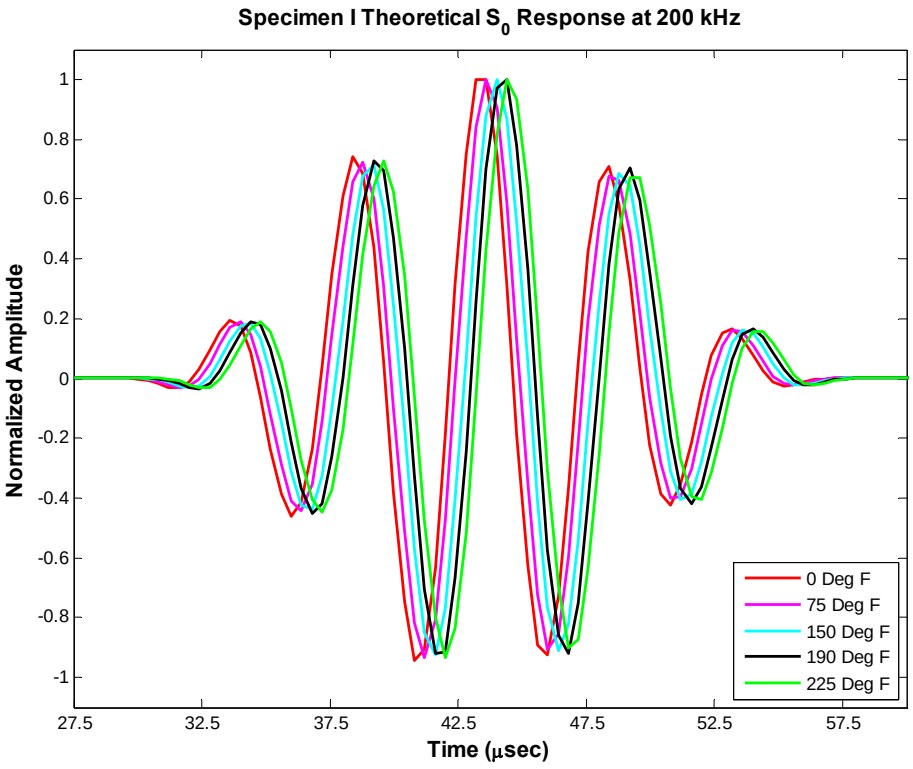

Figure 86: Specimen I Theoretical S_0 Response at 200 kHz

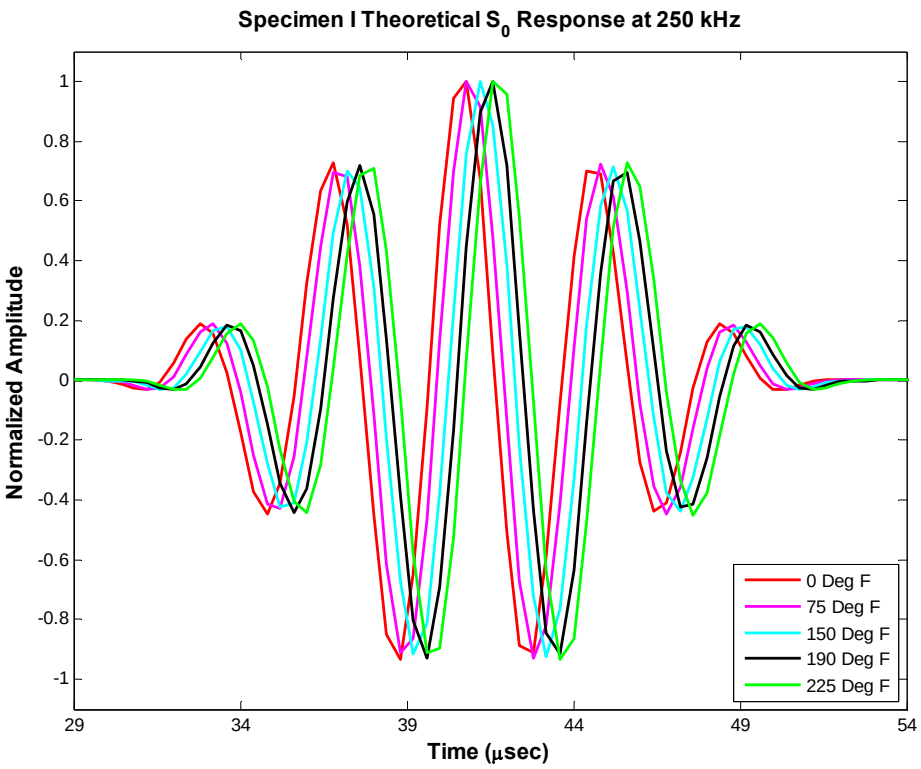

Figure 87: Specimen I Theoretical S_0 Response at 250 kHz

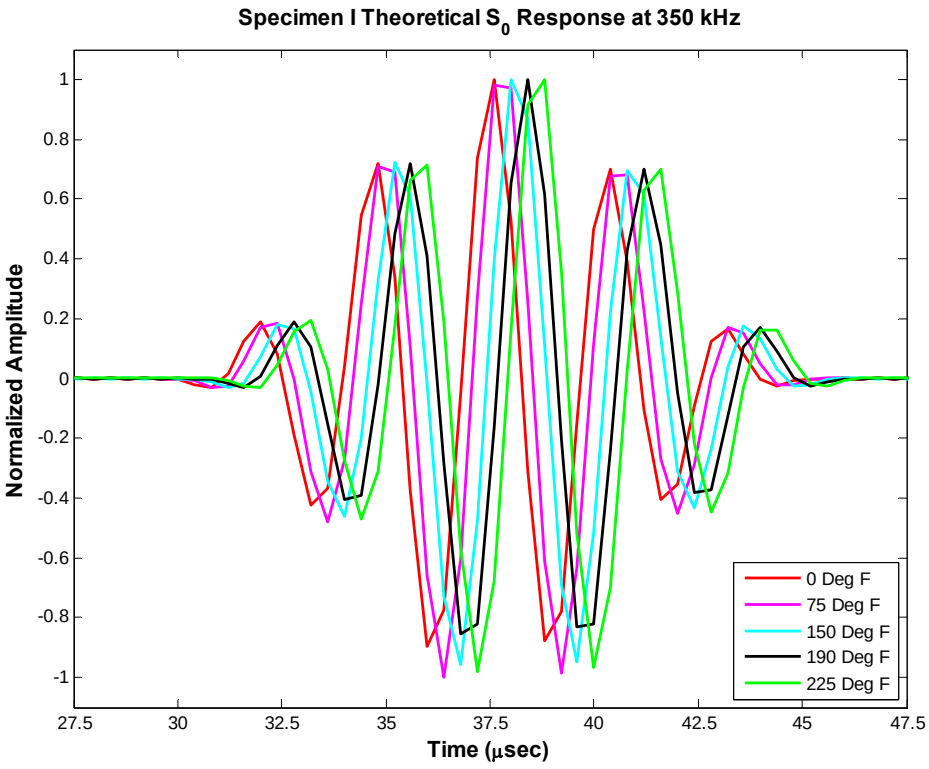

Figure 88: Specimen I Theoretical S_0 Response at 350 kHz

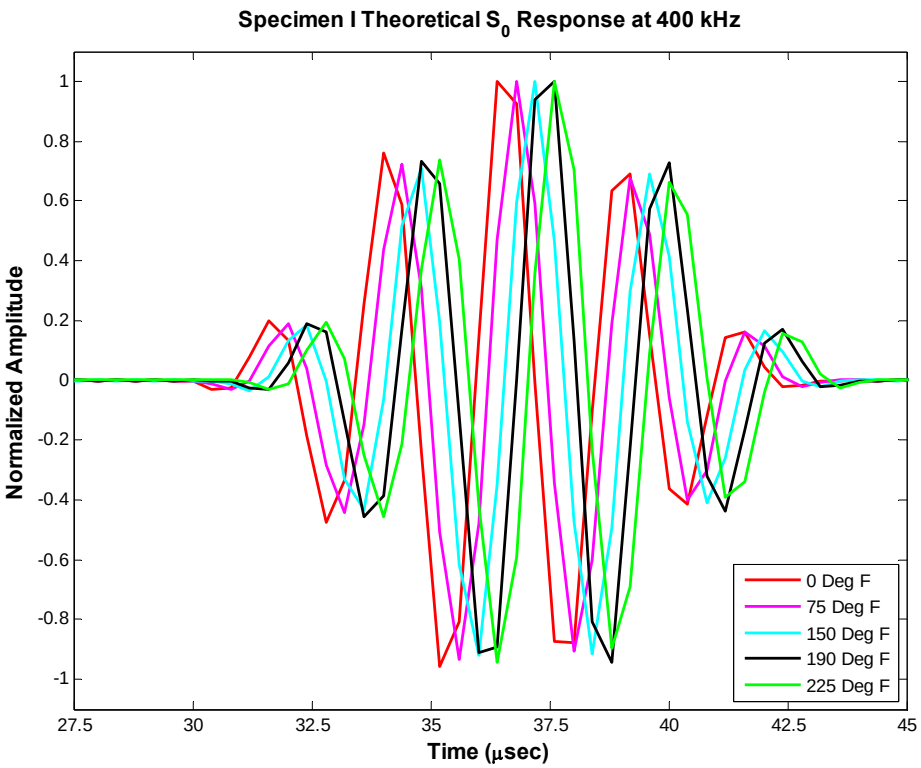

Figure 89: Specimen I Theoretical S_0 Response at 400 kHz

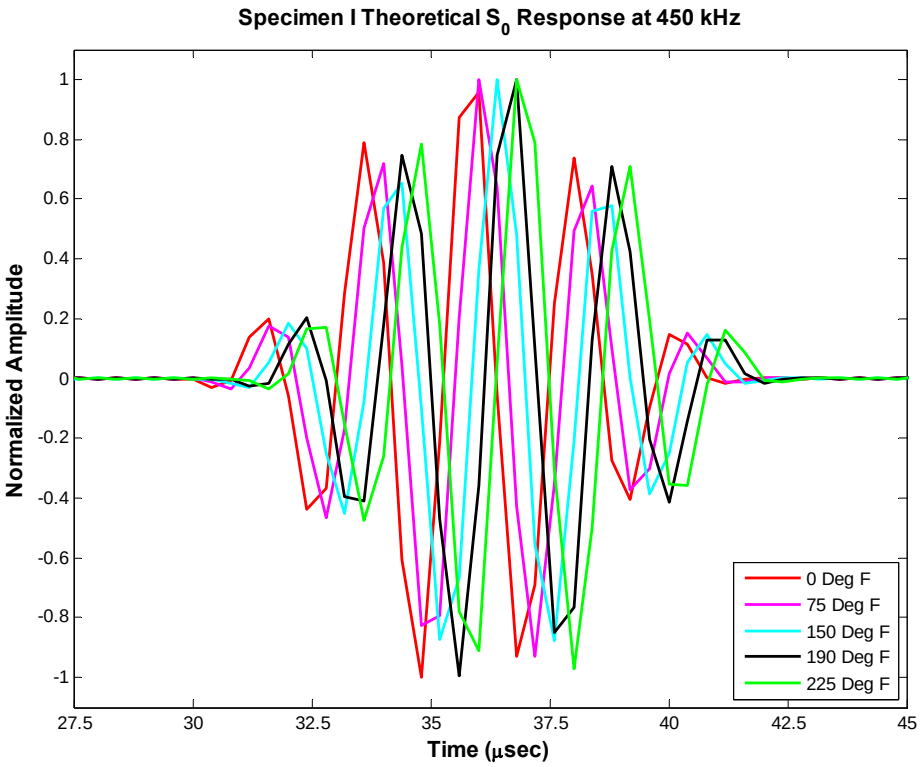

Figure 90: Specimen I Theoretical S_0 Response at 450 kHz

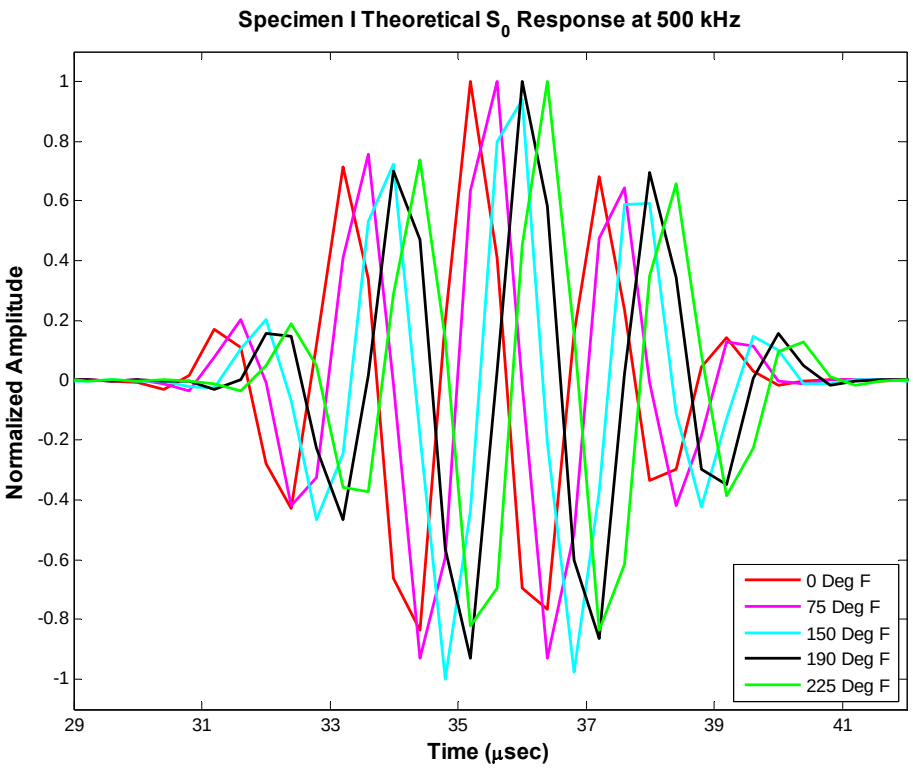

Figure 91: Specimen 1 Theoretical S_0 Response at 500 kHz

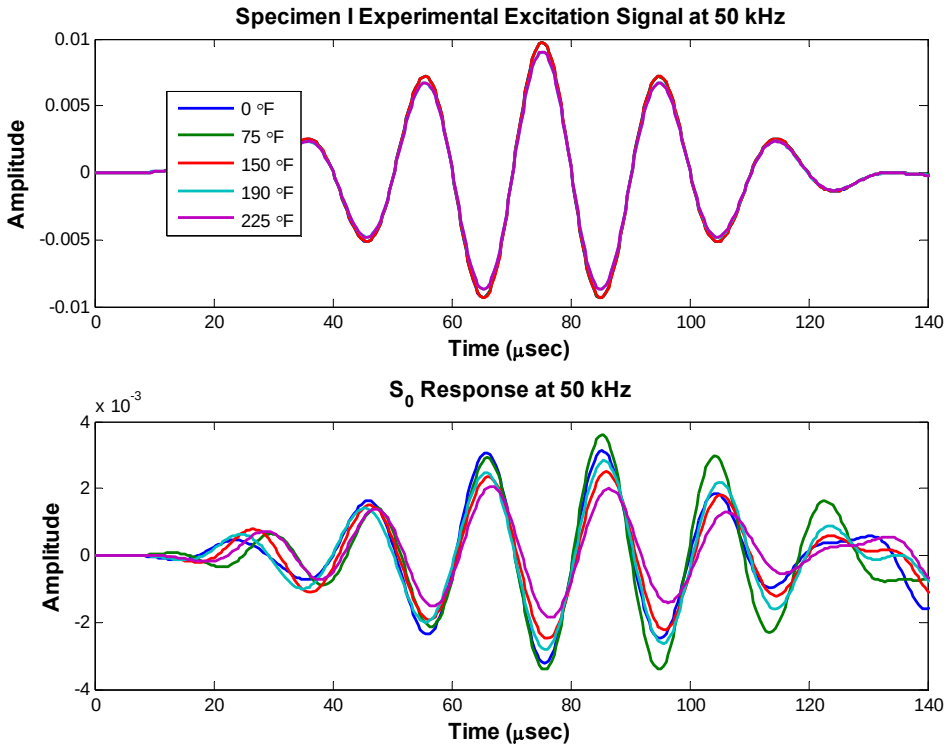

Figure 92: Specimen I Raw Signals at 50 kHz

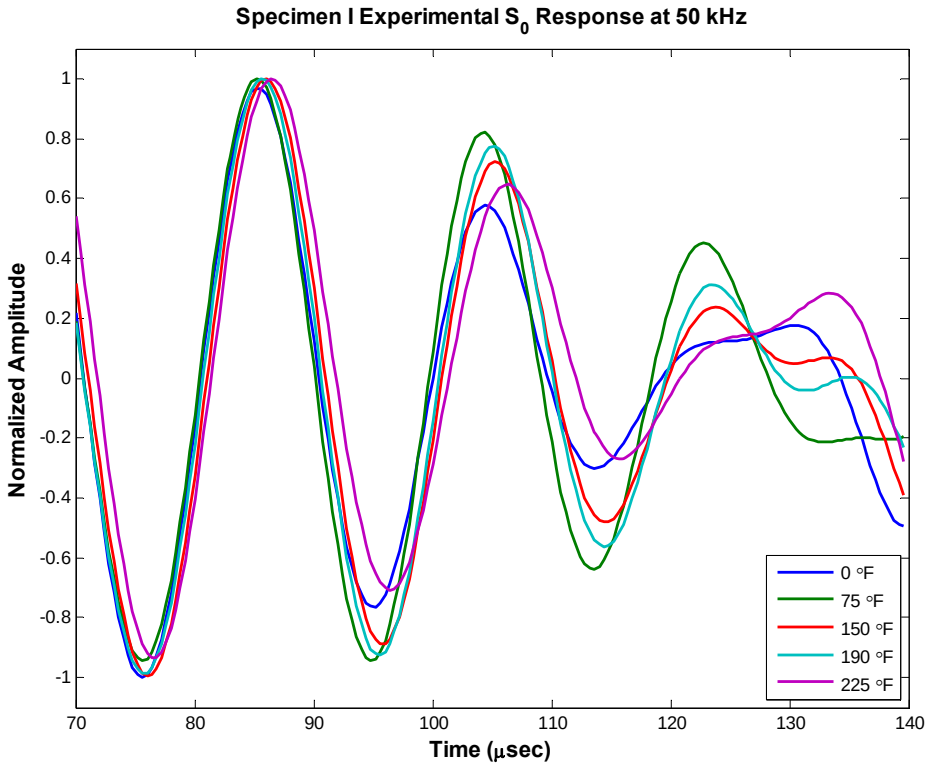

Figure 93: Specimen I Experimental S_0 Response at 50 kHz

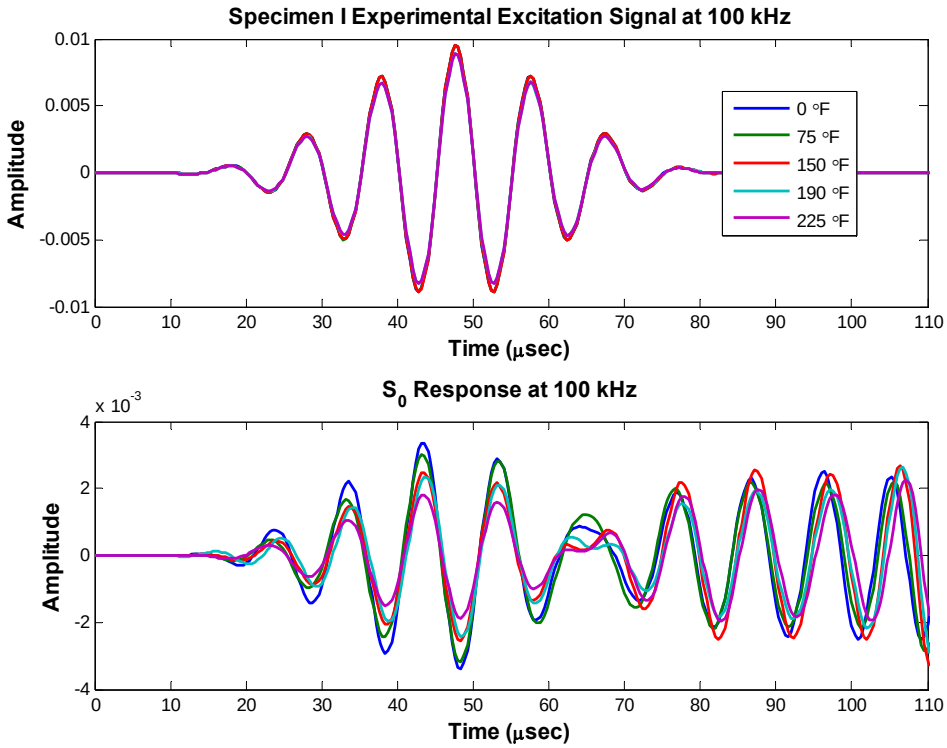

Figure 94: Specimen I Raw Signals at 100 kHz

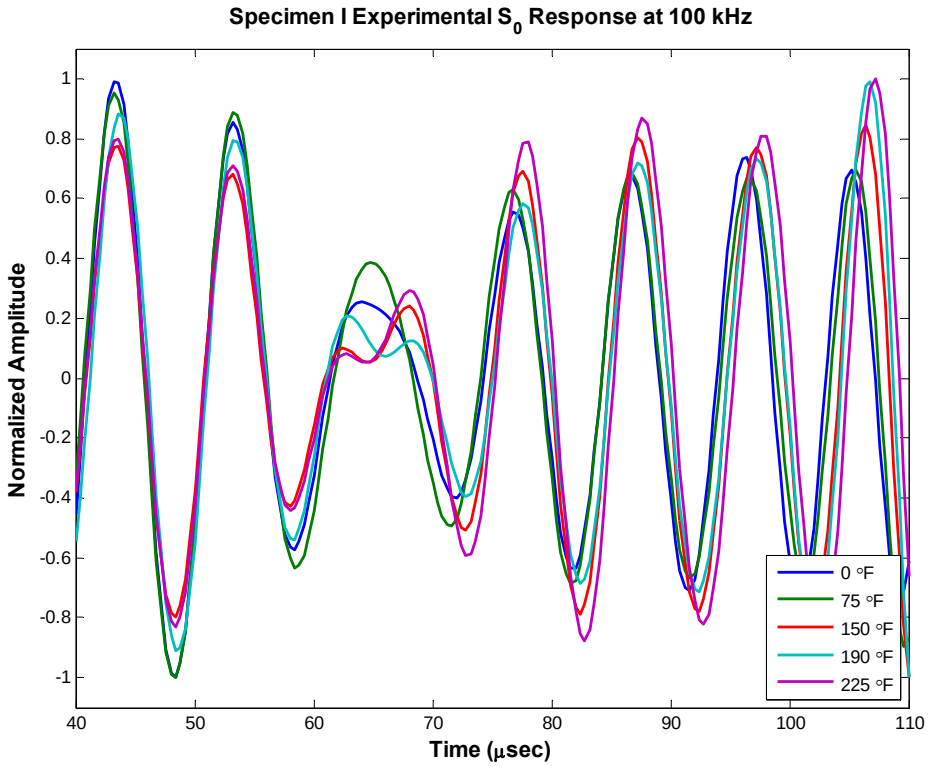

Figure 95: Specimen I Experimental S_0 Response at 100 kHz

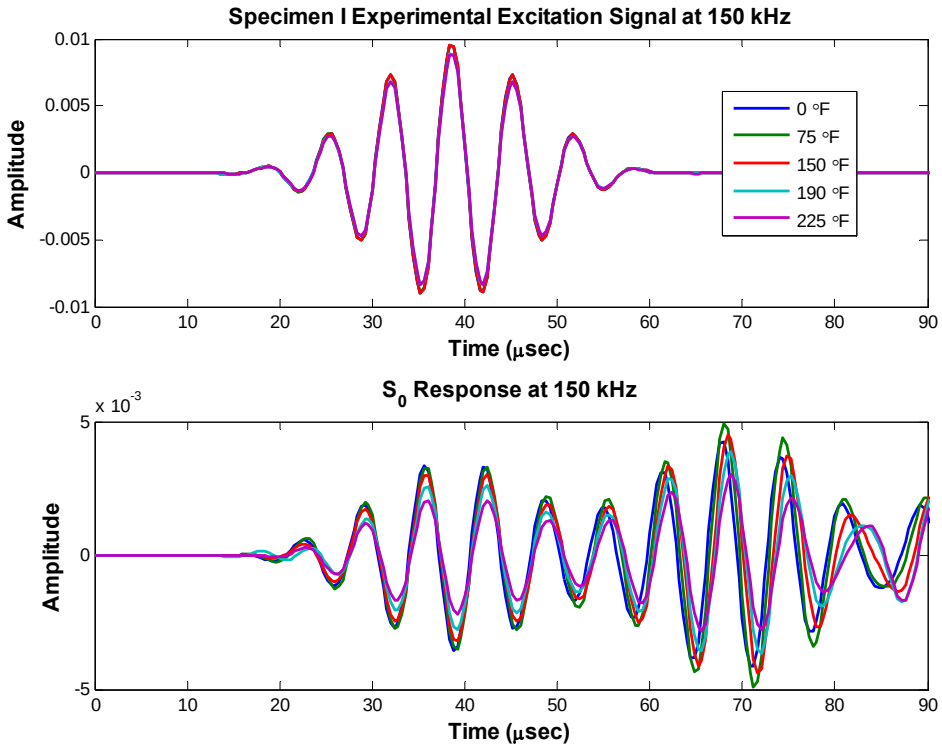

Figure 96: Specimen I Raw Signals at 150 kHz

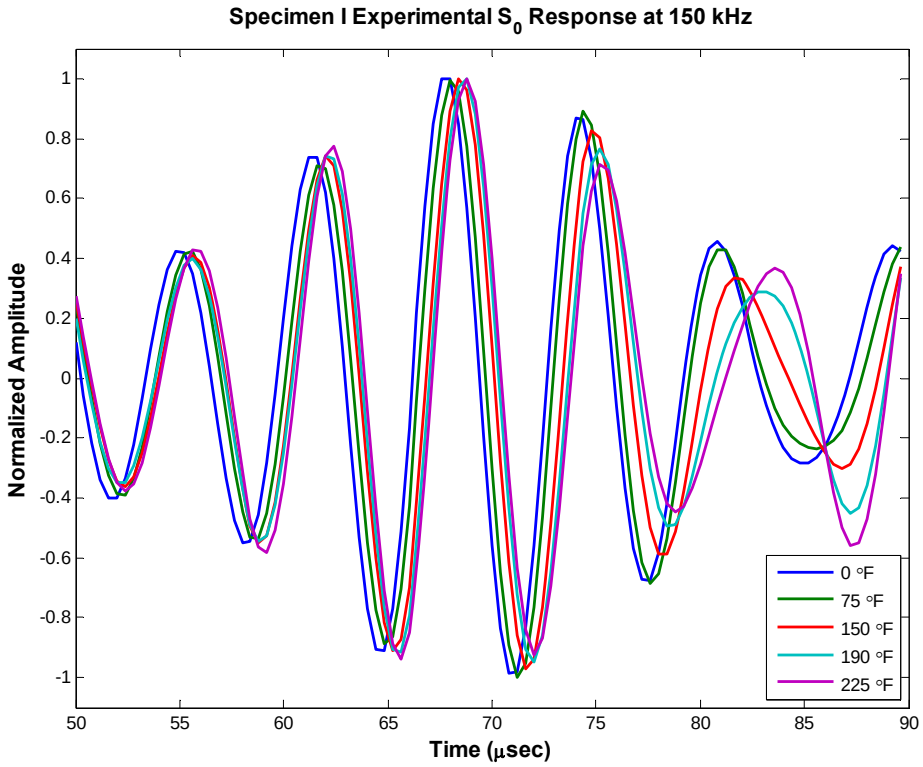

Figure 97: Specimen I Experimental S_0 Response at 150 kHz

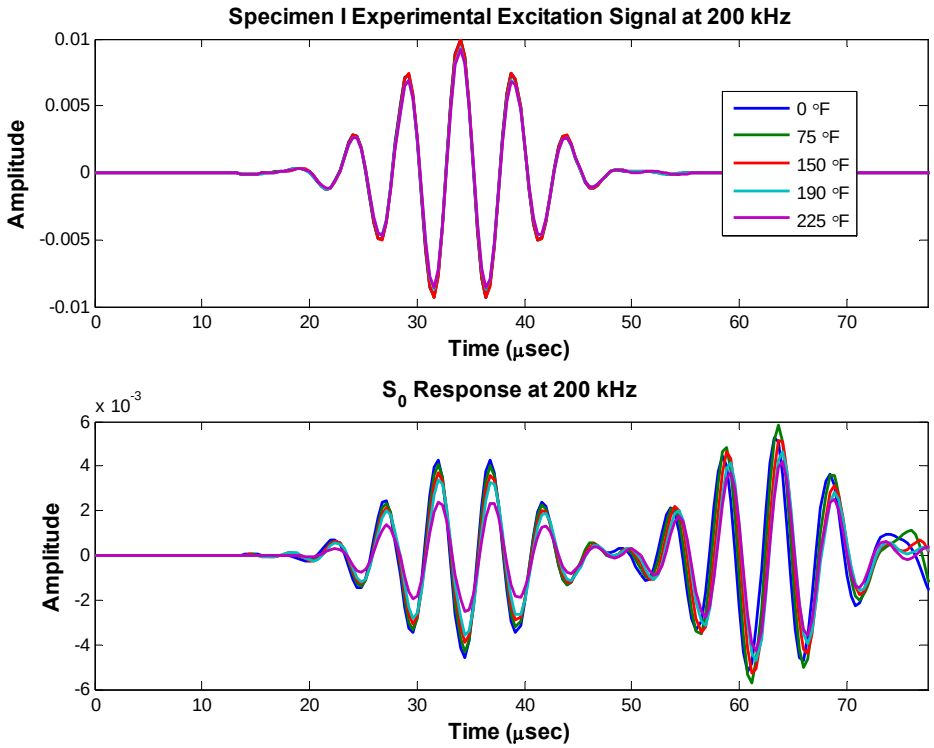

Figure 98: Specimen I Raw Signals at 200 kHz

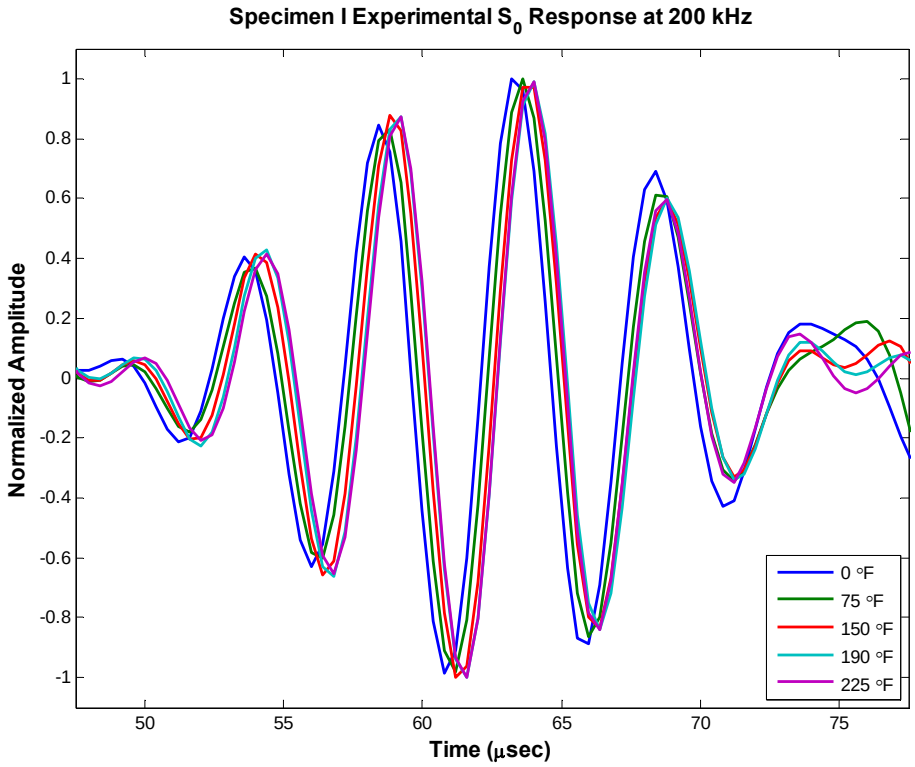

Figure 99: Specimen I Experimental S_0 Response at 200 kHz

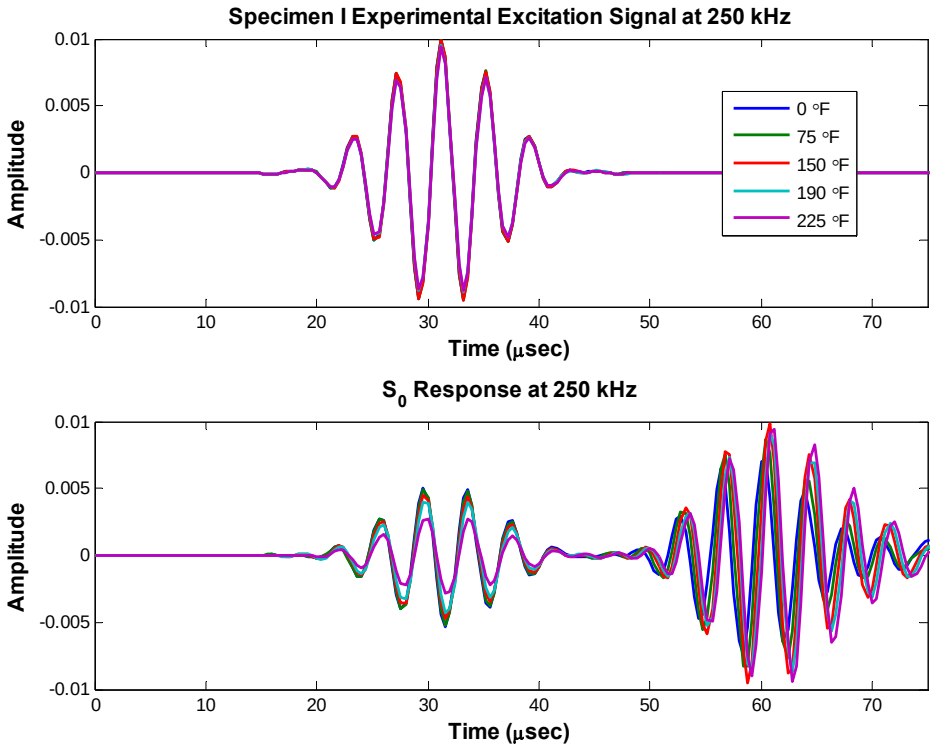

Figure 100: Specimen I Raw Signals at 250 kHz

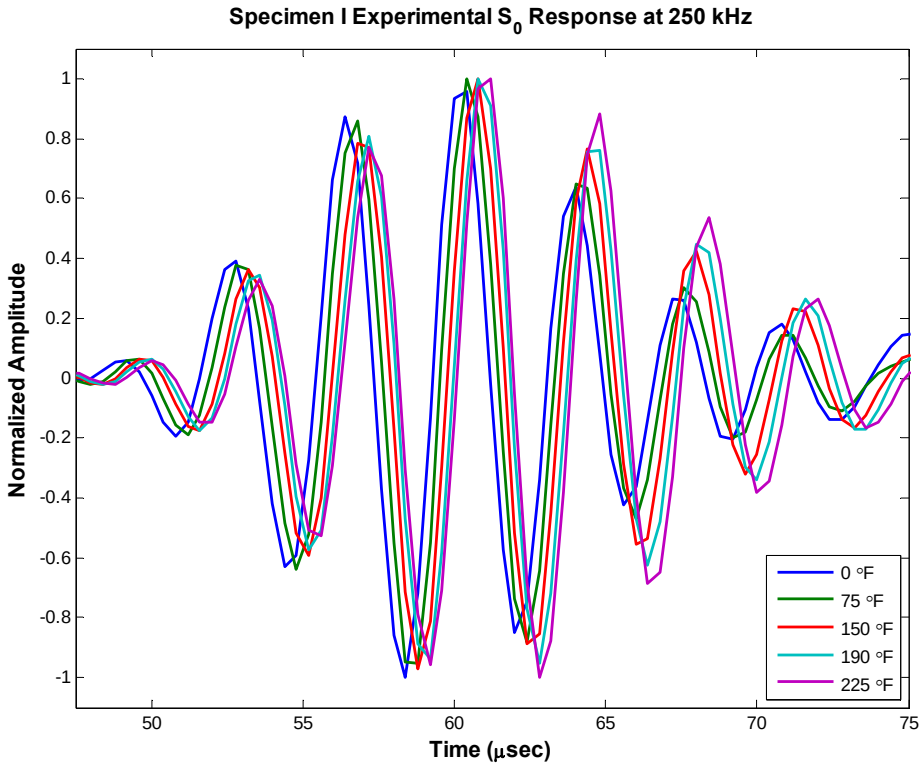

Figure 101: Specimen I Experimental S_0 Response at 250 kHz

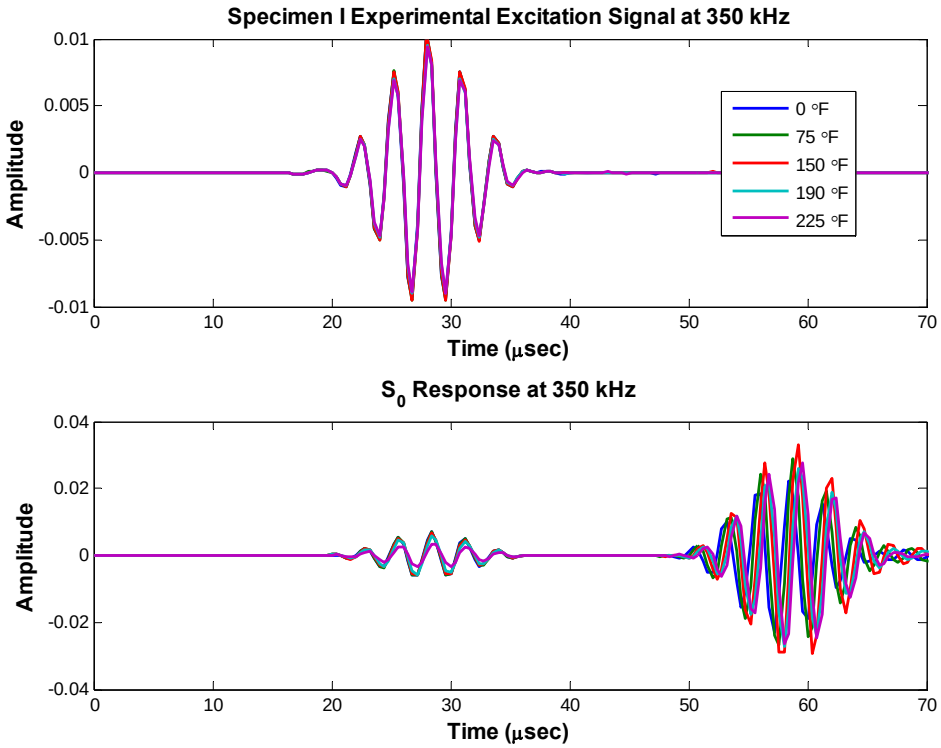

Figure 102: Specimen I Raw Signals at 350 kHz

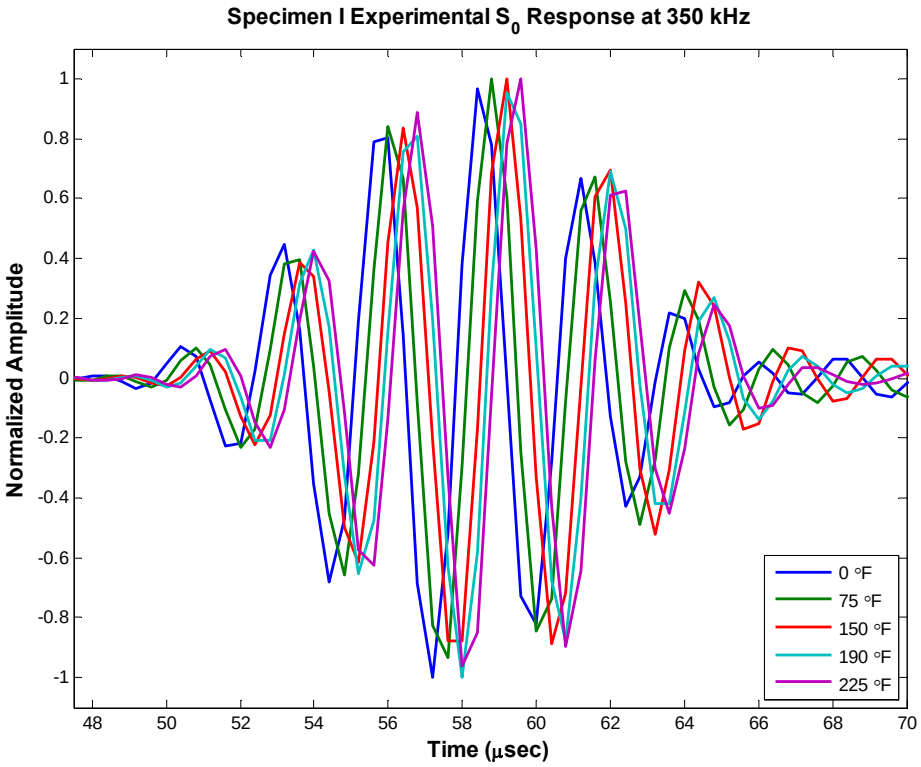

Figure 103: Specimen I Experimental S_0 Response at 350 kHz

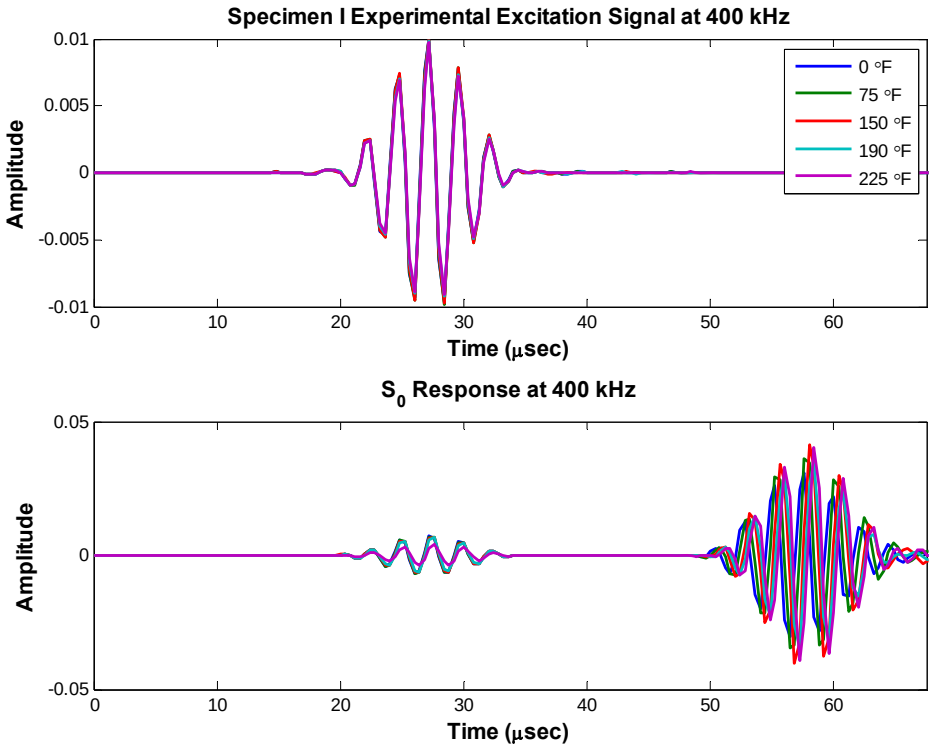

Figure 104: Specimen I Raw Signals at 400 kHz

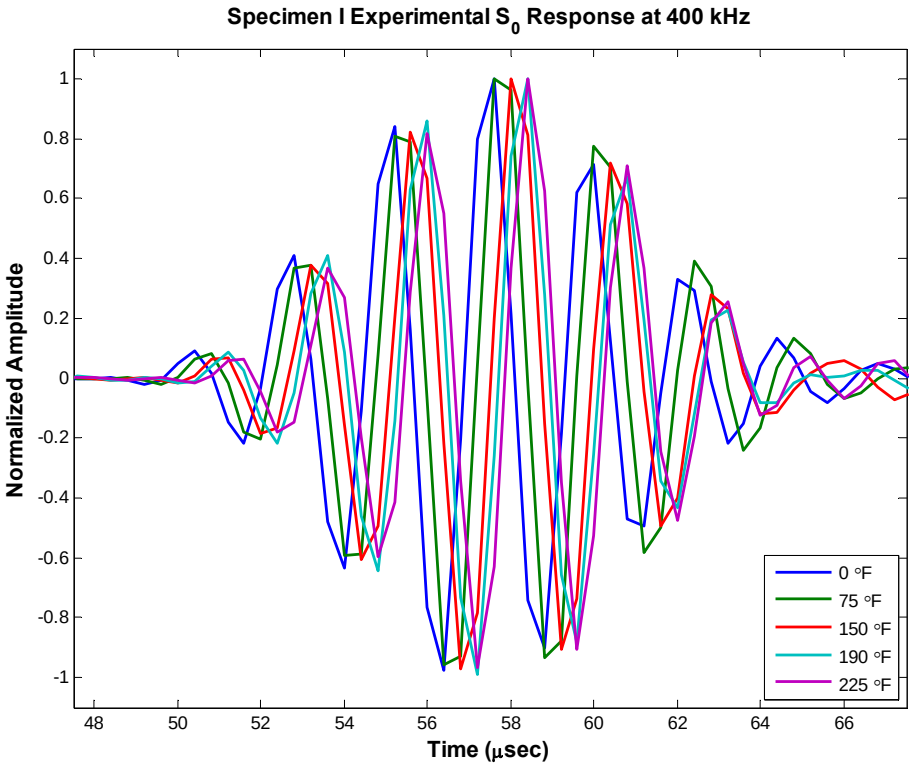

Figure 105: Specimen I Experimental S_0 Response at 400 kHz

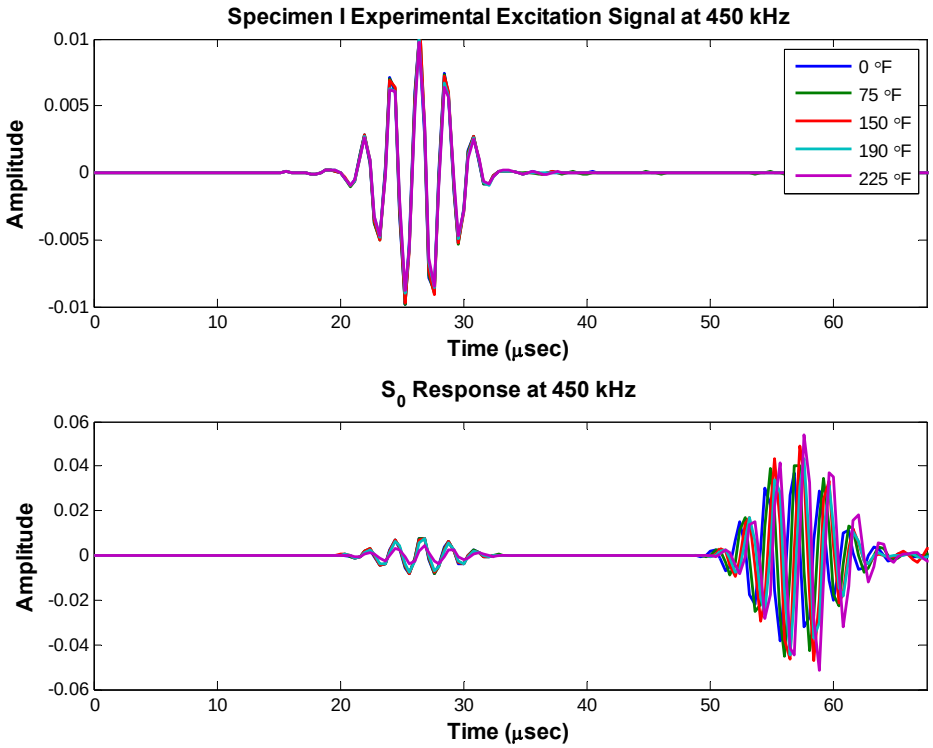

Figure 106: Specimen I Raw Signals at 450 kHz

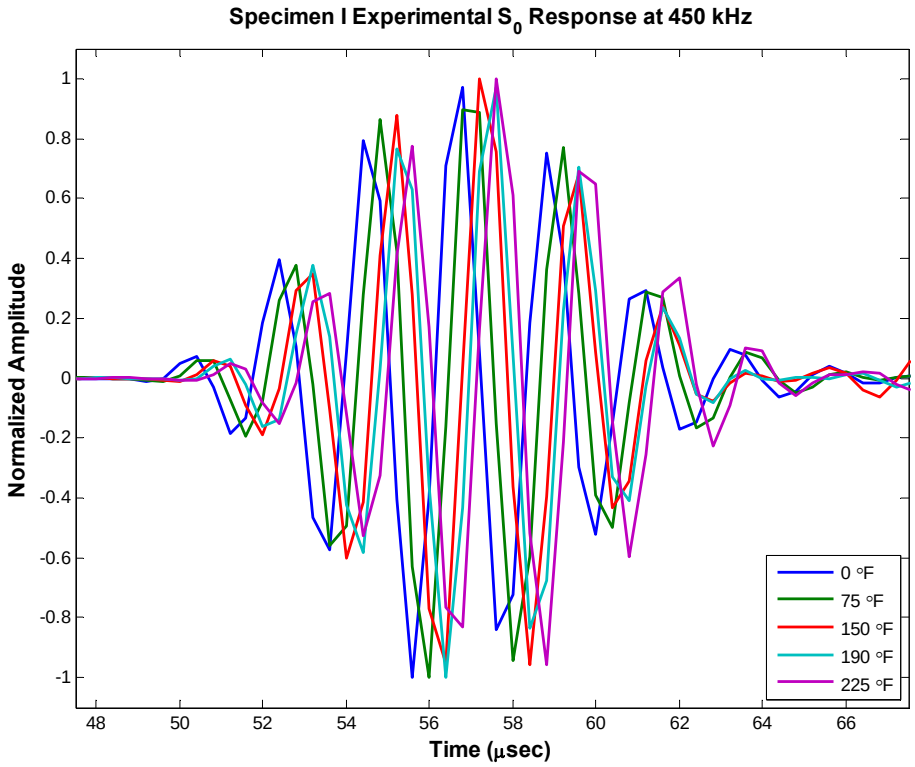

Figure 107: Specimen I Experimental S_0 Response at 450 kHz

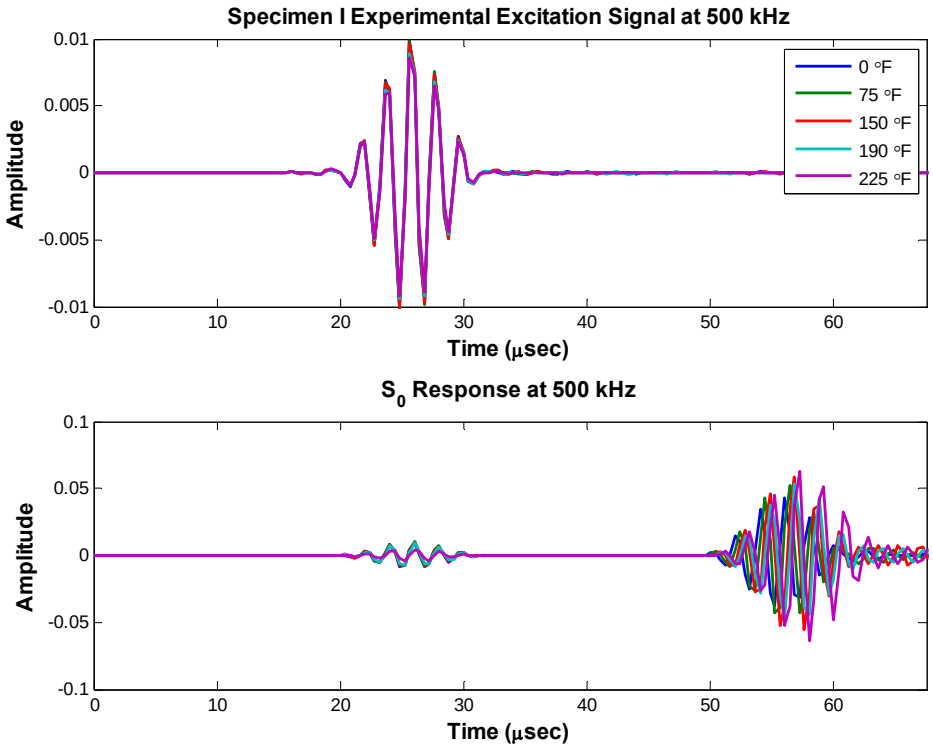

Figure 108: Specimen I Raw Signals at 450 kHz

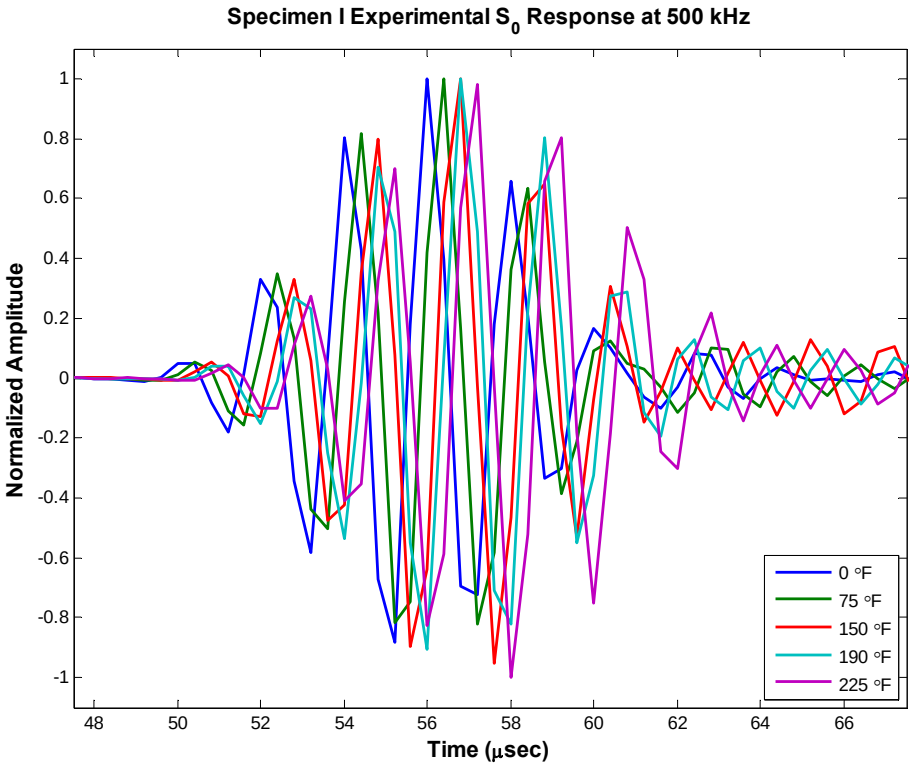

Figure 109: Specimen I Experimental S_0 Response at 500 kHz

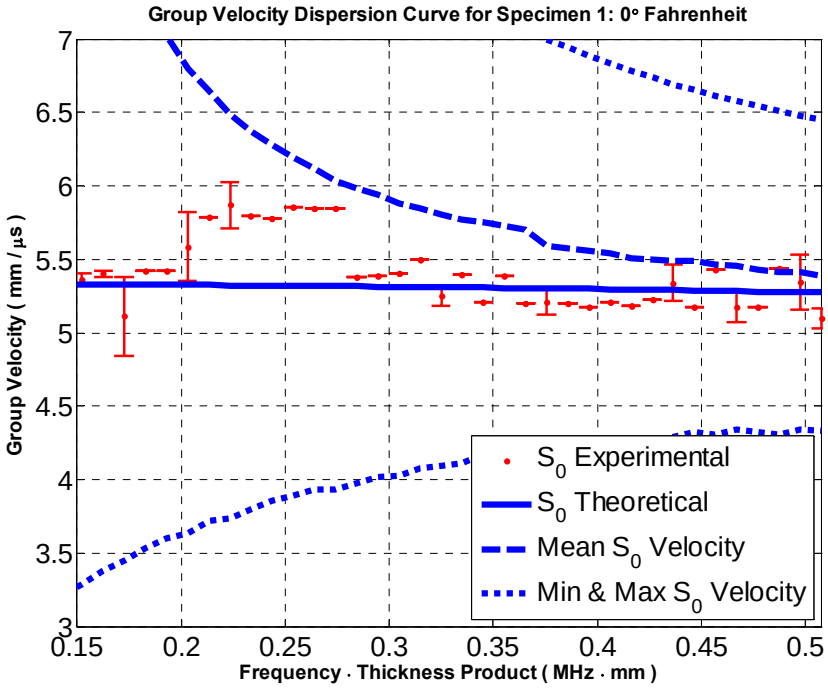

Figure 110: S_0 Group Velocity Dispersion Curve at 0°F

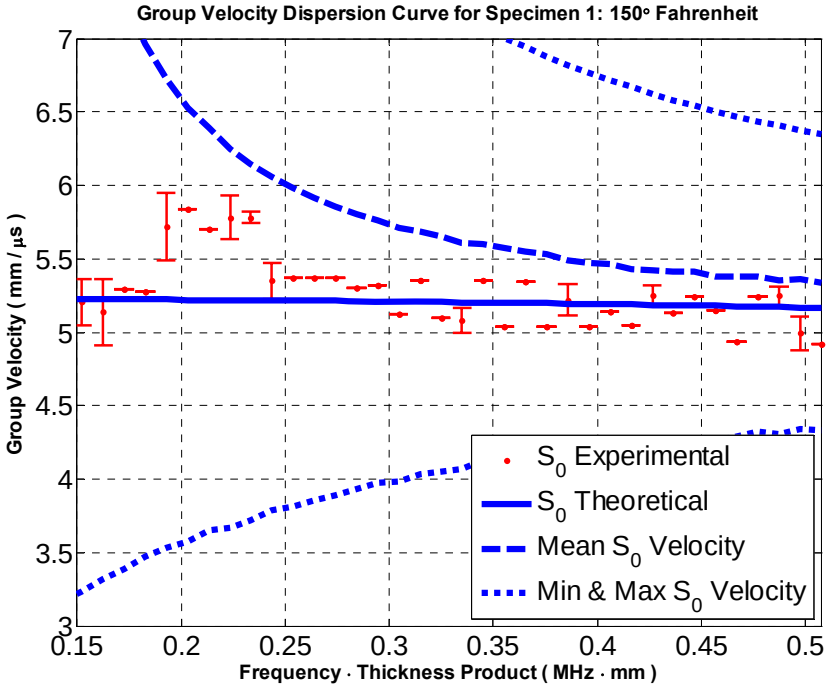

Figure 111: Group Velocity Dispersion Curve - 150°F

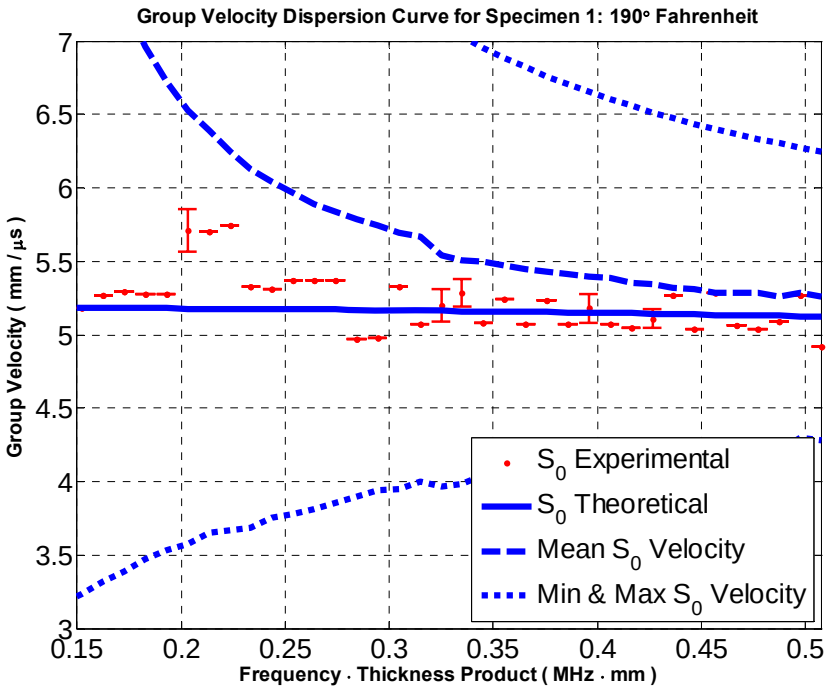

Figure 112: Group Velocity Dispersion Curve - 190°F

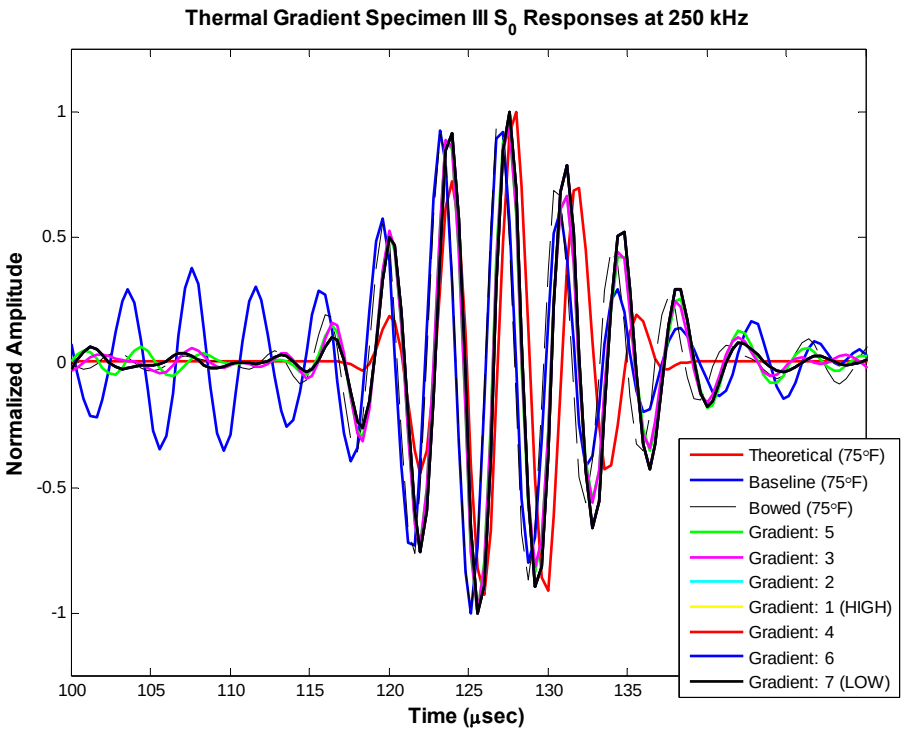

Figure 113: Specimen III Baseline versus Thermal Gradient S_0 Responses at 250 kHz

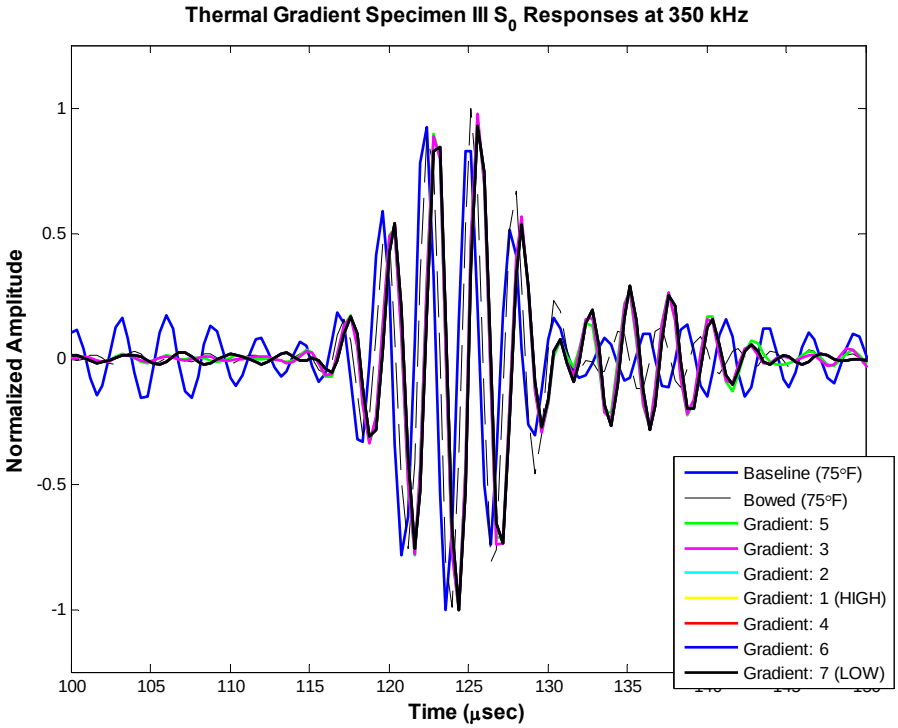

Figure 114: Specimen III Baseline versus Thermal Gradient S_0 Responses at 350 kHz

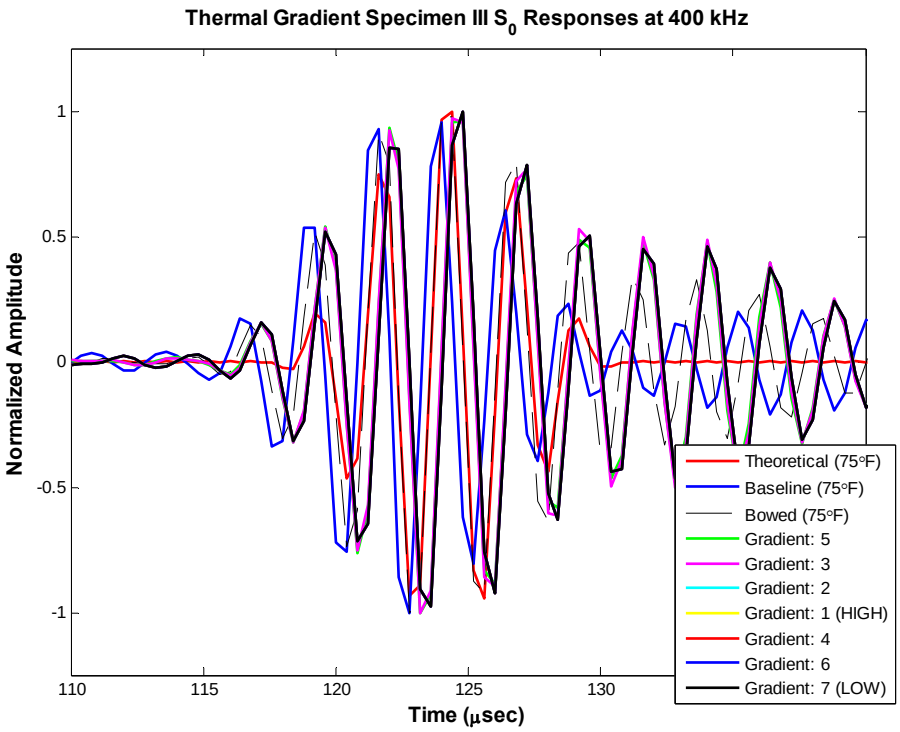

Figure 115: Specimen III Baseline versus Thermal Gradient S_0 Responses at 400 kHz

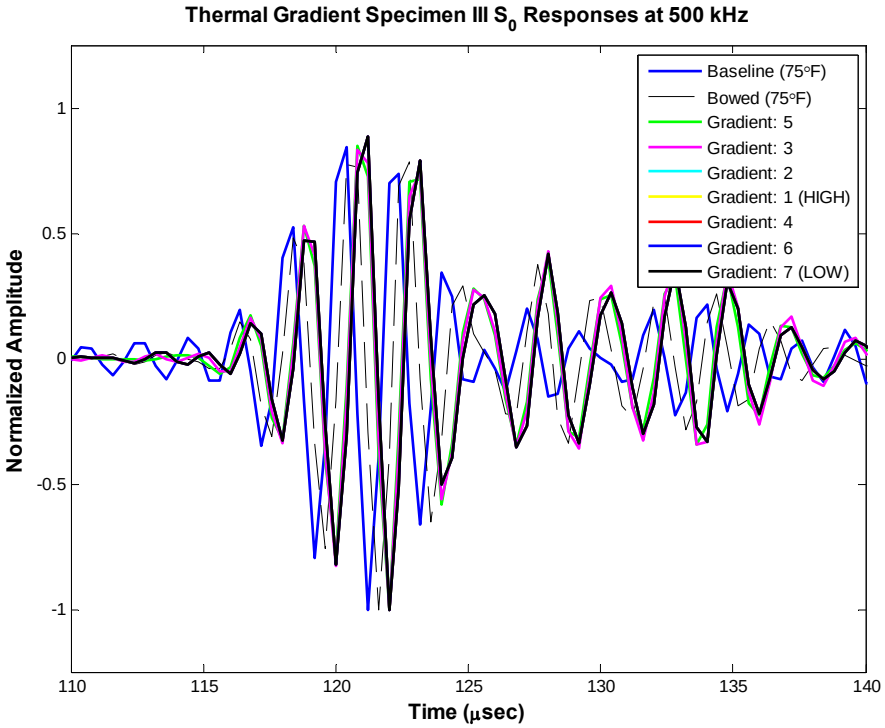

Figure 116: Specimen III Baseline versus Thermal Gradient S_0 Responses at 500 kHz

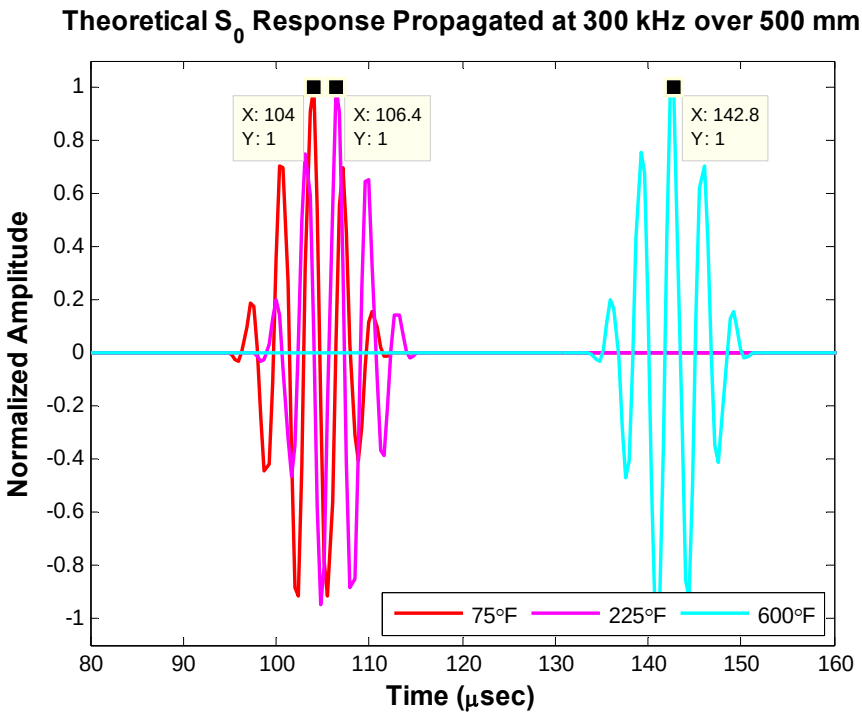

Figure 117: Theoretical Thermal Gradient S_0 Responses over 500 mm

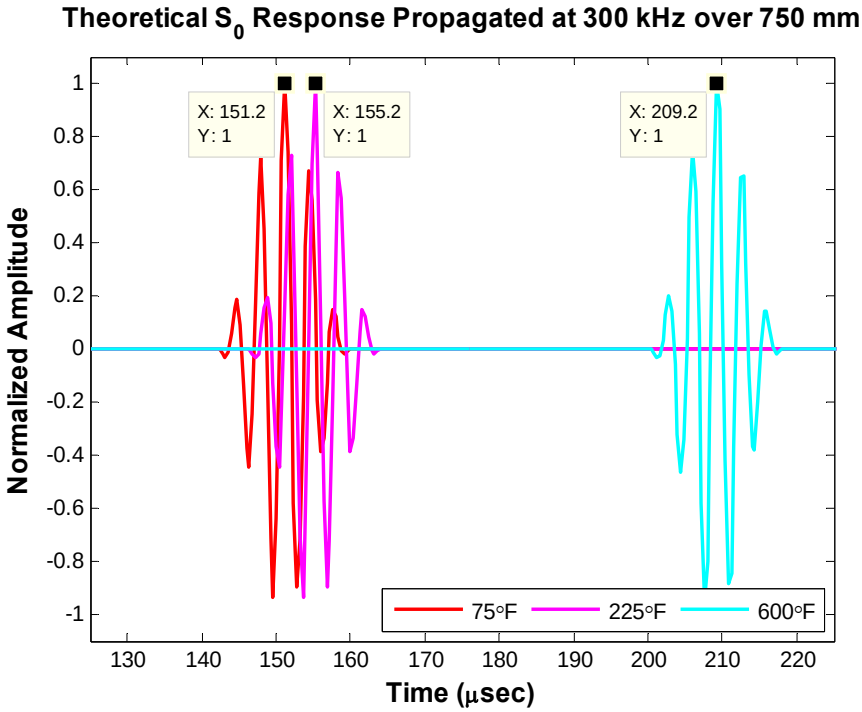

Figure 118: Theoretical Thermal Gradient S_0 Responses over 750 mm

APPENDIX D: MATLAB® CODE

AFRL/VASA: Modulus of Elasticity versus Temperature Curve

```
% AFRL/VASA: 20050302mpd
% Modulus versus Temperature from Steve Olson's alum_modulus_7075_mil5.xls
% file

%% Data
   tm = [0.155642  1.01735E+07
   20.0389 1.00978E+07
   45.6031 1.00725E+07
   62.6459 1.00220E+07
   84.6858 9.98273E+06
   104.411 9.92430E+06
   124.137 9.88046E+06
   145.506 9.79278E+06
   163.588 9.73432E+06
   183.313 9.64664E+06
   203.039 9.55896E+06
   222.764 9.47128E+06
   244.133 9.35437E+06
   263.859 9.23746E+06
   283.584 9.09132E+06
   303.31  8.95980E+06
   323.035 8.82827E+06
   341.117 8.66752E+06
   360.842 8.49216E+06
   382.212 8.28756E+06
   403.581 8.06836E+06
   423.306 7.84915E+06
   443.032 7.58610E+06
   462.757 7.32306E+06
   484.126 7.06001E+06
   502.208 6.76774E+06
   525.221 6.41701E+06
   544.947 6.05166E+06
   563.028 5.71555E+06
   584.398 5.33559E+06
   602.479 4.99947E+06];

%% PLOT
   figure;
   plot(tm(:,1),tm(:,2)./1E6,'bo-','LineWidth',2)
   xlabel('Temperature (\circF)','FontWeight','Bold','FontSize',14)
      xlim([0 600])
   ylabel('Modulus (1E6 psi)','FontWeight','Bold','FontSize',14);
   title('Modulus of Elasticity (E) versus Temperature','FontWeight','Bold','FontSize',14)
   grid on; hold on
```

Lt Andrews: Modulus of Elasticity versus Temperature Curve (Reference: Grisso)

```
% 1Lt Jennifer Andrews
% Thesis Code
% Modulus of Elasticity vs Temperature (taken from Grisso's work)
   close all
   clear all
   clc

%%
   %Note:  Temp_F = (9/5)*Tc+32
   Temp_F = [0:1:600]; %Deg Fahrenheit
   Temp_C = (Temp_F-32).*(5/9);
   T = Temp_C;

%% Modulus of Elasticity
   E = -1.3E-9*(T.^4)-9.2E-7*(T.^3)+0.00016*(T.^2)-0.0032*T+71;

%% Plot E versus T
   plot(T,E,'LineWidth',4)
   ylabel('Modulus of Elasticity (GPa)','FontWeight','Bold','FontSize',12)
   xlabel('Temperature (degrees Celsius)','FontWeight','Bold','FontSize',12)
      xlim([0 300])
   Title('Modulus of Elasticity (Aluminum) versus
Temperature','FontWeight','Bold','FontSize',12)
```

Lt Andrews: 5 ½ Cycle Hanning-windowed Excitation Signal

```
% 1Lt Jennifer Andrews
% Thesis Code
% 5 1/2 Cycle Hanning Window Excitation Signal
%%
   clear all
   close all
   clc

%% User Input
   % Specify Frequency
   fc = 300E3;

%%
   fc_title = fc/1E3;
   num_cycles = 5.5;
   fsamp = 2.5E6;

%% Excitation Signal at fc
   [ws,t] = WindowedSine(fc,num_cycles,fsamp);

%% PLOT
   plot(t./1E-6,ws,'LineWidth',2)
```

```
   xlabel('Time (\musec)','FontWeight','Bold','FontSize',12)
   ylabel('Normalized Amplitude','FontWeight','Bold','FontSize',12)
         ylim([-1.5 1.5])
   Title(['5 1/2 Cycle Hanning-window Excitation Signal at ' int2str(fc_title)
'kHz'],'FontWeight','Bold','FontSize',12)
```

AFRL/VASA: Function - Generates a Hanning-windowed Excitation Signal

```
function [ws,t] = WindowedSine(fc,num_cycles,fsamp);
   %   Creates windowed sinusoid
   %   INPUTS:
   %   fc = center frequency of burst (Hz)
   %   num_cycles = number of cycles, can be non-integer
   %   fsamp = sample rate of simulation (samples per second)

   % compute pulse duration
   duration = num_cycles / fc;

   t = [0: 1/fsamp : duration ]';
   num_samps = length(t);
   s = -sin(2*pi*fc*t);
   w = mrc_window(num_samps,'hanning');
   ws = w .* s
```

AFRL/VASA: Sub-Function - Generates a Window Function

```
function [w] = mrc_window(p,type)

%%% This function creates a bartlett, rectangular, hanning, blackman, or hamming
%%% window of size.  If the type is not specified it is assumed to be a hamming window.
%%% Note:  It will be very easy to add other types of windows as needed.

   % Set hamming window as default
      if ( nargin < 2 )
         type = 'hamming';
      end

      if ( mod(p,2) ~= 0 )
         half = (p+1)/2;
      else
         half = p/2;
      end

      i =( 0:(half-1)')/(p-1);
      if ( strcmp( type, 'hamming' ) )
         w = .54 - .46*cos(2*pi*i);
         if ( mod(p,2) ~=0 )
            w = [w w(end-1:-1:1)]';
         else
```

```
            w = [w w(end:-1:1)]';
        end
    elseif ( strcmp( type, 'hanning' ) )
        w = .5 - .5*cos(2*pi*i);
        if ( mod(p,2) ~=0 )
            w = [w w(end-1:-1:1)]';
        else
            w = [w w(end:-1:1)]';
        end
    elseif ( strcmp( type, 'bartlett' ) )
        w = 2*(0:((p-1)/2))/(p-1);
        if ( mod(p,2) ~= 0 )
            w = [w w((p-1)/2:-1:1)]';
        else
            w = [w w((p/2):-1:1)]';
        end

    elseif ( strcmp( type, 'blackman' ) )
        w = 0.42 - 0.5*cos(2*pi*i) + 0.08*cos(4*pi*i);
        if ( mod(p,2) ~=0 )
            w = [w w(end-1:-1:1)]';
        else
            w = [w w(end:-1:1)]';
        end

    elseif ( strcmp( type, 'rectangle' ) )
        w = ones(p,1);
    end
return
```

AFRL/VASA: Primary Function - Generates a Lamb Wave Response Signal

```
function [prop_sig, t, prop_sig_norm] = LambFourierDecomp(input_signal,...
   PadLength, ...
   LambWaveMode,...
   thickness, ...
   prop_distance, ...
   fsamp,...
   Temp,fd,i);

   % INPUTS:
   % input signal          % signal to propagate
   % PadLength             % specify length of padded signal to avoid time aliasing
   % LambWaveMode          % lamb wave mode to simulate; use proper phase velocity curve
   % thickness             % thickness of simulated plate (millimeters)
   % prop_distance         % distance to propagate input signal (meters)
   % delta_distance        % step size of distance (meters)
   % fsamp                 % sample rate of simulation (Hz)
```

```
   % OUTPUTS
   %   prop_sig = propagated signal
   %   t = time vector

   % FUNCTIONS CALLED:
   %         mrc_window
   %         mrc_spectrum
   %         fine_phase_velocity

   n_in = length(input_signal);
   npow2 = ceil(log(n_in)/log(2) );

%  Pad input sigal specified length
   tmp = zeros(1,PadLength);
   tmp(1:n_in) = input_signal;
   input_signal = tmp;

   t = [0 : 1: PadLength-1] / fsamp ;  % time sampling
   nt = length(t);                  % number of time samples

% Frequency vectors (in Hz and radians/sec)
   df = [0: fsamp/PadLength : fsamp/2 - fsamp/PadLength];
   omega = df*2*pi;

% Initialize output arrays to improve computation speed
   s_hat = zeros(nt,PadLength);
   s2_hat = zeros(1,nt);
   s2_prop = zeros(1,nt);

% DFT of pulse
   S = fft(input_signal,PadLength);

% For specified distance, at kth frequency component, obtain phase velocity
%  at freq corresponding to kth component and specified plate thickness
   for k = 1: PadLength/2
         %fd = thickness*df(k)/1e6;
         v = symm_fine_phase_velocity_temperature(fd,Temp);
         % v = fine_phase_velocity_atk(fd,LambWaveMode);
         s_hat(:,k) = S(k) * ...
            exp(-j*(omega(k)* prop_distance/v * ones(size(t)) - ...
            omega(k)*t)');
   end

% Synthesize the pulse at specified distance by summing across frequency
   prop_sig(1,:) = 2*real(sum(s_hat,2))';

% Normalize the response signal with respect to the maximum of the absolute value of the signal
   prop_sig_norm = prop_sig ./ max(abs(prop_sig));
```

AFRL/VASA: Sub-Function - Removes the Header in LabVIEW® data files

```
function X = data_guillotine(filenames,ncols,numhlines);

   % X = data_guillotine(fname,ncols)
   % fname = data filename holding data with a header
   % ncols = number of columns in the data file
   % numhlines = number of lines in header to remove; default = 22
   % NB:  Labview files use the first column for time index, then
   % follows with the excitation and response sensor data in columns.
   % Get rid of header from Labview data files!

% 20060712 - Number of lines in header are an optional input
   fid = fopen( filenames );

% Ditch the header
   if ~exist('numhlines','var') | isempty( numhlines )
      numhlines = 22;
   end

   for i = 1:numhlines
      dummy = fgetl(fid);
   end

   fmt_string = repmat('%g',1,ncols);

% Read the rest of the file
   [X,cnt]  = fscanf(fid, fmt_string );
   fclose(fid);
```

Lt Andrews: Displays the concept of Superposition using the LambFourierDecomp function

```
% Lt Jennifer Andrews
% Modified LambFourierDecomp to obtain s_hat as an output
% Run LambFourierDecomp - look at signal components added in over time
   clear all
   close all
   clc

%% Input Parameters
   freq = 3E5; %Center Frequency
   prop_dist = 300; %mm
   prop_dist_mtrs = prop_dist/1000; %User input: propagated distance in meters
   num_cycles = 5.5; %User Input: number of cycles in excitation signal
   samp_rate = 2.5e6; %User Input: sampling rate in Hz
   thickness = 1; %User Input: specimen thickness in mm
   fd = freq/1E6*thickness; %Frequency-thickness Product
   Temp = [75]; %User Input: specimen temperature

%% Create theoretical S0 response
```

```
   PadLength = 2048;
   for i = 1
      input_signal = WindowedSine(freq, num_cycles, samp_rate);
      [prop_sig, t, prop_sig_norm, s_hat] = LambFourierDecomp(input_signal,...
PadLength, ...
         'S0',...
         thickness, ...
         prop_dist_mtrs, ...
         samp_rate,Temp,fd);
   end
   t = t./1E-6; %Time in micro-seconds

%% Propagated Signal (Normalized)
   figure(1)
%        prop_sig(1,:) = 2*real(sum(s_hat,2))';
%        prop_sig_norm = prop_sig ./ max(abs(prop_sig));
      plot(t,prop_sig_norm,'LineWidth',2)
      title(['Signal Response: 300 kHz signal propagated over ' int2str(prop_dist) '
mm'],'FontWeight','BOLD','FontSize',12)
      xlabel('Time (\musec)','FontWeight','BOLD','FontSize',12)
         xlim([0 100])
      ylabel('Amplitude (Voltage) ','FontWeight','BOLD','FontSize',12)

%% Power Spectral Density
   figure(2)
      Y = fft(prop_sig_norm);
         N = length(Y);
      Pyy = Y.* conj(Y) / PadLength;
   % frequency vectors (in Hz and radians/sec)
      df = [0: samp_rate/PadLength : samp_rate/2 - samp_rate/PadLength];
      omega_vector = df.*(2*pi); %Why multiply by 2pi???
      plot(df./1E3,20*log10(Pyy(1:N/2)),'LineWidth',2)
         title('Power Spectral Density of Received Signal','FontWeight','BOLD','FontSize',12)
         xlabel('Frequency (kHz)','FontWeight','BOLD','FontSize',12)
            xlim([0 1000])
         ylabel('Magnitude (dB)','FontWeight','BOLD','FontSize',12)

%% Expanding signal content around the center frequency
      figure(3)
      fc=392;
      c=50;
      C1=fc - c;
      C2=fc + c;
      prop_sig = 2*real(sum(s_hat(:,C1:C2),2));
      plot(t,prop_sig ./max(abs(prop_sig)),'LineWidth',2)
      title(['Superposition: Center Frequency (300kHz)  +/- ' int2str(c) ' component
waves'],'FontWeight','Bold','FontSize',12)
      xlabel('Time (\musec)','FontWeight','Bold','FontSize',12)
      ylabel('Normalized Amplitude','FontWeight','Bold','FontSize',12)
```

```
xlim([0 150])
ylim([-1.5 1.5])

figure(4)
c=100;
C1=fc - c;
C2=fc + c;
prop_sig = 2*real(sum(s_hat(:,C1:C2),2));
plot(t,prop_sig./max(abs(prop_sig)),'LineWidth',2)
title(['Superposition: Center Frequency (300kHz)  +/- ' int2str(c) ' component
waves'],'FontWeight','Bold','FontSize',12)
xlabel('Time (\musec)','FontWeight','Bold','FontSize',12)
ylabel('Normalized Amplitude','FontWeight','Bold','FontSize',12)
xlim([0 150])
ylim([-1.5 1.5])

figure(5)
c=200;
C1=fc - c;
C2=fc + c;
prop_sig = 2*real(sum(s_hat(:,C1:C2),2));
plot(t,prop_sig./max(abs(prop_sig)),'LineWidth',2)
title(['Superposition: Center Frequency (300kHz)  +/- ' int2str(c) ' component
waves'],'FontWeight','Bold','FontSize',12)
xlabel('Time (\musec)','FontWeight','Bold','FontSize',12)
ylabel('Normalized Amplitude','FontWeight','Bold','FontSize',12)
xlim([0 150])
ylim([-1.5 1.5])

figure(6)
c=1024-fc;
C1=1;
C2=fc + c;
prop_sig = 2*real(sum(s_hat(:,C1:C2),2));
plot(t,prop_sig./max(abs(prop_sig)),'LineWidth',2)
title(['Superposition: All component waves'],'FontWeight','Bold','FontSize',12)
xlabel('Time (\musec)','FontWeight','Bold','FontSize',12)
ylabel('Normalized Amplitude','FontWeight','Bold','FontSize',12)
xlim([0 150])
ylim([-1.5 1.5])
```

AFRL/VASA: Sub-Function - Provides a Theoretical S_0 Group Velocity Value based on a Frequency-thickness Product and a Temperature Value

```
function fgv =  symm_fine_group_velocity_temperature(fd,temp);
%   fgv =  symm_fine_group_velocity_temperature(fd,temp)
%   Returns S0 group velocity (meters/sec) in aluminum for a given temperature
%   INPUT:
%       fd = frequency thickness product (MHz-mm); can be a vector of values
```

```
%       temp = temperature in degrees Fahrenheit, must be one of the set provided:
%                    = {0, 25, 50, 75, 100, 125, 150, 175, 190, 200, 225, 500, 550, 600}
%   OUTPUT:
%       fgv = phase velocity (meters/sec)
%             NOTE:  fgv/1000 => millimeters / usec

% Polynomial expansion used to fit data from Steve Olson's Root Finding Program
% Use polyfit and polyval; the selected order of polynomials was based on a
% visual fit of actual to approximated curve across fd = [0.01,2];

fd = fd(:);  % allows for possible evaluation at multiple points
min_fd = min(fd); max_fd = max(fd);

if min_fd < 0.01 || max_fd > 2
   fgv = - 1;
   return
else
   switch temp
      case 0
         coeffs = [-0.03771414746235
            -0.06609406890603
            0.16197465004562
            -0.38019687487521
            0.04801472894085
            5.32947410134224  ];

         fgv = 1e3 * polyval( coeffs, fd'); % the 1e3 term converts speed to m/s

      case 25
         coeffs = [-0.03453844229122
            -0.08454594665643
            0.19251782992134
            -0.40210726183557
            0.05346191414151
            5.30796943776990 ];
         fgv = 1e3 * polyval( coeffs, fd'); % the 1e3 term converts speed to m/s

      case 50
         coeffs = [-0.03274937045366
            -0.09396214535107
            0.20721427652177
            -0.41194093328316
            0.05574822068429
            5.29903652122057 ];
         fgv = 1e3 * polyval( coeffs, fd'); % the 1e3 term converts speed to m/s

      case 75
         coeffs = [-0.02958065650976
            -0.11116477617734
```

```
        0.23519370976088
        -0.43168333369008
        0.06071874667326
        5.28300800244965 ];
    fgv = 1e3 * polyval( coeffs, fd'); % the 1e3 term converts speed to m/s

case 100
    coeffs = [-0.02286653566366
        -0.14460359837475
        0.28898280086065
        -0.46854299523180
        0.06995258583008
        5.26584233436482 ];
    fgv = 1e3 * polyval( coeffs, fd'); % the 1e3 term converts speed to m/s

case 125
    coeffs = [-0.01878368253038
        -0.16634756992241
        0.32459279957130
        -0.49357624501156
        0.07623997281652
        5.24939615396701 ];
    fgv = 1e3 * polyval( coeffs, fd'); % the 1e3 term converts speed to m/s

case 150
    coeffs = [-0.01076572867631
        -0.20731932260796
        0.39009885640857
        -0.53839920874524
        0.08729887930565
        5.22239371630993 ];
    fgv = 1e3 * polyval( coeffs, fd'); % the 1e3 term converts speed to m/s


case 175
    coeffs = [-0.00219984056454
        -0.25045057101020
        0.45854981729179
        -0.58474787104732
        0.09860976672799
        5.19632737903971 ];
    fgv = 1e3 * polyval( coeffs, fd'); % the 1e3 term converts speed to m/s


case 190
    coeffs = [0.00620629794883
        -0.29171084763550
        0.52451089455619
        -0.62980411638718
```

```
        0.10998338084575
        5.17765224628654 ];
    fgv = 1e3 * polyval( coeffs, fd'); % the 1e3 term converts speed to m/s

case 200
    coeffs = [-0.03163922259345
        0.40552831199442
        -2.09520059849469
        5.89720469162116
        -10.13159968060309
        11.13503155525766
        -7.97258238450473
        3.62846818325202
        -1.05702932274158
        -0.05651368213046
        -0.01321010404268
        5.17321107420959 ];
    fgv = 1e3 * polyval( coeffs, fd'); % the 1e3 term converts speed to m/s

case 225
    coeffs = [-0.04909568892756
        0.58377575414420
        -2.86676916351367
        7.73629396616796
        -12.73325702412105
        13.28317574495995
        -8.84196218269797
        3.60872933012745
        -0.89243629600356
        -0.11633257226218
        -0.00608739880822
        5.14222679172513 ];
    fgv = 1e3 * polyval( coeffs, fd'); % the 1e3 term converts speed to m/s

case 500
    coeffs = 1e2*[-0.01820250682838
        0.17547683323663
        -0.72598808914928
        1.69228580838903
        -2.44965093086113
        2.28545591388524
        -1.38101813164313
        0.52792960413055
        -0.12190779968002
        0.01265525438527
        -0.00088469345954
        0.04362582965418 ];
    fgv = 1e3 * polyval( coeffs, fd'); % the 1e3 term converts speed to m/s
```

```
      case 550
         coeffs = 1e3*[0.00526436452725
            -0.05857881647880
            0.27917066595053
            -0.74702793963320
            1.23694546084896
            -1.31671333966854
            0.90610466228024
            -0.39510070269272
            0.10379720877583
            -0.01527142014610
            0.00099568624836
            0.00406055128251];
         fgv = 1e3 * polyval( coeffs, fd'); % the 1e3 term converts speed to m/s

      case 600
         coeffs = 1e3*[0.00876003281704
            -0.08686636847075
            0.36682254101450
            -0.86345420550187
            1.24648092737707
            -1.14427340051136
            0.66998024288823
            -0.24450082691471
            0.05261653289886
            -0.00638506849929
            0.00031498763846
            0.00375054806432 ];
         fgv = 1e3 * polyval( coeffs, fd'); % the 1e3 term converts speed to m/s

      otherwise
         disp('Unsupported temperature')
         fgv = [];
   end
end
return
```

AFRL/VASA: Sub-Function - Provides a Theoretical S_0 Phase Velocity Value based on a Frequency-thickness Product and a Temperature Value

```
function fpv =  symm_fine_phase_velocity_temperature( fd, temp );
%   fpv =  symm_fine_phase_velocity_temperature(fd,temp)
%   Returns S0 phase velocity (meters/sec)in aluminum for a given temperature
%   INPUT:
%      fd = frequency thickness product (MHz-mm); can be a vector of values
%      temp = temperature in degrees Fahrenheit, must be one of set:
%                  = {0, 25, 50, 75, 100, 125, 150, 175, 190, 225, 600}
%   OUTPUT:
%      fpv = phase velocity (meters/sec)
```

```
%         fpv/1000 => millimeters/usec

% Polynomial expansion used to fit data from Steve Olson's Root Finding Program
% Use polyfit and polyval; the selected order of polynomials was based on a
% visual fit of actual to approximated curve across fd = [0.01,2];

fd = fd(:);  % allows for possible evaluation at multiple points
min_fd = min(fd); max_fd = max(fd);

if min_fd < 0.01 || max_fd > 2
   fpv = - 1;
   return
else
   switch temp
      case 0
         coeffs = [-0.05142654709297
            0.16993288286982
            -0.24100699269294
            0.06501025649511
            -0.03139299715575
            5.33445759520220];

         fpv = 1e3 * polyval( coeffs, fd'); % the 1e3 term converts speed to m/s

      case 25
         coeffs = [-0.05313655342506
            0.17597647815818
            -0.24926123503776
            0.06938216345670
            -0.03236171402414
            5.31333398641870 ];
         fpv = 1e3 * polyval( coeffs, fd'); % the 1e3 term converts speed to m/s

      case 50
         coeffs = [-0.05378413396642
            0.17820497231257
            -0.25231032456288
            0.07105929649346
            -0.03279206525247
            5.30456449303111 ];
         fpv = 1e3 * polyval( coeffs, fd'); % the 1e3 term converts speed to m/s

      case 75
         coeffs = [-0.05507959466469
            0.18283473780074
            -0.25878777906218
            0.07466694280557
            -0.03365388253713
            5.28890170460593 ];
```

```
        fpv = 1e3 * polyval( coeffs, fd'); % the 1e3 term converts speed to m/s

    case 100
        coeffs = [-0.05636949658771
            0.18726567362737
            -0.26474597824300
            0.07779392926725
            -0.03437776385729
            5.27235220449814 ];
        fpv = 1e3 * polyval( coeffs, fd'); % the 1e3 term converts speed to m/s

    case 125
        coeffs = [-0.05776182834146
            0.19215889069200
            -0.27140615074052
            0.08136089064404
            -0.03521812591011
            5.25635541653454 ];
        fpv = 1e3 * polyval( coeffs, fd'); % the 1e3 term converts speed to m/s

    case 150
        coeffs = [-0.06009213310675
            0.20041459643570
            -0.28285321764051
            0.08773695163732
            -0.03676294576454
            5.23012173230380 ];
        fpv = 1e3 * polyval( coeffs, fd'); % the 1e3 term converts speed to m/s

    case 175
        coeffs = [-0.06224074229182
            0.20777568402492
            -0.29275654287881
            0.09305453654092
            -0.03808173833658
            5.20484290196241 ];
        fpv = 1e3 * polyval( coeffs, fd'); % the 1e3 term converts speed to m/s

    case 190
        coeffs = [   -0.06386743863999
            0.21345653682254
            -0.30049681482224
            0.09720554642296
            -0.03900502478225
            5.18692445333935 ];
        fpv = 1e3 * polyval( coeffs, fd'); % the 1e3 term converts speed to m/s


case 225
```

```
        coeffs = [0.01277993922954
            -0.12353223637959
            0.51191653087527
            -1.19397037452427
            1.72202041377808
            -1.59434838933529
            0.94821291882998
            -0.36787658715903
            0.08126191330675
            -0.08799422443185
            0.00060733201852
            5.14209345974537 ];
        fpv = 1e3 * polyval( coeffs, fd');

    case 600
        coeffs = 1e2* [0.02608076315068
            -0.29095598897656
            1.39021437440402
            -3.72576781639859
            6.16441540312900
            -6.53311220622451
            4.45289880924999
            -1.90827216853626
            0.48690552640556
            -0.06785420607551
            0.00403023304247
            0.03748966569755 ];
    fpv = 1e3 * polyval( coeffs, fd');

    otherwise
        disp('Unsupported temperature')
        fpv = [];
  end
end
return
```

Lt Andrews: Generates Theoretical Phase & Group Velocity Dispersion Curves for the Fundamental Symmetric Mode (S_0)

```
% 1Lt Jennifer Andrews
% Thesis Code
% Theoretical Phase and Group Velocity Dispersion Curves
  clear all
  close all
  clc

%%
  TEMP = [0 75 150 190 225 600]; %Temperatures
  thickness = 1; %Specimen Thickness
```

```
    freq_vector = [.1:.1:.6]; %1-6MHz
    fd = thickness*freq_vector; %Frequency-thickness Vector

%% Color Scheme for plotting
    for i = 1:7
        if i == 1
            color(i) = 'r';
        elseif i == 2
            color(i) = 'k';
        elseif i == 3
            color(i) = 'b';
        elseif i == 4
            color(i) = 'm';
        elseif i == 5
            color(i) = 'g';
        elseif i == 6
            color(i) = 'c';
        elseif i == 7
            color(i) = 'y';
        end
    end

%% Generating PV & GV Dispersion Curves
    for i = 1:length(TEMP)
        temp = TEMP(i);
        for j = 1:1:length(freq_vector)
            fpv(j) =  symm_fine_phase_velocity_temperature(fd(j),temp)
            fgv(j) =  symm_fine_group_velocity_temperature(fd(j),temp);
        end
        figure(1)
        plot(fd,fpv./1E3,'LineWidth',2,'Color',color(i));
        hold on
        figure(2)
        plot(fd,fgv./1E3,'LineWidth',2,'Color',color(i));
        hold on
    end

    figure(1)
    xlabel('Frequency-Thickness (MHz-mm)','FontWeight','BOLD','FontSize',12)
        xlim([.1 .6])
    ylabel('Phase Velocity (mm / \musec)','FontWeight','BOLD','FontSize',12)
    title('Phase Velocity Dispersion Curve: Symmetric (S_o)
Mode','FontWeight','BOLD','FontSize',12)
    legend([int2str(TEMP(1)) ' \circF'],[int2str(TEMP(2)) ' \circF'],[int2str(TEMP(3)) '
\circF'],[int2str(TEMP(4)) ' \circF'],[int2str(TEMP(5)) ' \circF'],[int2str(TEMP(6)) '
\circF'],'Location','SouthWest')
    hold off

    figure(2)
```

```
   xlabel('Frequency-Thickness (MHz-mm)','FontWeight','BOLD','FontSize',12)
      xlim([.1 .6])
   ylabel('Group Velocity (mm / \musec)','FontWeight','BOLD','FontSize',12)
   title('Group Velocity Dispersion Curve: Symmetric (S_o)
Mode','FontWeight','BOLD','FontSize',12)
   legend([int2str(TEMP(1)) ' \circF'],[int2str(TEMP(2)) ' \circF'],[int2str(TEMP(3)) '
\circF'],[int2str(TEMP(4)) ' \circF'],[int2str(TEMP(5)) ' \circF'],[int2str(TEMP(6)) '
\circF'],'Location','SouthWest')
   hold off
```

AFRL/VASA & Lt Andrews: Primary Function - Generates Theoretical & Experimental Group Velocity Dispersion Curves for the Fundamental Symmetric Mode (S_0)

```
% 1Lt Jennifer Andrews
% Thesis Code--Rewrote code based off of Martin DeSimio's original script (AFRL/VASA)

function [freqs,S0_speed_exp,S0_speed_theo,max_s0_vel,min_s0_vel,mean_s0_vel,e,r] =
experimental_dispersion2(params);

%% OVERVIEW
   % The following code calculates the symmetric wave speed (So) for each signal...
   % (in this analysis, the changing parameters include the freq-thickness products and the
temperature)
   % The So values are used to generate a Group Velocity (GV) dispersion
   % curve (So vs freq-thickness)

   %   INPUT:
   %   prop_dist = wave packet propagation distance
   %   th = aluminum plate thickness
   %   temp = temperature of specimen during experimental testing
   %   freq_range = [start_freq increment_freq end_freq]; range of frequencies
   %   num_cyles = number of cycles in sent wave packet (excitation signal)
   %   samp_rate = sampling rate of raw and theoretical data
   %   str_data_direct = path to experimental data files
   %   str_ident = string to identify files

   %   OUTPUT:
   %   S0_speed = vector of experimental symmetric speeds (mm/µsec)
   %   freqs = vector of frequencies for GV dispersion curves

%%  INPUTS
   prop_dist= params.prop_distance;
      prop_dist_mtrs = prop_dist/1000;
   th = params.thickness;
   temp = params.temperature;
   num_cycles = params.num_cycles;
   samp_rate = params.samp_rate;
```

```
% Data Files
   str_data_dir = params.str_data_dir;
   str_ident = params.str_fid;

   % Frequency Range Data
   start_freq = params.frequencies(1);
   increment_freq = params.frequencies(2);
   end_freq = params.frequencies(3);

%% Frequency Range
   freq_range = [start_freq:increment_freq:end_freq];
   freqs = freq_range; %simplify

%% Cleaning Up Data Files
   file_names = dir([str_data_dir str_ident]);
   numfiles = length(file_names);

   for i = 1:numfiles
         X = data_guillotine([str_data_dir file_names(i).name],3);
         e(:,i) = X(:,2); %Experimental Excitation
         r(:,i) = X(:,3); %Experimental Response
   end

%% DATA PROCESSING------------------------------------------------------
%(1) Compute 'Trigger Delay' between theoretical & experimental excitation
%    signals
%---------------------------------------------------------------------------
   peak_theo_signal_index = (0.5 * num_cycles ./ freqs) * samp_rate;
   [junk, peak_exp_signal_index] = max(abs(e),[],1);
   trigger_delay_index = round(peak_exp_signal_index - peak_theo_signal_index);

%(2) Estimate dispersion in response (index change/spread over original
%    signal duration)
%---------------------------------------------------------------------------
%   (A) Find frequency limits
       pulse_durat = num_cycles./freqs; %Pulse Duration
       pulse_durat_index = round(samp_rate*pulse_durat); %Pulse Duration Index
       BW = 2./pulse_durat; %Bandwidth
       freq_low = freqs - BW;
       freq_high = freqs + BW;

%   (B) Find group velocities (GV) corresponding to frequency limits
       freq_th_low = (freq_low * th)/ 1e6;
       freq_th_high = (freq_high * th)/ 1e6;
       GV_lower_freq_index = round(samp_rate * prop_dist_mtrs ./ ...
          symm_fine_group_velocity_temperature(freq_th_low,temp));

       GV_upper_freq_index = round(samp_rate * prop_dist_mtrs ./ ...
          symm_fine_group_velocity_temperature(freq_th_high,temp));
```

```
%   (C) Calculate Index Spread
       spread_index = abs(GV_upper_freq_index - GV_lower_freq_index);

% Additional Calculation --
%'Extent' of Response = pulse_durat_index + spread_index
   Extent_index = pulse_durat_index + spread_index;

%(3) Use Group Delay to find Propagation Delay
%-------------------------------------------------------
   Prop_Delay_index = round(samp_rate * prop_dist_mtrs ./ ...
      symm_fine_group_velocity_temperature(freqs/1e6,temp));

%(4) Compute wave packet limits in received waveform
%-------------------------------------------------------
   wavepacket_limits_index = [(trigger_delay_index + Prop_Delay_index)'...
    (trigger_delay_index + Prop_Delay_index + Extent_index)'];

%(5) Search received waveforms over computed wave packet limits
%-------------------------------------------------------
   for i = 1:length(freqs)
      constrained_response = zeros(size(r(:,1))); %r is the excitation response
      index_min = wavepacket_limits_index(i,1);
      index_max = wavepacket_limits_index(i,2);
      constrained_response(index_min:index_max) = r(index_min:index_max,i);

      %Use naive estimator: 'simple' max of absolute of constrained signal
      [Max_StatVal(i) TOA_index(i)] = max(abs(constrained_response));
           %Max_StatVal corresponds to amplitude
   end

%(6) Compute the 'Time of Flight' (TOF)
%-------------------------------------------------------
   TOF = (TOA_index - peak_theo_signal_index - trigger_delay_index) / samp_rate;

%(7) Compute the Group Velocity (GV) for the GV dispersion curve
%-------------------------------------------------------
   GV_exp = prop_dist_mtrs ./ TOF;
   S0_speed_exp = GV_exp ./ 1e3;
   S0_speed_theo = symm_fine_group_velocity_temperature(freqs./1e6,temp);
 close

%% PLOT Data: Overlay range of possible group velocities
      tof_s0min = wavepacket_limits_index(:,1) - peak_theo_signal_index' - trigger_delay_index';
      tof_s0max = wavepacket_limits_index(:,2) - peak_theo_signal_index' -
trigger_delay_index';
   % Clean up problems----
      neg_time =  tof_s0min <= 0 ;
      tof_s0min( neg_time ) = NaN;
```

```
   % Compute min and max velocities assuming TOA at window edges----
      max_s0_vel = prop_dist_mtrs * samp_rate ./ tof_s0min ;
      min_s0_vel = prop_dist_mtrs * samp_rate ./ tof_s0max ;
      mean_s0_vel = 0.5 * ( max_s0_vel + min_s0_vel );

%% PLOTS
      figure(1)
      set(gcf,'Color','w')
      set(gca,'FontSize',14)

   % Plot the theoretical and measured curves
      plot(freqs/1e6,S0_speed_theo/1e3,'b') ; % plot in mm/microsecond
      hold on;
      plot(freqs/1e6,S0_speed_exp,'b.') % plot in mm/microsecond
      legend('S0 - theory','S0 - measured','Location','NorthWest')

   % Add lines for velocity constraints
      plot(freqs'/1e6,max_s0_vel/1e3,'b:')
      plot(freqs'/1e6,min_s0_vel/1e3,'b:');
      plot( freqs'/1e6,mean_s0_vel/1e3,'b--')

   % FORMAT THE PLOT
      set(gca,'YLim',[0 8])
      xlabel('Frequency \cdot Thickness Product ( MHz \cdot mm )')
      ylabel('Group Velocity ( mm / \mus )')
      grid on
      legend('S0 - Theory','S0 - Experimental','Location','SouthEast')
```

Lt Andrews: S_0 Theoretical versus Experimental Response Comparisons - Wave Propagation and PSD Plots

```
% 1Lt Jennifer Andrews
% Thesis Code
% Theoretical vs Experimental S0 Response Wave Propagation Comparisons &...
% Power Spectral Densities
% Note: Signal data is normalized w.r.t. the maximum of the absolute value of the
% So responses
   clear all
   close all
   clc

%%  USER INPUTS (A): Temperature and Frequency
   TEMP = [0 75 225];
%      TEMP = [0 75 150 190 225];
   fcset = 1e3*[300];
   freq = 26;

   % 1 ==> 50 kHz
   % 6 ==> 100 kHz
```

```
% 11 ==> 150 kHz
% 16 ==> 200 kHz
% 21 ==> 250 kHz
% 26 ==> 300 kHz
% 31 ==> 350 kHz
% 36 ==> 400 kHz
% 41 ==> 450 kHz
% 46 ==> 500 kHz

if freq == 1                %NOTE: A0 Dominant @ 50 kHz
   flip=1;                  %Designates whether signal data should be flipped for analysis
   END_TIME = 351; %Visual Estimate: End of Response Signal for analysis
   XEx_END = 140;   %Excitation Signal: x-axis limit for plotting
   XResp_END = 160;%Response Signal: x-axis limit for plotting
elseif freq == 6           %NOTE: A0 Dominant @ 100 kHz
   flip=1;
   END_TIME = 251;
   XEx_END = 80;
   XResp_END = 110;
elseif freq == 11   %NOTE: GOOD PLOT @ 150 kHz
   flip=1;
   END_TIME = 201;
   XEx_END = 60;
   XResp_END = 90;
elseif freq == 16   %NOTE: GOOD PLOT @ 200 kHz
   flip=1;
   END_TIME = 201;
   XEx_END = 50;
   XResp_END = 80;
elseif freq == 21   %NOTE: *GREAT PLOT @ 250 kHz
   flip=1;
   END_TIME = 251;
   XEx_END = 50;
   XResp_END = 80;
   PSD_BEG = 116; %Visual Estimate: Start of PSD window
   PSD_END = 191; %Visual Estimate: End of PSD window
elseif freq == 26       %NOTE: GOOD PLOT @ 300 kHz
   flip=1;
   END_TIME = 251;
   XEx_END = 50;
   XResp_END = 80;
   PSD_BEG = 116;
   PSD_END = 191;
elseif freq == 31   %NOTE: GOOD PLOT @ 350 kHz
   flip=-1;
   END_TIME = 251;
   XEx_END = 50;
   XResp_END = 80;
   PSD_BEG = 116;
```

```
    PSD_END = 191;
  elseif freq == 36   % 400 kHz
    flip=-1;
    END_TIME = 251;
    XEx_END = 50;
    XResp_END = 80;
    PSD_BEG = 116;
    PSD_END = 191;
  elseif freq == 41   % 450 kHz: Sampling has an effect on signals
    flip=-1;
    END_TIME = 251;
    XEx_END = 50;
    XResp_END = 80;
  elseif freq == 46   % 500 kHz: Sampling has an effect on signals
    flip=-1;
    END_TIME = 251;
    XEx_END = 50;
    XResp_END = 80;
  else
    'WRONG INPUT'
  end

%% Loading Temperatures Based Data Files: Raw Excitation & Response Signals
  load('Isothermal_Wave_Propagation_0DegF.mat')
    E_0deg = -E(:,freq);
    R_0deg = flip*R(:,freq);
  load('Isothermal_Wave_Propagation_75DegF.mat')
    E_75deg = -E(:,freq);
    R_75deg = flip*R(:,freq);
  load('Isothermal_Wave_Propagation_150DegF.mat')
    E_150deg = -E(:,freq);
    R_150deg = flip*R(:,freq);
  load('Isothermal_Wave_Propagation_190DegF.mat')
    E_190deg = -E(:,freq);
    R_190deg = flip*R(:,freq);
  load('Isothermal_Wave_Propagation_225DegF.mat')
    E_225deg = -E(:,freq);
    R_225deg = flip*R(:,freq);

%% Specimen 1 Parameters
  th = 0.04; % (0.04 or 0.025 in)
    thickness = th/0.0394; %in ==> mm
  prop_dist1 = 158; %(158,509,511 mm)
    prop_dist = prop_dist1/1000; % mm ==> m

%% Theoretical Code Constants
  PadLength = 2048; %Frequency resolution
  LambWaveMode = 'S0'; %Wave mode
  fsamp = 2.5E6; %Sampling rate
```

```
   num_cycles = 5.5; %Cycles in excitation signal

%% Experimental Time Vector
   N = length(E_0deg(:,1));
   delta_t = 1/fsamp;
   T = [0:delta_t:(N-1)*delta_t]./1E-6;

%% Theoretical Analysis
   for i = 1:length(TEMP)
      Temp = TEMP(i);
   if Temp == 0
      E = E_0deg;
      R = R_0deg;
   elseif Temp == 75
      E = E_75deg;
      R = R_75deg;
   elseif Temp == 150
      E = E_150deg;
      R = R_150deg;
   elseif Temp == 190
      E = E_190deg;
      R = R_190deg;
   else
      E = E_225deg;
      R = R_225deg;
   end

   %% INPUT Signal
   nf = length(fcset);
   input_signal = zeros(nf,PadLength); %number of input frequency signals
   fd = (fcset./1E6)*thickness; %frequency-thickness (MHz-mm)

   for k = 1:nf
      ip = [WindowedSine(fcset(k),num_cycles,fsamp)]';
      input_signal(k,1:length(ip)) = ip;
      %%Propagated Signal
      [prop_sig(k,:), t , prop_sig_norm(k,:) ] = LambFourierDecomp_atk(input_signal(k,:),...
         PadLength, ...
         LambWaveMode,...
         thickness, ...
         prop_dist, ...
         fsamp,Temp,fd);
   end
   t = t./1E-6;

%% Color Scheme for plotting
   clear k
   for k = 1:7
       if k == 1
```

```
            color(k) = 'r';
        elseif k == 2
            color(k) = 'm';
        elseif k == 3
            color(k) = 'c';
        elseif k == 4
            color(k) = 'k';
        elseif k == 5
            color(k) = 'g';
        elseif k == 6
            color(k) = 'b';
        elseif k == 7
            color(k) = 'y';
       end
    end
    clear k

%% Excitation Signal: Time Delay between Theoretical and Experimental Results
       [C_raw,I_raw] = max((E(1:END_TIME,1)));
       [C_theor,I_theor] = max((input_signal));
       Time_Delay = T(I_raw)-t(I_theor)

%% Power Spectral Density Calculations & Plots
          %Theoretical PSD
             Y = fft(prop_sig_norm); %Fast Fourier Transform of Response Signal
                N_theo = length(Y);
             Pyy_theo = Y.* conj(Y)./PadLength; %Power Spectral Density
             %Same as approach used in Dr. Cobb's Vibrations Class
             df_theo = [0: fsamp/PadLength : fsamp/2 - fsamp/PadLength];
          %Experimental PSD
             R_PSD = R(PSD_BEG:PSD_END,1)./max(R(PSD_BEG:PSD_END,1));
             Y_exp = fft(R_PSD,PadLength);
                N_exp = length(Y_exp);
             Pyy_exp = Y_exp.*conj(Y_exp)./PadLength;
             df_exp = [0: fsamp/PadLength : fsamp/2 - fsamp/PadLength]; %Freq Vector

          %Plots
             figure(1)
             subplot(length(TEMP),1,i)
             plot(df_theo./1E3,20*log10(Pyy_theo(1,1:N_theo/2)),...
                 df_exp./1E3,20*log10(Pyy_exp(1:N_exp/2)),'LineWidth',2)
              hold on
                if i == 1
                   title(['Power Spectral Densities of S_0 Responses at ' int2str(fcset(1)./1e3) ' kHz '
int2str(Temp) '\circF' ],'FontWeight','Bold','FontSize',12)
                else
                   title([int2str(Temp) '\circF' ],'FontWeight','Bold','FontSize',12)
                end
```

```
            if i == length(TEMP)
               xlabel('Frequency (kHz)','FontWeight','BOLD','FontSize',12)

legend('Theoretical','Experimental','Location','SouthOutside','Orientation','horizontal')
%legend('0\circF','75\circF','150\circF','190\circF','225\circF','Location','SouthOutside','Orientatio
%...n','horizontal')
            end
               xlim([100 700])

            if i == round(length(TEMP)/2)
               ylabel('Magnitude (dB)','FontWeight','BOLD','FontSize',12)
            end
               ylim([-175 0])

%% Excitation & Response Plots (All signals normalized: max(abs(signal))
      figure(2)
      subplot(length(TEMP),1,i)%
      plot(T,E'./max(abs(E(1:END_TIME,1))),'LineWidth',2)
      hold on
      plot(t+Time_Delay,input_signal,color(1),'LineWidth',2) %Time Shifted Theoretical
Excitation Signal
         if i == length(TEMP)
            xlabel('Time (\musec)','FontWeight','Bold','FontSize',12)
            legend('Experimental','Theoretical','Location','SouthWest')
         end
            xlim([0 XEx_END])
            set(gca,'XTick',[0 : 5 : XEx_END])
         if i == round(length(TEMP)/2)
            ylabel('Normalized Amplitude','FontWeight','Bold','FontSize',12)
         end
            ylim([-1.1 1.1])
         if i == 1
            title(['Normalized Excitation Signal (' int2str(fcset(1)./1e3) ' kHz): ' int2str(Temp)
'\circF' ],'FontWeight','Bold','FontSize',12)
         else
            title([int2str(Temp) '\circF: ' ],'FontWeight','Bold','FontSize',12)
         end
      hold off

      figure(3)
      subplot(length(TEMP),1,i)
      plot(T,R'./max(abs(R(1:END_TIME,1))),'LineWidth',2)
      hold on
      plot(t+Time_Delay,prop_sig_norm,color(1),'LineWidth',2) %Time Shifted Theoretical
Response
            if i == length(TEMP)
               xlabel('Time (\musec)','FontWeight','Bold','FontSize',12)
               legend('Experimental','Theoretical','Location','SouthWest')
            end
```

```
            xlim([40 XResp_END])
            set(gca,'XTick',[40 : 5 : XResp_END])
        if i == round(length(TEMP)/2)
            ylabel('Normalized Amplitude','FontWeight','Bold','FontSize',12)
        end
            ylim([-1.1 1.1])
        if i == 1
            title(['Normalized S_0 Response at ' int2str(fcset(1)./1e3) ' kHz: Propagated over '
int2str(prop_dist*1000) ' mm ' int2str(Temp) '\circF'],'FontWeight','Bold','FontSize',12)
        else
            title([int2str(Temp) '\circF'],'FontWeight','Bold','FontSize',12)
        end
    hold off

%% Time Difference between theoretical and experimental responses
    [C_raw,I_raw] = max(abs(R(1:END_TIME,1)));
    [C_theor,I_theor] = max(abs(prop_sig_norm));
    Time_Difference = T(I_raw)-(t(I_theor)+Time_Delay)
end
```

Lt Andrews: Shift in Theoretical S_0 Response Signals due to Increasing Temperatures

```
% 1Lt Jennifer Andrews
% Thesis Code
% Shift in theoretical response signals due to increasing temperatures
  clear all
  close all
  clc

%% USER INPUTS...
  Temperature = [0 75 150 190 225];
  fcset = [250e3]; %Frequency input for excitation signal
  BEG = 29; %x-axis beginning limit (micro-sec)
  Increment = 5;
  END = 54; %x-axis end limit (micro-sec)

%% Constants
  PadLength = 2048; %Freq Resolution
  LambWaveMode = 'S0'; %Wave mode
  thickness = 0.04/0.0394; % mm
  prop_dist = 158/1000; % mm ==> m
  samp_rate = 2.5E6; %sampling rate
  num_cycles = 5.5; %cycles in excitation signal

%% Color Scheme for plotting
  for i = 1:7
      if i == 1
          color(i) = 'r';
      elseif i == 2
```

```
            color(i) = 'm';
        elseif i == 3
            color(i) = 'c';
        elseif i == 4
            color(i) = 'k';
        elseif i == 5
            color(i) = 'g';
        elseif i == 6
            color(i) = 'b';
        elseif i == 7
            color(i) = 'y';
        end
    end

%% INPUT Signal
    for i = 1:1:length(Temperature)
        Temp = Temperature(i);
        nf = length(fcset);
        input_signal = zeros(nf,PadLength); % # of input frequency signals
        fd = (fcset./1E6).*thickness;
      for k = 1:nf
        k;
        ip = [WindowedSine(fcset(k),num_cycles,samp_rate)]';
        input_signal(k,1:length(ip)) = ip;
        %%Propagated Signal
        [prop_sig, t , prop_sig_norm] = LambFourierDecomp_atk(input_signal,...
            PadLength, ...
            LambWaveMode,...
            thickness, ...
            prop_dist, ...
            samp_rate,Temp,fd,i);
      end
      t = t./1E-6;

%% Calculating Theoretical Peak Indices
      [C_theor,I_theor] = max(abs(prop_sig_norm));
      I_THEOR(i) = I_theor; %Max indices for different Temp waves
      TIME(:,1) = t';

%% Power Spectral Density Calculations & Plots
      figure(1)
      Y = fft(prop_sig_norm);
        N = length(Y);
      Pyy = Y.* conj(Y) / PadLength;
      % Frequency vectors (in Hz and radians/sec)
      df = [0: samp_rate/PadLength : samp_rate/2 - samp_rate/PadLength];
      omega_vector = df.*(2*pi); %Why multiply by 2pi???
      plot(df./1E3,20*log10(Pyy(1:N/2)),'Color',color(i),'LineWidth',2)
      hold on
```

```
        title('Power Spectral Density of Response Signal','FontWeight','BOLD','FontSize',12)
        xlabel('Frequency (kHz)','FontWeight','BOLD','FontSize',12)
           xlim([0 1000])
        ylabel('Magnitude (dB)','FontWeight','BOLD','FontSize',12)
        legend('0 Deg F','75 Deg F','150 Deg F','190 Deg F','Location','SouthEast')

%% Response Plots...

      figure(2)
      plot(t,prop_sig_norm,'Color',color(i),'LineWidth',2)
      hold on
        xlabel('Time (\musec)','FontWeight','Bold','FontSize',12)
           xlim([BEG END])
           set(gca,'XTick',[BEG : Increment : END])
        ylabel('Normalized Amplitude','FontWeight','Bold','FontSize',12)
           ylim([-1.1 1.1])
        title(['Specimen I Theoretical S_0 Response at ' int2str(fcset(1)./1e3) '
kHz'],'FontWeight','Bold','FontSize',12)
        legend('0 Deg F','75 Deg F','150 Deg F','190 Deg F','225 Deg F','Location','SouthEast')
   end

%% Time Difference between theoretical responses
      Time_Difference_2to1 = TIME(I_THEOR(2),1)-TIME(I_THEOR(1),1)
      Time_Difference_3to2 = TIME(I_THEOR(3),1)-TIME(I_THEOR(2),1)
      Time_Difference_4to3 = TIME(I_THEOR(4),1)-TIME(I_THEOR(3),1)
      Time_Difference_5to4 = TIME(I_THEOR(5),1)-TIME(I_THEOR(4),1)
      Time_Difference_4to1 = TIME(I_THEOR(4),1)-TIME(I_THEOR(1),1)
      Time_Difference_5to1 = TIME(I_THEOR(5),1)-TIME(I_THEOR(1),1)
```

Lt Andrews: Shift in Experimental S_0 Response Signals due to Increasing Temperatures

```
% 1Lt Jennifer Andrews
% Thesis Code
% Shift in experimental response signals due to increasing temperatures
% NOTE: Data normalized w.r.t. the max(abs(signal)
   clear all
   close all
   clc

%% LOAD DATA: USER INPUTS REQ'D
   freq = 26; % Input number corresponding to frequency
   % 1 ==> 50 kHz
   % 6 ==> 100 kHz
   % 11 ==> 150 kHz
   % 16 ==> 200 kHz
   % 21 ==> 250 kHz
   % 26 ==> 300 kHz
   % 31 ==> 350 kHz
   % 36 ==> 400 kHz
```

```
    % 41 ==> 450 kHz
    % 46 ==> 500 kHz

%% Visual estimates determined to capture and plot S0 Response Signals
    flip=1; %Required if raw signals must be flipped before plotting (flip=-1)
    if freq == 1
        %Normalized Plotting (x-axis limits)
        E_BEG = 1;   %Start of excitation signal
        E_END = 150; %End of excitation signal
        R_BEG = 70;  %Start of response signal
        R_END = 140; %End of response signal
        %Normalizing the signals w.r.t. the max(abs(signal)
        E_END_TIME = 1200; %End of excitation signal
        R_BEG_TIME = 175; %Start of response signal
        R_END_TIME = 350; %End of response signal
        %Frequency
        FREQ = 50;
    elseif freq == 6
        %Normalized Plotting
        E_BEG = 1;
        E_END = 150;
        R_BEG = 40;
        R_END = 110;
        %Normalizing
        E_END_TIME = 1200;
        R_BEG_TIME = 101;
        R_END_TIME = 276;
        %Frequency
        FREQ = 100;
    elseif freq == 11
        %Normalized Plotting
        E_BEG = 1;
        E_END = 80;
        R_BEG = 50;
        R_END = 90;
        %Normalizing
        E_END_TIME = 1200;
        R_BEG_TIME = 126;
        R_END_TIME = 225;
        %Frequency
        FREQ = 150;
    elseif freq == 16
        E_BEG = 17.5;
        E_END = 50;
        R_BEG = 47.5;
        R_END = 77.5;
        %Normalizing
        E_END_TIME = 130;
        R_BEG_TIME = 110;
```

```
    R_END_TIME = 200;
    %Frequency
    FREQ = 200;
elseif freq == 21
    E_BEG = 17.5;
    E_END = 45;
    R_BEG = 47.5;
    R_END = 75;
    %Normalizing
    E_END_TIME = 130;
    R_BEG_TIME = 110;
    R_END_TIME = 200;
    %Frequency
    FREQ = 250;
elseif freq == 26
    E_BEG = 17.5;
    E_END = 42.5;
    R_BEG = 47.5;
    R_END = 72.5;
    %Normalizing
    E_END_TIME = 125;
    R_BEG_TIME = 110;
    R_END_TIME = 200;
    %Frequency
    FREQ = 300;
elseif freq == 31
    flip = -1;
    E_BEG = 17.5;
    E_END = 37.5;
    R_BEG = 47.5;
    R_END = 70;
    %Normalizing
    E_END_TIME = 100;
    R_BEG_TIME = 110;
    R_END_TIME = 200;
    %Frequency
    FREQ = 350;
elseif freq == 36
    flip = -1;
    E_BEG = 17.5;
    E_END = 37.5;
    R_BEG = 47.5;
    R_END = 67.5;
    %Normalizing
    E_END_TIME = 100;
    R_BEG_TIME = 110;
    R_END_TIME = 200;
    %Frequency
    FREQ = 400;
```

```
elseif freq == 41
   flip = -1;
   E_BEG = 17.5;
   E_END = 37.5;
   R_BEG = 47.5;
   R_END = 67.5;
   %Normalizing
   E_END_TIME = 100;
   R_BEG_TIME = 110;
   R_END_TIME = 200;
   %Frequency
   FREQ = 450;
elseif freq == 46
   flip = -1;
   E_BEG = 17.5;
   E_END = 37.5;
   R_BEG = 47.5;
   R_END = 67.5;
   %Normalizing
   E_END_TIME = 100;
   R_BEG_TIME = 110;
   R_END_TIME = 200;
   %Frequency
   FREQ = 500;
else
   'WRONG INPUT'
end

load('Isothermal_Wave_Propagation_0DegF.mat')
   E_0deg = -E(:,freq);
   R_0deg = flip*R(:,freq);
load('Isothermal_Wave_Propagation_75DegF.mat')
   E_75deg = -E(:,freq);
   R_75deg = flip*R(:,freq);
load('Isothermal_Wave_Propagation_150DegF.mat')
   E_150deg = -E(:,freq);
   R_150deg = flip*R(:,freq);
load('Isothermal_Wave_Propagation_190DegF.mat')
   E_190deg = -E(:,freq);
   R_190deg = flip*R(:,freq);
load('Isothermal_Wave_Propagation_225DegF.mat')
   E_225deg = -E(:,freq);
   R_225deg = flip*R(:,freq);

% Excitation Signals
Oven0_E = E_0deg;
Oven75_E = E_75deg;
Oven150_E = E_150deg;
Oven190_E = E_190deg;
```

```
   Oven225_E = E_225deg;
   % Basic Time Response Plots
   Oven0_Resp_orig = R_0deg;
   Oven75_Resp_orig = R_75deg;
   Oven150_Resp_orig = R_150deg;
   Oven190_Resp_orig = R_190deg;
   Oven225_Resp_orig = R_225deg;
   % Normalized Time Response Plots
   Oven0_Resp = R_0deg(R_BEG_TIME:R_END_TIME,1);
   Oven75_Resp = R_75deg(R_BEG_TIME:R_END_TIME,1);
   Oven150_Resp = R_150deg(R_BEG_TIME:R_END_TIME,1);
   Oven190_Resp = R_190deg(R_BEG_TIME:R_END_TIME,1);
   Oven225_Resp = R_225deg(R_BEG_TIME:R_END_TIME,1);

   N = length(R_0deg');

%% EXPERIMENTAL TIME VECTOR
   samp_rate = 2.5E6;
   delta_t = 1/samp_rate;
   Time_Vector = [0 : delta_t : (N-1)*delta_t]./1E-6;

%% TIME SHIFT IN RESPONSES DUE TO VARYING TEMPERATURES
   [C_0,I_0] = max(abs(Oven0_Resp))
   [C_75,I_75] = max(abs(Oven75_Resp))
   [C_150,I_150] = max(abs(Oven150_Resp))
   [C_190,I_190] = max(abs(Oven190_Resp))
   [C_225,I_225] = max(abs(Oven225_Resp))

   Peak_Time_0 = Time_Vector(1,I_0);
   Peak_Time_75 = Time_Vector(1,I_75);
   Peak_Time_150 = Time_Vector(1,I_150);
   Peak_Time_190 = Time_Vector(1,I_190);
   Peak_Time_225 = Time_Vector(1,I_225);

   Time_Diff(1) = (Peak_Time_75 - Peak_Time_0); %micro-seconds
   Time_Diff(2) = (Peak_Time_150 - Peak_Time_75); %micro-seconds
   Time_Diff(3) = (Peak_Time_190 - Peak_Time_150); %micro-seconds
   Time_Diff(4) = (Peak_Time_225 - Peak_Time_190); %micro-seconds
   Time_Diff(5) = (Peak_Time_190 - Peak_Time_0); %micro-seconds
   Time_Diff(6) = (Peak_Time_225 - Peak_Time_0); %micro-seconds
   Time_Diff

%% Normalized Plots
   figure(1)

plot(Time_Vector(1,1:E_END_TIME),Oven0_E(1:E_END_TIME,1)./max(abs(Oven0_E(1:E_E
ND_TIME,1))),...
Time_Vector(1,1:E_END_TIME),Oven75_E(1:E_END_TIME,1)./max(abs(Oven75_E(1:E_END
_TIME,1))),...
```

```
Time_Vector(1,1:E_END_TIME),Oven150_E(1:E_END_TIME,1)./max(abs(Oven150_E(1:E_E
ND_TIME,1))),...
Time_Vector(1,1:E_END_TIME),Oven190_E(1:E_END_TIME,1)./max(abs(Oven190_E(1:E_E
ND_TIME,1))),...
Time_Vector(1,1:E_END_TIME),Oven225_E(1:E_END_TIME,1)./max(abs(Oven225_E(1:E_E
ND_TIME,1))),'LineWidth',2)
          xlabel('Time (\musec)','FontWeight','Bold','FontSize',12)
            xlim([E_BEG E_END])
          ylabel('Normalized Amplitude','FontWeight','Bold','FontSize',12)
            ylim([-1.1 1.1])
          title(['Specimen I Experimental Excitation Signal: ' int2str(FREQ) '
kHz'],'FontWeight','Bold','FontSize',12)
          legend('0 \circF','75 \circF','150 \circF','190 \circF','225 \circF','Location','SouthEast')
   figure(2)
   plot(Time_Vector(R_BEG_TIME:R_END_TIME),Oven0_Resp./max(abs(Oven0_Resp)),...
       Time_Vector(R_BEG_TIME:R_END_TIME),Oven75_Resp./max(abs(Oven75_Resp)),...
      Time_Vector(R_BEG_TIME:R_END_TIME),Oven150_Resp./max(abs(Oven150_Resp)),...
      Time_Vector(R_BEG_TIME:R_END_TIME),Oven190_Resp./max(abs(Oven190_Resp)),...
Time_Vector(R_BEG_TIME:R_END_TIME),Oven225_Resp./max(abs(Oven225_Resp)),'LineW
idth',2)
          xlabel('Time (\musec)','FontWeight','Bold','FontSize',12)
            xlim([R_BEG R_END])
          ylabel('Normalized Amplitude','FontWeight','Bold','FontSize',12)
            ylim([-1.1 1.1])
          title(['Specimen I Experimental S_0 Response at ' int2str(FREQ) '
kHz'],'FontWeight','Bold','FontSize',12)
          legend('0 \circF','75 \circF','150 \circF','190 \circF','225 \circF','Location','SouthEast')

%%  Raw Signal Plots
   Time_Vector = Time_Vector';
   figure(3)
   subplot(2,1,1)
   plot(Time_Vector,Oven0_E,...
       Time_Vector',Oven75_E,...
       Time_Vector',Oven150_E,...
       Time_Vector,Oven190_E,...
       Time_Vector,Oven225_E,'LineWidth',2)
          xlabel('Time (\musec)','FontWeight','Bold','FontSize',12)
          xlim([0 R_END])
          ylabel('Amplitude','FontWeight','Bold','FontSize',12)
          ylim([-.01 .01])
          title(['Specimen I Experimental Excitation Signal at ' int2str(FREQ) '
kHz'],'FontWeight','Bold','FontSize',12)
          legend('0 \circF','75 \circF','150 \circF','190 \circF','225 \circF','Location','Best')
   subplot(2,1,2)
   plot(Time_Vector,Oven0_Resp_orig,...
       Time_Vector,Oven75_Resp_orig,...
       Time_Vector,Oven150_Resp_orig,...
```

```
    Time_Vector,Oven190_Resp_orig,...
    Time_Vector,Oven225_Resp_orig,'LineWidth',2)
       xlabel('Time (\musec)','FontWeight','Bold','FontSize',12)
       xlim([0 R_END])
       ylabel('Amplitude','FontWeight','Bold','FontSize',12)
       title(['S_0 Response at ' int2str(FREQ) ' kHz'],'FontWeight','Bold','FontSize',12)
```

Lt Andrews: Generating Thermal Gradient Plots

```
% 1Lt Jennifer Andrews
% Thesis Code
% Thermal Gradient Plots (13 TCs: Temperature versus Location on propagation path)
   close all
   clear all
   clc

%% Loading Data
   load('TEST1.lvm')
      X1 = TEST1;
   load('TEST2.lvm')
      X2 = TEST2;
   load('TEST3.lvm')
      X3 = TEST3;
   load('TEST4.lvm')
      X4 = TEST4;
   load('TEST5.lvm')
      X5 = TEST5;
   load('TEST6.lvm')
      X6 = TEST6;
   load('TEST7.lvm')
      X7 = TEST7;

%% Marker Scheme for Plotting
   for i = 1:7
       if i == 1
          marker(i) = '+';
       elseif i == 2
          marker(i) = 'o';
       elseif i == 3
          marker(i) = '*';
       elseif i == 4
          marker(i) = '.';
       elseif i == 5
          marker(i) = 'x';
       elseif i == 6
          marker(i) = 's';
       elseif i == 7
          marker(i) = 'd';
      end
```

```
   end

%% Establishing naming convention
for Test = 1:1:7
      if Test == 1
         X = X1;
      elseif Test == 2
         X = X2;
      elseif Test == 3
         X = X3;
      elseif Test == 4
         X = X4;
      elseif Test == 5
         X = X5;
      elseif Test == 6
         X = X6;
      elseif Test == 7
         X = X7;
      end

      Time = X(:,1);
      Sender = X(:,14);
      Posit0 = X(:,6);
      Posit1 = X(:,11);
      Posit2 = X(:,10);
      Posit3 = X(:,3);
      Posit4 = X(:,9);
      Posit5 = X(:,4);
      Posit6 = X(:,8);
      Posit7 = X(:,5);
      Posit8 = X(:,7);
      Receiver = X(:,2);

      Temp_Sender = mean(Sender);
      Temp0 = mean(Posit0)
      Temp1 = mean(Posit1);
      Temp2 = mean(Posit2);
      Temp3 = mean(Posit3);
      Temp4 = mean(Posit4);
      Temp5 = mean(Posit5);
      Temp6 = mean(Posit6);
      Temp7 = mean(Posit7);
      Temp8 = mean(Posit8);
      Temp_Receiver = mean(Receiver);

      TempGradient = [Temp_Sender Temp8 Temp7 Temp6 Temp5 Temp4 Temp3 Temp2
Temp1 Temp0 Temp1 Temp2 Temp3 Temp4 Temp5 Temp6 Temp7 Temp8 Temp_Receiver]';

%% Est. x-axis (position location)
```

```
   Position = [-256 -226 -196 -166 -136 -106 -77 -47 -24 0 24 47 77 106 136 166 196 226 256]';

%% Plot Temp vs Location
   plot(Position,TempGradient,'MarkerType',marker(Test),'LineWidth',2)
   hold on
end
   grid on
   xlabel('Position (mm)','FontWeight','Bold','FontSize',12)
      xlim([-260 260])
   ylabel('Temperature (\circF)','FontWeight','Bold','FontSize',12)
   title('Specimen III: Thermal Gradients','FontWeight','Bold','FontSize',12)
   legend('Gradient 1','Gradient 2','Gradient 3','Gradient 4','Gradient 5','Gradient 6','Gradient 7')
hold off
```

Lt Andrews: Wave Propagation Results from Thermal Gradient Tests

```
% 1Lt Jennifer Andrews
% Thesis Code
% Thermal Gradient - Wave propagation comparisons (for 7 gradients)
% with theoretical, baseline, and post-bowing results
   clear all
   close all
   clc

%% %% USER INPUTS
   Freq = 450;
   fcset = 1e3* [Freq];
   Temp = [75];

%% Constants
   PadLength = 2048; %Freq Resolution
   LambWaveMode = 'S0';
   prop_dist = 512/1000; % meters
   thickness = 0.025/0.0394;
   fsamp = 2.5E6; %sampling rate
   num_cycles = 5.5;

%% LOAD RAW DATA
   [str_data_dir,str_fid] = Thermal_Gradient_DATA_LOADER_E(Freq);
   for k = 1:8
      str_data_dir2 = cell2mat(str_data_dir(k));
      file_name = dir([str_data_dir2 str_fid]);
      numfiles = length(file_name);
      for i = 1:numfiles
            X = data_guillotine([str_data_dir2 file_name.name],3);
            e(:,i) = X(:,2); %Experimental Excitation
            r(:,i) = X(:,3); %Experimental Response
      end
      E(:,k) = e;
```

```
    R(:,k) = r;
end

load('Isothermal_Wave_Propagation_Spec3_Baseline.mat')
% 31 ==> 200 kHz
% 41 ==> 250 kHz
% 51 ==> 300 kHz
% 61 ==> 350 kHz
% 71 ==> 400 kHz
% 81 ==> 450 kHz
% 91 ==> 500 kHz
if Freq == 200
    E(:,9) = Exp(:,31);
    R(:,9) = Resp(:,31);
    X_BEG = 100;
    X_END = 150;
    FLIP = 1;
    FLIP_EX = -1;
elseif Freq == 250
    E(:,9) = Exp(:,41);
    R(:,9) = Resp(:,41);
    X_BEG = 100;
    X_END = 150;
    FLIP = -1;
    FLIP_EX = -1;
elseif Freq == 300
    E(:,9) = Exp(:,51);
    R(:,9) = Resp(:,51);
    X_BEG = 100;
    X_END = 150;
    FLIP = -1;
    FLIP_EX = -1;
elseif Freq == 350
    E(:,9) = Exp(:,61);
    R(:,9) = Resp(:,61);
    X_BEG = 100;
    X_END = 150;
    FLIP = 1;
    FLIP_EX = -1;
elseif Freq == 400
    E(:,9) = Exp(:,71);
    R(:,9) = Resp(:,71);
    X_BEG = 110;
    X_END = 140;
    FLIP = 1;
    FLIP_EX = -1;
elseif Freq == 450
    E(:,9) = Exp(:,81);
    R(:,9) = Resp(:,81);
```

```
    X_BEG = 110;
    X_END = 140;
    FLIP = 1;
    FLIP_EX = -1;
  elseif Freq == 500
    E(:,9) = -Exp(:,91);
    R(:,9) = Resp(:,91);
    X_BEG = 110;
    X_END = 140;
    FLIP = 1;
    FLIP_EX = -1;
  else
    'WRONG!';
  end

%% Time Vector for Experimental Data
  delta_t = 1/fsamp;
  N = length(E(:,1));
  T = [0:delta_t:delta_t*(N-1)]./1E-6;
  T = T';

%% Experimental Excitation & Response Signals: Normalized w.r.t.
%  max(abs(Signal))
  E1 = E(:,1)/max(abs(E(:,1))); %Excitation Signal (Hanning Window Input)
  R1 = FLIP*R(:,1)/max(abs(R(1:375,1))); %Response Signal

  E2 = E(:,2)/max(abs(E(:,2))); %Excitation Signal (Hanning Window Input)
  R2 = FLIP*R(:,2)/max(abs(R(1:375,2))); %Response Signal

  E3 = E(:,3)/max(abs(E(:,3))); %Excitation Signal (Hanning Window Input)
  R3 = FLIP*R(:,3)/max(abs(R(1:375,3))); %Response Signal

  E4 = E(:,4)/max(abs(E(:,4))); %Excitation Signal (Hanning Window Input)
  R4 = FLIP*R(:,4)/max(abs(R(1:375,4))); %Response Signal

  E5 = E(:,5)/max(abs(E(:,5))); %Excitation Signal (Hanning Window Input)
  R5 = FLIP*R(:,5)/max(abs(R(1:375,5))); %Response Signal

  E6 = E(:,6)/max(abs(E(:,6))); %Excitation Signal (Hanning Window Input)
  R6 = FLIP*R(:,6)/max(abs(R(1:375,6)));%/max(abs(R(1:375,6))); %Response Signal

  E7 = E(:,7)/max(abs(E(:,7))); %Excitation Signal (Hanning Window Input)
  R7 = FLIP*R(:,7)/max(abs(R(1:375,7))); %Response Signal

  %Room Temp Post-Bowing
  E8 = E(:,8)/max(abs(E(:,8))); %Excitation Signal (Hanning Window Input)
  R8 = FLIP*R(:,8)/max(abs(R(1:375,8))); %Response Signal
```

```
%Baseline
   E9 = FLIP_EX*E(:,9)/max(abs(E(:,9))); %Excitation Signal (Hanning Window Input)
   R9 = FLIP*R(:,9)/max(abs(R(251:375,9))); %Response Signal

%% Theoretical INPUT Signal
      nf = length(fcset);
      input_signal = zeros(nf,PadLength); % # of input frequency signals
      fd = (fcset./1E6)*thickness; %fd must be in MHz-mm
      for k = 1:nf
         k;
         ip = [WindowedSine(fcset(k),num_cycles,fsamp)]';
         input_signal(k,1:length(ip)) = ip;
         %%Propagated Signal
         [prop_sig(k,:), t , prop_sig_norm(k,:) ] = LambFourierDecomp_atk(input_signal(k,:),...
            PadLength, ...
            LambWaveMode,...
            thickness, ...
            prop_dist, ...
            fsamp,Temp,fd);
      end
      t = t./1E-6;

%% Time Delay between Theoretical and Experimental Results
      [C_raw,I_raw] = max(abs(E(:,1)));
      [C_theor,I_theor] = max(abs(input_signal));
      Time_Delay = T(I_raw)-t(I_theor)

%% Time Delay between Theoretical and Baseline Results
      [C_raw,I_raw] = max(abs(E(:,9)));
      [C_theor,I_theor] = max(abs(input_signal));
      Time_Delay_Baseline = T(I_raw)-t(I_theor)

%% Color Scheme for plotting
   for i = 1:7
       if i == 1
          color(i) = 'r';
       elseif i == 2
          color(i) = 'b';
       elseif i == 3
          color(i) = 'k';
       elseif i == 4
          color(i) = 'g';
       elseif i == 5
          color(i) = 'm';
       elseif i == 6
          color(i) = 'c';
       elseif i == 7
          color(i) = 'y';
       end
```

```
    end

%% Excitation & Response Plots
%     figure(1)
%         %Excitation Signal - Hanning Window Input
%         plot(t+Time_Delay_Baseline,input_signal,'Color',color(1),'LineWidth',2)
%         hold on
%         plot(T,E9,'Color',color(2),'LineWidth',2)
%         hold on
%         plot(T,E8,'Color',color(3),'LineWidth',2)
%         hold on
%         plot(T,E1,'Color',color(4),'LineWidth',2)
%         hold on
%         plot(T,E2,'Color',color(5),'LineWidth',2)
%         hold on
%         plot(T,E3,'Color',color(6),'LineWidth',2)
%         hold on
%         plot(T,E4,'Color',color(7),'LineWidth',2)
%         hold on
%         plot(T,E5,'Color',color(1),'LineWidth',2)
%         hold on
%         plot(T,E6,'Color',color(2),'LineWidth',2)
%         hold on
%         plot(T,E7,'Color',color(3),'LineWidth',2)
%         hold on
%               xlabel('Time (\musec)')
%                  xlim([0 100])
%                  set(gca,'XTick',[0 : 10 : 100])
%               ylabel('Normalized Amplitude')
%               title(['Excitation Signal at ' int2str(fcset(1)./1E3) ' kHz'])
%               legend('Theoretical','Baseline','Room Temp','Gradient: 5','Gradient: 3','Gradient:
2','Gradient: 1 (HIGH)','Gradient: 4','Gradient: 6','Gradient: 7 (LOW)')
%         hold off

      %Response Signal: Normalized w.r.t. max(abs(E))
      figure(2)
      plot(t+Time_Delay_Baseline,prop_sig_norm,'Color',color(1),'LineWidth',2) %Theoretical
      hold on
      plot(T,R9,'Color',color(2),'LineWidth',2) %Baseline @ Room Temp
      hold on
      plot(T,R8,'Color',color(3),'LineWidth',2) %Post-Bowing @ Room Temp
      hold on
      plot(T,R1,'Color',color(4),'LineWidth',2)
      hold on
      plot(T,R2,'Color',color(5),'LineWidth',2)
      hold on
      plot(T,R3,'Color',color(6),'LineWidth',2)
      hold on
      plot(T,R4,'Color',color(7),'LineWidth',2)
```

```
        hold on
        plot(T,R5,'Color',color(1),'LineWidth',2)
        hold on
        plot(T,R6,'Color',color(2),'LineWidth',2)
        hold on
        plot(T,R7,'Color',color(3),'LineWidth',2)
        hold on
        title(['Thermal Gradient Specimen III S_0 Responses at ' int2str(Freq) '
kHz'],'FontWeight','Bold','FontSize',12)
%         legend('Baseline (75\circF)','Gradient: 5','Gradient: 3','Gradient: 2','Gradient: 1
(HIGH)','Gradient: 4','Gradient: 6','Gradient: 7 (LOW)')
        legend('Theoretical (75\circF)','Baseline (75\circF)','Post-bowing (75\circF)','Gradient:
5','Gradient: 3','Gradient: 2','Gradient: 1 (HIGH)','Gradient: 4','Gradient: 6','Gradient: 7 (LOW)')
        ylabel('Normalized Amplitude','FontWeight','Bold','FontSize',12)
          ylim([-1.25 1.25])
          xlim([X_BEG X_END])
        hold off
```

Lt Andrews: Final Theoretical S_0 Response comparison with temperatures up to 600°F

```
% 1Lt Jennifer Andrews
% Thesis Code
% THEORETICAL S0 Response Signal predictions for high temperatures
    clear all
    close all
    clc

%% USER INPUTS...
    Temperature = [0 75 150 225 600];
    fcset = [300e3];
    BEG = 180; %xlim_beg micro-sec
    Increment = 50;
    END = 300; %xlim_end micro-sec

%% Constants
    PadLength = 2048; %Freq Resolution
    LambWaveMode = 'S0';
    thickness = 1; % 1 mm
    prop_dist = 1000/1000; % mm ==> m
    samp_rate = 2.5E6; %sampling rate
    num_cycles = 5.5;

%% INPUT Signal
    for i = 1:1:length(Temperature)
          Temp = Temperature(i);
          nf = length(fcset);
          input_signal = zeros(nf,PadLength); % # of input frequency signals
          fd = (fcset./1E6).*thickness;
        for k = 1:nf
```

```
        k;
        ip = [WindowedSine(fcset(k),num_cycles,samp_rate)]';
        input_signal(k,1:length(ip)) = ip;
        %%Propagated Signal
        [prop_sig, t , prop_sig_norm] = LambFourierDecomp_atk(input_signal,...
            PadLength, ...
            LambWaveMode,...
            thickness, ...
            prop_dist, ...
            samp_rate,Temp,fd,i);
    end
    t = t./1E-6;

%% Calculating Theoretical Peak Indices
    [C_theor,I_theor] = max(prop_sig_norm);
    I_THEOR(i) = I_theor; %Max indices for different Temp waves
    TIME(:,1) = t';

%% Power Spectral Density Calculations & Plots
%       figure(1)
%       Y = fft(prop_sig_norm);
%          N = length(Y);
%       Pyy = Y.* conj(Y) / PadLength;
%       % Frequency vectors (in Hz and radians/sec)
%       df = [0: samp_rate/PadLength : samp_rate/2 - samp_rate/PadLength];
%       omega_vector = df.*(2*pi); %Why multiply by 2pi???
%       plot(df./1E3,20*log10(Pyy(1:N/2)),'Color',color(i),'LineWidth',2)
%       hold on
%          title('Power Spectral Density of Response Signal','FontWeight','BOLD','FontSize',12)
%          xlabel('Frequency (kHz)','FontWeight','BOLD','FontSize',12)
%             xlim([0 1000])
%          ylabel('Magnitude (dB)','FontWeight','BOLD','FontSize',12)
%          legend('0 Deg F','75 Deg F','150 Deg F','190 Deg F','Location','SouthEast')

%% Color Scheme for plotting
  for j = 1:7
      if j == 1
         color(j) = 'r';
      elseif j == 2
         color(j) = 'm';
      elseif j == 3
         color(j) = 'c';
      elseif j == 4
         color(j) = 'k';
      elseif j == 5
         color(j) = 'g';
      elseif j == 6
         color(j) = 'b';
      elseif j == 7
```

```
            color(j) = 'y';
        end
    end

%% Response Plots...
        figure(2)
        plot(t,prop_sig_norm,'Color',color(i),'LineWidth',2)
        hold on
            xlabel('Time (\musec)','FontWeight','Bold','FontSize',12)
                xlim([BEG END])
            ylabel('Normalized Amplitude','FontWeight','Bold','FontSize',12)
                ylim([-1.1 1.1])
            title(['Isothermal Theoretical S_0 Response propagated at ' int2str(fcset(1)./1e3) ' kHz
over ' int2str(prop_dist*1E3) ' mm'],'FontWeight','Bold','FontSize',12)
            legend('0\circF','75\circF','150\circF','225\circF','600\circF','Location','SouthEast')
    end

%% Time Difference between theoretical responses
        Time_Difference_2to1 = TIME(I_THEOR(2),1)-TIME(I_THEOR(1),1)
        Time_Difference_3to1 = TIME(I_THEOR(3),1)-TIME(I_THEOR(1),1)
        Time_Difference_4to1 = TIME(I_THEOR(4),1)-TIME(I_THEOR(1),1)
        Time_Difference_5to2 = TIME(I_THEOR(5),1)-TIME(I_THEOR(2),1)
        Time_Difference_5to1 = TIME(I_THEOR(5),1)-TIME(I_THEOR(1),1)
```

Lt Andrews: Theoretical Thermal Gradient Simulation

```
% 1Lt Jennifer Andrews
% Thesis Code
% THEORETICAL THERMAL GRADIENT
% Heat source at center of specimen
    clear all
    close all
    clc

%% Code Overview
    % Initially Propagate signal over 'x' mm (x = distance over one segment)
    % Continually use received signals as new signals and propagate over following
    % segments (Note: Individual segments are considered to be at
    % isothermal conditions)
    % Compare received signal over 1000 mm (five increments) to signal propagated
    % over 1000 mm (in one shot)!

%%  User Inputs
    fcset = 1e3*[150:50:500]; %Frequency of excitations signal
    Temp = [75 225 600 225 75]; % Temperatures over 5 increments
    beg_temp = 75; % Start temperature
    mid_temp = 600; % Mid Temperature
    avg_temp = 1; % Average or room temp (index)
```

```
%% Constants
   PadLength = 2048; %Freq Resolution
   LambWaveMode = 'S0';
   thickness = 1; % 1 mm
   prop_dist = 1000/1000; % mm ==> m
   num_increments = length(Temp);
   inc_dist = prop_dist/num_increments;
   fsamp = 2.5E6; %sampling rate
   num_cycles = 5.5;

%%  Basic Plot of Thermal Gradient (Temperature versus Distance)
   figure(5)
   plot([0 250 500 750 1000],Temp,'Color','r','LineWidth',2)
   Title('Simulated Thermal Gradient','FontWeight','Bold','FontSize',12)
   xlabel('Distance (mm)','FontWeight','Bold','FontSize',12)
   ylabel('Temperature (\circF)','FontWeight','Bold','FontSize',12)

%% Color Scheme for plotting
   for i = 1:7
       if i == 1
          color(i) = 'g';
       elseif i == 2
          color(i) = 'm';
       elseif i == 3
          color(i) = 'b';
       elseif i == 4
          color(i) = 'r';
       elseif i == 5
          color(i) = 'c';
       elseif i == 6
          color(i) = 'k';
       elseif i == 7
          color(i) = 'y';
      end
   end

%% INPUT Signal
   nf = length(fcset);
   input_signal = zeros(nf,PadLength); % # of input frequency signals
   fd = fcset.*thickness;
   j=1;
   for k = 1:nf
      ip = [WindowedSine(fcset(k),num_cycles,fsamp)]';
      input_signal_orig(k,1:length(ip)) = ip;
      %%Propagated Signal
      [prop_sig(k,:), t , prop_sig_norm(k,:) ] = LambFourierDecomp_atk(input_signal_orig(k,:),...
         PadLength, ...
         LambWaveMode,...
         thickness, ...
```

```
        inc_dist, ...
        fsamp,Temp(j),fd(k)./10^6);
    end
    t = t./1E-6;

%% PLOT (1st Segment)
    for i = 1:1:nf
        figure(1)
        subplot(num_increments-1,1,1)
        plot(t,prop_sig_norm(i,:),color(i))
        hold on
        if i == 1
        title(['Propagated Signal over a ' int2str(inc_dist*1000) ' mm segment'])%at ' int2str(fc) ' kHz
        end

        %TOF Calculation for First Segment
        temp = Temp(j);
        gv(j,i)  = symm_fine_group_velocity_temperature(fd(i)./(10^6),temp);
        TOF(j,i) = inc_dist / gv(j,i);
    end

%% Propagate Signal over Segments
    input_signal(1:nf,:) = prop_sig(1:nf,:); %1:nf ==> range of freq inputs
    for j = 2:1:num_increments-1 %Increments (between first and last leg)
       for i = 1:1:nf
        [prop_sig,t,prop_sig_norm] = LambFourierDecomp_atk(input_signal(i,:),...
              PadLength, ...
              LambWaveMode,...
              thickness, ...
              inc_dist, ...
              fsamp,Temp(j),fd(i)./10^6);
         t=t./1E-6;
         %%PLOT
         subplot(num_increments-1,1,j)
         plot(t,prop_sig_norm,color(i))
         if i == 1
         title(['Propagated Signal over a ' int2str(inc_dist*1000) ' mm segment'])%at ' int2str(fc) '
kHz
         end
         hold on

         input_signal(i,:) = prop_sig;

        %TOF Calculation for individual segments
        temp = Temp(j);
        gv(j,i)  = symm_fine_group_velocity_temperature(fd(i)./(10^6),temp);
        TOF(j,i) = inc_dist / gv(j,i);
        end
    end
```

```
%% Propagate signal over final segment: Response at Receiver
   j=j+1;
   for i = 1:1:nf
            [prop_sig,t,prop_sig_norm] = LambFourierDecomp_atk(input_signal(i,:),...
            PadLength, ...
            LambWaveMode,...
            thickness, ...
            inc_dist, ...
            fsamp,Temp(j),fd(i)./10^6);
       t1=t./1E-6;

       figure(2)
       plot(t1,prop_sig_norm,'Color','r','LineWidth',2)
       hold on

       %TOF Calculation for final segment
       temp = Temp(j);
       gv(j,i)  = symm_fine_group_velocity_temperature(fd(i)./(10^6),temp);
       TOF(j,i) = inc_dist / gv(j,i);
   end

    xlabel('Time (\musec)','FontWeight','Bold','FontSize',12)
        xlim([170 240])
    ylabel('Normalized Amplitude','FontWeight','Bold','FontSize',12)
        ylim([-1.25 1.25])
    title(['Theoretical Gradient: S_0 Response propagated at 300 kHz over '
int2str(prop_dist*1000) ' mm'],'FontWeight','Bold','FontSize',12)

%% PLOT: Original Signal propagated over whole length at Avg Temp
   for i = 1:nf
      [prop_sig,t,prop_sig_norm] = LambFourierDecomp_atk(input_signal_orig(i,:),...
            PadLength, ...
            LambWaveMode,...
            thickness, ...
            prop_dist, ...
            fsamp,75,fd(i)./1E6);
        t2=t./1E-6;
       figure(2)
       plot(t2,prop_sig_norm,'Color','b','LineWidth',2)
       hold on
       legend('Gradient','Room')
   end
   hold off

%% TOTAL TIME OF FLIGHT
   freq_vector = [.15:.1:.6]
   fd1 = freq_vector;
   for i = 1:round(length(Temp)/2)
```

```
        temp = Temp(i);
        for j = 1:1:length(freq_vector)
            fgv(j) =  symm_fine_group_velocity_temperature(fd1(j),temp);
        end
        figure(3)
        plot(fd1,fgv./1E3,'LineWidth',2,'Color',color(i));
        hold on
    end

    TOF_total(1,1:nf) = sum(TOF)
    GV(:,1) = prop_dist ./ (TOF_total)
    figure(3)
    plot(fd./1e6,GV*1e-3,'x','Color','r')
    xlabel('Frequency-Thickness Product(MHz-mm)','FontWeight','Bold','FontSize',12)
    xlim([.15 .5])
    ylim([3 6])
    ylabel('Group Velocity (mm/\musec)','FontWeight','Bold','FontSize',12)
    title('Group Velocity Dispersion Curve for Theoretical Thermal
Gradient','FontWeight','Bold','FontSize',12)
    legend('75\circF','225\circF','600\circF','Thermal Gradient')
```

Lt Andrews: Computing the Length (mm) and Duration (µsec) of Excitation Signals

```
% 1Lt Jennifer Andrews
% Thesis Code
% Calculating the Length & Duration of Excitation Signals
% Current parameters are based on Specimen I
    clear all
    close all
    clc

%% USER INPUTS
    thickness = .04/.0394; %Specimen thickness (mm)
    freq = [.5 1 1.5 2 2.5 3 3.5 4 4.5 5].*1E5; %Frequencies in Hz
    temp = [0 25 50 75 100 125 150 175 190 225 600]; %Temperatures in deg F
    cycles = 5.5; %Number of cycles in excitation signal

%% Computations
    fd = (freq/1E6)*thickness; %Frequency-thickness product in MHz-mm
    for k = 1:length(temp)
        TEMP = temp(k);
        for i = 1:length(freq)
            fpv(i) =  symm_fine_phase_velocity_temperature(fd(i),TEMP); %m/sec
        end
        Cycle_WaveLength(:,k) = (fpv*(1E3))./freq; %Length of one cycle (mm)
    end
    %Length of 5 1/2 cycle Hanning-window excitation signals (mm)
        Signal_Length = Cycle_WaveLength*cycles;
    %Pulse Duration of Excitation Signals (microseconds)
```

```
    Signal_Duration = ((5.5./freq')*1E6);
```

Lt Andrews: Theoretical Plots of Spatial versus Temporal Wave Propagation

```
% 1Lt Jennifer Andrews
% Thesis Code
% Example of Spatial versus Temporal Wave Propagation
  clear all
  close all
  clc

%% Constants
  A = 1;
  k = 3;
  f = 5;
  w = 2*pi*f;

  t_spat = 5;
  x_spat = [0:0.01:5]';
  t_temp = [0:0.01:1]';
  x_temp = 5;

  u1_spat = A*cos(k.*x_spat-w.*t_spat);
  u1_temp = A*cos(k.*x_temp-w.*t_temp);

  y=0;
  figure(1)
    subplot(2,1,1)
      plot(x_spat,u1_spat,x_spat,y*ones(length(x_spat),1),'Color','b','LineWidth',2)
      title('Spatial Propagation at t_0 = 5','FontWeight','BOLD','FontSize',12)
      xlabel('Distance (x)','FontWeight','BOLD','FontSize',12)
      ylabel('Amplitude','FontWeight','BOLD','FontSize',12)
      ylim([-2 2])
    subplot(2,1,2)
      plot(t_temp,u1_temp,t_temp,y*ones(length(t_temp),1),'Color','r','LineWidth',2)
      title('Temporal Propagation at x_0 = 5','FontWeight','BOLD','FontSize',12)
      xlabel('Time (t)','FontWeight','BOLD','FontSize',12)
      ylabel('Amplitude','FontWeight','BOLD','FontSize',12)
      ylim([-2 2])
```

Lt Andrews: Three methods illustrating the concept of Wave Superposition

```
% 1Lt Jennifer Andrews
% Thesis Code
% Basic Examples Demonstrating Wave Superposition - Comment out methods not in use
  clear all
  close all
  clc

%% Superposition of waves using k values
  k1 = 10;
```

```
    k2 = 11;
    k0 = (k1+k2)/2;
    delta_k = (k2-k1)/2; % Wave Number Spread of the Packet--the larger the spread the...
              % smaller the physical size of the packet; Cntrols the
              % distribution of the sine waves being superimposed
    delta_x = pi/(delta_k);

%% Sum of two sin functions
    figure(1)
       x = [-10:.01:10];
       A = sin(k1.*x);
       B = sin(k2.*x);

       WaveSuper = 2*sin(k0.*x).*cos(delta_k.*x);
       subplot(2,1,1)
       plot(x,A,'r',x,B,'b')
       title('Two Sine Waves','FontWeight','Bold','FontSize',12)
       ylabel('Displacement','FontWeight','Bold','FontSize',12)
       xlabel('X','FontWeight','Bold','FontSize',12)
       subplot(2,1,2)
       plot(x,WaveSuper)
       hold off
       xlabel('X','FontWeight','Bold','FontSize',12)
       ylabel('Displacement','FontWeight','Bold','FontSize',12)
       title('Superposition of 2 Sine Waves','FontWeight','Bold','FontSize',12)

%% Superposition Example (2 waves)
    k1 = 3;
    k2 = 5;
    delta_k = k2-k1;
    k_avg = (k1+k2)/2;

    w1 = 2*pi*2;
    w2 = 2*pi*2.5;
    delta_w = w2-w1;
    w_avg = (w1+w2)/2;

    A = 1;
    x = 5; %[0:0.01:10]';
    t = [0:0.01:10]';

    u1 = A*cos(k1.*x-w1.*t);
    u2 = A*cos(k2.*x-w2.*t);

    U1 = cos((0.5*delta_k).*x-(0.5*delta_w).*t);
    U2 = cos(k_avg.*x-w_avg.*t);

    U_total1 = 2*A*U1.*U2;
    U_total2 = u1+u2;
```

```
   figure(2)
      subplot(3,1,1)
      plot(t,u1,'Color','b','LineWidth',2)
      hold on
      plot(t,u2,'Color','r','LineWidth',2)
      legend('k = 4','k = 5','Location','SouthEast')
      title('Sinusoidal Signals with Differing Wavenumbers','FontWeight','BOLD','FontSize',12)
      xlabel('Time (sec)','FontWeight','BOLD','FontSize',12)
      ylabel('Amplitude','FontWeight','BOLD','FontSize',12)
      ylim([-2 2])

      subplot(3,1,2)
      plot(t,U1,'Color','b','LineWidth',2)
      hold on
      plot(t,U2,'Color','r','LineWidth',2)
      legend('Low Frequency Term','High Frequency Term','Location','SouthEast')
      title('High and Low Frequency Components of Superimposed
Signals','FontWeight','BOLD','FontSize',12)
      xlabel('Time (sec)','FontWeight','BOLD','FontSize',12)
      ylabel('Amplitude','FontWeight','BOLD','FontSize',12)
      ylim([-2 2])

      subplot(3,1,3)
      plot(t,U_total1,'.b','LineWidth',2)
      hold on
      plot(t,U_total2,'Color','r','LineWidth',2)
      legend('Basic Sum Approach','Equation 2.1.10','Location','SouthEast')
      title('Superimposed Sinusoidal Signals','FontWeight','BOLD','FontSize',12)
      xlabel('Time (sec)','FontWeight','BOLD','FontSize',12)
      ylabel('Amplitude','FontWeight','BOLD','FontSize',12)
      ylim([-3 3])
      hold off

%% MATLAB EXAMPLE
      t = linspace(0,10);
      x = linspace(0,10);
      k1 = 3;
      k2 = 5;
      w1 = 2*pi*5;
      w2 = 2*pi*6;
      a = sin(k1*x-w1*t);
      b = sin(k2*x-w2*t);

      figure(4)
      stem_handles = stem(x,a+b);
      hold on
      plot_handles = plot(x,a,'--r',x,b,'--g');
      hold off
```

```
    legend_handles = [stem_handles(1);plot_handles];
    legend(legend_handles,'a + b','a = sin(x)','b = cos(x)')
xlabel('Time in \musecs')
ylabel('Magnitude')
title('Linear Combination of Two Functions')
```

Bibliography

1. Cobb, Richard. MECH 719 Vibration Damping and Control Class Notes. Air Force Institute of Technology, Dayton, OH, Fall 2006.

2. Callister, Jr. W.D. Materials Science and Engineering: An Introduction. John Wiley and Sons, Inc.: New York, NY, 1997.

3. Derriso, M.M., S.E. Olson, M.P. DeSimio and B. Sanders. "Development of Automated Damage Detection Techniques," *Materials Damage Prognosis*, J.M. Larson, et. al., ed., TMS. Warrendale, PA (2005).

4. "FLIR Systems." http://www.flirthermography.com. 20 February 2007.

5. Giurgiutiu, Victor. "Multifunctional Vehicle Structural Health Monitoring Opportunities with Piezoelectric Wafer Active Sensors," *44th AIAA/ASME/ASCE/AHS Structures, Structural Dynamics, and Materials Conference*. 7-10 April 2003, Norfolk, VA. AIAA 2003-1568.

6. Giurgiutiu, Victor. "New Results in the Use of Piezoelectric Wafer Active Sensors for Structural Health Monitoring," *46th AIAA/ASME/ASCE/AHS/ASC Structures, Structural Dynamics & Materials Conference*. 18-21 April 2005, Austin, TX. AIAA 2005-2191.

7. Giurgiutiu, Victor, J. Bao and W. Zhao. "Piezoelectric Wafer Active Sensor Embedded Ultrasonics in Beams and Plates," *2003 Society for Experimental Mechanics*, 43(4): 428-449 (December 2003).

8. Giurgiutiu, Victor, Timir Datta and Michael L. Myrick. "Technology Review: Nano Piezo Sensors for Structural Health Monitoring, Damage Detection and Failure Prevention." Unpublished article. 25 May 2004.

9. Grisso, Benjamin L. *Considerations of the Impedance Method, Wave Propagation, and Wireless Systems for Structural Health Monitoring*. Master's thesis, Virginia Polytechnic Institute and State University, Blacksburg VA, 2004.

10. Grisso, Benjamin L., Donald J. Leo and Daniel J. Inman. "Temperature influences on the wave propagation technique for use in supplementing impedance-based structural health monitoring," *Health Monitoring and Smart Non-destructive Evaluation of Structural and Biological Systems III*. Proc. of SPIE Vol.5394, 222-232 (2004).

11. "Introduction to Ultrasonic Testing." http://www.ndt-ed.org/EducationResources/CommunityCollege/Ultrasonics/cc_ut_index.htm. 26 January 2007.

12. Kessler, Seth S., K.S. Amaratunga and B.L. Wardle. "An Assessment of Durability Requirements for Aircraft Structural Health Monitoring Sensors." *Proceedings of the 5th International Workshop on Structural Health Monitoring*, 12-14 September 2005, Stanford University, CA.

13. Konstantinidis, G., B. W. Drinkwater, and P. D. Wilcox. "The temperature stability of guided wave structural health monitoring systems," *Smart Material and Structures,* 15: 967-976 (2005).

14. Lamb, H. "On Waves in an Elastic Plate," *Proceedings of the Royal Society of London. Series A, Containing Papers of a Mathematical and Physical Character*, 93(648), 114-128 (1917).

15. Lempriere, Brian M. *Ultrasound and Elastic Waves*. New York: Academic Press, 2002.

16. Mal, Ajit. "Structural Health Monitoring." *Mechanics*, 33(11-12): 1-4 (2004).

17. "National Instruments." http://www.ni.com. 20 February 2007.

18. Olson, S.E., M.M. Derriso, M.P. DeSimio, and D.T. Thomas. "Analytical Modeling of Lamb Waves for Structural Health Monitoring," *in Proceedings of the 3rd European Workshop on Structural Health Monitoring,* Granada, Spain. 5-7 July 2006.

19. "OMEGA Engineering, Inc." http://www.omega.com. 20 February 2007.

20. "PROTHERM™." http://www.pro-therm.com. 20 February 2007.

21. Rose, J.L. *Ultrasonic Waves in Solid Media*. Cambridge University Press: Cambridge, MA, 1999.

22. Saada, Adel S. *Elasticity Theory and Applications*. Krieger Publishing Company: Malabar, Florida, 1993.

23. "Tacoma Narrows Bridge." http://en.wikipedia.org/wiki/Tacoma_Narrows_Bridge. October 2006.

24. Wait, Jeannette R., Gyuhae Park and Charles R. Farrar. "Integrated Structural Health Assessment Using Piezoelectric Active Sensors," *Shock and Vibration*, 12: 389-405 (2005).

25. Wardle, Brian L. and Jeffrey Chambers. "Durability of Lamb-wave Sensors for Structural Health Monitoring (SHM) of Aerospace Structures." Unpublished article. n. pg. http://web.mit.edu/aeroastro/www/people/wardle/documents/SHM_durability.doc.pdf. October 2006.

26. "Waves in One Dimension." http://www.physics.nmt.edu/~raymond/classes/ph13xbook/node3.html. 23 January 2007.

27. "Waves, the Wave Equation, and Phase Velocity." http://www.physics.gatech.edu/gcuo/lectures/3803/OpticsI02Waves.ppt. 23 January 2007.

28. Worlton, D.C. "Ultrasonic Testing with Lamb Waves," *Non-destructive Testing*, 15, 218-222 (1957).

Vita

First Lieutenant Jennifer Puri Andrews was selected as an ROTC scholarship recipient in 1999 and subsequently attended Texas A&M University for her undergraduate studies. During her four years at A&M, she was a member of the Texas Aggie Corps of Cadets and the Air Force Reserved Officer Training Corps. Additionally, she was the commander of her unit, Squadron 16, her senior year in college. In August of 2003, Lt Andrews graduated from Texas A&M University with a Bachelor's of Science in Mechanical Engineering and she was commissioned into the United States Air Force through Detachment 805.

Upon commissioning, Lt Andrews was assigned to Edwards Air Force Base, CA. She worked for the 419th Flight Test Squadron for two years as a B-1B Operations Engineer and a B-52H Flight Test Engineer. During this time, Lt Andrews logged approximately 45 hours of flight time on the B-52H and KC-135 and she was qualified as a B-1B test conductor.

In August of 2005, Lt Andrews was assigned to AFIT and was selected to enroll in the Astronautical Engineering Master's Program. Upon graduation, she will be assigned to Kirtland Air Force Base, where she will support Detachment 12 under Space and Missiles Command.

REPORT DOCUMENTATION PAGE

Form Approved
OMB No. 074-0188

1. REPORT DATE *(DD-MM-YYYY)*	**2. REPORT TYPE**	**3. DATES COVERED** *(From – To)*
22 Mar 07	Master's Thesis	Sept 2006 – Mar 2007

4. TITLE AND SUBTITLE

Lamb Wave Propagation in Varying Thermal Environments

5a. CONTRACT NUMBER

5b. GRANT NUMBER

5c. PROGRAM ELEMENT NUMBER

6. AUTHOR(S)

Andrews, Jennifer P., First Lieutenant, USAF

5d. PROJECT NUMBER

5e. TASK NUMBER

5f. WORK UNIT NUMBER

7. PERFORMING ORGANIZATION NAMES(S) AND ADDRESS(S)

Air Force Institute of Technology
Graduate School of Engineering and Management (AFIT/EN)
2950 Hobson Way
WPAFB OH 45433-7765

8. PERFORMING ORGANIZATION REPORT NUMBER

AFIT/GA/ENY/07-M01

9. SPONSORING/MONITORING AGENCY NAME(S) AND ADDRESS(ES)

AFRL/VASA
Attn: Mr. Mark Derriso
2130 8th Street
WPAFB OH 45433-7542 DSN: 785-8534

10. SPONSOR/MONITOR'S ACRONYM(S)

11. SPONSOR/MONITOR'S REPORT NUMBER(S)

12. DISTRIBUTION/AVAILABILITY STATEMENT

APPROVED FOR PUBLIC RELEASE; DISTRIBUTION UNLIMITED.

13. SUPPLEMENTARY NOTES

14. ABSTRACT

During flight, launch, and reentry, external surfaces on aerospace vehicles undergo extreme thermo-acoustic loads resulting in structural degradation. Structural health monitoring techniques are being devised to evaluate the health of these structures by locating and quantifying structural damage during and after flight. One such technique uses Lamb wave propagation to assess damage on the surface and through the thickness of thin materials.

The objective of this study was to assess the sensitivity of piezo-generated Lamb wave propagation to isothermal and thermal gradient environments using both theoretical and experimental methods. Experimental isothermal tests were conducted over a temperature range of 0-225°F. The changes in temperature-dependent material properties were correlated to measurable differences in the response signal's waveform and propagation speed. An analysis of the experimental signal response data demonstrated that elevated temperatures delay wave propagation, although the delays are minimal at the temperatures tested in this study. Both these results and experimental group velocity dispersion curves verified theoretical predictions. Subsequent experimental testing in thermal gradient environments, with peak temperatures ranging 114-280°F, also displayed an observable yet minimal delay in wave propagation. Finally, theoretical simulations at temperatures up to 600°F revealed significantly increased delays in wave propagation.

15. SUBJECT TERMS

Structural Health Monitoring, Nondestructive Testing, Piezoelectric Transducer, Rayleigh-Lamb Frequency Equations, Lamb Wave, Time of Arrival, Time of Flight, Group Velocity Dispersion Curve, Thermal Environment

16. SECURITY CLASSIFICATION OF:			**17. LIMITATION OF ABSTRACT**	**18. NUMBER OF PAGES**	**19a. NAME OF RESPONSIBLE PERSON**
REPORT	**ABSTRACT**	**c. THIS PAGE**			Dr. Anthony N. Palazotto
U	**U**	**U**	**UU**	201	**19b. TELEPHONE NUMBER** *(Include area code)* (937) 255-3636, ext 4599; e-mail: Anthony.Palazotto@afit.af.mil

Standard Form 298 (Rev: 8-98)
Prescribed by ANSI Std. Z39-18